School of Mathematical & Physical Sciences
Department of Mathematics

Mathematical modelling of cytokine-mediated immune response and autoimmunity

Farzad Fatehi Chenar

Supervised by Dr Konstantin Blyuss

Thesis submitted for the Degree of

Doctor of Philosophy in Mathematics

Declaration

I hereby declare that this Thesis is submitted at the University of Sussex for the title of Doctor of Philosophy in Mathematics, and this thesis has not been and will not be, submitted in whole or in part to another University for any other academic award. I also declare that this Thesis was composed by myself, under the supervision of Dr Konstantin Blyuss, and that the work contained therein is my own, except where stated otherwise, such as citations.

Signature:.....

Farzad Fatehi Chenar

Dedication

To my family

Acknowledgements

There are many people who deserve to be mentioned and thanked for their support throughout the period of this research. I must start by thanking the people who, more than anyone else, made this thesis possible, my supervisors Dr. Konstantin Blyuss and Dr. Yuliya Kyrychko, for their support, guidance and encouragement.

I would like to thank The CIRS and University of Sussex for providing the funding and support that enabled me to undertake this research and develop my skills and knowledge. I would also like to thank my postgraduate colleagues, including Davide Cusseddu, Silvio Fanzon, Victor Ogesa Juma and Matteo Perugini for their friendship and support.

Lastly, I would like to thank my family for their uncoditional love and consistent emotional support.

List of publications and author contributions

1. F. Fatehi Chenar, Y.N. Kyrychko, K.B. Blyuss, Mathematical model of immune response to hepatitis B, *J. Theor. Biol.* **447**, 98–110, 2018.

    - F. Fatehi Chenar developed the model, performed analytical and numerical analysis of the model, and wrote the bulk of the paper.
    - Y.N. Kyrychko conceived the goals of the study, assisted with the bifurcation analysis of the model, and edited the paper.
    - K.B. Blyuss conceived the goals of the study, assisted with model derivation, and wrote a portion of the paper.

2. F. Fatehi, Y.N. Kyrychko, R. Molchanov, K.B. Blyuss, Bifurcations and multistability in a model of cytokine-mediated autoimmunity, *Int. J. Bif. Chaos*, **29(3)**, 1950034, 2019.

    - F. Fatehi derived and analysed the model, performed numerical bifurcation and stability analyses, and wrote the bulk of the paper.
    - Y.N. Kyrychko assisted with numerical simulations, and edited the paper.
    - R. Molchanov advised on immunological background of the model and biological interpretation of results.
    - K.B. Blyuss conceived the goals of the study, and wrote a portion of the paper.

3. F. Fatehi, S.N. Kyrychko, A. Ross, Y.N. Kyrychko, K.B. Blyuss, Stochastic effects in autoimmune dynamics, *Front. Physiol.* **9**, 45, 2018.

- F. Fatehi derived the continuous-time Markov chain (CTMC) and stochastic differential equation (SDE) models, implemented the system size expansion, performed numerical simulations, and wrote the bulk of the paper.
- S.N. Kyrychko and A. Ross assisted with the numerical analysis and edited the paper.
- Y.N. Kyrychko conceived the goals of the study, and edited the paper.
- K.B. Blyuss conceived the goals of the study, and wrote a portion of the paper.

4. F. Fatehi, Y.N. Kyrychko, K.B. Blyuss, Effects of viral and cytokine delays on dynamics of autoimmunity, *Mathematics*, **6**, 66, 2018.

    - F. Fatehi developed the model, performed analytically and numerical analysis, and wrote the bulk of the paper.
    - Y.N. Kyrychko assisted with the numerical analysis, and wrote a portion of the paper.
    - K.B. Blyuss assisted with the model derivation, and edited the paper.

5. F. Fatehi, Y.N. Kyrychko, K.B. Blyuss, Stochastic dynamics in a time-delayed model for autoimmunity, 2019, submitted.

    - F. Fatehi conceived the goals of the study, performed analytical analysis, assisted with numerical analysis and simulations, and wrote the bulk of the paper.
    - Y.N. Kyrychko assisted with numerical analysis, and wrote a portion of the paper.
    - K.B. Blyuss conceived the goals of the study, assisted with numerical simulations, and edited the paper.

Glossary

Term	Definition
Clonal expansion	The explosive increase in the number of immune system's cells in the presence of an infection
Antigen	A structural molecule that binds specifically to an antibody
Leukocyte	A type of blood cell that is produced in the bone marrow and found in the blood and lymph tissue, which helps the body fight infection and other diseases
Macrophage	A type of white blood cell that surrounds and kills microorganisms, removes dead cells, and stimulates the action of other immune system cells
Cytolitic	Dissolution or destruction of a cell
Non-cytolitic cure	Curing an infected cell without dissolution or destruction of the cell
Epitope	A part of an antigen molecule that an antibody will recognize and bind to
Self-reactivity	The recognition of a self-antigen as a foreign antigen by the immune response
Autoreactive	An immune system's cell with high level of self-reactivity
Consuming reaction	When the reactants of an unfinished reaction cannot participate in a new reaction
fH bifurcation	fold-Hopf bifurcation is defined as the situation where the Jacobian matrix at an equilibrium has a zero eigenvalue and a pair of purely imaginary eigenvalues
Propensity function	When a system is in state $\mathbf{x}$, $a(\mathbf{x})$ is called a propensity function for the reaction R if $a(\mathbf{x})dt$ is the probability that one R event will occur in the next time interval dt

Abstract

One of the major outstanding challenges in immunology is the development of a comprehensive, quantitative and accurate approach to understanding the causes and dynamics of immune responses. The immune system normally protects the body against infections, but at the same time it is possible that it can fail to distinguish the host's own cells from the cells affected by the infection, which can lead to autoimmune disease. The question of what releases the auto-pathogenic potential of T lymphocytes is at the heart of understanding autoimmune disease. Among various possible causes of autoimmune disease, an important role is played by infections that can result in a breakdown of immune tolerance, primarily through the mechanism of molecular mimicry, where the introduction of pathogenic peptides that structurally resemble self-peptides, derived from infection, may induce T lymphocytes to proliferate and leave them with the ability to respond to self, as well as foreign antigens. Deterministic and stochastic models have been extensively used in the past to study the dynamics of immune responses and analyse a possible onset of autoimmunity. The main focus of this thesis is the development and analysis of mathematical models of immune response to infection, as well as the onset and progress of autoimmunity. Particular emphasis is made on developing new mathematical approaches for elucidating the roles played by various cytokines in the immune dynamics.

In the first part of the thesis I develop a mathematical model for dynamics of immune response to hepatitis B. This model explicitly includes contributions from innate and adaptive immune responses, as well as from cytokines. Analysis of the model identifies parameter regimes where the model exhibits clearance of infection, maintenance of a chronic infection, or periodic oscillations. Effects of nucleoside analogues and interferon treatments are analysed, and the critical drug efficiency is determined.

The second part of the thesis investigates the dynamics of immune response to a general viral infection and a possible onset of autoimmunity, which account for regulatory T cells, T cells with different activation thresholds, and cytokines. Feasibility and stability analyses of different steady states yield boundaries of stability and bifurcations in terms of system parameters. This model exhibits bi-stability and shows different regimes of normal clearance of viral infection, chronic infection, or autoimmune behaviour. Therefore, it can provide significant new insights into autoimmune dynamics.

To investigate the role of stochasticity in immune dynamics, I developed a stochastic version of the model, and the major result is that adding stochasticity can lead to the emergence of sustained oscillations around deterministically stable steady states, thus providing a possible explanation for experimentally observed variations in the progression of autoimmune disease. I also have investigated stochastic dynamics in the regime of bi-stability and computed the magnitude of these fluctuations.

I have also analysed the effects of different time delays, as well as the inhibiting effect of regulatory T cells on secretion of interleukin-2 on autoimmune dynamics. To this end, I have performed a systematic analysis of stability of all steady states of the corresponding model both analytically, and numerically. The identification of basins of attraction of different steady states and periodic solutions indicates that time delays can change the shape of these basins of attraction, and the new results show better qualitative agreement with the experimental observations.

My thesis culminates with the last part, where I explore stochastic effects in a time-delayed model for autoimmunity. The major achievement in this part of the thesis is the development of a new methodology for deriving an Itô stochastic delay differential equation (SDDE) from delay discrete stochastic models, as well as showing the equivalency of previously proposed methods. Using this equivalence, I derived a simpler SDDE model to perform numerical simulations. I have used a linear noise approximation (LNA) to determine the magnitude of stochastic fluctuations around deterministic steady states, and to obtain insights into how the coherence of stochastic oscillations around deterministically stable steady states depends on system parameters.

Contents

List of publications and author contributions **iv**

Abstract **vii**

1 Introduction **1**

1.1 Overview of immune response 1

1.2 Mathematical modelling in immunology 3

1.3 Thesis outline 11

2 Mathematical model of immune response to hepatitis B **13**

2.1 Background 13

2.2 Model derivation 15

2.3 Steady states and their stability 19

2.4 Numerical simulations 29

2.5 Discussion 36

3 Bifurcations and multi-stability in a model of cytokine-mediated autoimmunity **38**

3.1 Background 38

3.2 Model derivation 39

3.3 Steady states and their stability 45

3.4 Numerical stability analysis and simulations 48

3.5 Discussion 58

4 Stochastic effects in autoimmune dynamics **62**

4.1 Methods 63

4.1.1 Continuous-time Markov chain model of immune dynamics . . 63

4.1.2 Stochastic differential equation model 67
4.1.3 System size expansion 71
4.2 Results 79
4.3 Discussion 85

5 Effects of viral and cytokine delays on dynamics of autoimmunity 87
5.1 Model derivation 87
5.2 Stability analysis of the steady states 92
5.2.1 Stability analysis of the disease-free steady state 92
5.2.2 Stability analysis of the death, autoimmune and chronic steady states 93
5.3 Numerical stability analysis and simulations 98
5.4 Discussion 107

6 Stochastic dynamics in a time-delayed model for autoimmunity 110
6.1 Stochastic model: a delayed chemical master equation 111
6.2 Itô SDDE model 116
6.3 System size expansion and fluctuations 126
6.4 Numerical stability analysis and simulations 136
6.5 Discussion 145

7 Discussion 148
7.1 Summary 148
7.2 Future work 152

Bibliography 154

A Coefficients of the Hopf frequency function 178

B Construction of equivalent SDDE models 185

Chapter 1

Introduction

1.1 Overview of immune response

The term *immunity* comes from the Latin word *immunitas*, which refers to the protection from legal prosecution that was offered to Roman senators during their tenures in office. In biology, immunity means defence from disease particularly infectious disease. The *immune system* refers to the cells and molecules that are responsible for immunity, and their coordinated and collective response to the invasion of foreign matters is called the *immune response*.

The main role of the immune system is to effectively protect its host against parasites, which largely consists of identifying and destroying microbes and infected cells. Human immune system has two major components: innate immunity and adaptive immunity. Innate immune response is the early line of defence against microbes. Components of the innate immunity are as follows: (1) physical and chemical barriers, such as skin, mucosal epithelia and anti-microbial chemicals; (2) natural killer (NK) cells, macrophages, and dendritic cells; (3) blood proteins; and (4) cytokines which regulate some activities of the immune response. Innate immune response is non-specific, i.e. anything that is identified as foreign, is a target for the innate immune response.

Adaptive immune response is only stimulated upon encountering a foreign antigen presented on antigen-presenting cells (APCs), such as macrophages and dendritic cells [1]. Unlike innate immune response, adaptive immune response is specific, i.e. cells undergo clonal expansion by exposure to antigens, and it is able to distin-

guish between different microbes and molecules. Adaptive immunity has two forms, called humoral immunity and cell-mediated immunity. Humoral immunity is mediated by macromolecules found in the blood, called antibodies. Antigen-stimulated B lymphocytes (B cells) produce specific antibodies. Antibodies bind to microbial antigens, neutralise their infectivity, and eliminate them by various effector mechanisms, such as ingestion (phagocytosis). Viruses and some bacteria, which have survived against humoral immunity and proliferate inside host cells, are inaccessible to antibodies. In this case, cell-mediated immunity delivered by T lymphocytes (T cells) provides the defence against infection. T cells recognise antigens of intracellular microbes, and either destroy them through phagocytosis, or directly kill infected cells. Major T cell populations are helper T cells and cytotoxic T lymphocytes (CTLs). Helper T cells secrete cytokines, which stimulate the activation of T and B cells, macrophages and other leukocytes. CTLs are responsible for killing infected cells [1]. Moreover, in some diseases, such as hepatitis B, CTLs are able to induce non-cytolytic "cure" of infected cells [2, 3, 4].

As mentioned above, the immune system can only be viewed as effective when it can robustly identify and destroy pathogen-infected cells, while distinguishing such cells from healthy cells. Under normal conditions, once foreign epitopes are presented on APCs to T cells, this results in the proliferation of T cells and eliciting their effector function. T cells with high level of self-reactivity are removed from the system by two different mechanisms: central and peripheral tolerances. Central tolerance is associated with the removal of autoreactive T cells during their development in the thymus, while the peripheral tolerance is usually controlled by regulatory T cells [5]. However, these mechanisms are not perfect and sometimes cross-reactivity between epitopes associated with foreign and self-antigens can lead to a T cell response against healthy host cells [6, 7]. The breakdown of self-tolerance, i.e. a failure of self/non-self discrimination, results in a pathological immune response known as *autoimmune disease*, whereby T cells are attacking host's own healthy cells.

For many autoimmune diseases, the disease occurs in a specific organ or part of the body, such as retina in uveitis, central nervous system in multiple sclerosis, or pancreatic β-cells in type-1 diabetes [8, 9, 10]. It is extremely difficult to identify the specific causes of autoimmunity in individual patients, as it usually

has contributions from a number of internal and external factors, including a genetic predisposition, age, previous immune challenges, exposure to pathogens etc. [11, 12, 13, 14]. Even though genetic predisposition is known to play a very significant role, it is believed that some additional environmental triggers are required for the onset of autoimmunity, and these are usually represented by infections [15, 16]. A very recent work has experimentally identified a gut bacterium that, when present in mice and humans, can migrate to other parts of the body, facilitating subsequent triggering of autoimmune disease in those organs [17]. Various mechanisms of onset of pathogen-induced autoimmune disease have been identified, including *bystander activation* [18], where the infection releases autoantigen in an environment rich in cytokines that promote T cell activation, thus reducing the signal strength requirement for activation and allowing otherwise unresponsive autoreactive cells to be stimulated by the self-antigens, and *molecular mimicry* [19, 20], where the introduction of pathogenic peptides that structurally resemble self-peptides, derived from infection, may induce T lymphocytes to proliferate and leave them with the ability to respond to self as well as foreign antigens. Molecular mimicry is particularly important in the context of autoimmunity caused by viral infections.

1.2 Mathematical modelling in immunology

Mathematical modelling has been very effective in the analysis of different aspects of virus dynamics and the interactions between viruses and the immune system of the host [21, 22, 23, 24, 25], such as hepatitis B [26], influenza [27], HIV [28, 29, 30], and hepatitis C [31]. A nice review by Andrew et al. [32] discusses fundamental modelling and computational issues associated with modelling immune response, especially from the perspective of the possibility of making experimentally testable predictions.

In the context of modelling the dynamics of immune response to HBV infection, Ciupe et al. [33, 34] extended a standard model of immune response to study acute infection and the role of time delay associated with activation and expansion of effector cells. In a subsequent work, they also looked into the role of pre-existing or vaccine-induced antibodies in controlling the HBV infection [35]. Min et al. [36]

used a standard incidence function rather than a mass action to account for a finite liver size and susceptibility to HBV infection, while Gourley et al. [37] developed a time-delayed extension of this model. Hews et al. [38] used a logistic growth for hepatocyte population and a standard incidence to help the model better represent available data, and to achieve more realistic values for the basic reproduction number. Yousfi et al. [39] analysed possible mis-coordination between different branches of adaptive immune response, more specifically, between the CTLs and the antibodies, during HBV infection. In terms of the effects of cytokines on mediating immune response, Wiah et al. [40] studied a model that besides the CTLs and antibodies also includes α- and β-interferons, whose role is taken to convert susceptible hepatocytes into infection-resistant cells. Kim et al. [41] adapted an earlier model for hepatitis C to include cytokines implicitly through allowing effector cells to cause non-cytolytic recovery of the infected cells, and a similar approach has also been used by other researchers [42, 43, 44] who considered a constant rate of non-cytolytic cure alongside treatment.

Since the focus of all of these models was on the dynamics of immune response against HBV infection, they all assumed that the immune system is able to distinguish the host's own healthy cells from the cells affected by the infection, so that the immune response only targets infected cells. However, immune response is a complex process, which is not flawless, and cross-reactivity between epitopes associated with foreign and self-antigens can sometimes lead to autoimmune disease.

Over the years, a number of mathematical models have investigated various origins and aspects of immune response, with an emphasis on the onset and development of autoimmune disease. Some of the early models analysed interactions between regulatory and effector T cells without investigating specific causes of autoimmunity, but instead focusing on T cell vaccination [45]. Borghans and de Boer [46] and Borghans et al. [47] showed how autoimmune dynamics, which they defined as above-threshold oscillations in the number of autoreactive cells, can appear in such models. León et al. [48, 49, 50] studied interactions between different T cells, and how they can affect regulation of immune response and control of autoimmunity. Carneiro et al. [51] presented an overview of that work and compared two possible mechanisms of immune self-tolerance that are either based on control by specific

regulatory T cells, or result from tuning of T cell activation thresholds. Iwami et al. [52, 53] analysed a model of immune response to a viral infection with an emphasis on explicitly including the virus population, and also investigated the effects of different forms of the growth function for susceptible cells on autoimmune dynamics. Despite this model's ability to demonstrate the emergence of autoimmunity, since it does not allow for a viral expansion, it cannot support a regime of normal viral clearance. Alexander and Wahl [54] focused on how interactions of professional APCs with effector and regulatory T cells can control autoimmune response. Burroughs et al. [55, 56] demonstrated how autoimmunity can arise through bystander activation mediated by cytokines. An excellent overview of some of the latest development in mathematical modelling of autoimmune disease can be found in a special issue on "Theories and modelling of autoimmunity" [57].

Since T cells are known to be fundamental for the dynamics of autoimmunity, several different methodologies have been proposed for the analysis of various roles they play in coordinating immune response. Experimental evidence suggests that a major component in controlling autoimmune behaviour is provided by regulatory T cells, which are activated by autoantigens and act to shut down autoimmune responses [58, 59, 60], while impairment in the function of regulatory T cells results in autoimmune disease [61, 62]. To model this process, Alexander and Wahl [54] and Burroughs et al. [55, 56] explicitly included a separate compartment for regulatory T cells that are activated by autoantigens and suppress the activity of autoreactive T cells. Another theoretical approach supported by experimental evidence is the idea that T cells have the capacity to adjust their activation threshold for response to stimulation by autoantigens depending on various environmental conditions or endogenous stochastic variation, which allows them to perform a variety of different immune functions. The associated framework of *tunable activation thresholds* was proposed for analysis of thymic [63] and peripheral T cell dynamics [64, 65], and has been subsequently used to analyse differences in activation/response thresholds that are dependent on the activation state of the T cell [66]. van den Berg and Rand [67] and [68] developed and analysed stochastic models for tuning of activation thresholds. The importance of tuning lies in the fact that it provides an effective mechanism for improving sensitivity and specificity of T cell signalling in

a noisy environment [69, 70], and both murine and human experiments have confirmed that activation of T cells can indeed dynamically change during their circulation [71, 72, 73, 74]. It is noteworthy that the need for activation thresholds for T cells can be derived directly from the first principles of signal detection theory [75]. Blyuss and Nicholson [76, 77] proposed and analysed a mathematical model that includes two types of T cells with different activation thresholds and allows for a biologically realistic situation where infection and autoimmune response occur in different organs of the host. Depending on parameter values, this model can exhibit the regimes of normal viral clearance, a chronic infection, and an autoimmune state represented by endogenous oscillations in cell populations, associated with episodes of high viral production followed by long periods of quiescence. Such behaviour, associated in the clinical practice with relapses and remissions, has been observed in a number of autoimmune diseases, such as MS, autoimmune thyroid disease, and uveitis [78, 79, 80]. Despite its successes, this model has several limitations. One of those is the fact that the periodic oscillations in the model are only possible when the amount of free virus and the number of infected cells are also exhibiting oscillations, while in laboratory and clinical situations, one rather observes a situation where autoimmunity follows full clearance of the initial infection. Another issue is that this model does not exhibit bi-stability, which could explain clinical observations suggesting that patients with very similar parameters of immune response can have significantly different course and outcome of the infection. However, in the specific context of autoimmunity, León et al. [48] highlighted the importance of bi-stability between steady states with high populations of either regulatory, or effector T cells for effective representation of the adoptive transfer of tolerance. Roy et al. [81] developed a general kinetic model to capture the role of vitamin D in immunomodulatory responses, and they demonstrated that vitamin D extends the region of bi-stability, thus allowing immune regulation to be more robust with respect to changes in pathogenic stimulation. Baker et al. [82] analysed the dynamics of immune response during rheumatoid arthritis with particular emphasis on the effects of cytokines on bi-stability and treatment. Rapin et al. [83] proposed a simple model of autoimmunity that displays a bi-stability between stable steady states corresponding to a healthy state and autoimmunity. The authors have shown how

the system can be switched back to the healthy steady state by immunotherapy aimed at destabilising an autoimmune steady state. In Chapter 3, I will show how inclusion of regulatory T cells and the cytokine mediating T cell activity can allow one to overcome the above-mentioned difficulties and provide a more realistic representation of various regimes in the dynamics of autoimmunity.

Since immune response is known to be a complex multi-factor process [22], a number of studies have looked into various stochastic aspects of immune dynamics, such as T cell selection and proliferation. Deenick et al. [84] analysed stochastic effects of interleukin-2 (IL-2) on T cell proliferation from precursors. Blattman et al. [85] have shown that repertoires of the CTLs populations during primary response to a viral infection and in the memory pool are similar, thus providing further support to the theory of stochastic selection for the memory pool. Detours and Perelson [86] explored the distribution of possible outcomes during T cell selection with account for a variable affinity between T cell receptors and MHC-peptide complexes. Chao et al. [87] analysed a detailed stochastic model of T cell recruitment during immune response to a viral infection. Stirk et al. [88, 89] developed a stochastic model for T cell repertoire and investigated the role of competitive exclusion between different clonotypes. Using the methodology of continuous-time Markov processes, the authors computed extinction times, a limited multivariate probability distribution, as well as the size of fluctuations around the deterministic steady states. Reynolds et al. [90] used a similar methodology to investigate an important question of asymmetric cell division and its impact on the extinction of different T cell populations, and the expected lifetimes of naïve T cell clones. With regards to modelling autoimmune dynamics, Alexander and Wahl [54] studied the stochastic model of immune response with an emphasis on professional APCs to show that the probability of developing a chronic autoimmune response increases with the initial exposure to self-antigen or autoreactive effector T cells.

An important aspect of stochastic dynamics that has to be accounted for in the models is the so-called coherence resonance or stochastic amplification [91, 92], which denotes a situation where periodic solutions with decaying amplitudes in the deterministic model can result in sustained stochastic periodic oscillations in individual realisations of the same model [91, 92]. This suggests that whilst on

average the behaviour may show decaying-amplitude oscillations, individual realisations represented by stochastic oscillations can explain relapses/remissions in clinical manifestations of autoimmune disease as caused by endogenous stochasticity of the immune processes. Moreover, recent experimental data on the progression of uveitis (autoimmune inflammation in the eye) in rodent models [93, 94, 8] show noticeable variation in the progress of disease even in individual eyes of the same animal, as illustrated in Fig. 1.1. Since from a statistical point of view, one can consider the progress of autoimmune disease in each eye of the same animal as independent realisations of the same stochastic process, by computing the variance in the progress of disease it is possible to quantify the level of noise. This would allow us to study the contribution of stochastic processes to the unequal distribution of autoimmune disease in identical organs of the same host.

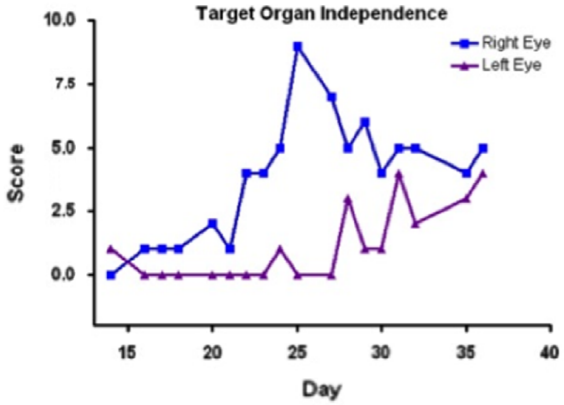

Figure 1.1: Unequal distribution of experimental autoimmune uveitis in C57BL/6 mice. Clinical disease score (y-axis) was obtained from photographs of the retina obtained throughout the course of the disease. These were analysed to produce a disease score by a trained individual, blinded to the origin of the pictures. These results compare two independent realisations of the same stochastic process, from [93, 94].

One of the fundamental features of the immune dynamics is the fact that various processes associated with development of infection, as well as with mounting the appropriate immune response, are characterised by time delays, which can be non-negligible, and thus have to be properly accounted for in mathematical models [95, 96, 97, 98]. In the specific context of viral infections, earlier mathematical models of influenza, HIV and HCV have highlighted the importance of including viral *lag phase* in the analysis of interactions between viruses and the immune system [99, 100, 101, 25]. This lag phase of the virus life cycle includes an *eclipse phase* consisting of virus attachment, cell penetration and uncoating, and a *latent phase*, which includes

virus assembly, maturation and release of new virions, and precise measurements of different stages of virus life cycle have been performed for several viruses that have been associated with triggering or exacerbating autoimmune disease [102, 103, 104, 105, 106, 107]. All of these processes result in a delayed production and release of virions, as well as in the delay between a cell becoming infectious and the time it becomes recognised as an infected cell by the CTLs [108].

The lag phase has been experimentally identified in viruses that are known to sometimes cause or exacerbate autoimmune disease, such as Epstein-Barr virus [103, 102] associated with multiple sclerosis (MS), systemic lupus erythematosus (SLE), rheumatoid arthritis and autoimmune thyroid disease, HSV-1 virus [106, 107] associated with autoimmune stromal keratitis, and the Coxsackie viruses [104, 105] associated with type-1 diabetes. In these cases, precise measurements of different stages of virus life cycle have been performed, and hence the details of the duration of lag phase are available and can be used in testing different time delay effects. Therefore, it is essential to correctly account for this in models of pathogen-induced autoimmunity.

Other time delays involved include a delay between infection and developing immune response [109, 110, 97, 111, 112], as well as the delay associated with the process of stimulation of T cells by the IL-2 cytokine and their subsequent proliferation. Kim et al. [113] have developed and analysed a very detailed model of immune regulation that includes various time delays associated with proliferation and stimulation of different types of T cells.

Since stochasticity and time delays are both essential features of the immune system, it is important to also consider interactions between these processes in the immune dynamics. Bratsun et al. [114] studied the combined effects of time delay and intrinsic noise in the context of gene regulation. They presented a truncated master equation for a set of biochemical reactions, some of which are delayed. They also introduced modifications to the Gillespie algorithm to incorporate delayed reactions. However, this delay stochastic simulation algorithm (DSSA) ignores the waiting time and only works for non-consuming delayed reactions [115]. Barrio et al. [115] analysed oscillatory regulation of Hes1 and presented a new algorithm, which takes into account the waiting time, but this method also only works for non-

consuming delayed reactions. As an alternative, these authors presented an algorithm for consuming delayed reactions termed the 'rejection algorithm', but did not prove that these algorithms can exactly simulate the dynamics of a delayed system. Cai [116] introduced a new algorithm called the 'direct algorithm' and showed that this method and the rejection method are exact, with the difference that his method generates less random variables and is faster. Zavala and Marquez-Lago [117] have used the rejection algorithm to study stochastic effects in a simple genetic circuit with negative feedback and transcriptional/translational delays. Later, Thanh et al. [118, 119] developed some new algorithms which are faster compared with these two algorithms. Delay chemical master equations (DCME) describes the exact probability distribution of finding the system in a particular state [114, 115]. Leier and Marquez-Lago [120] have presented a general framework of DCMEs, which covers both consuming and non-consuming delayed reactions. They have also described for the first time direct and closed solutions of the DCME for simple reaction schemes. Using DSSAs can be very computationally expensive [121, 122]. To overcome this limitation, Tian et al. [121] have developed a method for deriving stochastic delay differential equations (SDDEs), which are more computationally efficient, from a discrete delayed stochastic model, and they used the Euler-Maruyama method for numerical simulations. As an alternative, Niu et al. [123, 124] have introduced a strong predictor-corrector method for the numerical solution of SDDEs. They have indicated that the asymptotic mean-square stability bound (for more details see [125, 126]) of this method will be much larger than that of the Euler-Maruyama method, and also demonstrated that this implementation is much more efficient. Frank [127] has shown how the probability distribution of a SDDE can be described analytically as a solution of a delay Fokker-Planck equation (DFPE), and he has presented a method for deriving a DFPE from SDDEs [128]. Since solving a DCME or DFPE directly is computationally a very challenging task, to describe fluctuations in a delayed stochastic model Galla [129] has implemented the system size expansion, where the time evolution of each cell population is decomposed into deterministic and stochastic components. In this method the fluctuations around a deterministically stable steady state can be described as linear delay Langevin equations, which are easier to deal with [122, 130].

1.3 Thesis outline

In this thesis I focus on mathematical modelling of the effects of cytokines on mediating immune response to infection, as well as on the onset and development of autoimmune disease. When deriving models of immune response, I make a particular emphasis on the roles of time delays associated with different biological processes involved in developing immune response, as well as on stochastic properties of immune dynamics.

In Chapter 2, I focus on the interplay between various branches of the immune system during HBV infection, as well as the role of cytokines in mediating immune response and controlling viral replication. In Section 2.1 I give some general inormation about HBV infection and immune response against this infection. In Section 2.2 I discuss various biological aspects of the immune response against hepatitis B with particular emphasis on interactions between innate immune response as exemplified by NK cells, adaptive immune response represented by HBV-specific cytotoxic T cells and antibodies, and various cytokines, and develop the corresponding mathematical model. Section 2.3 contains systematic analysis of the steady states of the model and their stability, complemented by numerical analysis and identification of parameter regions where the model exhibits normal clearance of infection, maintenance of a chronic infection, or periodic oscillations. Section 2.4 contains results of numerical simulations in different parameter regimes, analysis of the effects of nucleoside analogues and interferon treatments, and determination of the critical drug efficiency. The results of the model are summarised in Section 2.5.

Chapter 3 follows a similar framework of studying immune response to viral infection, but now I make the emphasis on the breakdown of immune tolerance and study the onset of autoimmunity. Section 3.1 provides the key backgrounds of the new model and its advantage over the previous models. In Section 3.2 I derive a new mathematical model of immune response to a viral infection, with an emphasis on the role of T cells having different activation thresholds and cytokines mediating T cell activity, and a detailed analysis of this model is performed in Section 3.3. These analytical results are further extended in Section 3.4 to identify regimes of normal clearance of viral infection, chronic infection, or autoimmune behaviour, as well as the boundaries of stability and bifurcations of relevant steady states in

terms of system parameters and initial conditions. I perform numerical simulations to illustrate different dynamical scenarios, and to identify basins of attraction of different steady states and periodic solutions, highlighting the important role played by the initial conditions in determining the outcome of immune interactions. The Chapter concludes in Section 3.5 with the discussion of results.

Chapter 4 is devoted to analysis of the effects of stochasticity on the dynamics of immune response and autoimmunity. As a first step, in Section 4.1 I use the continuous-time Markov chain (CTMC) approach to derive a chemical master equation, which describes the probability distribution of cell populations over time. Subsequently, I develop an Itô stochastic differential equation model for finding stochastic trajectories. At the end of this section, I use van Kampen's system size expansion method to investigate sustained oscillations around deterministically stable steady states. Section 4.2 is concerned with the numerical simulations and analysis of stochastic dynamics in the regime of bi-stability, and the discussion of results is contained in Section 4.3.

In Chapter 5, I study the effects of viral and cytokine delays on dynamics of autoimmunity. After deriving the model and discussing its basic properties in Section 5.1, I then derive analytical conditions for local stability of the steady states in terms of system parameters and delays, identifying the conditions for stability and possible delay-induced Hopf bifurcation. Section 5.3 is concerned with extensive numerical bifurcation analyses of the model and numerical simulations to demonstrate behaviour in different dynamical regimes. The results and their biological interpretation are present in Section 5.4.

In Chapter 6, I investigate stochastic effects in a time-delayed model for autoimmunity. Using the discrete stochastic simulation method, in Section 6.1 I derive a delayed chemical master equation. Section 6.2 contains a new systematic method for deriving an Itô SDDE from a discrete stochastic delay model. In Section 6.3 I implement system size expansion method on the DCME to study fluctuations around deterministic attractors. Section 6.4 is concerned with numerical simulations and stability analysis of the model. The results are presented in Section 6.5.

The thesis concludes in Chapter 7 with a general discussion of results and open problems.

Chapter 2

Mathematical model of immune response to hepatitis B

This chapter is based on the publication F. Fatehi Chenar, Y.N. Kyrychko, K.B. Blyuss, Mathematical model of immune response to hepatitis B, *J. Theor. Biol.* **447**, 98–110, 2018.

In this chapter a new detailed mathematical model for dynamics of immune response to hepatitis B is proposed, which takes into account contributions from innate and adaptive immune responses, as well as cytokines. Stability analysis of different steady states is performed to identify parameter regions where the model exhibits clearance of infection, maintenance of a chronic infection, or periodic oscillations. Effects of nucleoside analogues and interferon treatments are analysed, and the critical drug efficiency is determined.

2.1 Background

Hepatitis B is a major viral infectious disease that affects a third of the world population, with 240-350 million people having a chronic infection [131, 132], and over 129 million new infections having occurred since 2013 [133]. This disease is a significant public health burden, causing 750,000 deaths annually [132], of which about 300,000 can be attributed to liver cirrhosis and hepatocellular carcinoma [134]. Whilst the prevalence of hepatitis B is relatively low (below 1%) in Western Europe and North America, it remains significant in south-east Asia and sub-Saharan Africa,

where 5-10% of the adult population are chronically infected [132].

The disease is caused by the hepatitis B virus (HBV), which is a hepatotropic noncytopathic DNA virus of the *Hepadnaviridae* family [135]. There are two main routes of transmission of the HBV virus. One is a vertical (perinatal) transmission from an infected mother to a child, resulting in subsequent infection, which in 90% of cases becomes chronic [136, 137]. The other possibility is a horizontal transmission between adults primarily through sexual contacts, intravenous drug use or poor sanitary habits. This type of transmission usually results in recovery, with only 5-10% of adults developing chronic infections [136, 137]. Multiple branches of the immune system are involved in mounting the response during different phases of the HBV infection. In many viral infections of humans, such as HIV, LCMV, Epstein-Barr, the main contribution to the immune response during the early stages of infection comes from the innate immune response, i.e. natural killer (NK) cells and antiviral cytokines, which aim at reducing the spread of the virus and facilitating the development of an adaptive immune response. Contrary to this general observation, early stages of HBV infection are characterised by a delayed viral production and the lack of production of IFN-α/β [138]. Several potential suggestions have been proposed to explain this, including the possibilities that the initial replication of HBV is very slow, or that the virus does not immediately reach the liver and remains for a period of time in other organs [138, 139], however, the exact mechanism is still largely unknown. Once the exponential phase of HBV expansions properly starts, it activates the innate response and the cytokines [2], which, in turn, induces adaptive immune response, with cytotoxic T lymphocytes (CTLs) being responsible for killing infected cells, and antibodies against HBV surface antigen (HBsAg) neutralizing virus particles and preventing (re)infection of cells. Interestingly, besides killing HBV-infected hepatocytes, CTLs are able to induce non-cytolytic "cure" of such cells [1, 2, 3]. An important role in the dynamics of immune response against HBV is played by cytokines, which reduce viral replication [140, 141, 142], activate NK and CTL cells [143, 3, 144], and facilitate induction of immunity in uninfected target cells [145, 40].

2.2 Model derivation

This model consists of nine cell populations as follows,

$T(t)$ is the number of susceptible cells at time t,

$I(t)$ is the number of infected cells at time t,

$F_1(t)$ is the amount of type-1 interferons at time t,

$F_2(t)$ is the amount of type-2 interferons at time t,

$N(t)$ is the number of NK cells at time t,

$E(t)$ is the number of effector T cells at time t,

$R(t)$ is the number of refractory cells at time t,

$V(t)$ is the viral load at time t,

$A(t)$ is the number of antibodies at time t.

In order to analyse various aspects of immune response to HBV infection, I build on the methodology of some earlier HBV models [146, 30, 147]. The host liver cells are divided into populations of uninfected cells $T(t)$, HBV-infected cells $I(t)$, and refractory cells $R(t)$. Healthy hepatocytes are assumed to be produced at a constant rate λ (cell day^{-1}), die at a rate d (day^{-1}) [34, 76], and they are infected by virions (free virus particles) at a rate β (cell^{-1}day^{-1}). New HBV virions $V(t)$ are produced by the infected cells at a rate p (day^{-1}), and they are cleared at a rate c (day^{-1}). Interactions between all cell populations are illustrated in Fig. 2.1.

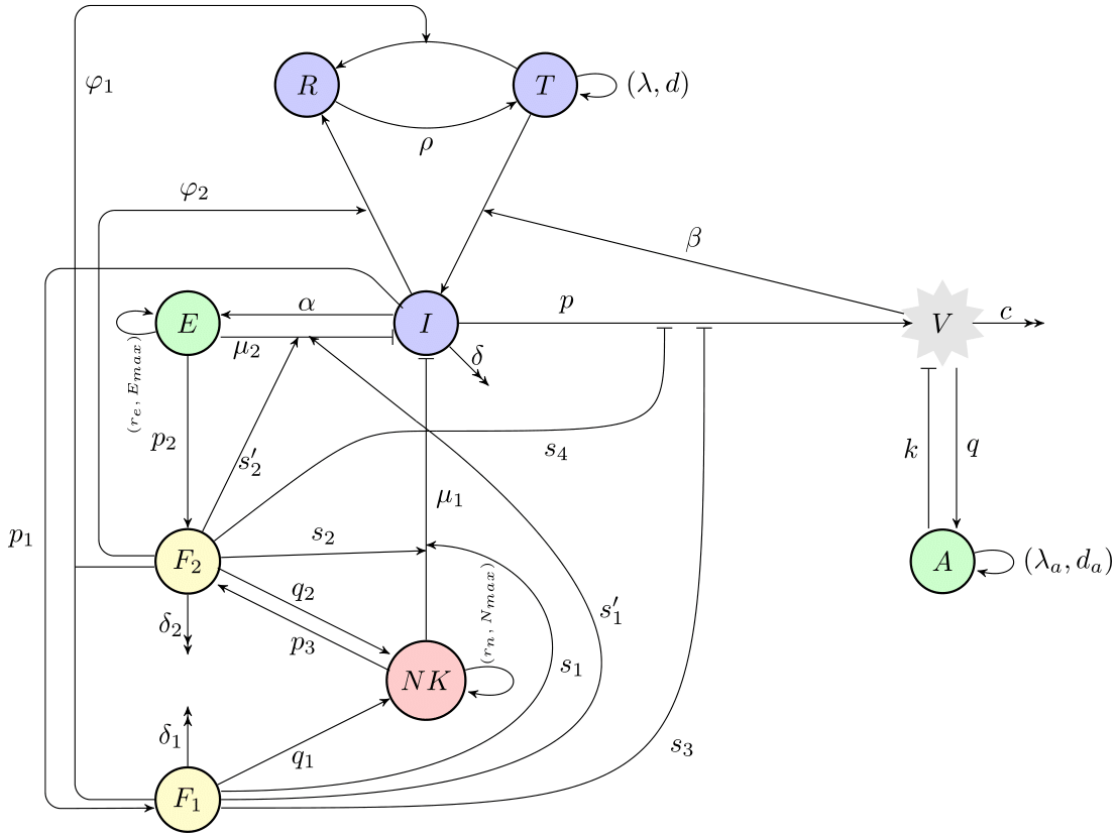

Figure 2.1: A diagram of immune response to HBV infection. Blue circles indicate host cells (uninfected, infected, and refractory cells), green circles denote adaptive immune response (antibodies, CTLs), yellow circles show cytokines (type-1 and type-2 interferon), red circle is the innate immune response (NK cells), and grey indicates virus particles (virions).

Adaptive immune response consists of HBsAg-specific antibodies $A(t)$ that destroy virions at a rate k (cell^{-1}day^{-1}), and HBV-specific CTLs, also referred to as effector cells, $E(t)$. After viral clearance, because of the long-lived plasma and memory B cells, antibody level is kept at some homeostatic level [35]. To model this, I assume that antibodies are produced at a constant rate λ_a (cell day^{-1}), and die at per capita rate d_a (day^{-1}). During infection, antibodies are produced at rate q (day^{-1}) proportional to the viral load. Whilst antibodies are responsible for eliminating free virus, CTLs instead kill infected cells at a rate μ_2 (cell^{-1}day^{-1}). Some models assume certain basal level of CTLs s/d_e in the absence of infection, where s is the source of CTLs, and $1/d_e$ is their average lifespan [33, 34]. We will instead assume the dynamics of effector cells in the absence of infection to have the form of logistic growth with the proliferation rate r_e (day^{-1}) and the carrying capacity E_{max}. Upon infection, the immune response is activated, and the population of

effector cells will expand at rate αIE (α cell^{-1} day^{-1}) [33, 34]. Similarly to effector cells, in the absence of infection, NK cells are assumed to obey logistic growth with the linear growth rate r_n (day^{-1}) and the carrying capacity N_{max}.

Let us now focus on the role of cytokines in the immune dynamics. Type-1 interferons IFN-α/β, to be denoted by $F_1(t)$, are produced by infected cells [148, 3] at a rate p_1 (day^{-1}), and they are destroyed at a rate δ_1 (day^{-1}). Type-2 interferons IFN-γ, denoted as $F_2(t)$, are produced by CTLs and NKs (natural killer cells) $N(t)$ [3, 140, 149, 150] at rates p_2 (day^{-1}) and p_3 (day^{-1}), respectively, and they are lost at a rate δ_2 (day^{-1}). Both types of interferons have the capacity to render the uninfected cells protected from infection through making them resistant to infection [40, 151, 152], or by turning them into refractory cells [145, 153]. Therefore, the combined effect of interferons making uninfected cells refractory is taken to be $\varphi_1(F_1+F_2)$ per uninfected cell, and refractory cells can lose their viral resistance at a rate ρ [33]. During infection, IFN-α/β are able to activate NK cells [154], while IFN-γ induces protein-10 (CXCL-10) that recruits NK cells [155, 143] and can also activate NK cells [3]. Hence, the combined effect of interferons on activating NK cells is taken to occur at a rate $q_1NF_1+q_2NF_2$ (q_i cell^{-1} day^{-1}). Besides positive contribution to the production of new NK cells, IFN-α/β also increase the cytotoxicity of NK cells and CTLs [1]. On the other hand, IFN-γ increases the expression of MHC antigen acting to help CTLs destroy infected cells [144], and it also enhances the activity of NK cells [156, 157]. Thus, both types of interferons increase cytolytic activity of NKs and CTLs, and hence, I will assume that NKs and CTLs destroy infected cells at rates $\mu_1(1+s_1F_1+s_2F_2)IN$ (s_i cell^{-1}) and $\mu_2(1+s_1'F_1+s_2'F_2)IE$ (s_i' cell^{-1}), respectively. Moreover, antiviral cytokines, such as IFN-γ and TNF-α, can non-cytopathically purify viruses from infected cells [3], so that HBV-specific CTLs and NK cells can effectively "cure" infected cells through a non-cytolytic antiviral activity mediated by IFN-γ [3, 140, 4, 158]. Hence, infected cells can be lost due to non-cytolytic response of IFN-γ at a rate φ_2IF_2 (φ_2 cell^{-1} day^{-1}). Studies have shown that IFN-γ can activate a number of intracellular mechanisms that suppress viral replication [140, 141, 142, 159], while IFN-α/β can stimulate the activation of intracellular antiviral pathways to limit the development and spread of viral replication [3]. Thus, both types of interferons help infected cells reduce production of

new virus particles, so infected cells produce virions at a rate $p/(1 + s_3F_1 + s_4F_2)$.

With the above assumptions, the complete model for immune response to HBV infection takes the form

$$\begin{aligned}
\frac{dT}{dt} &= \lambda - dT - \beta VT + \rho R - \varphi_1 T(F_1 + F_2),\\
\frac{dI}{dt} &= \beta VT - \delta I - \mu_1(1 + s_1F_1 + s_2F_2)IN - \mu_2(1 + s_1'F_1 + s_2'F_2)IE - \varphi_2 IF_2,\\
\frac{dF_1}{dt} &= p_1 I - \delta_1 F_1,\\
\frac{dF_2}{dt} &= p_2 E + p_3 N - \delta_2 F_2,\\
\frac{dN}{dt} &= r_n N\left(1 - \frac{N}{N_{max}}\right) + (q_1F_1 + q_2F_2)N,\\
\frac{dE}{dt} &= r_e E\left(1 - \frac{E}{E_{max}}\right) + \alpha IE,\\
\frac{dR}{dt} &= \varphi_1 T(F_1 + F_2) + \varphi_2 IF_2 - \rho R,\\
\frac{dV}{dt} &= \frac{p}{1 + s_3F_1 + s_4F_2} I - cV - kAV,\\
\frac{dA}{dt} &= \lambda_a - d_aA - kAV + qV.
\end{aligned} \tag{2.1}$$

All parameters are non-negative. To reduce the complexity of the model and the number of free parameters, I introduce the following rescaled parameters

$$\begin{aligned}
&\hat{d} = \frac{d}{r_n}, \quad \hat{\beta} = \frac{\beta\lambda_a}{d_a r_n}, \quad \hat{\rho} = \frac{\rho\lambda_a d}{r_n\lambda d_a}, \quad \hat{\delta} = \frac{\delta}{r_n}, \quad \hat{s}_i = s_i\frac{\lambda_a}{d_a}, \quad i = 1,2,3,4,\\
&\hat{\mu}_1 = \frac{\mu_1 N_{max}}{r_n}, \quad \hat{\mu}_2 = \frac{\mu_2 E_{max}}{r_n}, \quad \hat{\varphi}_i = \frac{\varphi_i\lambda_a}{d_a r_n}, \quad \hat{p}_1 = \frac{p_1}{r_n}, \quad \hat{p}_2 = \frac{p_2 d_a E_{max}}{r_n\lambda_a},\\
&\hat{p}_3 = \frac{p_3 d_a N_{max}}{r_n\lambda_a}, \quad \hat{r}_e = \frac{r_e}{r_n}, \quad \hat{\alpha} = \frac{\alpha\lambda_a}{r_n d_a}, \quad \hat{p} = \frac{p}{r_n}, \quad \hat{c} = \frac{c}{r_n}, \quad \hat{k} = \frac{k\lambda_a}{r_n d_a},\\
&\hat{d}_a = \frac{d_a}{r_n}, \quad \hat{q} = \frac{q}{r_n}, \quad \hat{s}_i' = s_i'\frac{\lambda_a}{d_a}, \quad \hat{\delta}_i = \frac{\delta_i}{r_n}, \quad \hat{q}_i = \frac{q_i\lambda_a}{r_n d_a}, \quad i = 1,2,
\end{aligned}$$

and new variables

$$\hat{t} = r_n t, \quad T = \frac{\lambda}{d}\hat{T}, \quad I = \frac{\lambda_a}{d_a}\hat{I}, \quad F_1 = \frac{\lambda_a}{d_a}\hat{F}_1, \quad F_2 = \frac{\lambda_a}{d_a}\hat{F}_2, \quad N = N_{max}\hat{N},$$

$$E = E_{max}\hat{E}, \quad R = \frac{\lambda_a}{d_a}\hat{R}, \quad V = \frac{\lambda_a}{d_a}\hat{V}, \quad A = \frac{\lambda_a}{d_a}\hat{A}.$$

Substituting these variables into the model (2.1) and dropping all hats gives the following non-dimensionalised system of equations

$$\begin{aligned}
\frac{dT}{dt} &= d(1-T) - \beta VT + \rho R - \varphi_1 T(F_1 + F_2),\\
\frac{dI}{dt} &= \beta VT - \delta I - \left[\mu_1(1 + s_1F_1 + s_2F_2)N + \mu_2(1 + s_1'F_1 + s_2'F_2)E + \varphi_2 F_2\right] I,\\
\frac{dF_1}{dt} &= p_1 I - \delta_1 F_1,\\
\frac{dF_2}{dt} &= p_2 E + p_3 N - \delta_2 F_2,\\
\frac{dN}{dt} &= N(1-N) + (q_1F_1 + q_2F_2)N,\\
\frac{dE}{dt} &= r_e E(1-E) + \alpha IE,\\
\frac{dR}{dt} &= \varphi_1 T(F_1 + F_2) + \varphi_2 IF_2 - \rho R,\\
\frac{dV}{dt} &= \frac{p}{1 + s_3F_1 + s_4F_2} I - cV - kAV,\\
\frac{dA}{dt} &= d_a(1-A) - kAV + qV.
\end{aligned} \tag{2.2}$$

It is straightforward to show that this system is well-posed, i.e. its solutions with non-negative initial conditions remain non-negative for all $t \geq 0$.

2.3 Steady states and their stability

We begin our analysis of the system (2.2) by looking at its steady states

$$S^* = (T^*, I^*, F_1^*, F_2^*, N^*, E^*, R^*, V^*, A^*),$$

that can be found by equating the right-hand sides of equations in (2.2) to zero and solving the resulting system of algebraic equations. Due to the high dimensionality of the system (2.2), it can admit a significant number of possible steady states. Hence, in order to systematically find and analyse all of them, I begin with steady states characterised by the absence of virus particles, i.e. $V^* = 0$, which immediately implies $I^* = F_1^* = 0$ and $T^* = A^* = 1$, which represents the clearance of infection. There are four such steady states,

$$S_1^* = (1,0,0,0,0,0,0,0,0,1), \quad S_2^* = \left(1,0,0,\frac{p_2}{\delta_2},0,1,\frac{\varphi_1 p_2}{\rho\delta_2},0,1\right),$$

$$S_3^* = \left(1,0,0,\frac{p_3}{\delta_2 - p_3 q_2},\frac{\delta_2}{\delta_2 - p_3 q_2},0,\frac{\varphi_1 p_3}{\rho(\delta_2 - p_3 q_2)},0,1\right),$$

$$S_4^* = \left(1,0,0,\frac{p_2+p_3}{\delta_2 - p_3 q_2},\frac{\delta_2 - p_3 q_2 + p_2 q_2 + p_3 q_2}{\delta_2 - p_3 q_2},1,\frac{\varphi_1(p_2+p_3)}{\rho(\delta_2 - p_3 q_2)},0,1\right).$$

Whilst the steady states S_1^* and S_2^* are feasible for any values of parameters, S_3^* and S_4^* are only biologically feasible, provided $\delta_2 - p_3 q_2 > 0$. Linearisation of the system (2.2) near each of these steady states shows that S_1^*, S_2^* and S_3^* are always unstable, while S_4^* is stable if the following condition holds

$$K < K_c, \qquad K = \frac{p\beta(\delta_2 - p_3 q_2)^3}{(c+k)(p_2 s_4 - p_3 q_2 + p_3 s_4 + \delta_2)}, \tag{2.3}$$

with

$$\begin{aligned} K_c = {} & \delta p_3^2 q_2^2 + \mu_1 p_2^2 q_2 s_2 - \mu_1 p_2 p_3 q_2^2 + \mu_1 p_2 p_3 q_2 s_2 - \mu_2 p_2 p_3 q_2 s_2' + \mu_2 p_3^2 q_2^2 - \mu_2 p_3^2 q_2 s_2' \\ & - 2\delta\delta_2 p_3 q_2 + \delta_2\mu_1 p_2 q_2 + \delta_2\mu_1 p_2 s_2 - \delta_2\mu_1 p_3 q_2 + \delta_2\mu_1 p_3 s_2 + \delta_2\mu_2 p_2 s_2' - 2\delta_2\mu_2 p_3 q_2 \\ & + \delta_2\mu_2 p_3 s_2' - p_2 p_3 q_2 \varphi_2 - p_3^2 q_2 \varphi_2 + \delta\delta_2^2 + \delta_2^2\mu_1 + \delta_2^2\mu_2 + \delta_2 p_2 \varphi_2 + \delta_2 p_3 \varphi_2. \end{aligned} \tag{2.4}$$

When $K = K_c$, equilibrium S_4^* undergoes a steady-state bifurcation, and for $K > K_c$, this steady state is unstable.

For $V^* \neq 0$, one has to distinguish between two cases, $k = q$ and $k \neq q$. For $k = q$, one finds $A^* = 1$, and there are four associated steady states with different combinations of $E^* = 0$ or $E^* \neq 0$, and $N^* = 0$ or $N^* \neq 0$. The first of these, S_5^*, characterised by the absence of CTLs and NKs, i.e. $E^* = 0$ and $N^* = 0$, has other

components given by

$$T^* = \frac{(c+k)(dp_1s_3+\delta\delta_1)}{cdp_1s_3+dkp_1s_3+\beta p\delta_1}, \quad I^* = \frac{d\delta_1(p\beta-c\delta-k\delta)}{\delta(cdp_1s_3+dkp_1s_3+\beta p\delta_1)},$$

$$F_1^* = \frac{dp_1(p\beta-c\delta-k\delta)}{\delta(cdp_1s_3+dkp_1s_3+\beta p\delta_1)}, \quad F_2^* = 0,$$

$$R^* = \frac{dp_1\varphi_1(c+k)(dp_1s_3+\delta\delta_1)(p\beta-c\delta-k\delta)}{\delta\rho(cdp_1s_3+dkp_1s_3+\beta p\delta_1)^2}, \quad V^* = \frac{d\delta_1(p\beta-c\delta-k\delta)}{\beta(c+k)(dp_1s_3+\delta\delta_1)},$$

and this steady state is always unstable. The steady state S_6^* with $E^* = 0$ and $N^* \neq 0$ has components given by

$$I^* = \frac{\delta_1 F_1^*}{p_1}, \quad F_2^* = \frac{1+q_1F_1^*}{a}, \quad N^* = \frac{\delta_2 F_2^*}{p_3}, \quad V^* = \frac{pI^*}{(c+k)(1+s_3F_1^*+s_4F_2^*)},$$

$$T^* = \frac{d+\varphi_2 I^* F_2^*}{d+\beta V^*}, \quad R^* = \frac{\varphi_1 T^*(F_1^*+F_2^*)+\varphi_2 I^* F_2^*}{\rho},$$

where F_1^* satisfies the cubic equation

$$b_3(F_1^*)^3 + b_2(F_1^*)^2 + b_1F_1^* + b_0 = 0,$$

where the coefficients b_1, b_2 and b_3 are always positive, and

$$b_0 = dp_1\left[-a^3pp_3\beta + (c+k)(a+s_4)(a^2p_3\delta + a\delta_2\mu_1 + ap_3\varphi_2 + s_2\delta_2\mu_1)\right],$$

$$a = \frac{\delta_2 - p_3q_2}{p_3}.$$

The steady state S_6^* is also always unstable.

Similarly, the steady state S_7^* with $E^* \neq 0$ and $N^* = 0$ has its state variables given by

$$I^* = \frac{\delta_1 F_1^*}{p_1}, \quad F_2^* = \frac{p_2}{\delta_2}\left(1+\frac{\alpha\delta_1F_1^*}{r_ep_1}\right), \quad V^* = \frac{pI^*}{(c+k)(1+s_3F_1^*+s_4F_2^*)},$$

$$E^* = \frac{r_e+\alpha I^*}{r_e}, \quad T^* = \frac{d+\varphi_2 I^* F_2^*}{d+\beta V^*}, \quad R^* = \frac{\varphi_1 T^*(F_1^*+F_2^*)+\varphi_2 I^* F_2^*}{\rho},$$

with F_1^* satisfying the cubic equation

$$m_3(F_1^*)^3 + m_2(F_1^*)^2 + m_1F_1^* + m_0 = 0,$$

where m_1, m_2 and m_3 are positive, and

$$m_0 = dp_1^3 r_e^3 \left[-\beta p \delta_2^2 + (c+k)(p_2 s_4 + \delta_2)(\mu_2 p_2 s_2' + \delta\delta_2 + \mu_2\delta_2 + \varphi_2 p_2) \right].$$

This steady state is unstable for any parameter values.

The last steady state S_8^* with $E^* \neq 0$ and $N^* \neq 0$ has components

$$I^* = \frac{\delta_1 F_1^*}{p_1}, \quad E^* = \frac{r_e + \alpha I^*}{r_e}, \quad F_2^* = \frac{\alpha p_2 \delta_1 F_1^* + r_e p_1 \left[p_2 + p_3(1 + q_1 F_1^*) \right]}{r_e p_1 (\delta_2 - p_3 q_2)},$$

$$N^* = \frac{\delta_2 F_2^* - p_2 E^*}{p_3}, \quad V^* = \frac{pI^*}{(c+k)(1 + s_3 F_1^* + s_4 F_2^*)},$$

$$T^* = \frac{d + \varphi_2 I^* F_2^*}{d + \beta V^*}, \quad R^* = \frac{\varphi_1 T^* (F_1^* + F_2^*) + \varphi_2 I^* F_2^*}{\rho},$$

and F_1^* satisfies a cubic equation. It does not prove possible to determine stability of this steady state in a closed form, so is has to be done numerically.

For $k \neq q$, we again have four options, depending on whether $E^* = 0$ or $E^* \neq 0$, and $N^* = 0$ or $N^* \neq 0$. Similar to the case $k = q$, the steady states S_9^* with $E^* = N^* = 0$, S_{10}^* with $E^* = 0$ and $N^* \neq 0$ and S_{11}^* with $E^* \neq 0$ and $N^* = 0$, are always unstable. The steady state S_{12}^* with all components being positive cannot be found in a closed form.

The cases $k = q$ and $k \neq q$ have to be considered separately, since for $k \neq q$ one has a relation $V^* = d_a(1 - A^*)/(kA^* - q)$, which cannot be directly used in the case $k = q$ with $A^* = 1$. However, it is straightforward to show that as $k \to q$, the steady states S_9^*, S_{10}^*, S_{11}^* and S_{12}^* converge to S_5^*, S_6^*, S_7^* and S_8^*, respectively. Of these steady states, only S_4^* and S_{12}^* (or equivalently S_8^* for $k = q$) can potentially change stability, as all other steady states are unstable for any parameter values.

To gain a better understanding of how stability of different steady states is affected by various parameters in the model, I perform numerical stability and bifurcation analysis. Baseline values of parameters are given in Table 2.1, though one should note that at this stage it is only feasible to explore different qualitative scenarios, as the actual values of many of these parameters have not yet been measured, or significant variations in their values have been reported.

Figure 2.2 shows regions of feasibility and stability of the disease-free steady state

S_4^*. Our earlier analysis indicates that this steady state is only feasible, provided $\delta_2 - p_3 q_2 > 0$, which means that this steady state can only exist if the rate p_3 of production of IFN-γ by NK cells, and the rate q_2 at which IFN-γ in turn upregulates the production of new NK cells, are not too large, as illustrated in Fig. 2.2(a) and (b).

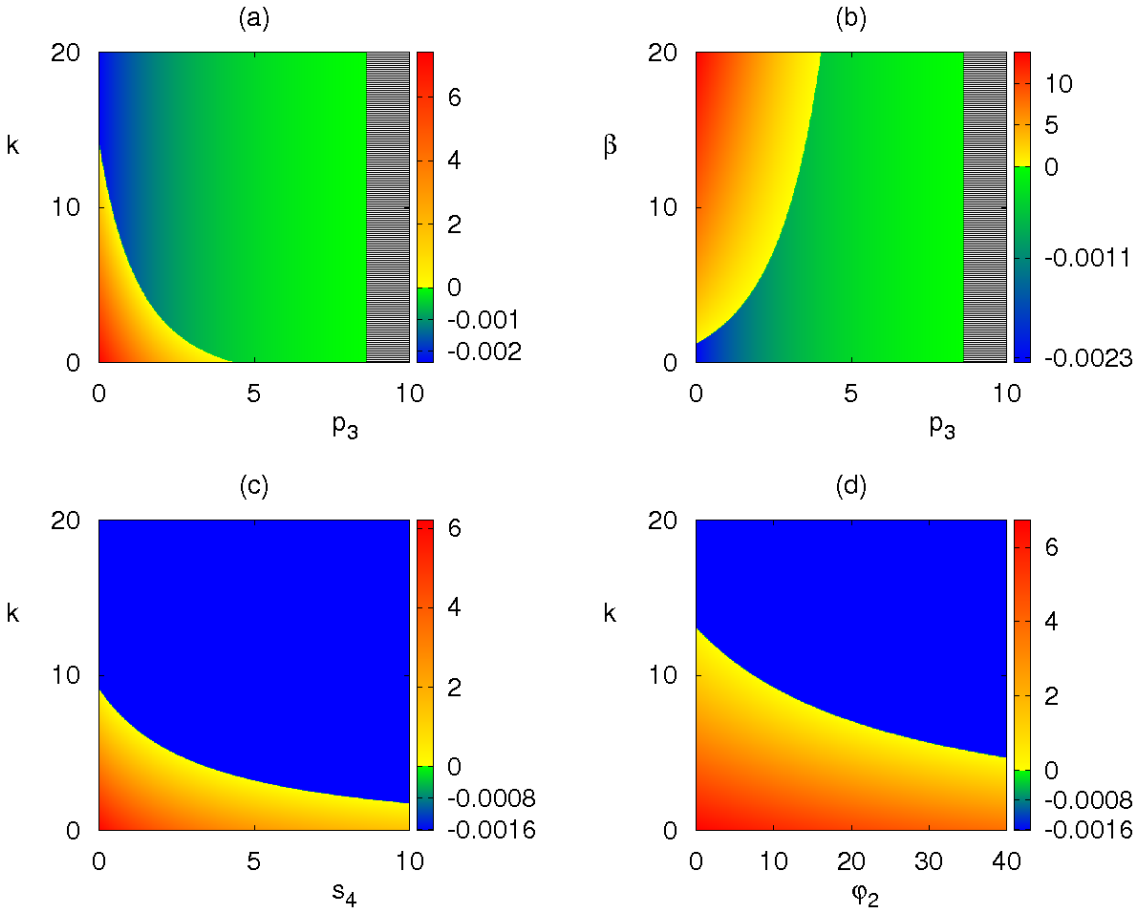

Figure 2.2: Stability of the disease-free steady state S_4^* with parameter values from Table 2.1. Black hatched area indicates the region where there are no feasible steady states. Colour code denotes maximum real part of the largest characteristic eigenvalue for the disease-free steady state S_4^* when it is feasible.

Stability of the disease-free steady state S_4^* is determined by the value of K defined in (2.3), and Figs. 2.2(a) and (b) suggest that increasing p_3 can stabilise this equilibrium if it were previously unstable, which should be expected, as increasing the number of NK cells and the amount of IFN-γ leads to a more effective eradication of the viral population. Similarly, increasing the rate of clearance of virions by antibodies k, the rate at which IFN-γ inhibits production of new virus particles s_4, or the rate of IFN-γ-induced conversion from infected cells to refractory cells φ_2, all lead to

the stabilisation of the disease-free steady state. At the same time, comparison of Fig. 2.2(a) with (c) and (d) indicates that if antibodies are not very effective, i.e. if k is small, it is easier to clear the infection, i.e. achieve stability of the disease-free steady state, by increasing production of IFN-γ by NK cells, since both s_4 and φ_2 have to be increased very significantly before the stability can be achieved.

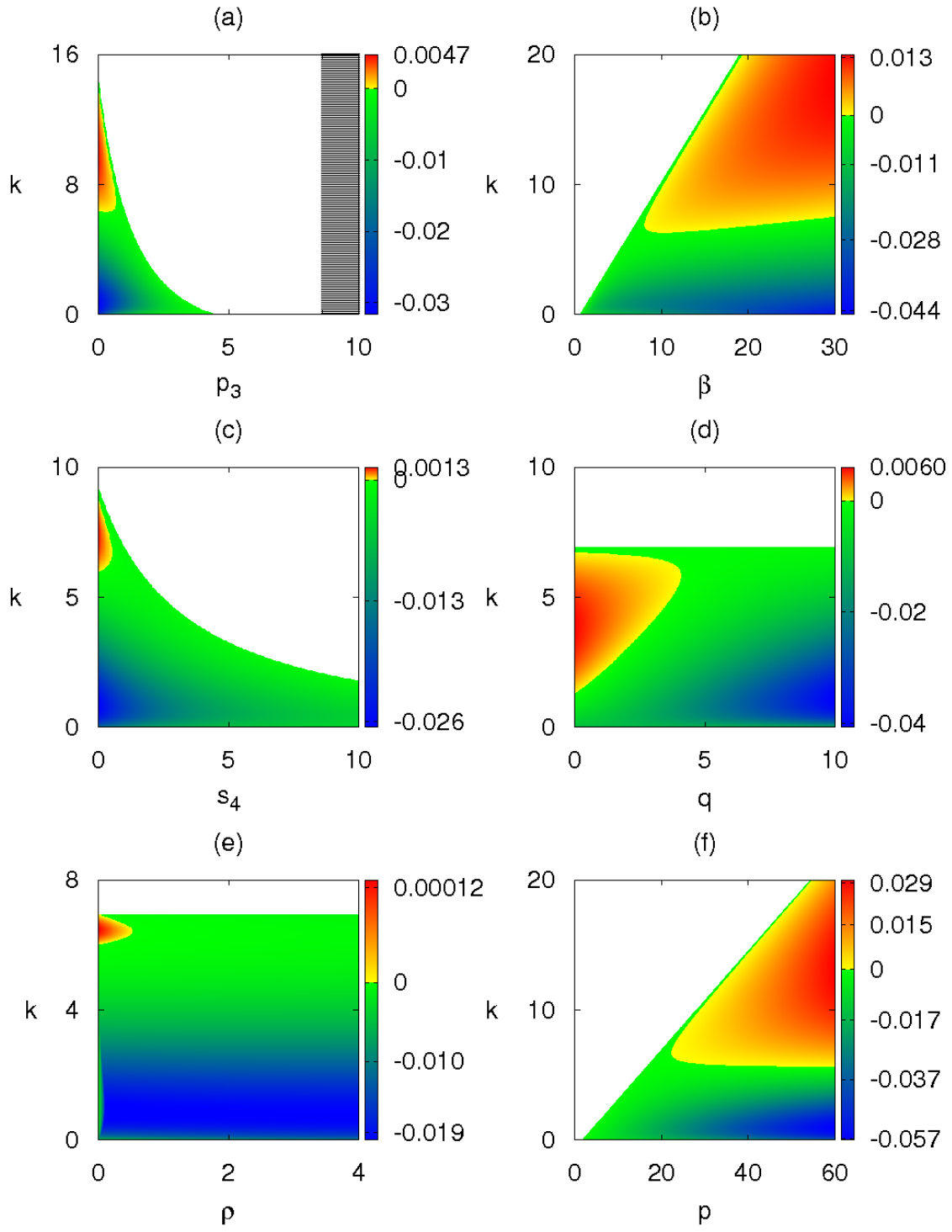

Figure 2.3: Stability of the endemic steady state S_{12}^* with parameter values from Table 2.1. White area shows the region where the endemic steady state is not feasible, but the disease-free steady state S_4^* is feasible and stable. Black hatched area indicates the region where there are no feasible steady states. Colour code denotes maximum real part of the largest characteristic eigenvalue for the endemic steady state S_{12}^* when it is feasible.

Figure 2.3 illustrates how regions of feasibility and stability of the endemic steady state S_{12}^* depend on system parameters. Comparison of Fig. 2.3(a) with Fig. 2.2(a)

suggests that as the disease-free steady state loses its stability, the endemic steady state becomes biologically feasible and stable. However, for very small values of p_3, there is a certain range of k values, for which the endemic steady state is also unstable, and one could expect the appearance of periodic solutions. This is illustrated in more detail in the bifurcation diagram shown in Fig. 2.4(a), which indicates that when one fixes some small value of p_3 and increases k, the endemic steady state does indeed lose its stability via a supercritical Hopf bifurcation, and then regains it at a (reverse) supercritical Hopf bifurcation for yet higher value of k.

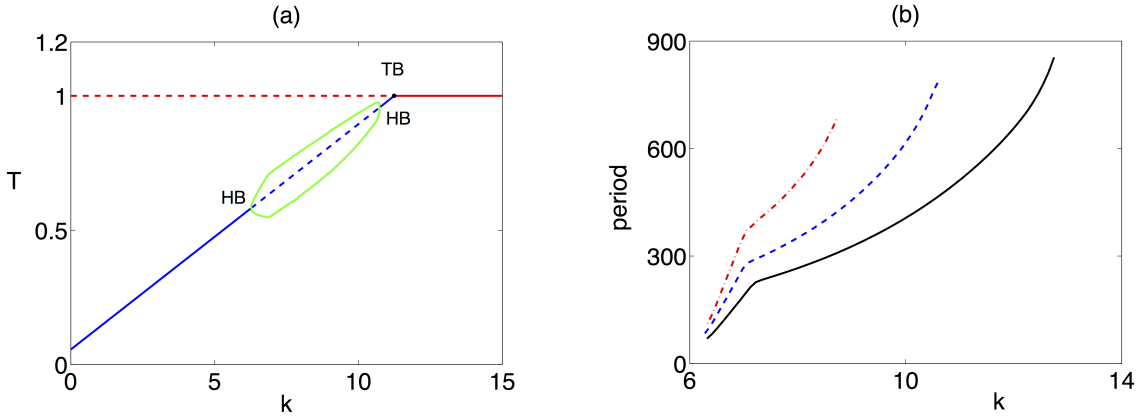

Figure 2.4: Bifurcation diagram (a) and periods of periodic solutions (b) with parameter values from Table 2.1. (a) In this figure $p_3 = 0.3$. The blue line shows the endemic steady state, and the red line shows the disease-free steady state, with solid (dashed) lines corresponding to stable (unstable) steady states. At $k = 6.277$ and $k = 10.74$ there is a Hopf bifurcation of the endemic steady steady state, and at $k = 11.2389$ there is a transcritical bifurcation. Between the two HB points there is a stable periodic solution, the minimum and maximum of T are shown in green. (b) This figure shows the dependence of the period of periodic solutions on k for $p_3 = 0.1$ (black), $p_3 = 0.3$ (blue), $p_3 = 0.5$ (red). This figure was computed using MATLAB.

In the range of k values where the endemic steady state S_{12}^* is unstable, one observes a stable periodic orbit, whose period increases with k but reduces with p_3, as shown in Fig. 2.4(b). The effects of varying s_4 and φ_2 on stability of S_{12}^* are similar to those of varying p_3, with the exception that for small k, increasing s_4 or φ_2 does not make this steady state infeasible, i.e. biologically irrelevant. Figures 2.3(b) and (f) are quite similar to each other in that for each value of k, there is some minimal value of the infection rate β or production rate of new virions p, above which the endemic steady state S_{12}^* becomes biologically feasible and stable. If k is small, then further increases of β or p do not have effect on stability, and S_{12}^* remains stable, whilst for higher k increasing either β or p results in the loss of stability through a supercritical

Hopf bifurcation. A very interesting behaviour is observed in Fig. 2.3(d), which shows that for k small or very large, the stability of S_{12}^* is unaffected by changes in the rate of production of new antibodies q, whereas for an intermediate range of k, S_{12}^* is unstable for small q but gains stability as q is increased. This is quite counter-intuitive, as one would normally expect that if more antibodies are produced for the same viral load, this would help clear the infection. Since k is also the rate at which antibodies are binding free virus and, hence, are removed, this means that it is the balance between k and q that determines whether the infection is maintained at a steady level, i.e. S_{12}^* is stable, or if periodic oscillations appear in the dynamics. Similar behaviour can be observed in Fig. 2.3(e), which shows that the endemic steady state S_{12}^* is unstable for small ρ, i.e. for long periods of viral resistance, but it stabilises as the duration of viral resistance reduces, i.e. for higher values of ρ.

In order to better understand the role of cytokines in system's dynamics, I present in Fig. 2.5 stability of the endemic steady state depending on cytokine-related parameters. Figures 2.5(a) and (b) suggest that increasing the rates s_1 and s_2 at which IFN-α/β and IFN-γ enhance cytolytic activity of NK cells, or the rates s_3 and s_4 at which these interferons inhibit production of new virions, results in stabilisation of the endemic steady state S_{12}^*. One should note, however, that while increasing the rates s_1 or s_3, associated with IFN-α/β only acts to make the endemic steady state more stable, increasing the rates s_2 or s_4 associated with IFN-γ can actually make the endemic steady state biologically irrelevant, thus helping clear the infection by moving the system to a stable disease-free steady state. This suggests the profoundly different effects of IFN-α/β and IFN-γ on viral dynamics. A similar phenomenon is observed when one investigates the role of cytokines in producing refractory cells from either uninfected or infected cells. Increasing the rate φ_1 of conversion of uninfected cells into refractory cells, which involves contributions from both types of interferon, results in destabilisation of the endemic steady state. On the other hand, increasing the rate φ_2 of non-cytolytic cure of infected cells by IFN-γ initially stabilises the endemic steady state, but subsequent increase makes the endemic steady state infeasible, thus leading to clearance of infection, as shown in Fig. 2.5(c).

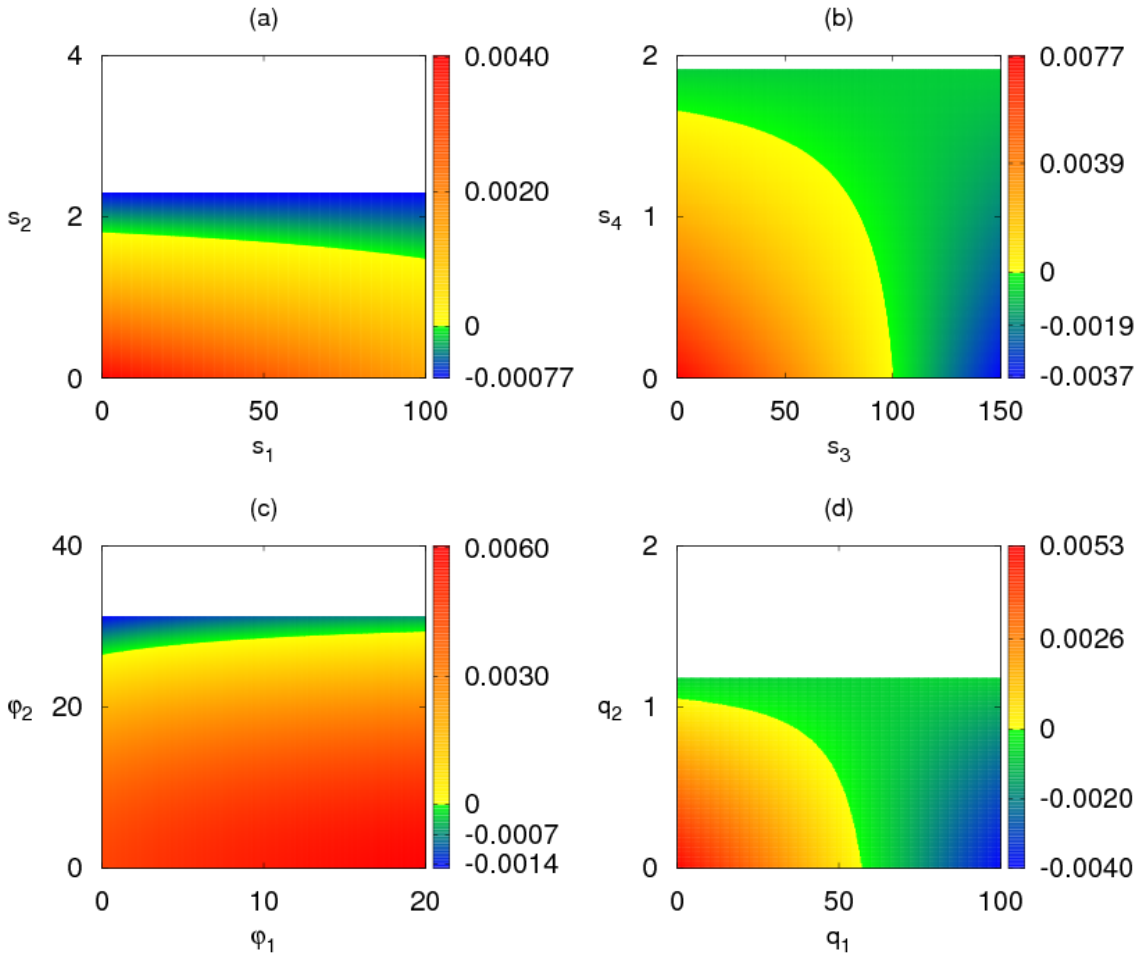

Figure 2.5: Stability of the endemic steady state S^*_{12} with parameter values from Table 2.1. White area shows the region where the endemic steady state is not feasible, but the disease-free steady state S^*_4 is feasible and stable. Colour code denotes maximum real part of the largest characteristic eigenvalue for the endemic steady state S^*_{12} when it is feasible.

We have also looked into the effects of both types of interferon on enhancing cytotoxic activity of CTLs, as represented by parameters s'_1 and s'_2. In this case, numerical calculations suggest that the stability of the endemic steady state is not sensitive to s'_1, implying that this particular contribution from IFN-α/β does not help clear the infection. In this respect, IFN-γ plays a more important role, since increasing s'_2 above a certain level makes the endemic steady state biologically irrelevant, so the system reverts to a stable disease-free state. Finally, Figure 2.5(d) shows that increasing the rates q_1 and q_2 of cytokine-related activation of NK cells leads to stabilisation of the endemic steady state, however, increasing the rate q_2 associated with IFN-γ beyond certain level results in this steady state becoming biologically irrelevant, thus eradicating the viral infection.

Table 2.1: Table of baseline parameter values

Parameter	Value	Definition
d	0.003	Natural death rate of uninfected cells
β	7	Infection rate
ρ	5	Rate of missing refractory state
φ_1	14	Rate of IFN-induced conversion from uninfected cells to refractory cells
δ	0.56	Natural death rate of infected cells
μ_1	5	Death rate of infected cells by NK cells
s_1	1.5	Effect of IFN-α/β on NK cells to kill infected cells
s_2	0.6	Effect of IFN-γ on NK cells to kill infected cells
μ_2	0.14	Death rate of infected cells by HBV-specific CTLs
s_1'	1.9	Effect of IFN-α/β on the HBV-specific CTLs
s_2'	2	Effect of IFN-γ on the HBV-specific CTLs
φ_2	21	Rate of IFN-γ-induced conversion from infected cells to refractory cells
p_1	1	Production rate of IFN-α/β by infected cells
δ_1	4.9	Natural death rate of IFN-α/β
p_2	0.5	Production rate of IFN-γ by HBV-specific CTLs
p_3	0.9	Production rate of IFN-γ by NK cells
δ_2	5.16	Natural death rate of IFN-γ
q_1	0.8	Production rate of NK cells by IFN-α/β
q_2	0.6	Production rate of NK cells by IFN-γ
r_e	0.5	Maximal growth rate of HBV specific cytotoxic T cells
α	1	Antigen-dependent proliferation rate of HBV-specific CTLs
p	20	Production rate of free virus
s_3	1.7	Effect of IFN-α/β on the production of free viruses
s_4	1	Effect of IFN-γ on the production of free viruses
c	0.67	Natural clearance rate of free viruses
k	2	Clearance rate of free viruses by antibodies
d_a	0.332	Natural death rate of free antibodies
q	5	Production rate of free antibody by free viruses

2.4 Numerical simulations

To demonstrate different types of dynamical behaviour that can be exhibited by the model (2.2) in various parameter regimes, I solve this system numerically using MATLAB ode45 routine implementing Runge-Kutta method of the fourth order, with the absolute and relative tolerances set to 1e-13, the baseline values of parameters given in Table 2.1, and the initial condition

$$\begin{aligned}(T(0), I(0), F_1(0), F_2(0), N(0), &E(0), R(0), V(0), A(0)) \\ &= (0.9, 0, 0, 0, 0.1, 0.2, 0, 0.33, 0.1). \qquad (2.5)\end{aligned}$$

Note that since there are significant differences in the reported values of many of the model parameters, and some of them have not even been measured yet, I fix the values of these parameters randomly to be able to do some qualitative analysis of the model and show different possible dynamics of the model mathematically. The results are shown in Figs. 2.6, 2.7, 2.8. In all these figures, the free virus $V(t)$ exhibits the behaviour that is qualitatively similar to that of the number of infected cells, hence, I plot instead the dynamics of the population of refractory cells $R(t)$.

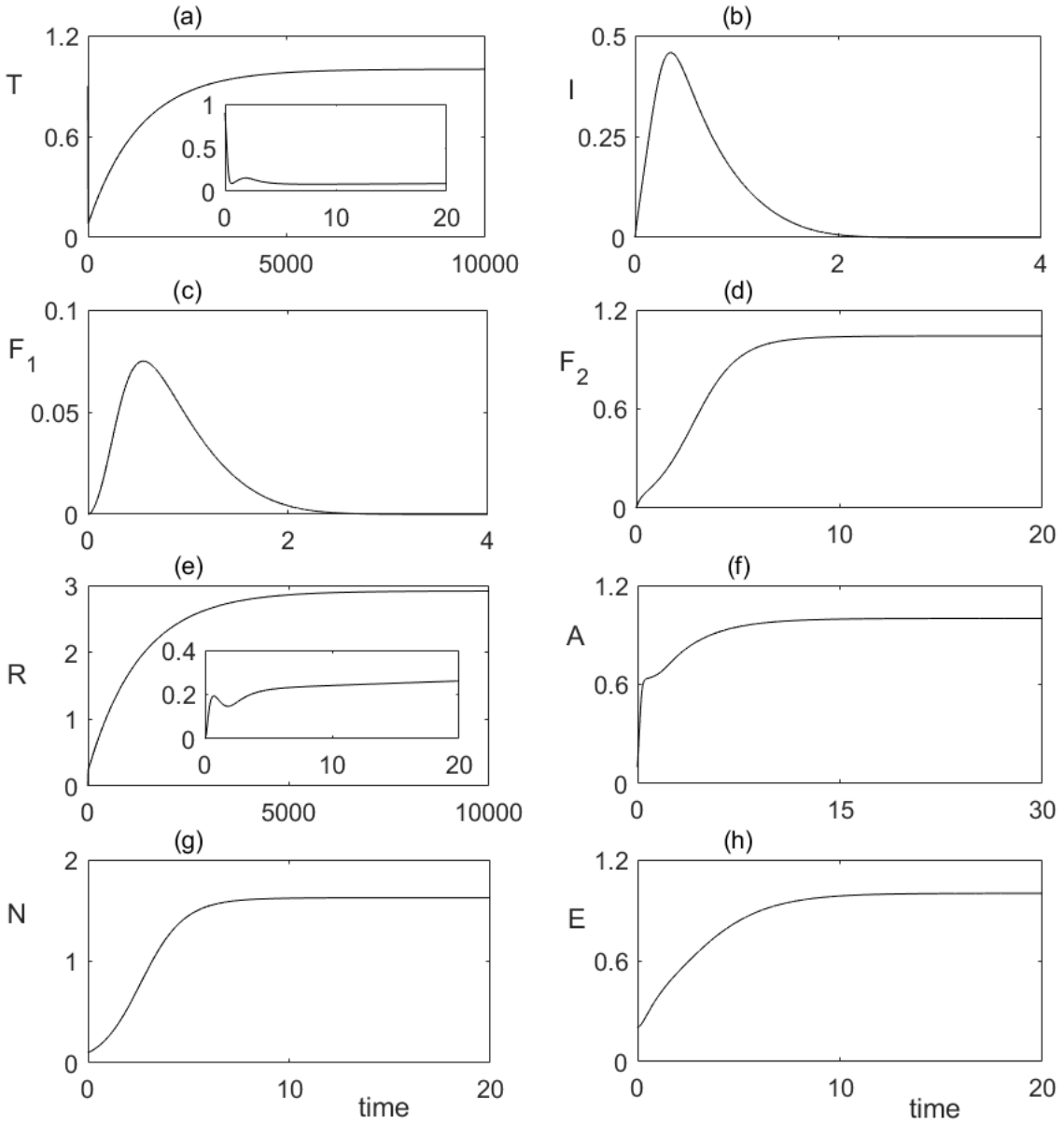

Figure 2.6: Numerical solution of the model (2.2) with parameter values from Table 2.1, and $p_3 = 3$, $k = 8$. In this case, the disease-free steady state S_4^* is stable, so immune system is able to clear the initial infection.

Figure 2.6 illustrates the dynamics of immune response when the condition (2.3) holds. In this case, the initial viral growth leads to an increase in the numbers of NKs and CTLs, as well as both types of interferons, which results in the successful clearance of the HBV infection, upon which type-1 interferons are also destroyed, and the system settles on a stable disease-free steady state S_4^*.

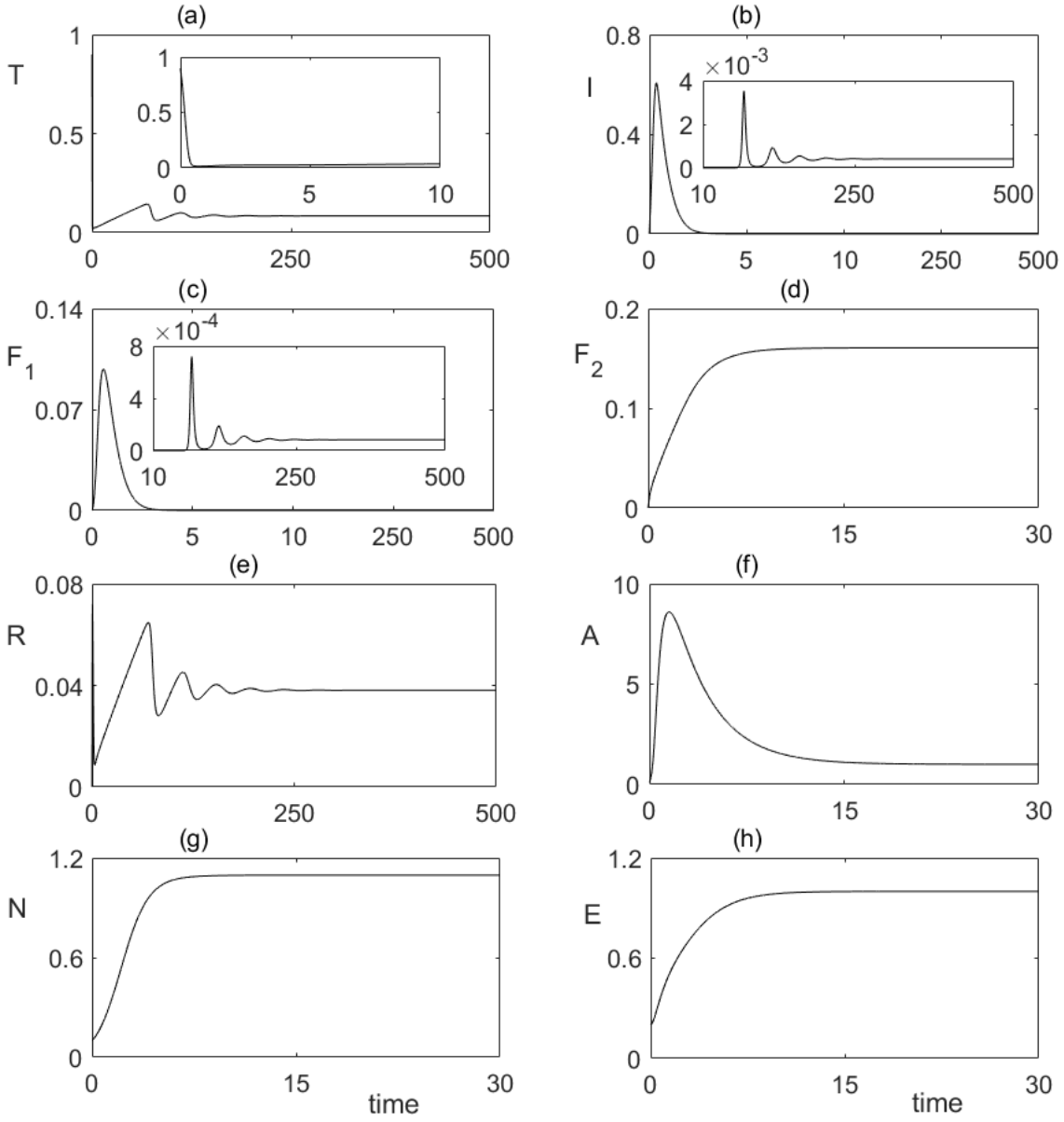

Figure 2.7: Numerical solution of the model (2.2) with parameter values from Table 2.1, and $p_3 = 0.3$, $k = 0.3$. In this case, the system approaches a stable endemic steady state S_{12}^*.

Figure 2.7 shows the dynamics in the case where the endemic steady state S_{12}^* is feasible and stable. One observes that the initial viral growth is suppressed by the

combined effects of different branches of the immune system. However, the approach to the endemic steady state is oscillatory with the amplitude of oscillations decaying, with each subsequent viral peak being smaller than the previous one.

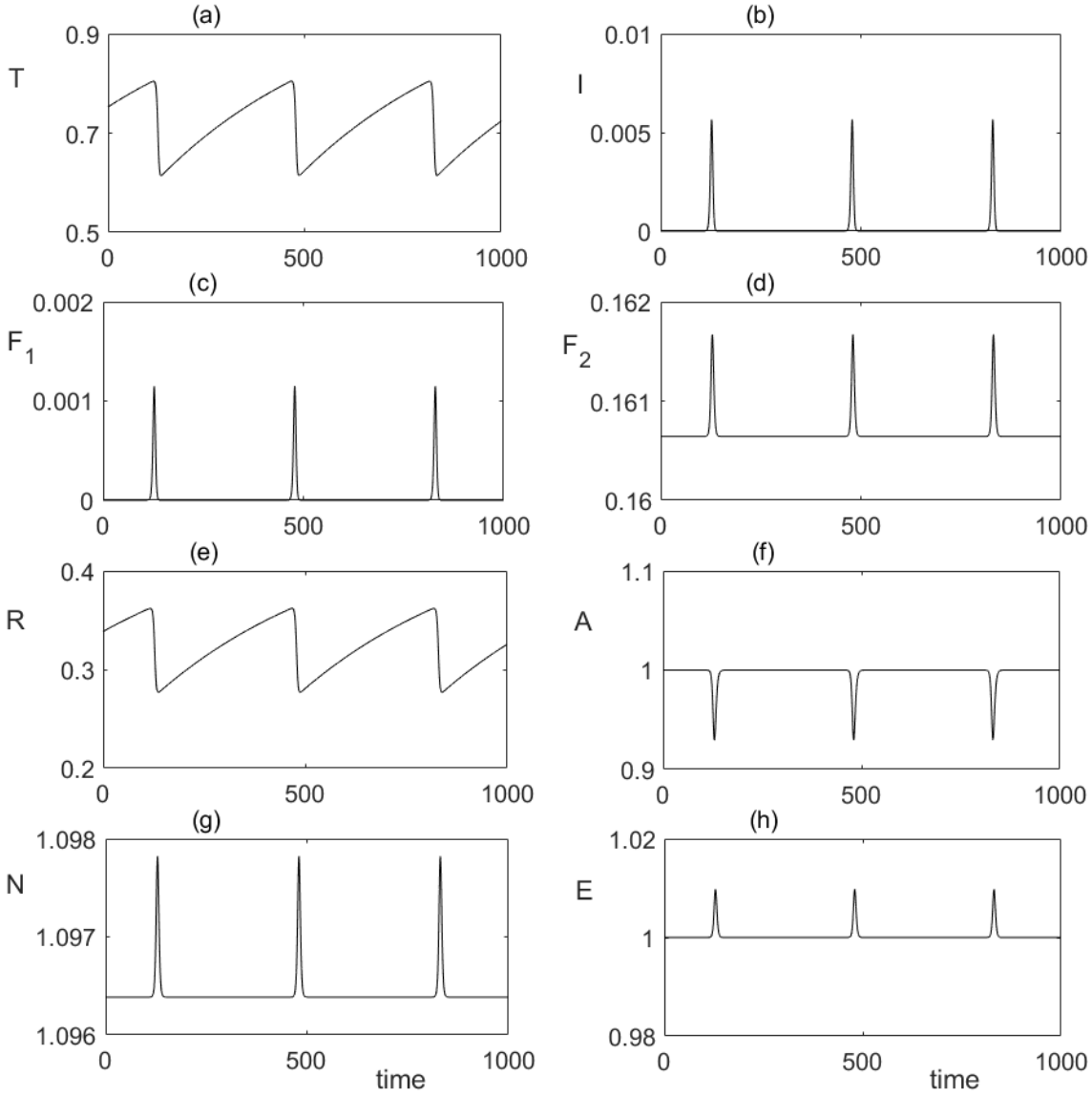

Figure 2.8: Numerical solution of the model (2.2) with parameter values from Table 2.1, and $p_3 = 0.3$, $k = 8$. In this case, both the disease-free S_4^* and the endemic steady state S_{12}^* are unstable, and the system exhibits a periodic solution.

In the case when the endemic state is unstable due to Hopf bifurcation, one observes stable oscillations, as shown in Fig. 2.8. Biologically, these would correspond to the so-called "flare-ups" [160, 161], where the infection is never completely cleared, but through the interactions between the virus and the immune system, there are periods of very low viral activity followed by the periods of acute viral growth. This

situation is reminiscent of the infection-induced autoimmune reaction, where initial viral infection can lead to a breakdown of immune tolerance, so that even in the absence of any exogenous factors or subsequent infections, patients exhibit periods of remission and relapses [76, 77]. It is worth noting that the behaviour shown in Fig. 2.8 has the hallmarks of slow-fast dynamics, or relaxation oscillations, that are not uncommon in models of immune response [162, 163]. At every "flare-up", there is a significant growth in the number of infected cells that triggers the proliferation of both types of interferon, as well as the growth in the populations of CTLs and natural killer cells. All of them are growing very quickly, resulting in a fast immune response that reduces the infection, but as the number of infected cells subsides, so do all the various populations associated with the immune response. Hence, the infection is not completely cleared but rather is kept in check at a very small level. Now, as the population of susceptible cells recovers, which is happening on a much longer time-scale, more of these cells become the target of free virus, resulting in a new episode of high viral load, and the cycle repeats.

As a next step, I look into effects of antiviral treatments on HBV. There are two main types of drugs used to treat HBV infection: nucleot(s)ide analogues (NAs), such as lamivudine, adefovir, entecavir, tenofovir, telbivudine, famciclovir, telbivudine, clevudine, and IFN-based therapy, which includes stand-alone IFN-α (roferon, intron) or pegylated interferon peg-IFN-α2a/2b [42, 41, 164, 44, 131]. These treatments individually [165, 146] and in combinations [166, 43] result in either reduction of the production of new virus particles, or in blocking *de novo* infections. Mathematically, one can represent these two effects by a modified viral production rate $(1-\epsilon)p$ and a modified transmission rate $(1-\eta)\beta$, where $0 \leq \epsilon \leq 1$ and $0 \leq \eta \leq 1$ are drug efficacies associated with inhibiting viral production and preventing new infections, respectively. In order to characterise the overall effectiveness of treatment, it can be helpful to consider a cumulative parameter describing the total drug effectiveness ϵ_{tot}, which is defined as $1-\epsilon_{tot} = (1-\eta)(1-\epsilon)$ [42]. This would allow one to determine a critical drug efficacy, ϵ_c, corresponding to stability boundary of the disease-free steady state S_4^*, so that this steady state would be stable for $\epsilon_{tot} > \epsilon_c$. With these modifications, new equations for the numbers of healthy and

infected cells, as well as the free virus, have the non-dimensional form

$$\frac{dT}{dt} = d(1-T) - \beta(1-\eta)VT + \rho R - \varphi_1 T(F_1+F_2),$$

$$\frac{dI}{dt} = \beta(1-\eta)VT - \delta I - \mu_1(1+s_1F_1+s_2F_2)IN - \mu_2(1+s_1'F_1+s_2'F_2)IE - \varphi_2 IF_2,$$

$$\frac{dV}{dt} = \frac{p(1-\epsilon)}{1+s_3F_1+s_4F_2}I - cV - kAV, \tag{2.6}$$

with the rest of the equations remaining the same as in the main model (2.2).

Figure 2.9 (a) shows that for parameter values from Table 2.1, if $\eta > 0.7646$, then pure NAs therapy is sufficient to destabilise the endemic steady state and thus clear the infection, and similarly, if $\epsilon > 0.7646$, then just IFN-therapy can make the disease-free steady state S_4^* stable. This Figure also suggests that disease clearance can be achieved if the combined efficacy ϵ_{tot} exceeds some critical value ϵ_c.

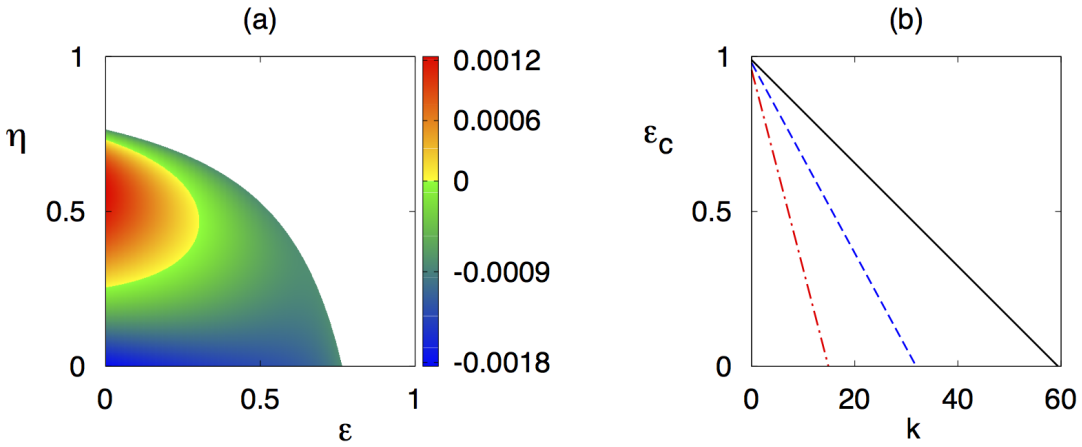

Figure 2.9: Effects of NAs and interferon therapy on the dynamics of HBV with parameter values from Table 2.1, and $k = 7$, $\beta = 30$.(a) Stability plot for the endemic steady state S_{12}^*, with the colour code denoting maximum real part of the largest characteristic eigenvalue for the endemic steady state when it is feasible. White area shows the region where the endemic steady state S_{12}^* is not feasible, and the disease-free steady state S_4^* is stable. (b) Dependence of the critical drug efficacy (ϵ_c) on k, with disease being cleared for $\epsilon_{tot} > \epsilon_c$, with $p_3 = 0.1$ (black line), $p_3 = 0.9$ (blue line), $p_3 = 2$ (red line).

Figure 2.9 (b) illustrates how this critical combined efficacy ϵ_c varies with the rate k of clearance of free virus by antibodies and the rate p_3 of production of type-2 interferons by NK cells. One observes that the critical combined efficacy ϵ_c decreases with k, implying that the faster the free virus is cleared by antibodies, the less

stringent is the requirement on the efficacy of treatment to clear the infection, and for sufficiently high k the disease clearance can be achieved even in the absence of treatment. Surprisingly, for the same value of k, having a higher rate of production of type-2 interferons by NK cells requires a higher combined efficacy ϵ_c for viral clearance.

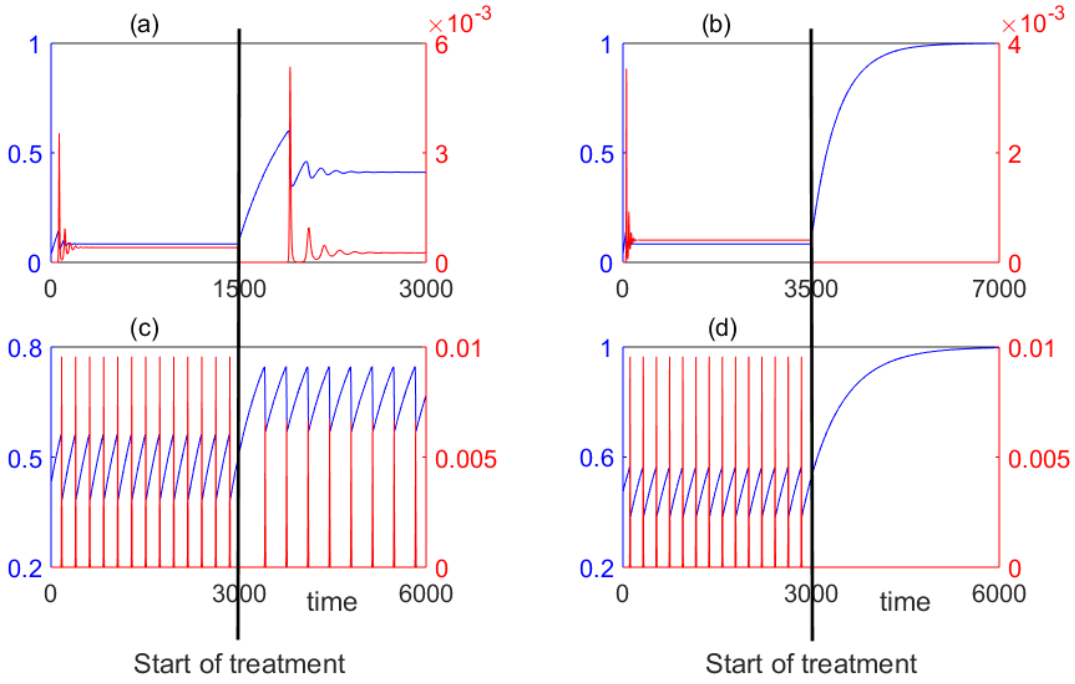

Figure 2.10: Numerical solution of the model (2.2) with treatment (2.6) parameter values from Table 2.1 and the initial condition (2.5) and ($k = 0.3$, $p = 0.3$) in (a-b), and ($k = 8$, $p = 0.3$) in (c-d). In all plots, blue colour denotes a rescaled number of uninfected cells $T(t)$, and red colour denotes a rescaled number of infected cells $I(t)$. (a)-(b) Treatment of the chronic infection with $\epsilon_{tot} < \epsilon_c$ ($\eta = 0.6$, $\epsilon = 0.5$) (a), and $\epsilon_{tot} > \epsilon_c$ ($\eta = 0.9$, $\epsilon = 0.6$) (b). (c)-(d) Treatment of the relapsing infection with $\epsilon_{tot} < \epsilon_c$ ($\eta = 0.2$, $\epsilon = 0.1$) (c), and $\epsilon_{tot} > \epsilon_c$ ($\eta = 0.2$, $\epsilon = 0.4$) (d).

Figure 2.10 illustrates the effect of using combined NAs and interferon therapy on chronic and relapsing HBV infections. In both regimes, application of treatment with sub-optimal efficacy, i.e. with $\epsilon_{tot} < \epsilon_c$, does not cause qualitative change in the system dynamics but results in an increased number of uninfected cells and a decreased number of infected cells. On the contrary, for $\epsilon_{tot} > \epsilon_c$, in both cases the number of infected cells is reduced to zero, and the system approaches a stable disease-free steady state S_4^*, which corresponds to a successful clearance of infection.

2.5 Discussion

In this chapter I have derived and analysed a new model for HBV infection with particular emphasis on interactions between different branches of immune system, including innate immune response as exemplified by NK cells, adaptive immune response represented by HBV-specific cytotoxic T cells and antibodies, and various cytokines. During infection the cytokines play an important role in recruitment of innate and adaptive immune factors, and they also help them to be more effective, as well as facilitate non-cytolytic cure of infected cells.

Stability analysis of the steady states has shown how various parameters affect the dynamics of immune response, with some of the results being intuitively clear, and others being quite unexpected. Naturally, increasing the number of NK cells, the rate of clearance of free virus by antibodies, the rate of inhibition of viral production by IFN-γ, or the rate of conversion from infected to refractory cells, all facilitate a more efficient clearance of infection, making the disease-free steady state stable. Once the disease-free steady state loses its stability, the endemic equilibrium becomes biologically feasible and stable. For sufficiently small values of the rate of production of IFN-γ by NK cells, the endemic steady state can lose its stability via Hopf bifurcation, giving rise to stable periodic solutions. We have found that for a very small or a very large rate of free virus clearance by antibodies, the stability of the endemic steady state is unaffected by how quickly the new antibodies are produced, whereas for an intermediate range of virus clearance rate, this steady state is unstable for low production of antibodies, and gains stability as the rate of antibody production is increased. This is a very surprising result, as normally one would expect that a higher rate of production of antibodies for the same viral load leads to a clearance of infection, rather than stabilisation of a chronic state. The implication of this observation is that it is not the individual rates of production of antibodies and viral clearance, but rather the balance between them that determines whether the system maintains a chronic infection or exhibits periodic oscillations.

In terms of the role of cytokines on mediating various branches of immune response, a surprising result of the analysis is that increasing the rates at which IFN-α/β and IFN-γ increase cytolytic activity of NK cells or inhibit production of free virus, actually leads to stabilisation of the endemic steady state. The major differ-

ence in the effects of cytokines IFN-α/β and IFN-γ lies in the observation that whilst increasing the rates associated with IFN-α/β just results in the stabilisation of an otherwise unstable endemic steady state, increasing the same rates for IFN-γ can result in making the endemic steady state biologically irrelevant, thus qualitatively changing the dynamics. The same result holds for IFN-γ-facilitated non-cytolytic cure of infected cells. If the production of IFN-γ by NK cells is too high, this makes all steady states of the system unstable, leading to persistent oscillations, thus maintaining the infection.

We have also looked into modelling the dynamics of HBV treatment with nucleot(s)ide analogues and/or stand-alone or pegylated interferons. Since these treatments are known to act by reducing the appearance of new infections and blocking production of free virus, I have looked at how the combined drug efficacy depends on these two properties. Numerical studies have shown the existence of a minimum drug efficacy required to clear the infection, and, unexpectedly, this critical drug efficacy is actually increasing with the rate of production of IFN-γ by NK cells.

There are several directions in which the model presented in this chapter can be extended. One important aspect of the immune dynamics is the non-instantaneous nature of several important processes, such as the lag between infection and recruitment of CTLs, production of new virus particles once a cell becomes infected, the time required for viral cell entry etc [99, 167]. Mathematically, this can be represented by including discrete or distributed time delay for each of the associated processes, which would make the model more realistic but would also make the analysis much more involved. Furthermore, it is known that antibodies do not kill the virus particles directly, but rather stick to them, creating a virus-antibody complex [35]. These complexes are not stable forever and can experience some dissociation, hence, explicitly including them into the model can provide better insights into the dynamics. The immune response is not perfect, and the breakdown of self-tolerance results in autoimmune disease [6, 7]. In Chapter 3 I propose a mathematical model of immune response to a viral infection and subsequent autoimmunity to study the dynamics of autoimmune diseases.

Chapter 3

Bifurcations and multi-stability in a model of cytokine-mediated autoimmunity

This chapter is based on the publication F. Fatehi, Y.N. Kyrychko, R. Molchanov, K.B. Blyuss, Bifurcations and multistability in a model of cytokine-mediated autoimmunity, *Int. J. Bif. Chaos*, **29(3)**, 1950034, 2019.

This chapter investigates the dynamics of immune response and autoimmunity with particular emphasis on the role of regulatory T cells (Tregs), T cells with different activation thresholds, and cytokines in mediating T cell activity. Analysis of the steady states yields parameter regions corresponding to regimes of normal clearance of viral infection, chronic infection, or autoimmune behaviour, and the boundaries of stability and bifurcations of relevant steady states are found in terms of system parameters. Numerical simulations are performed to illustrate different dynamical scenarios, and to identify basins of attraction of different steady states and periodic solutions, highlighting the important role played by the initial conditions in determining the outcome of immune interactions.

3.1 Background

Autoimmune disease is a pathological condition characterised by the failure of the immune system to efficiently discriminate between self-antigens and foreign antigens,

resulting in unwanted destruction of healthy organ cells. In the case of normal functioning, recognition of foreign epitopes presented on antigen presenting cells (APCs) to T lymphocytes results in proliferation and effector function from T cells, while cross-reactivity between epitopes leads to the possibility of T cell response against self-antigens [6, 7]. During an infection T cells with high level of self-reactivity are removed from the system by Tregs [5].

A particularly important role in the immune dynamics, and more specifically, in the performance of T cells, is played by cytokines. Activated T cells produce growth cytokines (primarily, interleukin-2, IL-2), and expression of IL-2 receptor by these T cells triggers cytokine-driven proliferation [168, 169]. Importantly, whereas IL-2 appears to be essential for proliferation of regulatory T cells [170], these T cells do not actually produce IL-2 even upon activation [171, 170].

In the next section, I use the model that has been presented by Blyuss and Nicholson [76] and show how by adding the effects of Tregs and IL-2 to that model we can develope a new model which can provide a more realistic representation of autoimmune dynamics.

3.2 Model derivation

This model consists of eight cell populations as follows,
$A(t)$ is the number of susceptible cells at time t,
$F(t)$ is the number of infected cells at time t,
$T_{in}(t)$ is the number of naïve T cells at time t,
$T_{reg}(t)$ is the number of regulatory T cells at time t,
$T_{nor}(t)$ is the number of activated T cells which acts against foreign antigen at time t,
$T_{aut}(t)$ is the number of autoreactive T cells which acts against self antigen at time t,
$I(t)$ is the amount of interleukin 2 (IL-2) at time t,
$V(t)$ is the viral load at time t.

To analyse the dynamics of immune response to infection and possible onset of autoimmunity, I use an approach similar to some of the earlier models of immune

response [76, 77, 172, 21]. The underlying idea is the mechanism of molecular mimicry, where immune response against an infection can lead to a breakdown of immune tolerance due to cross-reaction with one or more self-antigens that share some of their immunological characteristics with a pathogen [20, 19]. Experimental evidence suggests that while antibodies are important in a wider picture of immune response to viral infections, within the context of autoimmunity, B cells can be dispensable, so that autoimmune disease can develop even in their absence [173]. Moreover, it has been shown in some studies that the development of antibodies can itself depend on prior interactions of T cells with a pathogen [174]. Hence, in this chapter I rather focus on the role of T cells and associated cytokines.

We consider a situation where both infection and autoimmune response are targeting the same organ of the body, and the population of healthy cell in this organ is denoted by $A(t)$. These cells are assumed to follow logistic growth with the proliferation rate r (day^{-1}) and the carrying capacity N in the absence of infection or autoimmune response, as is common in models of viral dynamics [52, 175]. At the same time, one should be mindful of the fact that different functional forms of the growth of healthy cells can also have an effect on autoimmune dynamics, as has been shown by Iwami et al. [52, 53].

During a viral infection, some number of healthy cells become infected by free virus particles, at which point they move to the compartment of infected cells, denoted by $F(t)$. After a certain period of time, these infected cells will be producing virions, or free virus particles, $V(t)$ at a rate k (day^{-1}), and the rate of natural clearance of virions is denoted by c (day^{-1}). These virions then go on to infect other as yet uninfected cells at a rate β (cell^{-1} day^{-1}), which is an effective rate incorporating time constants associated with various biological processes, such as the movement of virions, cell entry, and an eclipse phase, during which the cells are infected but are not yet recognised as such by the immune system [28, 95, 32].

In terms of immune dynamics, T cell response originates in the lymph nodes. Stimulation of naïve T cells results in their proliferation, differentiation into activated T cells, and subsequent migration to the infected tissue. Once activated, T cells bearing the CD8$^+$ receptor become cytotoxic T cells that are able to destroy infected cells, whereas if they have a CD4$^+$ receptor, they turn into helper T cells

[1, 113]. Tregs perform an important role of suppressing the autoreactive T cells, and are a part of $CD4^+$ T cell population [176, 177, 178]. Since in this chapter I am trying to understand self and non-self discrimination mechanisms of the immune response, I consider two populations of naïve $CD8^+$ T cells that respond to self-antigens and foreign antigens, while focusing on one population of $CD4^+$ T cells representing regulatory T cells. Kim et al. [113] have considered a situation where each population of naïve T cells is maintained at a certain level supported by homeostasis in the absence of infection. Burroughs et al. [179, 55] and Segel et al. [45] in their models have instead considered a constant influx of new T cells from the thymus. In this model, for simplicity, I consider a single population of naïve T cells which includes Tregs, foreign-reactive and self-reactive T cells, and, similarly to earlier work, the population of these naïve T cells is assumed to be maintained at a certain level by homeostasis [76, 52, 53, 175]. It is thus assumed that in the absence of infection, these cells are produced at a constant rate λ_{in} (cell day^{-1}), and they die at a rate d_{in} (day^{-1}). Once activated, these cells differentiate into either regulatory T cells, whose main role is the control of immune response against self- and foreign antigens [1, 60], as well as prevention of autoimmune disease [60, 54, 51, 180], or effector cells that are able to eliminate infected cells. We denote by α the rate at which naïve T cells (T_{in}) are activated, and for simplicity we assume that all types of T cells have the same activation rate. Since T_{in} includes different kinds of naïve T cells, it is assumed that a constant proportion p_1 of them will develop into regulatory T cells T_{reg}, and a proportion p_2 will become normal activated T cells T_{nor} that are able to recognise infected cells expressing foreign antigen and destroy these cells at rate μ_F (cell^{-1} day^{-1}). The remaining proportion $(1-p_1-p_2)$ of T cells will become autoreactive cells T_{aut} with a lower threshold for activation by healthy cells, hence, they will be destroying both infected and healthy cells at rate μ_a (cell^{-1} day^{-1}).

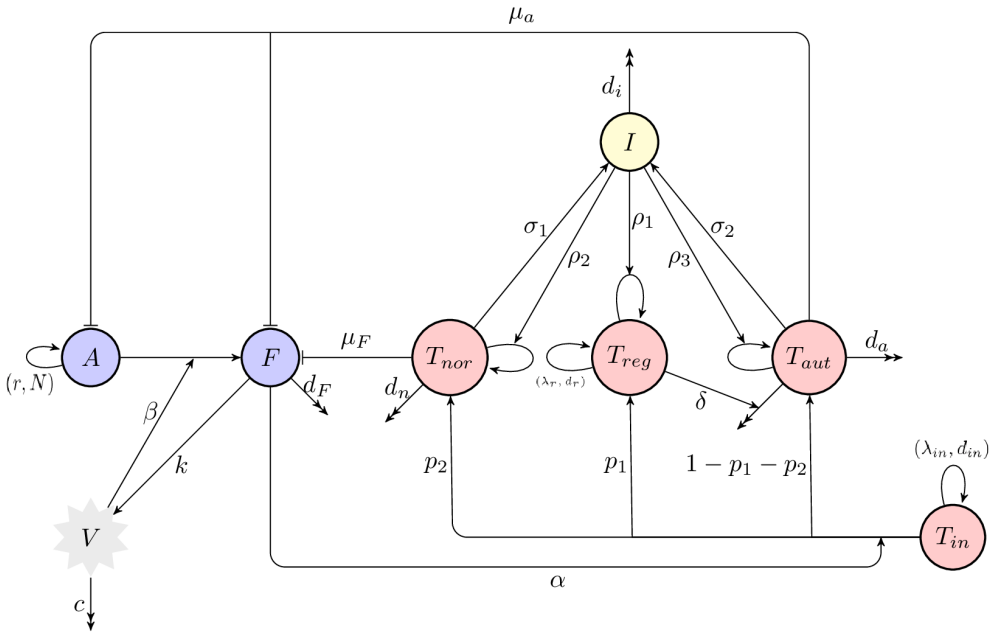

Figure 3.1: A schematic diagram of immune response to an infection. Blue circles indicate host cells (uninfected and infected cells), red circles denote different T cells (naïve, regulatory, normal activated, and autoreactive T cells), yellow circle shows cytokines (interleukin 2), and grey indicates virus particles (virions). Single arrow-headed and bar-headed lines indicate, respectively, production/proliferation and destroying of one cell population from/by another. Double arrows indicate natural clearance.

Unlike the work by Blyuss and Nicholson [76, 77], [55] and [113] have not explicitly modelled the production of autoreactive T cells from normal activated T cells, and in the present model I also do not include this feature, as the model already accounts for the influx of each population of T cells directly to the tissue.

Similarly to other models of autoimmune dynamics [55, 179, 181], regulatory T cells in our model are assumed to have their own homeostatic mechanism, and they are assumed to be produced at constant rate λ_r (cell day^{-1}) and die at rate d_r (day^{-1}). One of the main effects of regulatory T cells is to suppress the proliferation of autoreactive T cells. Part of this suppression occurs through the inhibition of interleukin 2 (IL-2) by T cells [182, 183]. Moreover, there is evidence for both cell-to-cell inhibition, and soluble mediators such as IL-10 and TNF-β [179, 55, 58, 113]. There is some experimental evidence suggesting that the suppression by Tregs is antigen-specific [184, 185, 186], which implies that Tregs are able to discriminate between T cells responding to self-antigens and T cells responding to foreign antigen [60]. León et al. [48] and Carneiro et al. [187] have proposed a model that considers antigen-specific suppression by Tregs, thus endowing Tregs with a mechanism for

self/non-self discrimination. Baecher-Allan et al. [188] have proposed a model for the T cell receptor (TCR) signal strength, where Tregs suppress the activation of autoreactive T cells, while the T cells reactive to foreign antigen are refractory to the suppression. Thus, in this chapter I only consider direct suppression of autoreactive T cells by Tregs, which is assumed to occur at rate δ (cell^{-1} day^{-1}), and, unlike the work by Burroughs et al. [55] and Kim et al. [113], I am assuming Tregs do not suppress the normal activated T cells T_{nor}. Among various cytokines involved in the process of immune response, a particularly important role is played by IL-2, to be denoted by $I(t)$, which is an essential factor in the growth of T cells. Whilst this cytokine promotes the growth of both regulatory and effector T cells, regulatory T cells do not secrete IL-2 [1, 55, 179]. Therefore, in this model I assume that T_{nor} and T_{aut} produce IL-2 at rates σ_1 (day^{-1}) and σ_2 (day^{-1}). On the other hand, whilst regulatory T cells do not produce IL-2, similar to other T cells they need this cytokine for their activation and proliferation [189, 190]. Thus, I assume that IL-2 promotes proliferation of T_{reg}, T_{nor} and T_{aut} at rates ρ_1 (cell^{-1} day^{-1}), ρ_2 (cell^{-1} day^{-1}) and ρ_3 (cell^{-1} day^{-1}), respectively. Although it is also possible to include in the model inhibition of IL-2 by T cells [179, 190], our analysis shows that this would not qualitatively change the behaviour of the model.

With the above assumptions, the model for dynamics of immune response to a viral infection with account for Tregs, T cells with different activation thresholds

and IL-2, as illustrated in Fig. 3.1, takes the form

$$\begin{aligned}
\frac{dA}{dt} &= rA\left(1-\frac{A}{N}\right) - \beta AV - \mu_a T_{aut} A,\\
\frac{dF}{dt} &= \beta AV - d_F F - \mu_F T_{nor} F - \mu_a T_{aut} F,\\
\frac{dT_{in}}{dt} &= \lambda_{in} - d_{in} T_{in} - \alpha T_{in} F,\\
\frac{dT_{reg}}{dt} &= \lambda_r - d_r T_{reg} + p_1 \alpha T_{in} F + \rho_1 I T_{reg},\\
\frac{dT_{nor}}{dt} &= p_2 \alpha T_{in} F - d_n T_{nor} + \rho_2 I T_{nor},\\
\frac{dT_{aut}}{dt} &= (1-p_1-p_2)\alpha T_{in} F - d_a T_{aut} - \delta T_{reg} T_{aut} + \rho_3 I T_{aut},\\
\frac{dI}{dt} &= \sigma_1 T_{nor} + \sigma_2 T_{aut} - d_i I,\\
\frac{dV}{dt} &= kF - cV,
\end{aligned} \tag{3.1}$$

with $0 \leq p_1 + p_2 \leq 1$. Introducing non-dimensional variables

$$\hat{t} = rt, \quad A = N\hat{A}, \quad F = N\hat{F}, \quad T_{in} = \frac{\lambda_{in}}{d_{in}}\hat{T}_{in}, \quad T_{reg} = \frac{\lambda_{in}}{d_{in}}\hat{T}_{reg},$$
$$T_{nor} = \frac{\lambda_{in}}{d_{in}}\hat{T}_{nor}, \quad T_{aut} = \frac{\lambda_{in}}{d_{in}}\hat{T}_{aut}, \quad I = \frac{\lambda_{in}}{d_{in}}\hat{I}, \quad V = N\hat{V},$$

yields a rescaled model

$$
\begin{aligned}
\frac{dA}{dt} &= A\left(1-A\right) - \beta AV - \mu_a T_{aut} A, \\
\frac{dF}{dt} &= \beta AV - d_F F - \mu_F T_{nor} F - \mu_a T_{aut} F, \\
\frac{dT_{in}}{dt} &= d_{in}\left(1-T_{in}\right) - \alpha T_{in} F, \\
\frac{dT_{reg}}{dt} &= \lambda_r - d_r T_{reg} + p_1 \alpha T_{in} F + \rho_1 I T_{reg}, \\
\frac{dT_{nor}}{dt} &= p_2 \alpha T_{in} F - d_n T_{nor} + \rho_2 I T_{nor}, \\
\frac{dT_{aut}}{dt} &= (1-p_1-p_2)\alpha T_{in} F - d_a T_{aut} - \delta T_{reg} T_{aut} + \rho_3 I T_{aut}, \\
\frac{dI}{dt} &= \sigma_1 T_{nor} + \sigma_2 T_{aut} - d_i I, \\
\frac{dV}{dt} &= kF - cV,
\end{aligned}
\tag{3.2}
$$

where

$$
\begin{aligned}
&\hat{\beta} = \frac{\beta N}{r}, \quad \hat{\mu}_a = \frac{\mu_a \lambda_{in}}{r d_{in}}, \quad \hat{d}_F = \frac{d_F}{r}, \quad \hat{\mu}_F = \frac{\mu_F \lambda_{in}}{r d_{in}}, \quad \hat{d}_{in} = \frac{d_{in}}{r}, \\
&\hat{\alpha} = \frac{\alpha N}{r}, \quad \hat{\lambda}_r = \frac{\lambda_r d_{in}}{\lambda_{in} r}, \quad \hat{d}_n = \frac{d_n}{r}, \quad \hat{d}_a = \frac{d_a}{r}, \quad \hat{\rho}_i = \frac{\rho_i \lambda_{in}}{r d_{in}}, \quad i = 1,2,3, \\
&\hat{\delta} = \frac{\delta \lambda_{in}}{r d_{in}}, \quad \hat{\sigma}_1 = \frac{\sigma_1}{r}, \quad \hat{\sigma}_2 = \frac{\sigma_2}{r}, \quad \hat{d}_i = \frac{d_i}{r}, \quad \hat{k} = \frac{k}{r}, \quad \hat{c} = \frac{c}{r}, \quad \hat{d}_r = \frac{d_r}{r},
\end{aligned}
$$

and all hats in variables and parameters have been dropped for simplicity of notation. The model (3.2) is clearly well-posed, i.e. its solutions remain non-negative for $t \geq 0$ for any non-negative initial conditions.

3.3 Steady states and their stability

As a first step in the analysis of model (3.2), I look at its steady states

$$
S^* = \left(A^*, F^*, T_{in}^*, T_{reg}^*, T_{nor}^*, T_{aut}^*, I^*, V^*\right),
$$

that can be found by equating to zero the right-hand sides of equations (3.2) and solving the resulting system of algebraic equations. High dimensionality of the system (3.2) results in a large number of possible steady states, so I now systematically

study all of them. First, I consider a situation where at a steady state, there is no free virus population, i.e. $V^* = 0$, which immediately implies $F^* = 0$ and $T^*_{in} = 1$. In this case there are four possible steady states depending on whether T^*_{nor} and T^*_{aut} are each equal to zero or being positive. If $T^*_{nor} = T^*_{aut} = 0$, there are two steady states

$$S^*_1 = \left(0, 0, 1, \frac{\lambda_r}{d_r}, 0, 0, 0, 0\right), \quad S^*_2 = \left(1, 0, 1, \frac{\lambda_r}{d_r}, 0, 0, 0, 0\right),$$

of which S^*_1 is always unstable, and S^*_2 is stable if $cd_F - k\beta > 0$, unstable if $cd_F - k\beta < 0$, and undergoes a steady-state bifurcation at $cd_F - k\beta = 0$. For $T^*_{nor} \neq 0$ and $T^*_{aut} = 0$, we again have two steady states

$$S^*_3 = \left(0, 0, 1, \frac{\lambda_r \rho_2}{\rho_2 d_r - \rho_1 d_n}, \frac{d_i d_n}{\sigma_1 \rho_2}, 0, \frac{d_n}{\rho_2}, 0\right),$$
$$S^*_4 = \left(1, 0, 1, \frac{\lambda_r \rho_2}{\rho_2 d_r - \rho_1 d_n}, \frac{d_i d_n}{\sigma_1 \rho_2}, 0, \frac{d_n}{\rho_2}, 0\right),$$

but they are both unstable for any values of parameters.

In the case when $T^*_{nor} = 0$ and $T^*_{aut} \neq 0$, we have steady states S^*_5 and S^*_6,

$$S^*_5 = \left(0, 0, 1, T^*_{reg}, 0, \frac{d_i\left(d_a + \delta T^*_{reg}\right)}{\rho_3 \sigma_2}, \frac{d_a + \delta T^*_{reg}}{\rho_3}, 0\right),$$

$$S^*_6 = \left(1 - \frac{\mu_a d_i\left(d_a + \delta T^*_{reg}\right)}{\rho_3 \sigma_2}, 0, 1, T^*_{reg}, 0, \frac{d_i\left(d_a + \delta T^*_{reg}\right)}{\rho_3 \sigma_2}, \frac{d_a + \delta T^*_{reg}}{\rho_3}, 0\right),$$

where

$$T^*_{reg} = \frac{d_r \rho_3 - \rho_1 d_a \pm \sqrt{\left(d_r \rho_3 - \rho_1 d_a\right)^2 - 4\rho_1 \delta \lambda_r \rho_3}}{2\rho_1 \delta}.$$

The steady state S^*_5 (respectively, S^*_6) is stable if the following conditions hold

$$P < \frac{d_a + \delta T^*_{reg}}{\rho_3} < \frac{d_n}{\rho_2}, \quad \delta \rho_1 \left(T^*_{reg}\right)^2 > \lambda_r \rho_3,$$

$$\rho_3 \lambda_r^2 + \rho_3 d_i \lambda_r T^*_{reg} - \rho_3 d_i d_a \left(T^*_{reg}\right)^2 - \delta(\rho_1 d_a + \rho_3 d_i)\left(T^*_{reg}\right)^3 - \rho_1 \delta^2 \left(T^*_{reg}\right)^4 > 0,$$

where

$$P = \begin{cases} \dfrac{\sigma_2}{\mu_a d_i}, & \text{for } S_5^*, \\ \dfrac{\sigma_2 \left(\beta k - c d_F\right)}{\mu_a d_i \left(c + \beta k\right)}, & \text{for } S_6^*. \end{cases}$$

This steady state undergoes a steady-state bifurcation if

$$\frac{d_a + \delta T_{reg}^*}{\rho_3} = P, \quad \text{or} \quad \frac{d_a + \delta T_{reg}^*}{\rho_3} = \frac{d_n}{\rho_2}, \quad \text{or} \quad \delta \rho_1 \left(T_{reg}^*\right)^2 = \lambda_r \rho_3,$$

and a Hopf bifurcation if

$$P < \frac{d_a + \delta T_{reg}^*}{\rho_3} < \frac{d_n}{\rho_2}, \quad \delta \rho_1 \left(T_{reg}^*\right)^2 > \lambda_r \rho_3,$$

$$\rho_3 \lambda_r^2 + \rho_3 d_i \lambda_r T_{reg}^* - \rho_3 d_i d_a \left(T_{reg}^*\right)^2 - \delta(\rho_1 d_a + \rho_3 d_i) \left(T_{reg}^*\right)^3 - \rho_1 \delta^2 \left(T_{reg}^*\right)^4 = 0.$$

The steady state with $T_{nor}^* \neq 0$ and $T_{aut}^* \neq 0$ only exists for a particular combination of parameters, namely, when

$$\delta \rho_2^2 \lambda_r = (\rho_3 d_n - \rho_2 d_a)(\rho_2 d_r - \rho_1 d_n),$$

and is always unstable.

When $V^* \neq 0$, all other state variables are also non-zero. In this case, the steady

state S_7^* has T_{nor}^* and T_{aut}^* satisfying the following system of equations

$$\begin{aligned}
&\alpha c\mu_a\rho_2\sigma_2(\beta k+c)(T_{aut}^*)^2T_{nor}^*+\alpha c\rho_2(\beta k\mu_a\sigma_1+c\mu_F\sigma_2+c\mu_a\sigma_1)T_{aut}^*(T_{nor}^*)^2\\
&-(\alpha\beta ckd_id_n\mu_a+\beta^2k^2d_{in}\rho_2\sigma_2+\alpha\beta ck\rho_2\sigma_2-\alpha c^2d_F\rho_2\sigma_2+\alpha c^2d_id_n\mu_a)T_{aut}^*\\
&T_{nor}^*+\alpha cd_id_{in}\mu_ap_2(\beta k+c)T_{aut}^*+\alpha c^2\mu_F\rho_2\sigma_1(T_{nor})^3-(\beta^2k^2d_{in}\rho_2\sigma_1\\
&+\alpha\beta ck\rho_2\sigma_1-\alpha c^2d_F\rho_2\sigma_1+\alpha c^2d_id_n\mu_F)(T_{nor}^*)^2+d_i(\alpha c^2d_{in}\mu_Fp_2\\
&+\beta^2k^2d_{in}d_n+\alpha\beta ckd_n-\alpha c^2d_Fd_n)T_{nor}^*-\alpha cd_id_{in}p_2(cd_F-k\beta)=0,
\end{aligned}$$

$$\begin{aligned}
&p_2\rho_1\rho_3{\sigma_2}^2(T_{aut}^*)^3+\sigma_2(-\delta d_ip_1\rho_2+p_1\rho_1\rho_2\sigma_2+p_2\rho_1\rho_2\sigma_2+2p_2\rho_1\rho_3\sigma_1\\
&-\rho_1\rho_2\sigma_2)(T_{aut}^*)^2T_{nor}^*-d_ip_2\sigma_2(d_a\rho_1+d_r\rho_3)(T_{aut}^*)^2+\sigma_1(-\delta d_ip_1\rho_2\\
&+2p_1\rho_1\rho_2\sigma_2+2p_2\rho_1\rho_2\sigma_2+p_2\rho_1\rho_3\sigma_1-2\rho_1\rho_2\sigma_2)T_{aut}^*(T_{nor}^*)^2+d_i(\delta d_id_np_1\\
&-d_ap_2\rho_1\sigma_1-d_np_1\rho_1\sigma_2-d_np_2\rho_1\sigma_2-d_rp_1\rho_2\sigma_2-d_rp_2\rho_2\sigma_2-d_rp_2\rho_3\sigma_1\\
&+d_n\rho_1\sigma_2+d_r\rho_2\sigma_2)T_{aut}^*T_{nor}^*+p_2{d_i}^2(\delta\lambda_r+d_ad_r)T_{aut}^*+(1-p_1-p_2)T_{nor}^*\\
&\left[-\rho_1\rho_2{\sigma_1}^2(T_{nor}^*)^2+d_i\sigma_1(d_n\rho_1+d_r\rho_2)T_{nor}^*-{d_i}^2d_nd_r\right]=0,
\end{aligned}$$

with the rest of state variables being given by

$$I^*=\frac{\sigma_1T_{nor}^*+\sigma_2T_{aut}^*}{d_i},\quad A^*=\frac{c\left(d_F+\mu_FT_{nor}^*+\mu_aT_{aut}^*\right)}{k\beta},\quad V^*=\frac{1-A^*-\mu_aT_{aut}^*}{\beta},$$

$$F^*=\frac{cV^*}{k},\quad T_{in}^*=\frac{d_{in}}{d_{in}+\alpha F^*},\quad T_{reg}^*=\frac{\lambda_r+p_1\alpha T_{in}^*F^*}{d_r-\rho_1I^*}.$$

It does not prove possible to analyse stability of this steady state analytically, hence, one has to resort to numerical calculations.

Remark. Inclusion of a term corresponding to production of autoreactive T cells directly from normal activated T cells in a manner similar to Blyuss and Nicholson [76, 77] would make the steady states S_3^* and S_4^* infeasible, while having no major effect on stability of other steady states. Hence, it suffices to consider the above model without explicitly modelling the transition from T_{nor} to T_{aut}.

3.4 Numerical stability analysis and simulations

To investigate various dynamical scenarios that can be exhibited by the model, I now perform a comprehensive numerical analysis of stability of different steady

states and identify their possible bifurcations using MATLAB routine ode45 with the absolute and relative tolerances set to 1e-13. Analytical results from the previous section suggest that the disease-free steady state S_2^* is stable when $k\beta < cd_F$, and unstable when $k\beta > cd_F$. As will be shown below, there are some major differences in dynamics between these two parameter combinations, hence, I will analyse them separately. Since there are significant differences in the reported values of many of the model parameters, and some of them have not yet been properly measured, I fix the baseline values as given in Table 1, and perform a sweep of parameter space to identify the effects of varying these parameters. Since prior to the start of infection, the numbers of infected cells, normal activated T cells, and the amount of IL-2 are all equal to zero, the initial condition for the model is taken to be

$$(A(0), F(0), T_{in}(0), T_{reg}(0), T_{nor}(0), T_{aut}(0), I(0), V(0)) = (0.9, 0, 0.8, 0.7, 0, 0, 0, 0.4), \tag{3.3}$$

Table 3.1: Table of parameters

Parameter	Value	Definition
β	3	Infection rate
μ_a	20	The rate of killing of uninfected cells by autoreactive T cells
d_F	1.1	Natural death rate of infected cells
μ_F	6	The rate of killing of infected cells by the normal T cells
d_{in}	1	Growth rate of naïve T cells
α	0.4	Rate of activation of naïve T cells by infected cells
λ_r	3	Growth rate of regulatory T cells
d_r	0.4	Natural death rate of regulatory T cells
p_1	0.4	Rate of conversion of naïve T cells into regulatory T cells
p_2	0.4	Rate of conversion of naïve T cells into normal T cells
ρ_1	10	Proliferation rate of regulatory T cells by interleukin 2 (IL-2)
ρ_2	0.8	Proliferation rate of normal T cells by interleukin-2 (IL-2)
ρ_3	2	Proliferation rate of autoreactive T cells by interleukin 2 (IL-2)
d_n	1	Natural death rate of normal T cells
d_a	0.001	Natural death rate of autoreactive T cells
δ	0.002	Rate of clearance of autoreactive T cells by regulatory T cells
σ_1	0.15	Rate of production of interleukin-2 (IL-2) by normal T cells
σ_2	0.2	Rate of production of interleukin-2 (IL-2) by autoreactive T cells
d_i	0.6	Natural clearance rate of IL-2
k	2	Rate of production of free virus
c	6	Natural clearance rate of free virus

which indicates the presence of some number of free virus particles. Here the initial values of $A(0)$ and $T_{in}(0)$ are chosen randomly, with the only requirement that they

do not exceed unity, in light of the fact that I am considering a non-dimensionalised model. For analysis of basins of attraction, the values of $T_{reg}(0)$ and $V(0)$ will be varied.

Figure 3.2 illustrates how system dynamics is affected by the parameters. Since the condition $k\beta < cd_F$ holds, the disease-free steady state S_2^* is always stable.

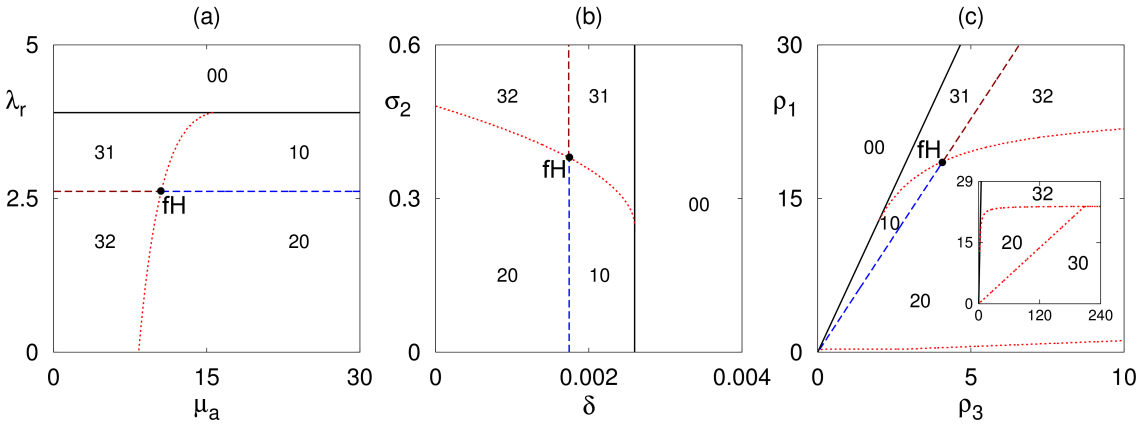

Figure 3.2: Regions of feasibility and stability of the steady states S_5^* and S_6^* with parameter values from Table 1. Black and red curves indicate the boundaries of feasibility and the steady-state bifurcation, whereas dashed lines (blue/brown) show the boundaries of Hopf bifurcation of the steady states S_5^* and S_6^*, respectively, with 'fH' indicating the fold-Hopf bifurcation. The first digit of the index refers to S_5^*, while the second corresponds to S_6^*, and they indicate that in that parameter region the respective steady state is unfeasible (index is '0'), stable (index is '1'), unstable via Hopf bifurcation with a periodic orbit around this steady state (index is '2'), or unstable via a steady-state bifurcation (index is '3'). In all plots, the condition $k\beta < cd_F$ holds, so the disease-free steady state S_2^* is also stable.

However, the system can also have two other biologically feasible steady states S_5^* and S_6^*, which only exist, provided regulatory T cells do not grow too rapidly and do not clear autoreactive T cells too quickly. In the case where autoreactive T cells are very effective in killing infected cells (i.e. for higher μ_a), or when they are producing IL-2 at a slow rate (smaller σ_2), only the steady state S_5^* is feasible, which has the zero population of host cells A, while the steady state S_6^* with $A > 0$ can only exist when μ_a is relatively low (or σ_2 is high), and S_5^* is unstable. Provided the steady states S_5^* and S_6^* are feasible, decreasing the growth rate λ_r of regulatory T cells results in a supercritical Hopf bifurcation, which gives rise to stable periodic solutions around these steady states. Since the steady state S_5^* is characterised by $A = 0$, both regimes where this steady state is stable, or unstable with oscillations around it, biologically correspond to a situation where the host cells are dead. On the other hand, a periodic solution around S_6^* corresponds to a proper autoimmune

response, whereby the infection is cleared, but the immune system still exhibits endogenous oscillations, as illustrated in Fig. 3.4(a)-(b). At the intersection of the lines of Hopf bifurcation and the steady-state bifurcation, one has the fold-Hopf (also known as zero-Hopf or saddle-node Hopf) bifurcation [191]. Importantly, the steady states S_5^* and S_6^* can only exist if the rate ρ_3 at which IL-2 promotes proliferation of autoreactive T cells is sufficiently high, and this minimum value of the rate ρ_3 increases linearly with the rate ρ_1 at which IL-2 promotes proliferation of regulatory T cells. Once feasible, the steady states S_5^* and S_6^* are stable for smaller values of ρ_3 and then undergo Hopf bifurcation, when ρ_3 is sufficiently increased.

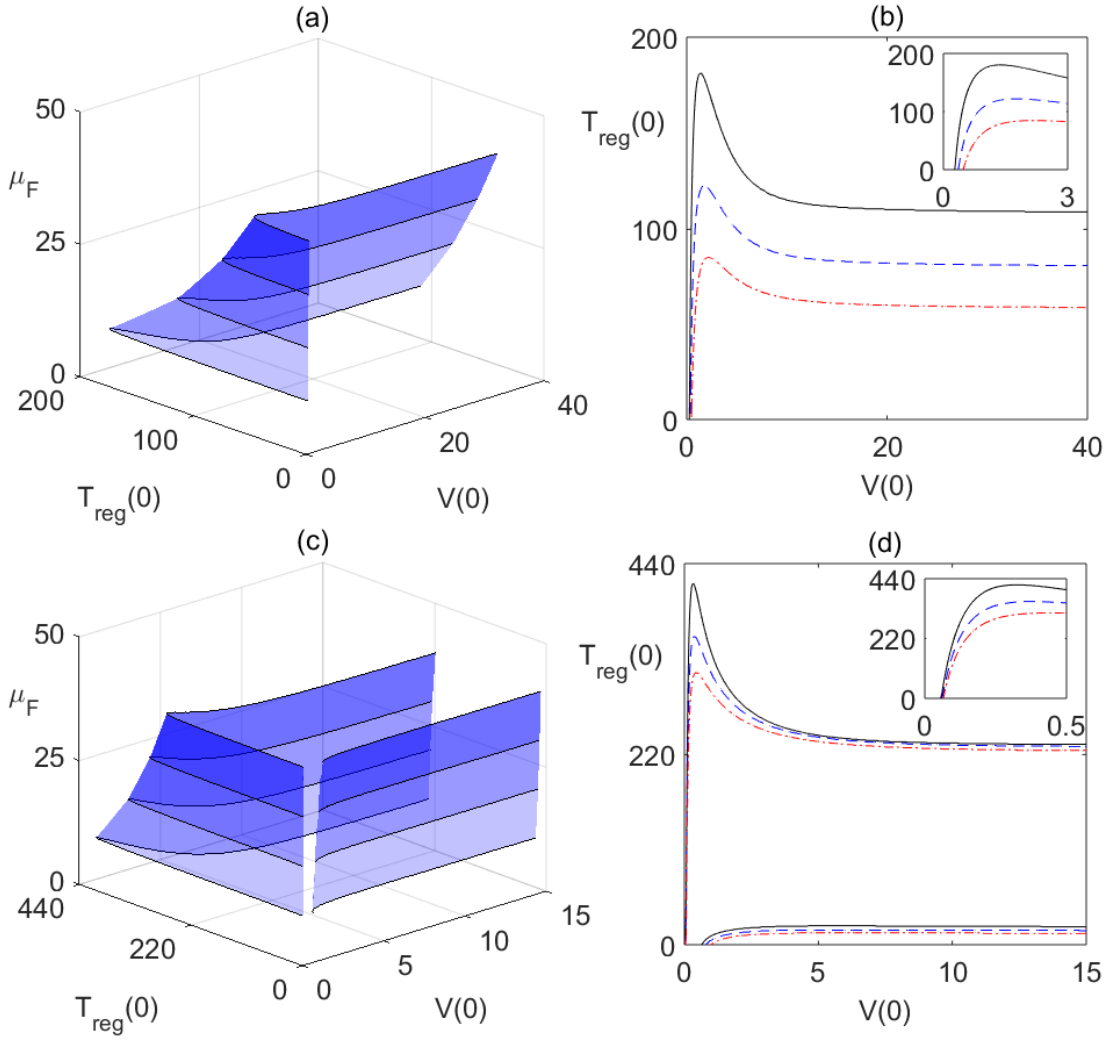

Figure 3.3: Regions of bi-stability with parameter values from Table 1 and initial condition (3.3). (a), (b) $\lambda_r = 2.5$, $\mu_a = 5$, with $\mu_F = 10$ (black), $\mu_F = 20$ (blue), $\mu_F = 30$ (red). The system exhibits autoimmune response to the right of the surface in (a) and below the curves in (b), while to the left of the surface in (a) and above the curves in (b) it tends to a stable disease-free steady state S_2^*. (c), (d) $\rho_1 = 30$, $\rho_3 = 8$. The system exhibits autoimmune response inside the region bounded by the surfaces in (c), or by the curves in (d), and outside it tends to a stable disease-free steady state S_2^*.

Since for all parameter combinations in Fig. 3.2 the steady state S_2^* is stable, this means that the system can exhibit bi-stability between steady states and/or periodic solutions. To investigate this in more detail, I choose parameter values in the '32' region in Fig. 3.2, where periodic oscillations around the steady state S_6^* are possible. While previous works on multi-stability in models of autoimmunity focussed mainly on identifying parameter regions associated with bi-stability [192, 82, 193], the structure of basins of attraction associated with different dynamical states has remained largely unexplored. To analyse basins of attraction in our model, due to high dimensionality of the phase space, I fix initial conditions for all state variables, and consider different initial amounts of free virus $V(0)$ and regulatory T cells $T_{reg}(0)$, as illustrated in Fig. 3.3. Biologically, this corresponds to varying the initial level of infection, as well as the initial state of the immune system, which can be primed by previous exposures to other pathogens. This Figure shows that if the initial number of regulatory T cells is sufficiently high, the system is able to successfully eliminate infection without any lasting consequences, settling on a stable disease-free steady state.

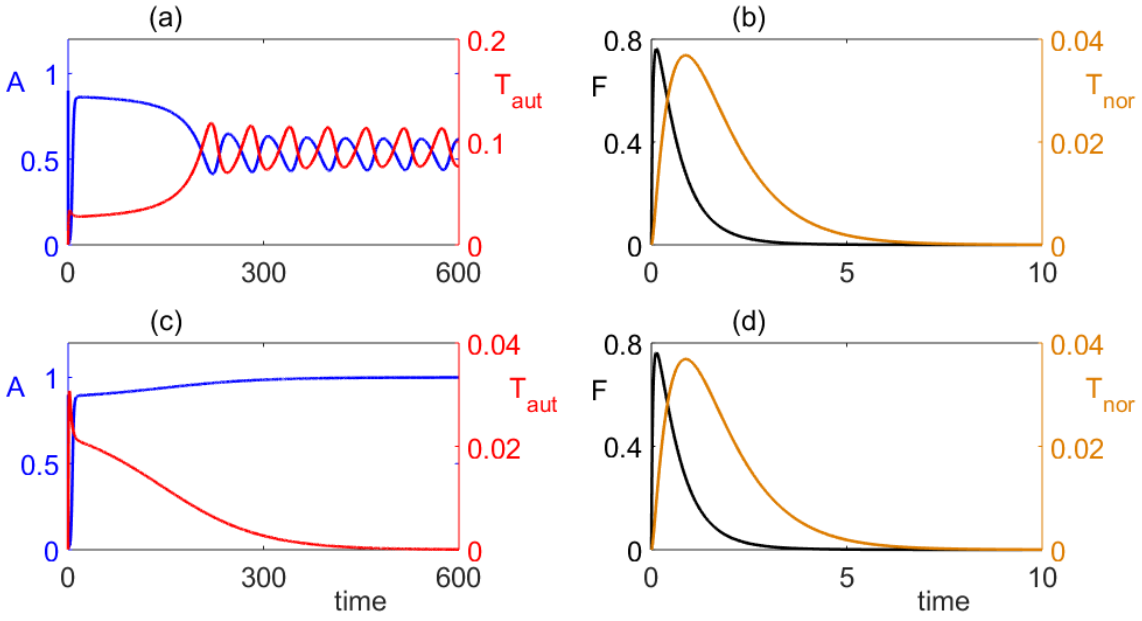

Figure 3.4: Simulation of the model (3.2) with parameter values from Table 1, except for $\lambda_r = 2.5$, $\mu_a = 5$, $\mu_F = 10$, and the initial condition (3.3). (a), (b) $V(0) = 10$, $T_{reg}(0) = 100$, the system exhibits periodic behaviour around S_6^*, i.e. clearance of infection followed by the onset of autoimmune response. (c), (d) $V(0) = 10$, $T_{reg}(0) = 150$, the model converges to a stable disease-free steady state S_2^*.

Interestingly, for very small initial amounts of free virus, a higher amount of regulatory T cells is required to clear the infection. For lower values of $T_{reg}(0)$, the

system exhibits stable periodic oscillations around the steady state S_6^*, which biologically represents the regime of autoimmune response. One can also observe that the minimum value of $T_{reg}(0)$ needed to achieve a disease-free steady state reduces with increasing the rate μ_F at which normal T cells are able to kill infected cells. Figure 3.4 illustrates temporary evolution of the system in the regime of bi-stability between a stable disease-free steady state and a periodic solution, corresponding to autoimmunity. The dynamics of regulatory T cells (not shown in this figure) mimics that of autoreactive T cells.

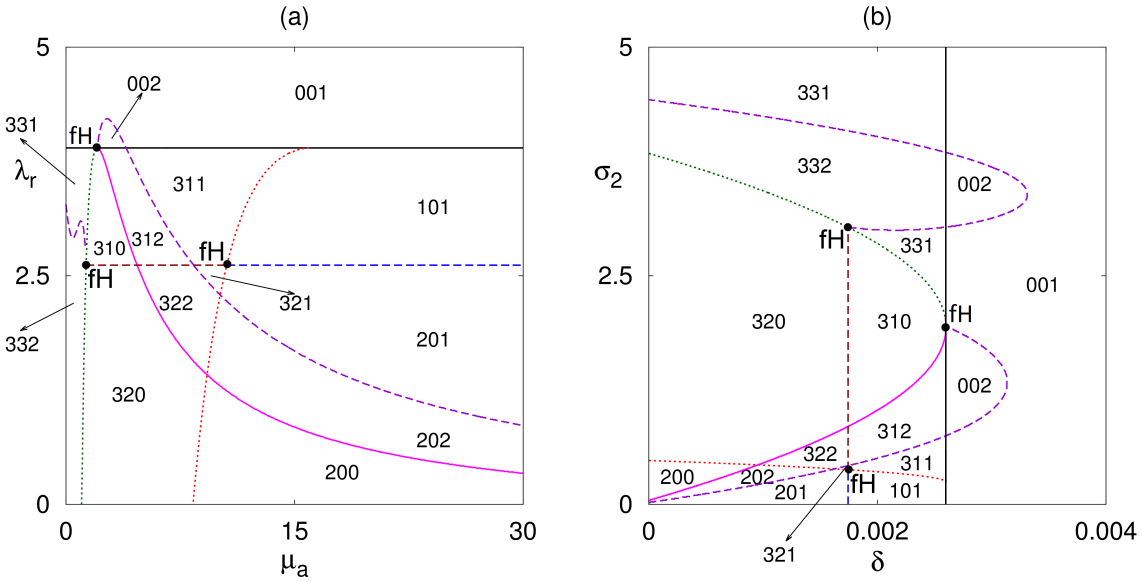

Figure 3.5: Regions of feasibility and stability of the steady states S_5^*, S_6^*, and S_7^* with parameter values from Table 1. Black and magenta curves indicates the boundaries of feasibility for S_5^*/S_6^* and S_7^*, dashed curves are the boundaries of Hopf bifurcation for S_5^*/S_6^* (blue/brown) or S_7^* (purple), and dotted lines are the boundaries of the steady-state bifurcation of S_5^* (red) and S_6^* (green), with 'fH' indicating the location of the fold-Hopf bifurcation. The first digit of the index refers to S_5^*, the second corresponds to S_6^*, and the third corresponds to S_7^*. These indices indicate that in that parameter region the respective steady state is unfeasible (index is '0'), stable (index is '1'), unstable via Hopf bifurcation with a periodic orbit around this steady state (index is '2'), or unstable via a steady-state bifurcation (index is '3'). In all plots, the condition $k\beta > cd_F$ holds, so the disease-free steady state S_2^* is unstable.

Next, I consider a situation described by the combination of parameters satisfying $k\beta > cd_F$, so the disease-free steady state S_2^* is unstable, and the system can only have steady states S_5^*, S_6^*, and S_7^*. Figure 3.5 shows how feasibility and stability of these steady states depend on parameters. Naturally, this figure is identical to Fig. 3.2 in terms of indicating stability and bifurcations of the steady states S_5^* and S_6^*. One should note that unlike the case considered earlier, now for sufficiently high

rate σ_2 of production of IL-2, or sufficiently small rate μ_a at which autoreactive T cells are killing infected cells, the steady state S_6^* can also undergo a steady-state bifurcation due to the fact that the condition $k\beta > cd_F$ holds. Beyond this stability boundary, i.e. for very high values of σ_2 or very small values of μ_a, both steady states S_5^* and S_6^* are unstable, and the system settles either on the steady state S_7^*, or an a periodic solution around this steady state. In the parameter region, where only the steady state S_7^* is feasible, this steady state can only be unstable, giving rise to stable periodic oscillations, for sufficiently small values of δ or λ_r, whereas for higher values of those parameters this steady state is stable.

Figure 3.6 demonstrates the basins of attraction of the steady states S_5^*, S_6^* and S_7^*, as well as periodic solutions around them. As it has already been mentioned, this is the first time when basins of attraction for different steady states and periodic solutions are identified in a model of cytokine-mediated immune response and autoimmunity. Figure (a) shows that if the initial amount of free virus is sufficiently small, the system will converge to S_7^* for any value of $T_{reg}(0)$. For higher values of $V(0)$, the system exhibits bi-stability, where for smaller initial numbers of regulatory T cells $T_{reg}(0)$ it converges to the stable steady state S_5^* corresponding to the death of susceptible organ cells, while for higher values of $T_{reg}(0)$, the system settles on the stable steady state S_7^*. While the critical value of $T_{reg}(0)$ at which the transition between the two steady state takes place initially increases with $V(0)$, eventually it settles on some steady level, so that for higher initial amounts of free virus, this critical value no longer depends on $V(0)$. Figure (b) illustrates a qualitatively similar behaviour for higher rates of production of IL-2 and clearance of autoreactive T cells, in which case there is a bi-stability between S_6^* and S_7^*, but with the difference that there is also a small region for small values of $T_{reg}(0)$ and intermediate values of $V(0)$, where the system also converges to S_7^*. Figures (c) and (d) illustrate bi-stability between a periodic solution around S_7^* and either the stable steady state S_6^*, or a periodic solution around this steady state.

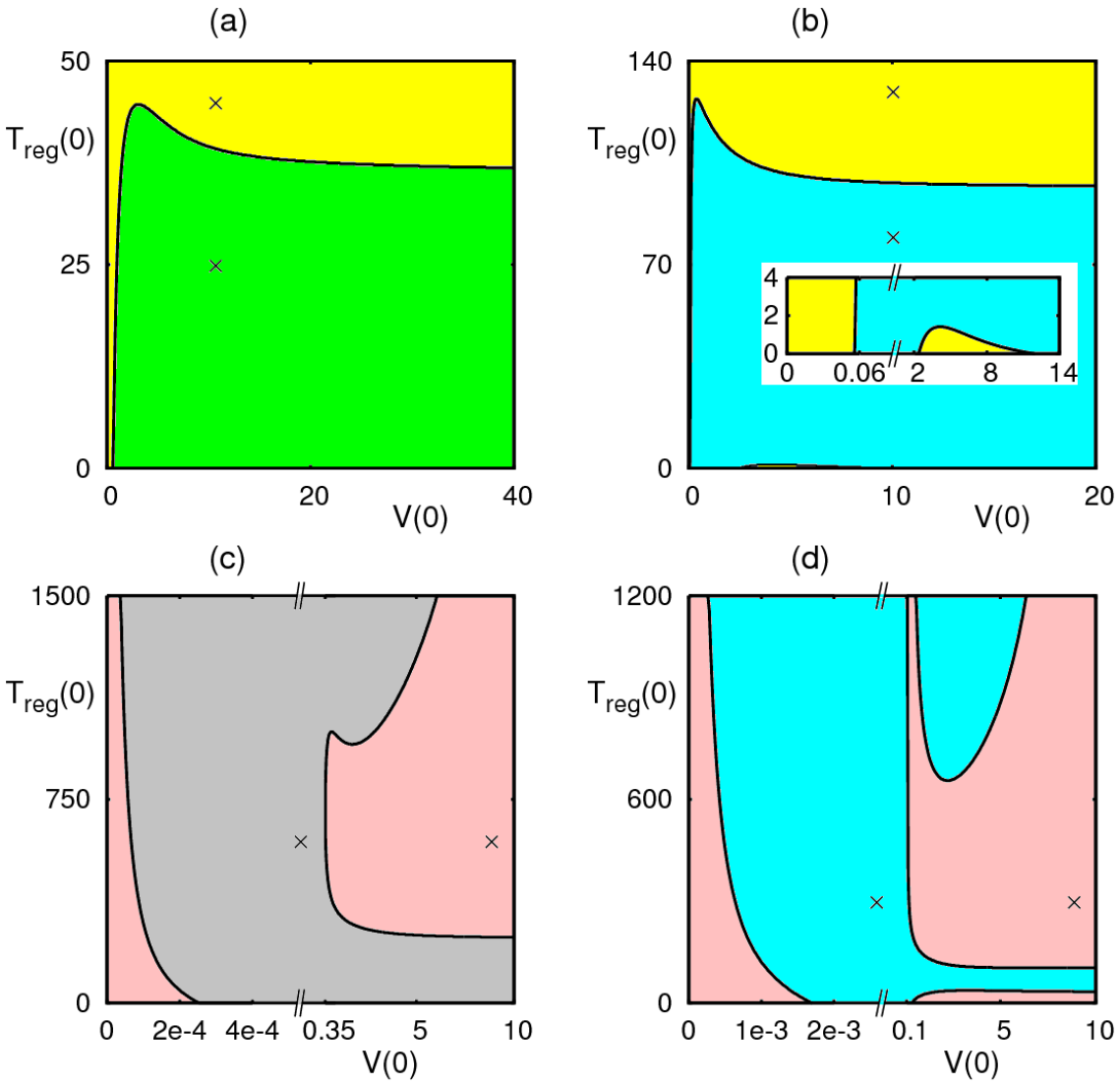

Figure 3.6: Regions of bi-stability in the system (3.2) with the initial condition (3.3), parameter values from Table 1, and $\beta = 4$, $k = 2.1$. (a) $\delta = 0.002$, $\sigma_2 = 0.2$, (b) $\delta = 0.0024$, $\sigma_2 = 0.5$, (c) $\delta = 0.0017$, $\sigma_2 = 0.42$, (d) $\delta = 0.0024$, $\sigma_2 = 0.7$. Green, blue and yellow are the basins of attraction of the steady states S_5^*, S_6^*, and S_7^*, respectively. Grey and pink are the basins of attraction of periodic solutions around S_6^* and S_7^*, respectively.

Numerical simulations in Figs. 3.7, 3.8, 3.9, and 3.10 show the dynamics of the model in the case when $k\beta > cd_F$ for the same parameter values but different initial conditions, thus illustrating various bi-stability scenarios shown in Fig. 3.6, in which crosses indicate the values of specific initial conditions used for simulations. Figure 3.7 demonstrates how for sufficiently small initial number of regulatory T cells the infection can result in the death of organ cells, in which case the system approaches a stable steady state S_5^*. On the other hand, for a higher number of Tregs, the system goes to a stable steady state S_7^* which represents a persistent (chronic) infection. In this case, one observes some kind of balance maintained with

the help of regulatory T cells: while the immune system is not able to clear the infection, at the same time it prevents infection from destroying the organ cells.

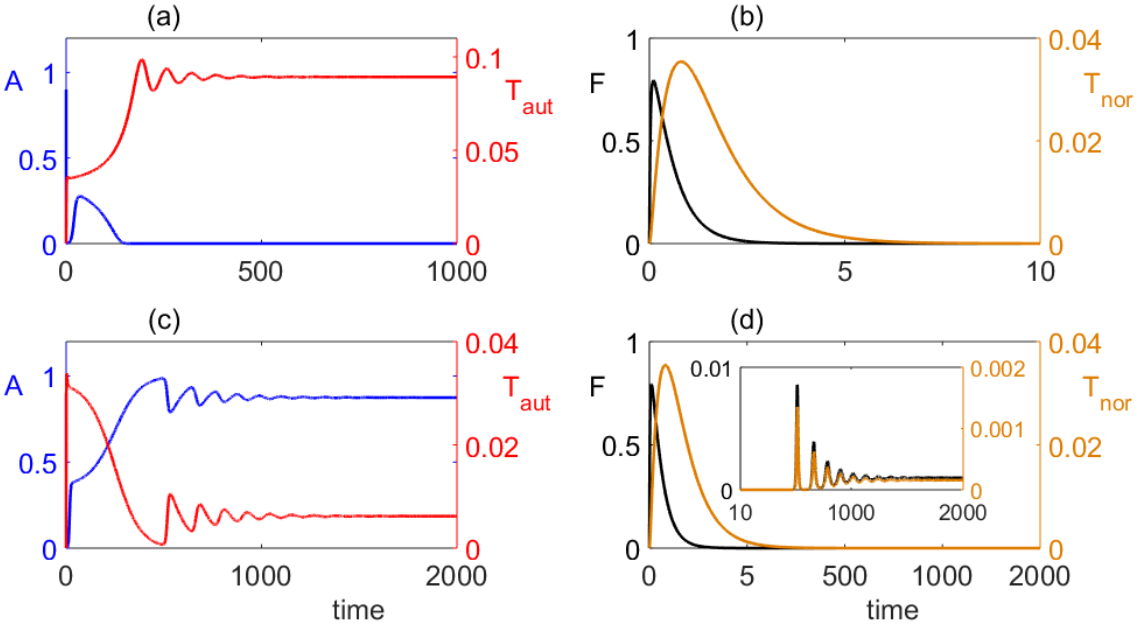

Figure 3.7: Numerical solution of the model (3.2) with the initial condition (3.3), parameter values from Table 1, and $\beta = 4$, $k = 2.1$, $\delta = 0.002$, $\sigma_2 = 0.2$. In (a) and (b) $V(0) = 10$ and $T_{reg}(0) = 25$. The model converges to the S_5^*. In (c) and (d) $V(0) = 10$ and $T_{reg}(0) = 45$. The model converges to the S_7^*. The dynamic of T_{reg} has a same behaviour as T_{aut}.

Figure 3.8 illustrates a similar behaviour, where bi-stability takes place between the steady states S_6^* and S_7^*. In this case, for a smaller number of regulatory T cells, the system favours the regime of normal clearance of infection, where after the initial growth, the numbers of infected cells and activated T cells responding to foreign antigen go to zero. For higher numbers of regulatory T cells, the system again approaches a stable steady state S_7^* describing a persistent infection. This is a really interesting and counter-intuitive result, which suggests that whilst regulatory T cells play a major role in reducing autoimmune response during normal disease clearance, when they are present in high numbers, the are actually promoting the persistence of infection.

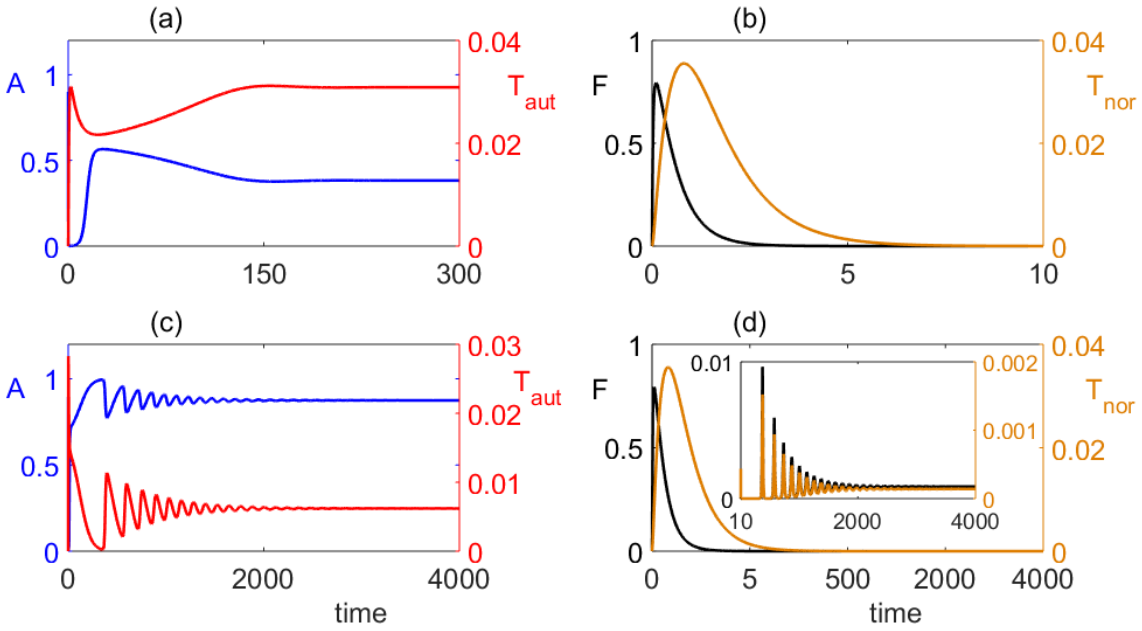

Figure 3.8: Numerical solution of the model (3.2) with the initial condition (3.3), parameter values from Table 1, and $\beta = 4$, $k = 2.1$, $\delta = 0.0024$, $\sigma_2 = 0.5$. (a), (b) $V(0) = 10$, $T_{reg}(0) = 80$. The system converges to S_6^*. (c), (d) $V(0) = 10$, $T_{reg}(0) = 130$. The system converges to S_7^*. The dynamics of T_{reg} is the same as T_{aut}.

Figure 3.9 illustrates a regime of bi-stability between periodic solutions around the steady states S_6^* and S_7^*. Similarly to the case of stable disease-free steady state considered earlier, the periodic solution around S_6^* biologically corresponds to the regime of autoimmune response, where upon clearance of the initial infection, the immune systems maintains endogenous oscillations, in which the growth of autoreactive T cells results in the destruction of some healthy organ cells, after which the number of autoreactive T cells decreases, and the organ cells recover.

One should note that since these oscillations take place around the steady state S_6^*, the mean concentration of organ cells is much lower than what it was before the infection. In the case of periodic oscillations around the steady state S_7^*, initially one observes a similar behaviour in terms of rapid growth of infected cells, followed by an expansion in the population of activated T cells recognising foreign antigen, but after the number of infected cells decreases, rather than go to zero, it settles on periodic oscillations around some small positive level. This suggests that the infection is not cleared, but rather than being chronic, there are intervals of quiescence where the level of infection is very small, followed by regular intervals of rapid growth of infection and autoreactive T cells, which causes significant reduction in the number of uninfected organ cells. After this infection is significantly reduced by the activated T cells, the cycle repeats.

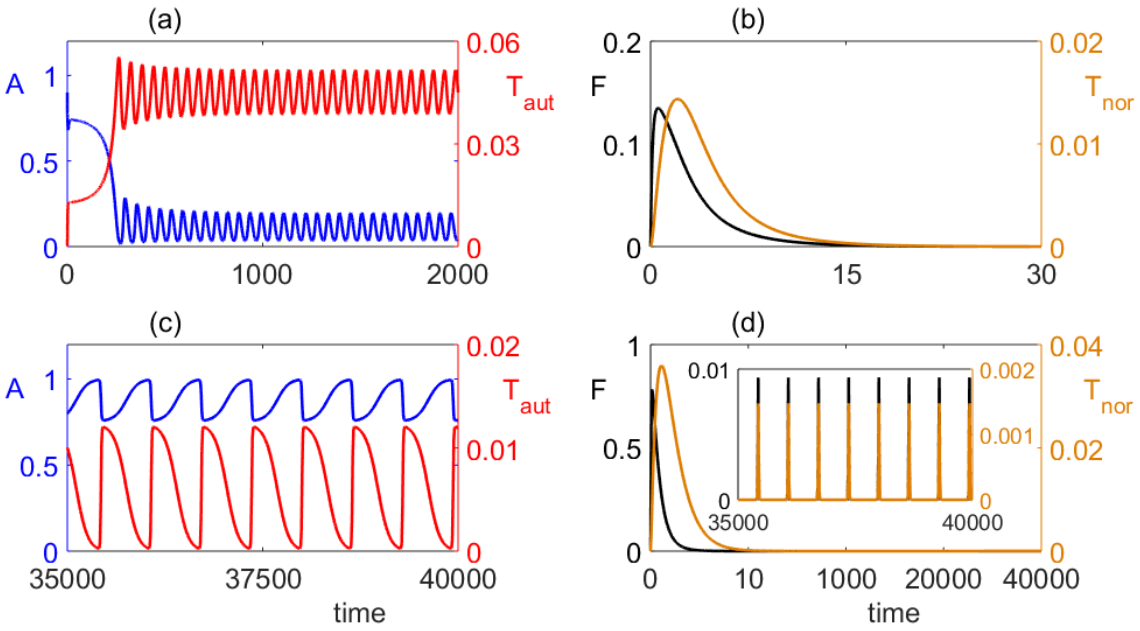

Figure 3.9: Numerical solution of the model (3.2) with the initial condition (3.3), parameter values from Table 1, and $\beta = 4$, $k = 2.1$, $\delta = 0.0017$, $\sigma_2 = 0.42$. (a), (b) $V(0) = 0.3$, $T_{reg}(0) = 600$. This system exhibits periodic oscillations around S_6^*, i.e. an autoimmune response. (c), (d) $V(0) = 9$, $T_{reg}(0) = 600$. The system exhibits periodic oscillations around S_7^*. The dynamics of T_{reg} is the same as T_{aut}.

Finally, Figure 3.10 demonstrates a situation where the system has a bi-stability between a stable steady state S_6^* and a periodic solution around S_7^*. The difference from the previous case is that instead of autoimmune regime, the system can now successfully clear the infection, without having any subsequent oscillations. Although the infection itself is cleared, it leaves an imprint on the dynamics in the form of a reduced number of organ cells and a non-zero number of autoreactive T cells.

3.5 Discussion

In this chapter I have developed and studied a model of immune response to a viral infection, with an emphasis on the role of cytokine mediating T cell activity, and T cells having different activation thresholds. Stability analysis of the model's steady states has allowed us to identify regimes with different dynamical behaviour depending on system parameters. When the product of infection rate and the rate of production of new virus particles is smaller than the product of the rates of viral clearance and death of infected cells, the immune system is able to successfully

clear the infection without further consequences for either the host organ cells, or the immune system. In this case, the system settles on a stable disease-free steady state, characterised by the absence of infected cells and free virus, as well as zero amount of normal or autoreactive T cells. Another biologically feasible steady state that can exist in some parameter regimes is the state that also has no infected cells or free virus, but maintains non-zero levels of activated T cells. We have derived analytical conditions for steady-state and Hopf bifurcations of this state. When the disease-free steady state is unstable, the model also possesses a steady state with all cell populations being positive, which biologically corresponds to a state of chronic infection.

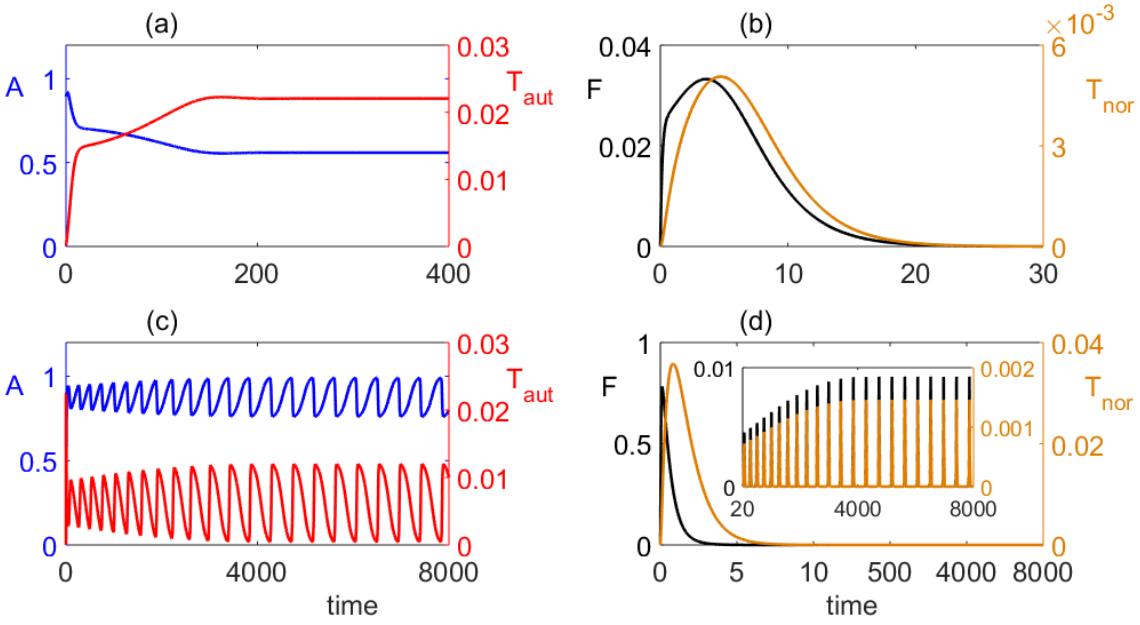

Figure 3.10: Numerical simulation of the model (3.2) with the initial condition (3.3), parameter values from Table 1, and $\beta = 4$, $k = 2.1$, $\delta = 0.0024$, $\sigma_2 = 0.7$. (a), (b) $V(0) = 0.05$, $T_{reg}(0) = 300$. The system converges to S_6^*. (c), (d) $V(0) = 9$, $T_{reg}(0) = 300$. The system exhibits periodic oscillations around S_7^*. The dynamics of T_{reg} is the same as T_{aut}.

To investigate how the system behaves in different parameter regimes, I have solved it numerically, paying particular attention to cases where more than one steady state can be feasible. This has allowed us to identify regions of multi-stability, where for the same parameter values, depending on the initial conditions the system can approach either two distinct steady states, or a steady state and a periodic solution. In the case where the disease-free steady state is stable, such a regime has a very important potential clinical significance, as effectively it suggests that

whether or not a given patient is able to clear the infection or will go on to develop autoimmunity depends not only on the rate of performance of their immune system, but also on the magnitude of viral challenge they experience and the amount of regulatory T cells they have before the infection. Numerical simulations for the autoimmune regime illustrate how initial infection leads to a rapid growth in the number of infected cells, resulting in the growth of populations of normal and autoreactive T cells, which clear the infection, but on a longer time-scale the system exhibits sustained periodic oscillations that can be associated with periods of relapses and remission, characteristic for many autoimmune diseases. For the case where the disease-free steady state is unstable, the bi-stability can occur between an autoimmune steady state and a chronic state, or a period orbit around the latter. A number of earlier models have looked into bi-stability in the immune dynamics, and the model analysed in this chapter provides further clues regarding the important role played by cytokines in controlling the dynamics of immune response. In the regime of bi-stability, I have discovered that the initial state of the immune system, and the initial viral load determine the course and outcome of the immune response, a result that would be interesting to test in an experimental setting.

There are several directions in which the model presented in this chapter could be extended to make it more realistic. One possibility is to include in the model other potentially relevant aspects of immune system dynamics, such as antibodies and memory T cells [194, 195], or the effects of T cells on secretion of IL-2 [179]. This is particularly important from the perspective that clinically the onset of autoimmune disease is often taking place on a much longer scale than the timescale of a regular immune response to a viral infection, so memory T cells can be expected to play a more substantial role. Another aspect that is particularly relevant for our model is the fact that activation thresholds can themselves change during the process of immune response, hence, one could explicitly include the dynamics of activation thresholds as an extra component of the model [63, 66, 67, 68]. To account for the fact that immune response is a very complex multi-factor process, it is important to investigate the effects of stochasticity on the dynamics of immune response. Therefore, in the next chapter I analyse the effects of stochasticity on the dynamics of the model 3.2. Many viruses are known to have a non-negligible lag phase in their virus

cycle, which includes such processes as virus attachment, cell penetration and uncoating, virus assembly, maturation, and release of new virions. All these processes result in the delay in production and release of new virus particles, thus having an impact on the dynamics of immune response and potential onset and development of autoimmune disease. Mathematically, the lag phase can be represented using time delays in the relevant terms of the model, and the available data on lag phase for viruses associated with triggering or exacerbating autoimmune diseases can be used to validate the model. Thus in Chapter 5 I study the dynamics of immune response with particular emphasis on the role of time delays and the effects of T cells on secretion of IL-2.

Chapter 4

Stochastic effects in autoimmune dynamics

This chapter is based on the publication F. Fatehi, S.N. Kyrychko, A. Ross, Y.N. Kyrychko, K.B. Blyuss, Stochastic effects in autoimmune dynamics, *Front. Physiol.* **9**, 45, 2018.

In this chapter I propose and analyse a stochastic model of immune response to a viral infection and subsequent autoimmunity, with account for the populations of T cells with different activation thresholds, regulatory T cells, and cytokines. I show analytically and numerically how stochasticity can result in sustained oscillations around deterministically stable steady states, and I also investigate stochastic dynamics in the regime of bi-stability. These results provide a possible explanation for experimentally observed variations in the progression of autoimmune disease. Computations of the variance of stochastic fluctuations provide practically important insights into how the size of these fluctuations depends on various biological parameters, and this also gives a headway for comparison with experimental data on variation in the observed numbers of T cells and organ cells affected by infection. In the next section starting with a system of ordinary differential equations, I apply the methodology of continuous-time Markov chains (CTMC) to derive a Kolmogorov, or chemical master equation, describing the dynamics of a probability distribution of finding the system in a particular state. To make further analytical and numerical progress, I derive an Itô stochastic differential equation, whose solutions provide similar stochastic paths to those of the CTMC models. This then

allows me to numerically study the stationary multivariate probability distributions for the states in the model, explore stochastic amplification, determine how the magnitude of stochastic fluctuations around deterministic steady states depends on various parameters, and investigate the effects of initial conditions on the outcome in the case of bi-stability between different dynamical states. These results suggest that the experimentally observed variation in the progression of autoimmune disease can be attributed to stochastic amplification, and they also provide insights into how the variance of fluctuations depends on parameters, which can guide new laboratory experiments.

4.1 Methods

4.1.1 Continuous-time Markov chain model of immune dynamics

In Chapter 3 I introduced and analysed a deterministic model for autoimmune dynamics with account for the populations of T cells with different activation thresholds and cytokines. The analysis showed that depending on parameters and initial conditions, the model can support the regimes of *normal disease clearance*, where an initial infection is cleared without further consequences for immune dynamics, *chronic infection* characterised by a persistent presence of infected cells in the body, the state of *autoimmune behaviour* where after clearance of initial infection, the immune system supports stable endogenous oscillations in the number of autoreactive T cells, which can be interpreted in the clinical practice of autoimmune disease as periods of relapses and remissions, and the state where this steady state is stable. In this chapter unlike the model (3.1), I consider the situation where the process of producing virions by infected cells is quite fast, hence, I do not explicitly incorporate a separate compartment for free virus. Therefore, the new deterministic model for immune response to a viral infection, as illustrated in a diagram shown in Fig. 4.1, has the form

$$
\begin{aligned}
\frac{dA}{dt} &= rA\left(1-\frac{A}{N}\right) - \beta AF - \mu_a T_{aut} A,\\
\frac{dF}{dt} &= \beta AF - d_F F - \mu_F T_{nor} F - \mu_a T_{aut} F,\\
\frac{dT_{in}}{dt} &= \lambda_{in} - d_{in} T_{in} - \alpha T_{in} F,\\
\frac{dT_{reg}}{dt} &= \lambda_r - d_r T_{reg} + p_1 \alpha T_{in} F + \rho_1 I T_{reg},\\
\frac{dT_{nor}}{dt} &= p_2 \alpha T_{in} F - d_n T_{nor} + \rho_2 I T_{nor},\\
\frac{dT_{aut}}{dt} &= (1-p_1-p_2)\alpha T_{in} F - d_a T_{aut} - \delta T_{reg} T_{aut} + \rho_3 I T_{aut},\\
\frac{dI}{dt} &= \sigma_1 T_{nor} + \sigma_2 T_{aut} - d_i I,
\end{aligned}
\tag{4.1}
$$

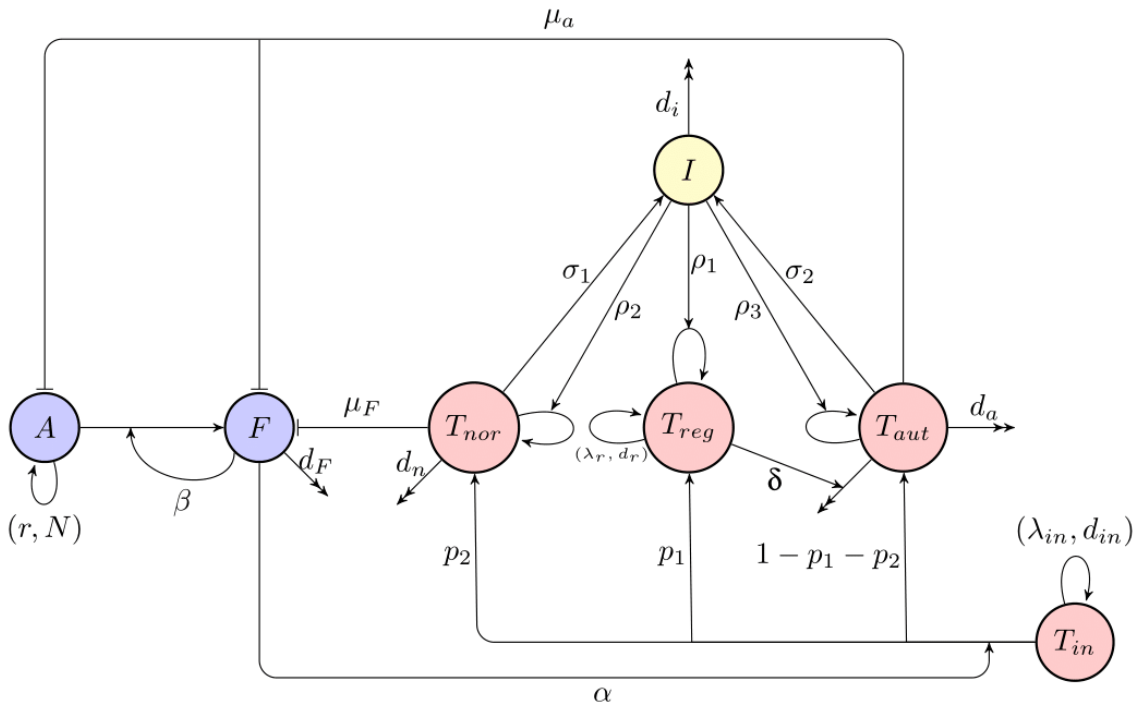

Figure 4.1: A schematic diagram of immune response to infection. Blue indicates host cells (susceptible and infected), red denotes T cells (naïve, regulatory, normal activated, and autoreactive), yellow shows cytokines (interleukin-2).

As a first step in the analysis of stochastic effects in immune dynamics, I construct a CTMC model based on the ODE model (4.1) using the methodology developed earlier in the context of modelling stochastic effects in epidemic and immunological models [196, 197, 88]. To this end, I introduce variables $X_1(t), \ldots, X_7(t) \in \{0, 1, 2, \ldots\}$ as discrete random variables representing the number of uninfected cells,

infected cells, naïve T cells, regulatory T cells, normal activated T cells, autoreactive T cells, and interleukin-2 at time t, respectively. Let the initial condition be fixed as

$$\mathbf{X}_0 = (X_1(0), \ldots, X_7(0)) = (n_{10}, n_{20}, n_{30}, n_{40}, n_{50}, n_{60}, n_{70}).$$

The probability of finding the system in the state $\mathbf{n} = (n_1, n_2, n_3, n_4, n_5, n_6, n_7)$ with $n_i \in \{0, 1, 2, ...\}$ at time t we denote as

$$P(\mathbf{n}, t) = \text{Prob}\{\mathbf{X}(t) = \mathbf{n} | \mathbf{X}(0) = \mathbf{X}_0\}.$$

Let Δt be sufficiently small such that $\Delta X_i(t) = X_i(t + \Delta t) - X_i(t)$, and the probability of $\Delta X_i(t) \notin \{-1, 0, 1\}$ is $o(\Delta t)$ for $1 \leq i \leq 7$. The CTMC can then be formulated as a birth and death process in each of the variables [196]. The infinitesimal transition probabilities corresponding to Fig. 4.1 are as follows,

$$\text{Prob}(\Delta\mathbf{X}=\mathbf{i}|\mathbf{X}=\mathbf{n})=\begin{cases} q_1\Delta t+o(\Delta t), & \mathbf{i}=(1,0,0,0,0,0,0),\\ q_2\Delta t+o(\Delta t), & \mathbf{i}=(-1,0,0,0,0,0,0),\\ q_3\Delta t+o(\Delta t), & \mathbf{i}=(-1,1,0,0,0,0,0),\\ q_4\Delta t+o(\Delta t), & \mathbf{i}=(0,0,1,0,0,0,0),\\ q_5\Delta t+o(\Delta t), & \mathbf{i}=(0,0,-1,0,0,0,0),\\ q_6\Delta t+o(\Delta t), & \mathbf{i}=(0,0,-1,0,1,0,0),\\ q_7\Delta t+o(\Delta t), & \mathbf{i}=(0,0,-1,0,1,0,0),\\ q_8\Delta t+o(\Delta t), & \mathbf{i}=(0,0,-1,0,0,1,0),\\ q_9\Delta t+o(\Delta t), & \mathbf{i}=(0,-1,0,0,0,0,0),\\ q_{10}\Delta t+o(\Delta t), & \mathbf{i}=(0,0,0,1,0,0,0),\\ q_{11}\Delta t+o(\Delta t), & \mathbf{i}=(0,0,0,-1,0,0,0),\\ q_{12}\Delta t+o(\Delta t), & \mathbf{i}=(0,0,0,0,1,0,0),\\ q_{13}\Delta t+o(\Delta t), & \mathbf{i}=(0,0,0,0,-1,0,0),\\ q_{14}\Delta t+o(\Delta t), & \mathbf{i}=(0,0,0,0,0,1,0),\\ q_{15}\Delta t+o(\Delta t), & \mathbf{i}=(0,0,0,0,0,-1,0),\\ q_{16}\Delta t+o(\Delta t), & \mathbf{i}=(0,0,0,0,0,0,1),\\ q_{17}\Delta t+o(\Delta t), & \mathbf{i}=(0,0,0,0,0,0,-1),\\ 1-\sum\limits_{i=1}^{17}q_i\Delta t+o(\Delta t), & \mathbf{i}=(0,0,0,0,0,0,0),\\ o(\Delta t), & \text{otherwise,}\end{cases}\tag{4.2}$$

where

$$q_1=b_1n_1+b_2n_1^2,\quad q_2=d_1n_1+d_2n_1^2+\mu_an_1n_6,\quad q_3=\beta n_1n_2,\quad q_4=\lambda_{in},$$
$$q_5=d_{in}n_3,\quad q_6=p_1\alpha n_2n_3,\quad q_7=p_2\alpha n_2n_3,\quad q_8=(1-p_1-p_2)\alpha n_2n_3,$$
$$q_9=(d_F+\mu_Fn_5+\mu_an_6)n_2,\quad q_{10}=\lambda_r+\rho_1n_4n_7,\quad q_{11}=d_rn_4,\quad q_{12}=\rho_2n_5n_7,$$
$$q_{13}=d_nn_5,\quad q_{14}=\rho_3n_6n_7,\quad q_{15}=(d_a+\delta n_4)n_6,\quad q_{16}=\sigma_1n_5+\sigma_2n_6,\quad q_{17}=d_in_7.$$

Here, $b_1 n_1 + b_2 n_1^2$ and $d_1 n_1 + d_2 n_1^2$ are natural birth and death rates for uninfected cells with $b_1 - d_1 = r$ and $d_2 - b_2 = r/N$ [196]. In this model for the numerical simulations I used $b_2 = 0$.

The probabilities $P(\mathbf{n}, t)$ satisfy the following master equation (forward Kolmogorov equation) as $\Delta t \to 0$ [198, 199, 91].

$$\begin{aligned}\frac{dP(\mathbf{n},t)}{dt} =&\{(\varepsilon_1^- - 1)q_1 + (\varepsilon_1^+ - 1)q_2 + (\varepsilon_1^+\varepsilon_2^- - 1)q_3 + (\varepsilon_3^- - 1)q_4 + (\varepsilon_3^+ - 1)q_5 \\ &+ (\varepsilon_3^+\varepsilon_4^- - 1)q_6 + (\varepsilon_3^+\varepsilon_5^- - 1)q_7 + (\varepsilon_3^+\varepsilon_6^- - 1)q_8 + (\varepsilon_2^+ - 1)q_9 \\ &+ (\varepsilon_4^- - 1)q_{10} + (\varepsilon_4^+ - 1)q_{11} + (\varepsilon_5^- - 1)q_{12} + (\varepsilon_5^+ - 1)q_{13} + (\varepsilon_6^- - 1)q_{14} \\ &+ (\varepsilon_6^+ - 1)q_{15} + (\varepsilon_7^- - 1)q_{16} + (\varepsilon_7^+ - 1)q_{17}\}P(\mathbf{n},t). \end{aligned} \tag{4.3}$$

where the operators $\varepsilon_i^{\pm}$ are defined as follows,

$$\varepsilon_i^{\pm} f(n_1, n_2, n_3, n_4, n_5, n_6, n_7, t) = f(n_1, ..., n_i \pm 1, ..., n_7, t), \text{ for each } 1 \le i \le 7,$$

and if $n_i < 0$ for any $1 \le i \le 7$, then $P(\mathbf{n}, t) = 0$.

By solving this master equation, one can find the probability density function for this model. However, since this is a high-dimensional difference-differential equation, solving it is a very challenging task. Normally, the number of events occurring in a small time step in the CTMC model is extremely large, hence using the CTMC model for plotting stochastic trajectories is computationally intensive [200]. A much more computationally efficient approach is to use chemical Langevin equations [201, 202], also known as Itô stochastic differential equation (SDE) models, which provide similar sample paths to those of the CTMC models [200]. While both Itô and Stratonovich interpretations of stochastic calculus can be applied [203], in biological applications Itô formulation is more frequently used due to its non-anticipatory nature and a closer connection to numerical implementation [204, 205, 196].

4.1.2 Stochastic differential equation model

To derive Itô SDE model, let $\mathbf{Y}(t) = (Y_1(t), Y_2(t), Y_3(t), Y_4(t), Y_5(t), Y_6(t), Y_7(t))$ be a continuous random vector for the sizes of various cell compartments at time t.

Table 4.1: Possible state changes $\Delta\mathbf{Y}$ during a small time interval Δt

i	$(\Delta\mathbf{Y})_i^T$	Probability $P_i\Delta t$
1	$(1,0,0,0,0,0,0)$	$(b_1Y_1 + b_2{Y_1}^2)\Delta t$
2	$(-1,0,0,0,0,0,0)$	$(d_1Y_1 + d_2{Y_1}^2 + \mu_aY_6Y_1)\Delta t$
3	$(-1,1,0,0,0,0,0)$	$\beta Y_1Y_2\Delta t$
4	$(0,0,1,0,0,0,0)$	$\lambda_{in}\Delta t$
5	$(0,0,-1,0,0,0,0)$	$d_{in}Y_3\Delta t$
6	$(0,0,-1,1,0,0,0)$	$p_1\alpha Y_3Y_2\Delta t$
7	$(0,0,-1,0,1,0,0)$	$p_2\alpha Y_3Y_2\Delta t$
8	$(0,0,-1,0,0,1,0)$	$(1-p_1-p_2)\alpha Y_3Y_2\Delta t$
9	$(0,-1,0,0,0,0,0)$	$(d_F + \mu_FY_5 + \mu_aY_6)Y_2\Delta t$
10	$(0,0,0,1,0,0,0)$	$(\lambda_r + \rho_1Y_7Y_4)\Delta t$
11	$(0,0,0,-1,0,0,0)$	$d_rY_4\Delta t$
12	$(0,0,0,0,1,0,0)$	$\rho_2Y_7Y_5\Delta t$
13	$(0,0,0,0,-1,0,0)$	$d_nY_5\Delta t$
14	$(0,0,0,0,0,1,0)$	$\rho_3Y_7Y_6\Delta t$
15	$(0,0,0,0,0,-1,0)$	$(d_a + \delta Y_4)Y_6\Delta t$
16	$(0,0,0,0,0,0,1)$	$(\sigma_1Y_5 + \sigma_2Y_6)\Delta t$
17	$(0,0,0,0,0,0,-1)$	$d_iY_7\Delta t$
18	$(0,0,0,0,0,0,0)$	$1 - \sum_{i=1}^{17} P_i\Delta t$

Similar to the CTMC model, I assume that Δt is small enough so that during this time interval at most one change can occur in state variables. These changes together with their probabilities are listed in Table 4.1 [205], which is again based on Fig. 4.1 and transitions in the CTMC model (4.2). Using this table of possible state changes, one can compute the expectation vector and covariance matrix of $\Delta\mathbf{Y}$ for sufficiently small Δt [200, 206]. The expectation vector to order Δt is given by

$$\mathbb{E}(\Delta\mathbf{Y}) \approx \sum_{i=1}^{17} P_i(\Delta\mathbf{Y})_i\Delta t = \boldsymbol{\mu}\Delta t,$$

where

$$\boldsymbol{\mu} = \begin{pmatrix} P_1 - P_2 - P_3 \\ P_3 - P_9 \\ P_4 - P_5 - P_6 - P_7 - P_8 \\ P_6 + P_{10} - P_{11} \\ P_7 + P_{12} - P_{13} \\ P_8 + P_{14} - P_{15} \\ P_{16} - P_{17} \end{pmatrix}$$

is the drift vector, which has the same form as the right-hand side of the deterministic model (4.1). The covariance matrix is obtained by keeping terms of order Δt only, i.e.

$$\mathrm{cov}(\Delta\mathbf{Y}) = \mathbb{E}\left[(\Delta\mathbf{Y})(\Delta\mathbf{Y})^T\right] - \mathbb{E}\left[\Delta\mathbf{Y}\right]\left(\mathbb{E}\left[\Delta\mathbf{Y}\right]\right)^T \approx \mathbb{E}\left[(\Delta\mathbf{Y})(\Delta\mathbf{Y})^T\right]$$

$$= \sum_{i=1}^{17} P_i(\Delta\mathbf{Y})_i(\Delta\mathbf{Y}_i)^T\Delta t = \Sigma\Delta t,$$

where

$$\Sigma = \begin{pmatrix} P_1+P_2+P_3 & -P_3 & 0 & 0 & 0 & 0 & 0 \\ -P_3 & P_3+P_9 & 0 & 0 & 0 & 0 & 0 \\ 0 & 0 & P_4+P_5+P_6+P_7+P_8 & -P_6 & -P_7 & -P_8 & 0 \\ 0 & 0 & -P_6 & P_6+P_{10}+P_{11} & 0 & 0 & 0 \\ 0 & 0 & -P_7 & 0 & P_7+P_{12}+P_{13} & 0 & 0 \\ 0 & 0 & -P_8 & 0 & 0 & P_8+P_{14}+P_{15} & 0 \\ 0 & 0 & 0 & 0 & 0 & 0 & P_{16}+P_{17} \end{pmatrix}$$

is a 7×7 covariance matrix. To derive Itô SDE model, I need to find a diffusion matrix H defined according to $HH^T = \Sigma$. Although this matrix is not unique, different forms of this matrix give equivalent systems [205, 206].

If one rewrites the covariance matrix Σ in the form

$$\Sigma = \begin{pmatrix} U & \mathbf{0} & \mathbf{0} \\ \mathbf{0} & W & \mathbf{0} \\ \mathbf{0} & \mathbf{0} & Z \end{pmatrix},$$

with

$$U = \begin{pmatrix} P_1+P_2+P_3 & -P_3 \\ -P_3 & P_3+P_9 \end{pmatrix}, \quad Z = P_{16}+P_{17},$$

and

$$W = \begin{pmatrix} P_4+P_5+P_6+P_7+P_8 & -P_6 & -P_7 & -P_8 \\ -P_6 & P_6+P_{10}+P_{11} & 0 & 0 \\ -P_7 & 0 & P_7+P_{12}+P_{13} & 0 \\ -P_8 & 0 & 0 & P_8+P_{14}+P_{15} \end{pmatrix},$$

we can define three matrices H_1, H_2 and H_3 as follows,

$$H_1 = \begin{pmatrix} \sqrt{P_1 + P_2} & -\sqrt{P_3} & 0 \\ 0 & \sqrt{P_3} & \sqrt{P_9} \end{pmatrix}, \quad H_3 = \sqrt{P_{16} + P_{17}},$$

$$H_2 = \begin{pmatrix} \sqrt{P_4 + P_5} & -\sqrt{P_6} & -\sqrt{P_7} & -\sqrt{P_8} & 0 & 0 & 0 \\ 0 & \sqrt{P_6} & 0 & 0 & \sqrt{P_{10} + P_{11}} & 0 & 0 \\ 0 & 0 & \sqrt{P_7} & 0 & 0 & \sqrt{P_{12} + P_{13}} & 0 \\ 0 & 0 & 0 & \sqrt{P_8} & 0 & 0 & \sqrt{P_{14} + P_{15}} \end{pmatrix}.$$

Now if we consider

$$H = \begin{pmatrix} H_1 & \mathbf{0} & \mathbf{0} \\ \mathbf{0} & H_2 & \mathbf{0} \\ \mathbf{0} & \mathbf{0} & H_3 \end{pmatrix},$$

then $HH^T = \Sigma$, where H is a 7×11 matrix. The Itô SDE model now has the form

$$\begin{cases} d\mathbf{Y}(t) = \boldsymbol{\mu} dt + H d\mathbf{W}(t), \\ \mathbf{Y}(0) = (A(0), F(0), T_{in}(0), T_{reg}(0), T_{nor}(0), T_{aut}(0), I(0))^T, \end{cases} \tag{4.4}$$

and $\mathbf{W}(t) = [W_1(t), W_2(t), ..., W_{11}(t)]^T$ is a vector of eleven independent Wiener processes [205].

In order to make further analytical progress, I find an approximate probability density function for the model (4.4) as given by an approximate solution of the master equation [205, 199]. Let $P(\mathbf{Y}, t)$ be the probability density function of the model (4.4). Then $P(\mathbf{Y}, t)$ satisfies the following Fokker-Planck equation [205, 207] which is an approximation of the master equation

$$\begin{cases} \dfrac{\partial P(\mathbf{Y}, t)}{\partial t} = -\sum_{i=1}^{7} \dfrac{\partial}{\partial y_i} \left[\mu_i P(\mathbf{Y}, t)\right] + \dfrac{1}{2} \sum_{i=1}^{7} \sum_{j=1}^{7} \dfrac{\partial^2}{\partial y_i \partial y_j} \left[\Sigma_{ij} P(\mathbf{Y}, t)\right], \\ \\ P(\mathbf{Y}, 0) = \delta_7(\mathbf{Y} - \mathbf{Y}_0). \end{cases}$$

By solving this PDE, one can find the probability density function of our model, but since this equation is high-dimensional and linear, solving it analytically is impossible. Hence, I use another approach, a so-called system size expansion or

van Kampen's Ω-expansion [199], which is a method for constructing a continuous approximation to a discrete stochastic model [88, 89], which allows one to study stochastic fluctuations around deterministic attractors [208].

4.1.3 System size expansion

In order to apply the van Kampen's approach, I consider fluctuations within a systematic expansion of the master equation for a large system size Ω. Specifically, one can write each $n_i(t)$ as a deterministic part of order Ω plus a fluctuation of order $\Omega^{1/2}$ as follows,

$$n_i(t) = \Omega x_i(t) + \Omega^{1/2}\zeta_i(t), \quad i = 1, \ldots, 7, \tag{4.5}$$

where $x_i(t)$ and $\zeta_i(t)$ are two continuous variables, and $\Omega x_i(t) = \mathbb{E}[n_i(t)]$. The probability density $P(\mathbf{n}, t)$ satisfying the master equation (4.3) is now represented by the probability density $\Pi(\boldsymbol{\zeta}, t)$, i.e. $\Pi(\boldsymbol{\zeta}, t) = P(\mathbf{n}, t) = P\left(\Omega\mathbf{x} + \Omega^{1/2}\boldsymbol{\zeta}, t\right)$, which implies

$$\frac{dP(\mathbf{n}, t)}{dt} = \frac{\partial \Pi}{\partial t} - \sum_{i=1}^{7} \Omega^{1/2} \frac{dx_i}{dt} \frac{\partial \Pi}{\partial \zeta_i}. \tag{4.6}$$

To expand the master equation (4.3) in a power series in $\Omega^{-1/2}$, I use the following expansion for the step operators

$$\varepsilon_i^{\pm} = 1 \pm \Omega^{-1/2} \frac{\partial}{\partial \zeta_i} + \frac{1}{2}\Omega^{-1} \frac{\partial^2}{\partial \zeta_i^2} \pm \cdots. \tag{4.7}$$

Therefore

$$\begin{aligned} \varepsilon_i^+ \varepsilon_j^- &= \left(1 + \Omega^{-1/2} \frac{\partial}{\partial \zeta_i} + \frac{1}{2}\Omega^{-1} \frac{\partial^2}{\partial \zeta_i^2} + \cdots\right)\left(1 - \Omega^{-1/2} \frac{\partial}{\partial \zeta_j} + \frac{1}{2}\Omega^{-1} \frac{\partial^2}{\partial \zeta_j^2} - \cdots\right) \\ &= 1 + \Omega^{-1/2}\left(\frac{\partial}{\partial \zeta_i} - \frac{\partial}{\partial \zeta_j}\right) + \Omega^{-1}\left(\frac{1}{2}\frac{\partial^2}{\partial \zeta_i^2} - \frac{\partial^2}{\partial \zeta_i \partial \zeta_j} + \frac{1}{2}\frac{\partial^2}{\partial \zeta_j^2}\right) + \cdots, \end{aligned} \tag{4.8}$$

for $1 \leq i, j \leq 7$. One can simplify q_i's as follows,

$$\begin{aligned} q_1 &= b_1 n_1 + b_2 {n_1}^2 = b_1\left(\Omega x_1 + \Omega^{1/2}\zeta_1\right) + b_2\left(\Omega^2 x_1^2 + \Omega\zeta_1^2 + 2\Omega^{3/2} x_1 \zeta_1\right) \\ &= b_1\left(\Omega x_1 + \Omega^{1/2}\zeta_1\right) + \underbrace{b_2\Omega}_{\widetilde{b}_2}\left(\Omega x_1^2 + \zeta_1^2 + 2\Omega^{1/2} x_1 \zeta_1\right) \\ &= \widetilde{b}_2\zeta_1^2 + \left(b_1\zeta_1 + 2\widetilde{b}_2 x_1 \zeta_1\right)\Omega^{1/2} + \left(b_1 x_1 + \widetilde{b}_2 x_1^2\right)\Omega, \end{aligned}$$

$$
\begin{aligned}
q_2 &= d_1 n_1 + d_2 {n_1}^2 + \mu_a n_6 n_1 \\
&= d_1 \left(\Omega x_1 + \Omega^{1/2}\zeta_1\right) + d_2 \left(\Omega^2 x_1^2 + \Omega\zeta_1^2 + 2\Omega^{3/2} x_1\zeta_1\right) + \mu_a \left(\Omega x_1 + \Omega^{1/2}\zeta_1\right)\left(\Omega x_6 + \Omega^{1/2}\zeta_6\right) \\
&= d_1 \left(\Omega x_1 + \Omega^{1/2}\zeta_1\right) + \underbrace{d_2\Omega}_{\widetilde{d}_2}\left(\Omega x_1^2 + \zeta_1^2 + 2\Omega^{1/2} x_1\zeta_1\right) + \underbrace{\mu_a\Omega}_{\widetilde{\mu}_a}\left(\Omega^{1/2} x_1 + \zeta_1\right)\left(\Omega^{1/2} x_6 + \zeta_6\right) \\
&= d_1 \left(\Omega x_1 + \Omega^{1/2}\zeta_1\right) + \widetilde{d}_2 \left(\Omega x_1^2 + \zeta_1^2 + 2\Omega^{1/2} x_1\zeta_1\right) + \widetilde{\mu}_a \left(\Omega x_1 x_6 + \Omega^{1/2} x_1\zeta_6 + \Omega^{1/2} x_6\zeta_1 + \zeta_1\zeta_6\right) \\
&= \widetilde{\mu}_a\zeta_1\zeta_6 + \left(d_1\zeta_1 + 2\widetilde{d}_2 x_1\zeta_1 + \widetilde{\mu}_a x_1\zeta_6 + \widetilde{\mu}_a x_6\zeta_1\right)\Omega^{1/2} + \left(d_1 x_1 + \widetilde{d}_2 x_1^2 + \widetilde{\mu}_a x_1 x_6\right)\Omega,
\end{aligned}
$$

$$
\begin{aligned}
q_3 &= \beta n_1 n_2 = \beta \left(\Omega x_1 + \Omega^{1/2}\zeta_1\right)\left(\Omega x_2 + \Omega^{1/2}\zeta_2\right) = \underbrace{\beta\Omega}_{\widetilde{\beta}}\left(\Omega^{1/2} x_1 + \zeta_1\right)\left(\Omega^{1/2} x_2 + \zeta_2\right) \\
&= \widetilde{\beta}\left(\Omega x_1 x_2 + \Omega^{1/2} x_1\zeta_2 + \Omega^{1/2} x_2\zeta_1 + \zeta_1\zeta_2\right) \\
&= \widetilde{\beta}\zeta_1\zeta_2 + \left(\widetilde{\beta} x_1\zeta_2 + \widetilde{\beta} x_2\zeta_1\right)\Omega^{1/2} + \widetilde{\beta} x_1 x_2\Omega,
\end{aligned}
$$

$$
q_4 = \lambda_{in} = \underbrace{\frac{\lambda_{in}}{\Omega}}_{\widetilde{\lambda}_{in}}\Omega = \widetilde{\lambda}_{in}\Omega,
$$

$$
q_5 = d_{in} n_3 = d_{in}\left(\Omega x_3 + \Omega^{1/2}\zeta_3\right) = d_{in}\zeta_3\Omega^{1/2} + d_{in} x_3\Omega,
$$

In a similar way we can easily show

$$
q_6 = p_1\widetilde{\alpha}\zeta_2\zeta_3 + \left(p_1\widetilde{\alpha} x_2\zeta_3 + p_1\widetilde{\alpha} x_3\zeta_2\right)\Omega^{1/2} + p_1\widetilde{\alpha} x_2 x_3\Omega,
$$

$$
q_7 = p_2\widetilde{\alpha}\zeta_2\zeta_3 + \left(p_2\widetilde{\alpha} x_2\zeta_3 + p_2\widetilde{\alpha} x_3\zeta_2\right)\Omega^{1/2} + p_2\widetilde{\alpha} x_2 x_3\Omega,
$$

$$
q_8 = (1 - p_1 - p_2)\left[\widetilde{\alpha}\zeta_2\zeta_3 + \widetilde{\alpha} x_2\zeta_3 + \widetilde{\alpha} x_3\zeta_2\Omega^{1/2} + \widetilde{\alpha} x_2 x_3\Omega\right],
$$

$$
\begin{aligned}
q_9 = &\left(\widetilde{\mu}_F\zeta_2\zeta_5 + \widetilde{\mu}_a\zeta_2\zeta_6\right) + \left(d_F + \widetilde{\mu}_F x_2\zeta_5 + \widetilde{\mu}_F x_5\zeta_2 + \widetilde{\mu}_a x_2\zeta_6 + \widetilde{\mu}_a x_6\zeta_2\right)\Omega^{1/2} \\
&+ \left(d_F x_2 + \widetilde{\mu}_F x_2 x_5 + \widetilde{\mu}_a x_2 x_6\right)\Omega,
\end{aligned}
$$

$$
q_{10} = \widetilde{\rho}_1\zeta_4\zeta_7 + \left(\widetilde{\rho}_1 x_4\zeta_7 + \widetilde{\rho}_1 x_7\zeta_4\right)\Omega^{1/2} + \left(\widetilde{\lambda}_r + \widetilde{\rho}_1 x_4 x_7\right)\Omega,
$$

$$q_{11} = d_r\zeta_4\Omega^{1/2} + d_r x_4\Omega,$$

$$q_{12} = \widetilde{\rho}_2\zeta_5\zeta_7 + \left(\widetilde{\rho}_2 x_5\zeta_7 + \widetilde{\rho}_2 x_7\zeta_5\right)\Omega^{1/2} + \widetilde{\rho}_2 x_5 x_7\Omega,$$

$$q_{13} = d_n\zeta_5\Omega^{1/2} + d_n x_5\Omega,$$

$$q_{14} = \widetilde{\rho}_3\zeta_6\zeta_7 + \left(\widetilde{\rho}_3 x_6\zeta_7 + \widetilde{\rho}_3 x_7\zeta_6\right)\Omega^{1/2} + \widetilde{\rho}_3 x_6 x_7\Omega,$$

$$q_{15} = \widetilde{\delta}\zeta_4\zeta_6 + \left(d_a\zeta_6 + \widetilde{\delta}x_4\zeta_6 + \widetilde{\delta}x_6\zeta_4\right)\Omega^{1/2} + \left(d_a x_6 + \widetilde{\delta}x_4 x_6\right)\Omega,$$

$$q_{16} = \left(\sigma_1\zeta_5 + \sigma_2\zeta_6\right)\Omega^{1/2} + (\sigma_1 x_5 + \sigma_2 x_6)\Omega,$$

$$q_{17} = d_i\zeta_7\Omega^{1/2} + d_i x_5\Omega,$$

where

$$\mu_F = \frac{\widetilde{\mu}_F}{\Omega}, \quad \alpha = \frac{\widetilde{\alpha}}{\Omega}, \quad \delta = \frac{\widetilde{\delta}}{\Omega}, \quad \rho_i = \frac{\widetilde{\rho}_i}{\Omega},\ i = 1,2,3, \quad \lambda_r = \widetilde{\lambda}_r\Omega.$$

If we substitute equations (4.6), (4.7), (4.8), and q_i's in the master equation (4.3), it is clear that on the right side we have terms of order $\Omega^{1/2}$, Ω^0, and $\Omega^{-n/2}$, for $n \in \mathbb{N}$, but on the left side we have just terms of order $\Omega^{1/2}$ and Ω^0. To derive a linear Fokker-Planck equation I ignore those terms of order $\Omega^{-n/2}$, for $n \in \mathbb{N}$. Therefore, I substitute the following expansions

$$\begin{aligned}
\varepsilon_i^{\pm} - 1 &= \pm\Omega^{-1/2}\frac{\partial}{\partial\zeta_i} + \frac{1}{2}\Omega^{-1}\frac{\partial^2}{\partial\zeta_i^2}, \\
\varepsilon_i^{+}\varepsilon_j^{-} - 1 &= \Omega^{-1/2}\left(\frac{\partial}{\partial\zeta_i} - \frac{\partial}{\partial\zeta_j}\right) + \Omega^{-1}\left(\frac{1}{2}\frac{\partial^2}{\partial\zeta_i^2} - \frac{\partial^2}{\partial\zeta_i\partial\zeta_j} + \frac{1}{2}\frac{\partial^2}{\partial\zeta_j^2}\right),
\end{aligned}$$

for $1 \leq i, j \leq 7$, and in q_i's I do not consider constant terms (terms of order Ω^0).

It is clear that terms of order $\Omega^{1/2}$ are proportional to $\dfrac{\partial \Pi}{\partial \zeta_i}$ for $i = 1, 2, ..., 7$. Now if we consider terms of order $\Omega^{1/2}$ we would have

$$-\Omega^{1/2}\frac{dx_1}{dt}\frac{\partial \Pi}{\partial \zeta_1} = \left(-\Omega^{-1/2}\frac{\partial}{\partial \zeta_1}\right)\left[\left(b_1 x_1 + \widetilde{b}_2 x_1^2\right)\Omega\right]\Pi + \left(\Omega^{-1/2}\frac{\partial}{\partial \zeta_1}\right)\left[\widetilde{\beta} x_1 x_2 \Omega\right]\Pi + \left(\Omega^{-1/2}\frac{\partial}{\partial \zeta_1}\right)\left[\left(d_1 x_1 + \widetilde{d}_2 x_1^2 + \widetilde{\mu}_a x_1 x_6\right)\Omega\right]\Pi,$$

$$-\Omega^{1/2}\frac{dx_2}{dt}\frac{\partial \Pi}{\partial \zeta_2} = \left(-\Omega^{-1/2}\frac{\partial}{\partial \zeta_2}\right)\left[\widetilde{\beta} x_1 x_2 \Omega\right]\Pi + \left(\Omega^{-1/2}\frac{\partial}{\partial \zeta_2}\right)\left[\left(d_F x_2 + \widetilde{\mu}_F x_2 x_5 + \widetilde{\mu}_a x_2 x_6\right)\Omega\right]\Pi,$$

$$-\Omega^{1/2}\frac{dx_3}{dt}\frac{\partial \Pi}{\partial \zeta_3} = \left(-\Omega^{-1/2}\frac{\partial}{\partial \zeta_3}\right)\left[\widetilde{\lambda}_{in}\Omega\right]\Pi + \left(\Omega^{-1/2}\frac{\partial}{\partial \zeta_3}\right)\left[d_{in} x_3 \Omega\right]\Pi + \left(\Omega^{-1/2}\frac{\partial}{\partial \zeta_3}\right)\left[p_1 \widetilde{\alpha} x_2 x_3 \Omega\right]\Pi + \left(\Omega^{-1/2}\frac{\partial}{\partial \zeta_3}\right)\left[p_2 \widetilde{\alpha} x_2 x_3 \Omega\right]\Pi + \left(\Omega^{-1/2}\frac{\partial}{\partial \zeta_3}\right)\left[(1 - p_1 - p_2)\widetilde{\alpha} x_2 x_3 \Omega\right]\Pi,$$

$$-\Omega^{1/2}\frac{dx_4}{dt}\frac{\partial \Pi}{\partial \zeta_4} = \left(-\Omega^{-1/2}\frac{\partial}{\partial \zeta_4}\right)\left[p_1 \widetilde{\alpha} x_2 x_3 \Omega\right]\Pi + \left(-\Omega^{-1/2}\frac{\partial}{\partial \zeta_4}\right)\left[\left(\widetilde{\lambda}_r + \widetilde{\rho}_1 x_4 x_7\right)\Omega\right]\Pi + \left(\Omega^{-1/2}\frac{\partial}{\partial \zeta_4}\right)\left[d_r x_4 \Omega\right]\Pi,$$

$$-\Omega^{1/2}\frac{dx_5}{dt}\frac{\partial \Pi}{\partial \zeta_5} = \left(-\Omega^{-1/2}\frac{\partial}{\partial \zeta_5}\right)\left[p_2 \widetilde{\alpha} x_2 x_3 \Omega\right]\Pi + \left(-\Omega^{-1/2}\frac{\partial}{\partial \zeta_5}\right)\left[\widetilde{\rho}_2 x_5 x_7 \Omega\right]\Pi - \left(\Omega^{-1/2}\frac{\partial}{\partial \zeta_5}\right)\left[d_n x_5 \Omega\right]\Pi,$$

$$-\Omega^{1/2}\frac{dx_6}{dt}\frac{\partial \Pi}{\partial \zeta_6} = \left(-\Omega^{-1/2}\frac{\partial}{\partial \zeta_6}\right)\left[(1 - p_1 - p_2)\widetilde{\alpha} x_2 x_3 \Omega\right]\Pi + \left(-\Omega^{-1/2}\frac{\partial}{\partial \zeta_6}\right)\left[\widetilde{\rho}_3 x_6 x_7 \Omega\right]\Pi + \left(\Omega^{-1/2}\frac{\partial}{\partial \zeta_6}\right)\left[\left(d_a x_6 + \widetilde{\delta} x_4 x_6\right)\Omega\right]\Pi,$$

$$-\Omega^{1/2}\frac{dx_7}{dt}\frac{\partial \Pi}{\partial \zeta_7} = \left(-\Omega^{-1/2}\frac{\partial}{\partial \zeta_7}\right)\left[(\sigma_1 x_5 + \sigma_2 x_6)\Omega\right]\Pi + \left(\Omega^{-1/2}\frac{\partial}{\partial \zeta_7}\right)\left[d_i x_5 \Omega\right]\Pi.$$

Thus we derive a deterministic model for the macroscopic behaviour as follows,

$$\begin{aligned}
\frac{dx_1}{dt} &= b_1x_1 + \widetilde{b}_2x_1^2 - d_1x_1 - \widetilde{d}_2x_1^2 - \widetilde{\beta}x_1x_2 - \widetilde{\mu}_ax_1x_6,\\
\frac{dx_2}{dt} &= \widetilde{\beta}x_1x_2 - d_Fx_2 - \widetilde{\mu}_Fx_2x_5 - \widetilde{\mu}_ax_2x_6,\\
\frac{dx_3}{dt} &= \widetilde{\lambda}_{in} - d_{in}x_3 - \widetilde{\alpha}x_2x_3,\\
\frac{dx_4}{dt} &= \widetilde{\lambda}_r - d_rx_4 + p_1\widetilde{\alpha}x_2x_3 + \widetilde{\rho}_1x_4x_7,\\
\frac{dx_5}{dt} &= p_2\widetilde{\alpha}x_2x_3 - d_nx_5 + \widetilde{\rho}_2x_5x_7,\\
\frac{dx_6}{dt} &= (1-p_1-p_2)\widetilde{\alpha}x_2x_3 - d_ax_6 - \widetilde{\delta}x_4x_6 + \widetilde{\rho}_3x_6x_7,\\
\frac{dx_7}{dt} &= \sigma_1x_5 + \sigma_2x_6 - d_ix_7.
\end{aligned} \tag{4.9}$$

Model (4.9) has been analysed in Chapter 3, and it can have at most four biologically feasible steady states. The first one, a disease-free steady state, is given by

$$S_1^* = \left(\frac{b_1-d_1}{\widetilde{d}_2-\widetilde{b}_2}, 0, \frac{\widetilde{\lambda}_{in}}{d_{in}}, \frac{\widetilde{\lambda}_r}{d_r}, 0, 0, 0\right),$$

and it is stable if $d_F > \widetilde{\beta}$. The second and third steady states can be found as

$$S_2^* = \left(0, 0, \frac{\widetilde{\lambda}_{in}}{d_{in}}, x_4^*, 0, \frac{d_i\left(d_a+\widetilde{\delta}x_4^*\right)}{\widetilde{\rho}_3\sigma_2}, \frac{d_a+\widetilde{\delta}x_4^*}{\widetilde{\rho}_3}\right),$$

and

$$S_3^* = \left(\frac{\widetilde{\rho}_3\sigma_2(b_1-d_1) - \widetilde{\mu}_ad_i\left(d_a+\widetilde{\delta}x_4^*\right)}{\widetilde{\rho}_3\sigma_2\left(\widetilde{d}_2-\widetilde{b}_2\right)}, 0, \frac{\widetilde{\lambda}_{in}}{d_{in}}, x_4^*, 0, \frac{d_i\left(d_a+\widetilde{\delta}x_4^*\right)}{\widetilde{\rho}_3\sigma_2}, \frac{d_a+\widetilde{\delta}x_4^*}{\widetilde{\rho}_3}\right),$$

where x_4^* satisfies the following quadratic equation

$$\widetilde{\rho}_1\widetilde{\delta}\left(x_4^*\right)^2 + \left(\widetilde{\rho}_1d_a - \widetilde{\rho}_3d_r\right)x_4^* + \widetilde{\rho}_3\widetilde{\lambda}_r = 0. \tag{4.10}$$

These steady states are stable, provided

$$\frac{\sigma_2}{\widetilde{\mu}_ad_i}K < \frac{d_a+\widetilde{\delta}x_4^*}{\widetilde{\rho}_3} < \frac{d_n}{\widetilde{\rho}_2}, \quad \widetilde{\delta}\widetilde{\rho}_1(x_4^*)^2 > \widetilde{\lambda}_r\widetilde{\rho}_3,$$

$$\widetilde{\rho}_3\widetilde{\lambda}_r^2 + \widetilde{\rho}_3d_i\widetilde{\lambda}_rx_4^* - \widetilde{\rho}_3d_id_a(x_4^*)^2 - \widetilde{\delta}(\widetilde{\rho}_1d_a + \widetilde{\rho}_3d_i)(x_4^*)^3 - \widetilde{\rho}_1\widetilde{\delta}^2(x_4^*)^4 > 0,$$

where $K = 1$ for S_2^*, and $K = \left(\widetilde{\beta} - d_F\right) / \left(1 + \widetilde{\beta}\right)$ for S_3^*. Biologically, the steady state S_2^* represents the death of organ cells, while S_3^* corresponds to an autoimmune regime.

The last steady state S_4^* has all of its components positive and corresponds to the state of chronic infection.

Terms of order Ω^0 give the following Fokker-Planck equation

$$
\begin{aligned}
\frac{\partial \Pi}{\partial t} =& - b_1 \frac{\partial(\zeta_1 \Pi)}{\partial \zeta_1} - 2\widetilde{b}_2 x_1 \frac{\partial(\zeta_1 \Pi)}{\partial \zeta_1} + d_1 \frac{\partial(\zeta_1 \Pi)}{\partial \zeta_1} + 2\widetilde{d}_2 x_1 \frac{\partial(\zeta_1 \Pi)}{\partial \zeta_1} + \widetilde{\mu}_a x_1 \frac{\partial(\zeta_6 \Pi)}{\partial \zeta_1} \\
&+ \widetilde{\mu}_a x_6 \frac{\partial(\zeta_1 \Pi)}{\partial \zeta_1} + \widetilde{\beta} x_1 \frac{\partial(\zeta_2 \Pi)}{\partial \zeta_1} + \widetilde{\beta} x_2 \frac{\partial(\zeta_1 \Pi)}{\partial \zeta_1} - \widetilde{\beta} x_1 \frac{\partial(\zeta_2 \Pi)}{\partial \zeta_2} - \widetilde{\beta} x_2 \frac{\partial(\zeta_1 \Pi)}{\partial \zeta_2} \\
&+ d_F \frac{\partial(\zeta_2 \Pi)}{\partial \zeta_2} + \widetilde{\mu}_F x_2 \frac{\partial(\zeta_5 \Pi)}{\partial \zeta_2} + \widetilde{\mu}_F x_5 \frac{\partial(\zeta_2 \Pi)}{\partial \zeta_2} + \widetilde{\mu}_a x_2 \frac{\partial(\zeta_6 \Pi)}{\partial \zeta_2} + \widetilde{\mu}_a x_6 \frac{\partial(\zeta_2 \Pi)}{\partial \zeta_2} \\
&+ d_{in} \frac{\partial(\zeta_3 \Pi)}{\partial \zeta_3} + p_1 \widetilde{\alpha} x_2 \frac{\partial(\zeta_3 \Pi)}{\partial \zeta_3} + p_1 \widetilde{\alpha} x_3 \frac{\partial(\zeta_2 \Pi)}{\partial \zeta_3} + p_2 \widetilde{\alpha} x_2 \frac{\partial(\zeta_3 \Pi)}{\partial \zeta_3} + p_2 \widetilde{\alpha} x_3 \frac{\partial(\zeta_2 \Pi)}{\partial \zeta_3} \\
&+ (1 - p_1 - p_2) \widetilde{\alpha} x_2 \frac{\partial(\zeta_3 \Pi)}{\partial \zeta_3} + (1 - p_1 - p_2) \widetilde{\alpha} x_3 \frac{\partial(\zeta_2 \Pi)}{\partial \zeta_3} - p_1 \widetilde{\alpha} x_2 \frac{\partial(\zeta_3 \Pi)}{\partial \zeta_4} \\
&- p_1 \widetilde{\alpha} x_3 \frac{\partial(\zeta_2 \Pi)}{\partial \zeta_4} - \widetilde{\rho}_1 x_4 \frac{\partial(\zeta_7 \Pi)}{\partial \zeta_4} - \widetilde{\rho}_1 x_7 \frac{\partial(\zeta_4 \Pi)}{\partial \zeta_4} + d_r \frac{\partial(\zeta_4 \Pi)}{\partial \zeta_4} - p_2 \widetilde{\alpha} x_2 \frac{\partial(\zeta_3 \Pi)}{\partial \zeta_5} \\
&- p_2 \widetilde{\alpha} x_3 \frac{\partial(\zeta_2 \Pi)}{\partial \zeta_5} - \widetilde{\rho}_2 x_5 \frac{\partial(\zeta_7 \Pi)}{\partial \zeta_5} - \widetilde{\rho}_2 x_7 \frac{\partial(\zeta_5 \Pi)}{\partial \zeta_5} + d_n \frac{\partial(\zeta_5 \Pi)}{\partial \zeta_5} \\
&- (1 - p_1 - p_2) \widetilde{\alpha} x_2 \frac{\partial(\zeta_3 \Pi)}{\partial \zeta_6} - (1 - p_1 - p_2) \widetilde{\alpha} x_3 \frac{\partial(\zeta_2 \Pi)}{\partial \zeta_6} - \widetilde{\rho}_3 x_6 \frac{\partial(\zeta_7 \Pi)}{\partial \zeta_6} \\
&- \widetilde{\rho}_3 x_7 \frac{\partial(\zeta_6 \Pi)}{\partial \zeta_6} + d_a \frac{\partial(\zeta_6 \Pi)}{\partial \zeta_6} + \widetilde{\delta} x_4 \frac{\partial(\zeta_6 \Pi)}{\partial \zeta_6} + \widetilde{\delta} x_6 \frac{\partial(\zeta_4 \Pi)}{\partial \zeta_6} - \sigma_1 \frac{\partial(\zeta_5 \Pi)}{\partial \zeta_7} \\
&- \sigma_2 \frac{\partial(\zeta_6 \Pi)}{\partial \zeta_7} + d_i \frac{\partial(\zeta_7 \Pi)}{\partial \zeta_7} + \frac{1}{2} b_1 x_1 \frac{\partial^2 \Pi}{\partial \zeta_1^2} + \frac{1}{2} \widetilde{b}_2 x_1^2 \frac{\partial^2 \Pi}{\partial \zeta_1^2} + \frac{1}{2} d_1 x_1 \frac{\partial^2 \Pi}{\partial \zeta_1^2} + \frac{1}{2} \widetilde{d}_2 x_1^2 \frac{\partial^2 \Pi}{\partial \zeta_1^2} \\
&+ \frac{1}{2} \widetilde{\mu}_a x_1 x_6 \frac{\partial^2 \Pi}{\partial \zeta_1^2} + \frac{1}{2} \widetilde{\beta} x_1 x_2 \frac{\partial^2 \Pi}{\partial \zeta_1^2} + \frac{1}{2} \widetilde{\beta} x_1 x_2 \frac{\partial^2 \Pi}{\partial \zeta_2^2} + \frac{1}{2} d_F x_2 \frac{\partial^2 \Pi}{\partial \zeta_2^2} + \frac{1}{2} \widetilde{\mu}_F x_2 x_5 \frac{\partial^2 \Pi}{\partial \zeta_2^2} \\
&+ \frac{1}{2} \widetilde{\mu}_a x_2 x_6 \frac{\partial^2 \Pi}{\partial \zeta_2^2} + \frac{1}{2} \widetilde{\lambda}_{in} \frac{\partial^2 \Pi}{\partial \zeta_3^2} + \frac{1}{2} d_{in} x_3 \frac{\partial^2 \Pi}{\partial \zeta_3^2} + \frac{1}{2} p_1 \widetilde{\alpha} x_2 x_3 \frac{\partial^2 \Pi}{\partial \zeta_3^2} + \frac{1}{2} p_2 \widetilde{\alpha} x_2 x_3 \frac{\partial^2 \Pi}{\partial \zeta_3^2} \\
&+ \frac{1}{2} (1 - p_1 - p_2) \widetilde{\alpha} x_2 x_3 \frac{\partial^2 \Pi}{\partial \zeta_3^2} + \frac{1}{2} p_1 \widetilde{\alpha} x_2 x_3 \frac{\partial^2 \Pi}{\partial \zeta_4^2} + \frac{1}{2} \widetilde{\lambda}_r \frac{\partial^2 \Pi}{\partial \zeta_4^2} + \frac{1}{2} \widetilde{\rho}_1 x_4 x_7 \frac{\partial^2 \Pi}{\partial \zeta_4^2} \\
&+ \frac{1}{2} d_r x_4 \frac{\partial^2 \Pi}{\partial \zeta_4^2} + \frac{1}{2} p_2 \widetilde{\alpha} x_2 x_3 \frac{\partial^2 \Pi}{\partial \zeta_5^2} + \frac{1}{2} \widetilde{\rho}_2 x_5 x_7 \frac{\partial^2 \Pi}{\partial \zeta_5^2} + \frac{1}{2} d_n x_5 \frac{\partial^2 \Pi}{\partial \zeta_5^2} + \frac{1}{2} \widetilde{\rho}_3 x_6 x_7 \frac{\partial^2 \Pi}{\partial \zeta_6^2} \\
&+ \frac{1}{2} (1 - p_1 - p_2) \widetilde{\alpha} x_2 x_3 \frac{\partial^2 \Pi}{\partial \zeta_6^2} + \frac{1}{2} d_a x_6 \frac{\partial^2 \Pi}{\partial \zeta_6^2} + \frac{1}{2} \widetilde{\delta} x_4 x_6 \frac{\partial^2 \Pi}{\partial \zeta_6^2} + \frac{1}{2} \sigma_1 x_5 \frac{\partial^2 \Pi}{\partial \zeta_7^2} \\
&+ \frac{1}{2} \sigma_2 x_6 \frac{\partial^2 \Pi}{\partial \zeta_7^2} + \frac{1}{2} d_i x_7 \frac{\partial^2 \Pi}{\partial \zeta_7^2} - \widetilde{\beta} x_1 x_2 \frac{\partial^2 \Pi}{\partial \zeta_1 \partial \zeta_2} - p_1 \widetilde{\alpha} x_2 x_3 \frac{\partial^2 \Pi}{\partial \zeta_3 \partial \zeta_4} \\
&- p_2 \widetilde{\alpha} x_2 x_3 \frac{\partial^2 \Pi}{\partial \zeta_3 \partial \zeta_5} - (1 - p_1 - p_2) \widetilde{\alpha} x_2 x_3 \frac{\partial^2 \Pi}{\partial \zeta_3 \partial \zeta_6}.
\end{aligned}
$$

If we gather it, it would be as follows,

$$
\begin{aligned}
\frac{\partial \Pi}{\partial t} = -\Bigg[& \left(b_1 + 2\widetilde{b}_2 x_1 - d_1 - 2\widetilde{d}_2 x_1 - \widetilde{\mu}_a x_6 - \widetilde{\beta} x_2\right) \frac{\partial(\zeta_1 \Pi)}{\partial \zeta_1} - \widetilde{\beta} x_1 \frac{\partial(\zeta_2 \Pi)}{\partial \zeta_1} \\
& - \widetilde{\mu}_a x_1 \frac{\partial(\zeta_6 \Pi)}{\partial \zeta_1} + \widetilde{\beta} x_2 \frac{\partial(\zeta_1 \Pi)}{\partial \zeta_2} + \left(\widetilde{\beta} x_1 - d_F - \widetilde{\mu}_F x_5 - \widetilde{\mu}_a x_6\right) \frac{\partial(\zeta_2 \Pi)}{\partial \zeta_2} \\
& - \widetilde{\mu}_F x_2 \frac{\partial(\zeta_5 \Pi)}{\partial \zeta_2} - \widetilde{\mu}_a x_2 \frac{\partial(\zeta_6 \Pi)}{\partial \zeta_2} - \widetilde{\alpha} x_3 \frac{\partial(\zeta_2 \Pi)}{\partial \zeta_3} - (d_{in} + \widetilde{\alpha} x_2) \frac{\partial(\zeta_3 \Pi)}{\partial \zeta_3} \\
& + p_1 \widetilde{\alpha} x_3 \frac{\partial(\zeta_2 \Pi)}{\partial \zeta_4} + p_1 \widetilde{\alpha} x_2 \frac{\partial(\zeta_3 \Pi)}{\partial \zeta_4} + (\widetilde{\rho}_1 x_7 - d_r) \frac{\partial(\zeta_4 \Pi)}{\partial \zeta_4} + \widetilde{\rho}_1 x_4 \frac{\partial(\zeta_7 \Pi)}{\partial \zeta_4} \\
& + p_2 \widetilde{\alpha} x_3 \frac{\partial(\zeta_2 \Pi)}{\partial \zeta_5} + p_2 \widetilde{\alpha} x_2 \frac{\partial(\zeta_3 \Pi)}{\partial \zeta_5} + (\widetilde{\rho}_2 x_7 - d_n) \frac{\partial(\zeta_5 \Pi)}{\partial \zeta_5} + \widetilde{\rho}_2 x_5 \frac{\partial(\zeta_7 \Pi)}{\partial \zeta_5} \\
& + (1 - p_1 - p_2) \widetilde{\alpha} x_3 \frac{\partial(\zeta_2 \Pi)}{\partial \zeta_6} + (1 - p_1 - p_2) \widetilde{\alpha} x_2 \frac{\partial(\zeta_3 \Pi)}{\partial \zeta_6} - \widetilde{\delta} x_6 \frac{\partial(\zeta_4 \Pi)}{\partial \zeta_6} \\
& + \left(\widetilde{\rho}_3 x_7 - d_a - \widetilde{\delta}\right) x_4 \frac{\partial(\zeta_6 \Pi)}{\partial \zeta_6} + \widetilde{\rho}_3 x_6 \frac{\partial(\zeta_7 \Pi)}{\partial \zeta_6} + \\
& \sigma_1 \frac{\partial(\zeta_5 \Pi)}{\partial \zeta_7} + \sigma_2 \frac{\partial(\zeta_6 \Pi)}{\partial \zeta_7} - d_i \frac{\partial(\zeta_7 \Pi)}{\partial \zeta_7} \Bigg] \\
+ \frac{1}{2} \Bigg\{ & \left(b_1 x_1 + \widetilde{b}_2 x_1^2 + d_1 x_1 + \widetilde{d}_2 x_1^2 + \widetilde{\beta} x_1 x_2 + \widetilde{\mu}_a x_1 x_6\right) \frac{\partial^2 \Pi}{\partial \zeta_1^2} - 2\widetilde{\beta} x_1 x_2 \frac{\partial^2 \Pi}{\partial \zeta_1 \partial \zeta_2} \\
& + \left(\widetilde{\beta} x_1 x_2 + d_F x_2 + \widetilde{\mu}_F x_2 x_5 + \widetilde{\mu}_a x_2 x_6\right) \frac{\partial^2 \Pi}{\partial \zeta_2^2} + \left(\widetilde{\lambda}_{in} + d_{in} x_3 + \widetilde{\alpha} x_2 x_3\right) \frac{\partial^2 \Pi}{\partial \zeta_3^2} \\
& - 2p_1 \widetilde{\alpha} x_2 x_3 \frac{\partial^2 \Pi}{\partial \zeta_3 \partial \zeta_4} - 2p_2 \widetilde{\alpha} x_2 x_3 \frac{\partial^2 \Pi}{\partial \zeta_3 \partial \zeta_5} - 2(1 - p_1 - p_2) \widetilde{\alpha} x_2 x_3 \frac{\partial^2 \Pi}{\partial \zeta_3 \partial \zeta_6} \\
& + \left(\widetilde{\lambda}_r + d_r x_4 + p_1 \widetilde{\alpha} x_2 x_3 + \widetilde{\rho}_1 x_4 x_7\right) \frac{\partial^2 \Pi}{\partial \zeta_4^2} + (p_2 \widetilde{\alpha} x_2 x_3 + d_n x_5 + \widetilde{\rho}_2 x_5 x_7) \frac{\partial^2 \Pi}{\partial \zeta_5^2} \\
& + \left[(1 - p_1 - p_2) \widetilde{\alpha} x_2 x_3 + d_a x_6 + \widetilde{\delta} x_4 x_6 + \widetilde{\rho}_3 x_6 x_7\right] \frac{\partial^2 \Pi}{\partial \zeta_6^2} \\
& + (\sigma_1 x_5 + \sigma_2 x_6 + d_i x_7) \frac{\partial^2 \Pi}{\partial \zeta_7^2} \Bigg\}.
\end{aligned}
$$

Therefore, at the next order, stochastic fluctuations are determined by linear stochastic processes, hence, this is known as a linear noise approximation [199, 209]. The dynamics of these fluctuations is described by the following Fokker-Planck equation

$$
\frac{\partial \Pi(\boldsymbol{\zeta}, t)}{\partial t} = -\sum_{i,j} A_{ij} \frac{\partial}{\partial \zeta_i} (\zeta_j \Pi) + \frac{1}{2} \sum_{i,j} B_{ij} \frac{\partial^2 \Pi}{\partial \zeta_i \partial \zeta_j}, \tag{4.11}
$$

where A is the Jacobian matrix of system (4.9)

$$A = \begin{pmatrix} A_{11} & -\widetilde{\beta}x_1 & 0 & 0 & 0 & -\widetilde{\mu}_a x_1 & 0 \\ \widetilde{\beta}x_2 & A_{22} & 0 & 0 & -\widetilde{\mu}_F x_2 & -\widetilde{\mu}_a x_2 & 0 \\ 0 & -\widetilde{\alpha}x_3 & -d_{in} - \widetilde{\alpha}x_2 & 0 & 0 & 0 & 0 \\ 0 & p_1\widetilde{\alpha}x_3 & p_1\widetilde{\alpha}x_2 & \widetilde{\rho}_1 x_7 - d_r & 0 & 0 & \widetilde{\rho}_1 x_4 \\ 0 & p_2\widetilde{\alpha}x_3 & p_2\widetilde{\alpha}x_2 & 0 & \widetilde{\rho}_2 x_7 - d_n & 0 & \widetilde{\rho}_2 x_5 \\ 0 & p_3\widetilde{\alpha}x_3 & p_3\widetilde{\alpha}x_2 & -\widetilde{\delta}x_6 & 0 & \widetilde{\rho}_3 x_7 - d_a - \widetilde{\delta}x_4 & \widetilde{\rho}_3 x_6 \\ 0 & 0 & 0 & 0 & \sigma_1 & \sigma_2 & -d_i \end{pmatrix},$$

with $A_{11} = b_1 + 2\widetilde{b}_2 x_1 - d_1 - 2\widetilde{d}_2 x_1 - \widetilde{\mu}_a x_6 - \widetilde{\beta}x_2$, $A_{22} = \widetilde{\beta}x_1 - d_F - \widetilde{\mu}_F x_5 - \widetilde{\mu}_a x_6$ and $p_3 = 1 - p_1 - p_2$, and B is a 7×7 symmetric matrix given by

$$B_{ij} = \begin{cases} b_1 x_1 + \widetilde{b}_2 x_1^2 + d_1 x_1 + \widetilde{d}_2 x_1^2 + \widetilde{\beta}x_1 x_2 + \widetilde{\mu}_a x_1 x_6, & \text{if } (i,j) = (1,1), \\ \widetilde{\beta}x_1 x_2 + d_F x_2 + \widetilde{\mu}_F x_2 x_5 + \widetilde{\mu}_a x_2 x_6, & \text{if } (i,j) = (2,2), \\ \widetilde{\lambda}_{in} + d_{in} x_3 + \widetilde{\alpha}x_2 x_3, & \text{if } (i,j) = (3,3), \\ \widetilde{\lambda}_r + d_r x_4 + p_1\widetilde{\alpha}x_2 x_3 + \widetilde{\rho}_1 x_4 x_7, & \text{if } (i,j) = (4,4), \\ p_2\widetilde{\alpha}x_2 x_3 + d_n x_5 + \widetilde{\rho}_2 x_5 x_7, & \text{if } (i,j) = (5,5), \\ (1-p_1-p_2)\widetilde{\alpha}x_2 x_3 + d_a x_6 + \widetilde{\delta}x_4 x_6 + \widetilde{\rho}_3 x_6 x_7, & \text{if } (i,j) = (6,6), \\ \sigma_1 x_5 + \sigma_2 x_6 + d_i x_7, & \text{if } (i,j) = (7,7), \\ -\widetilde{\beta}x_1 x_2, & \text{if } (i,j) = (1,2) \text{ or } (2,1), \\ -p_1\widetilde{\alpha}x_2 x_3, & \text{if } (i,j) = (3,4) \text{ or } (4,3), \\ -p_2\widetilde{\alpha}x_2 x_3, & \text{if } (i,j) = (3,5) \text{ or } (5,3), \\ -(1-p_1-p_2)\widetilde{\alpha}x_2 x_3, & \text{if } (i,j) = (3,6) \text{ or } (6,3), \\ 0, & \text{otherwise.} \end{cases}$$

Since the Fokker-Planck equation (4.11) has constant coefficients and Dirac delta initial condition, the probability density $\Pi(\boldsymbol{\zeta}, t)$ is Gaussian [199], and hence, just the first two moments are enough to characterise it [210, 211]. Due to the way the system size expansion was introduced in (4.5), the mean values of fluctuations for all variables are zero, i.e. $\langle \zeta_i(t) \rangle = 0$ for all $1 \leq i \leq 7$, while the covariance matrix Ξ with $\Xi_{ij} = \langle \zeta_i(t)\zeta_j(t) \rangle - \langle \zeta_i(t) \rangle \langle \zeta_j(t) \rangle = \langle \zeta_i(t)\zeta_j(t) \rangle$ satisfies the following

equation [199, 211]

$$\partial_t \Xi = A\Xi + \Xi A^T + B, \tag{4.12}$$

where A^T is the transpose of A.

We are mainly interested in the dynamics of fluctuations when the oscillations of the deterministic model have died out, and the system is in a stationary state, i.e. the fluctuations take place around the steady states [208]. If the model (4.9) tends to a steady state as $t \to \infty$, then in the equation (4.11) one can substitute the values of x_i's with the corresponding constant components of that steady state to study the fluctuations around it, as described by the linear Fokker-Planck equation. At any steady state, the covariance matrix Ξ is independent of time, and the fluctuations are described by a Gaussian distribution with the zero mean and the stationary covariance satisfying the equation

$$A\Xi + \Xi A^T + B = 0.$$

In order to be able to relate the results of this analysis to simulations, it is convenient to express the covariance matrix in terms of actual numbers of cells in each compartment, rather than deviations from stationary values. To this end, I instead use the covariance matrix C defined as $C_{ij} = \langle (n_i - \langle n_i \rangle)(n_j - \langle n_j \rangle) \rangle$, which, in light of the relation $C_{ij} = \Omega \Xi_{ij}$, satisfies the following Lyapunov equation [211]

$$AC + CA^T + \Omega B = 0. \tag{4.13}$$

This equation can be solved numerically for each of the stable steady states to determine the variance of fluctuations around that steady state depending on system parameters.

4.2 Results

To simulate the dynamics of the model, I solve the system (4.4) numerically in MATLAB using the Euler-Maruyama method [196] with parameter values given in

Table 4.2, and $\Omega = 1000$. The initial condition is chosen to be of the form

$$(x_1(0), x_2(0), x_3(0), x_4(0), x_5(0), x_6(0), x_7(0)) = (18, 2, 7.2, 6.3, 0, 0, 0), \qquad (4.14)$$

which corresponds to a small number of host cells being initially infected.

Table 4.2: Table of parameters

Parameter	value	Parameter	value
b_1	2.5	d_r	0.8
$\widetilde{b}_2$	0	p_1	0.4
d_1	0.5	$\widetilde{\rho}_1$	$10/9$
$\widetilde{d}_2$	0.1	p_2	0.4
$\widetilde{\beta}$	0.1	d_n	2
$\widetilde{\mu}_a$	$40/9$	$\widetilde{\rho}_2$	$4/45$
d_F	2.2	d_a	0.002
$\widetilde{\mu}_F$	$4/3$	$\widetilde{\delta}$	$1/4500$
$\widetilde{\lambda}_{in}$	18	$\widetilde{\rho}_3$	$2/9$
d_{in}	2	σ_1	0.3
$\widetilde{\alpha}$	0.04	σ_2	0.4
$\widetilde{\lambda}_r$	108	d_i	1.2

Figure 4.2 shows the results of 20000 simulations with the initial condition (4.14) and $\sigma_2 = 1$. In the deterministic model (4.9), for $\sigma_2 = 1$ both steady states S_1^* (disease-free) and S_3^* (autoimmune state) are stable, but with the initial condition (4.14) the system is in the basin of attraction of S_3^*. In the stochastic model, the majority of trajectories also enter the attraction region of S_3^*, but a small proportion of them went into the basin of attraction of S_1^*. This figure illustrates a single stochastic path around S_1^*, and a single stochastic path around S_3^*, together with the deterministic trajectory. These individual solutions indicate that whilst deterministically, the system exhibits decaying oscillations around S_3^*, the same behaviour is observed in the stochastic simulations only upon taking an average of a very large number of simulations. At the same time, individual realisations exhibit sustained stochastic oscillations in a manner similar to that observed in models of stochastic amplification in epidemics [91, 92]. Figure 4.2 also illustrates the size of areas of one standard deviation from the mean for trajectories in the basins of attraction S_1^* and S_3^*, in which individual stochastic trajectories may exhibit stochastic oscillations [212, 90].

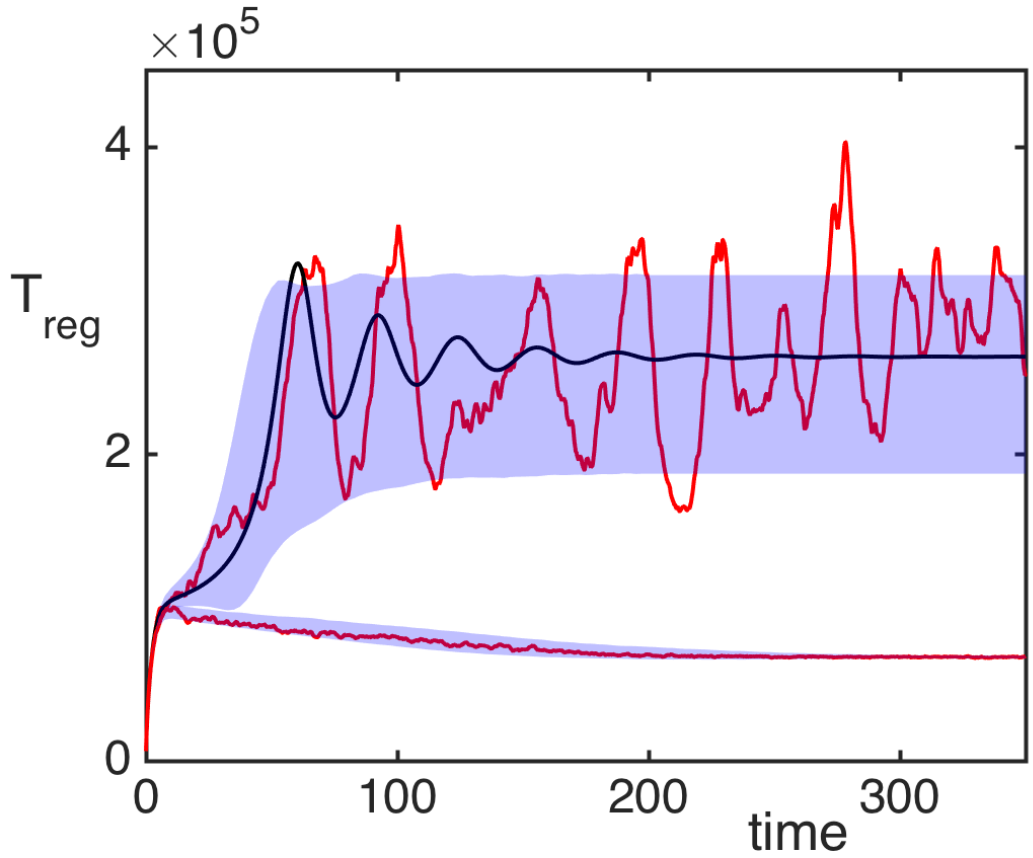

Figure 4.2: Numerical simulation of the model (4.4) with parameter values from Table 4.2, $\sigma_2 = 1$, and the initial condition (4.14). Red curves are two sample paths that have entered the basins of attraction of S_1^* or S_3^*, black curve is the deterministic trajectory from (4.1), and the shaded areas indicate the regions of one standard deviation from the mean.

Figures 4.3 (a) and (b) show temporal evolution of the probability distribution in the case of bi-stability between the steady states S_1^* and S_3^*, as illustrated in Fig. 4.2. They indicate that after some initial transient, the system reaches a stationary bimodal normal distribution. The width of the probability distribution around each stable steady state, as described by its variance or standard deviation, gives the size of fluctuations around this steady state observed in individual stochastic realisations, as is shown in Fig. 4.2. Similar behaviour has been observed in stochastic realisations of other deterministic models with bi-stability [213, 214, 215]. For the parameter values given in Table 4.2, the deterministic system exhibits a bi-stability between S_1^* and S_2^*, and with the initial condition

$$(x_1(0), x_2(0), x_3(0), x_4(0), x_5(0), x_6(0), x_7(0)) = (18, 9, 7.2, 6.3, 0, 0, 0), \qquad (4.15)$$

it is in the basin of attraction of S_2^*. Due to stochasticity, the stationary probability

distribution in this case is also bimodal, with the majority of solutions being distributed around S_2^*, and a very small number being centred around S_1^*, as can be seen in Figs. 4.3 (c) and (d). Increasing the system size Ω is known to result in the bimodal distribution becoming unimodal due to the size of fluctuations scaling as $\Omega^{-1/2}$ [200], which results in a reduced variability in trajectories [216, 215], and the same conclusion holds for the system (4.4).

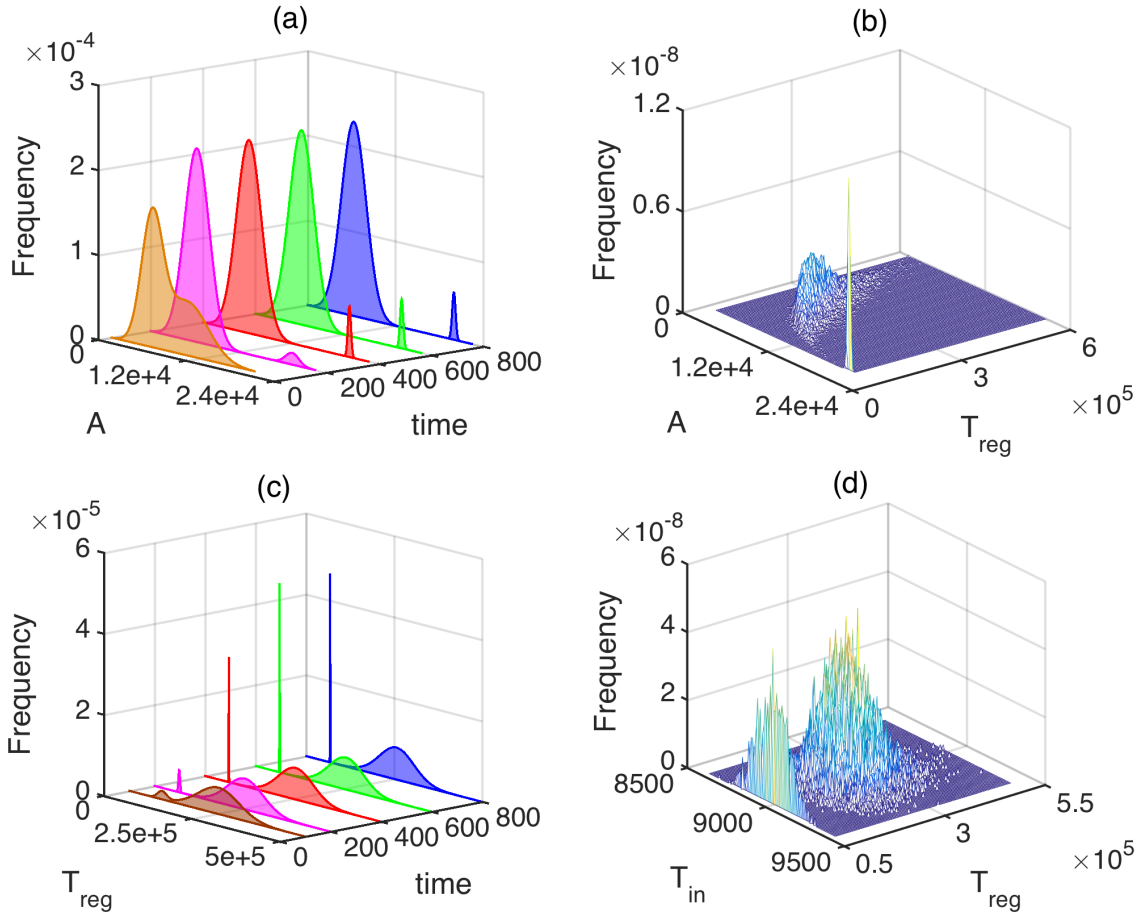

Figure 4.3: Probability distribution of solutions out of 20000 simulations. (a) and (b) with parameters from Table 4.2, but $\sigma_2 = 1$ and the initial condition (4.14). (c) and (d) with parameters from Table 4.2 and the initial condition (4.15). In (a) and (c), the probability histogram is fit to a bimodal normal distribution at different times. (b) and (d) illustrate stationary joint probability histograms.

To gain better insights into the role of initial conditions, in Fig. 4.4 I fix all parameter values, and vary initial numbers of infected cells and regulatory T cells. For the parameter combination illustrated in Fig. 4.4 (a), the deterministic model exhibits a bi-stability between a stable disease-free steady state S_1^* and a periodic oscillation around the state S_3^*, which biologically corresponds to an autoimmune regime. In the deterministic case, the black boundary provides a clear separation

of the basins of attraction of these two dynamical states, in a manner similar to that investigated recently in the context of within-cell dynamics of RNA interference [217].

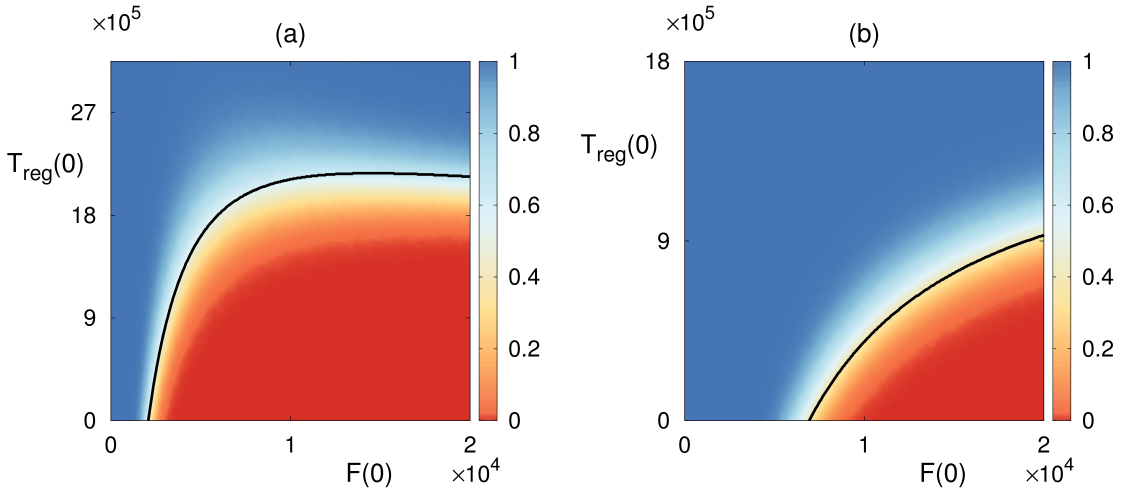

Figure 4.4: Probability of solution entering and staying in the basin of attraction of the disease-free steady state S_1^* in the bi-stability regime with $A(0) = 18000$ and $T_{in}(0) = 7200$. Black curves are the boundaries between different basins of attraction in the deterministic model. (a) With parameter values from Table 4.2, $\widetilde{\lambda}_r = 45$ and $\widetilde{\mu}_a = 10/9$, in the region below the black curve, the deterministic model exhibits a periodic solution around S_3^*, and above this curve is the deterministic basin of attraction of S_1^*. (b) With parameter values from Table 4.2, area below the black curve is the basin of attraction of S_2^*, and above it is again the basin of attraction of S_1^*.

For stochastic simulations, the colour indicates the probability of the solution going to a disease-free state S_1^*, and it shows that even in the case where deterministically the system is in the basin of attraction of one of the states, there is a non-zero probability that it will actually end up at another state, with this probability varying smoothly across the deterministic basin boundary. This figure suggests that if the initial number of infected cells is sufficiently small, or if the number of regulatory T cells is sufficiently large, the system tends to clear the infection and approach the disease-free state. On the contrary, for higher numbers of infected cells and lower numbers of regulatory cells, autoimmune regime appears to be a more likely outcome. Qualitatively similar behaviour is observed for another combination of parameters illustrated in Fig. 4.4 (b), in which case the deterministic system has a bi-stability between a disease-free steady state S_1^*, and a state S_2^* which represents the death of host cells.

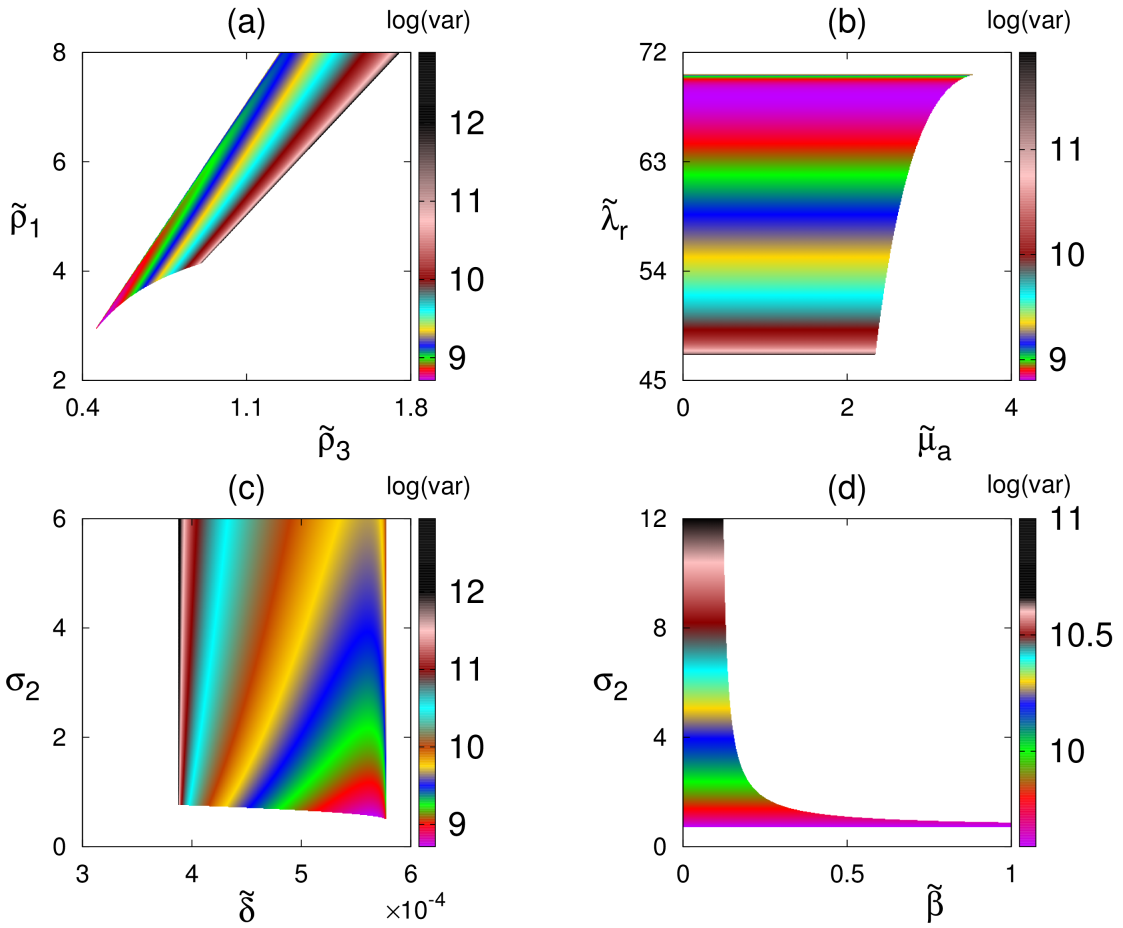

Figure 4.5: Variance of the number of regulatory T cells T_{reg} with parameter values from Table 4.2. Coloured regions indicate areas in respective parameter planes in which the autoimmune steady state S_3^* is deterministically stable.

In order to understand how biological parameters affect the size of fluctuations around steady states, in Fig. 4.5 I explore several parameter planes by first identifying parameter regions where the deterministic system has a stable steady state S_3^*, and then for each combination of parameters inside these regions, I use the Bartels-Stewart method [218, 219] to numerically solve the Lyapunov equation (4.13) and compute the variance in the number of regulatory T cell when the deterministic model is at the steady state S_3^*. One should note that in this method the variance goes to infinity as one approaches a bifurcation. Therefore, this method can only be used when a steady state is stable, and we are not close to bifurcation boundaries. The value of variance gives the square of the magnitude of oscillations observed in individual stochastic realisations. One should note that getting closer to the deterministic boundary of stability of S_3^* increases the stochastic variance of fluctuations around this steady state. The reason for this is that closer parameters are to the de-

terministic stability boundary, the less stable is the steady state, hence the larger is the amplitude of stochastic oscillations around it. Moreover, the variance increases with the rate of production of IL-2 by autoreactive T cells and the rate at which regulatory T cells suppress autoreactive T cells; it decreases with the higher rate of production of regulatory T cells, and it appears to not depend on the rate at which autoreactive T cells destroy infected cells, or on the infection rate.

4.3 Discussion

In this chapter I have analysed stochastic aspects of immune response against a viral infection with account for the populations of T cells with different activation thresholds, as well as cytokines mediating T cell activity. The CTMC model has provided an exact master equation, for which I applied a van Kampen's expansions to derive a linear Fokker-Planck equation that characterises fluctuations around the deterministic solutions. We have also explored actual stochastic trajectories of the system by deriving an SDE model and solving it numerically.

One biologically important aspect I have looked at is the influence of stochasticity on the dynamics of the system in the case where deterministically it exhibits a bi-stability between either two steady states, or a steady state and a periodic solution. In such a situation, bi-stability in the deterministic version of the model translates in the stochastic case into a stationary bimodal distribution for the probability density. To obtain further insights into details of how stochasticity affects bi-stability, I have investigated how for the fixed parameter values time evolution of the system changes depending on the initial numbers of the regulatory T cells and infected cells.

Our analysis reinforces the need to distinguish mean dynamics from individuals realisations: where in the deterministic case the system can approach a stable steady state (which represents mean behaviour of a very large number of simulations), individual realisations can exhibit sustained stochastic oscillations around that steady state, as we have seen in numerical simulations. Since in the clinical or laboratory setting one is usually dealing with single measurements of some specific biological quantities rather than their averaged values, the stochastic oscillations exhibited by our model may quite well explain observed variability in the measured levels of

infection or T cell populations. To better understand the magnitude of stochastic fluctuations around the deterministic steady states, I have solved the Lyapunov equation, which has provided us with a quantitative information on the dependence of variance of fluctuations on system parameters.

There are several directions in which the work presented in this chapter can be extended. Whilst I have used numerical simulations to compute the probability of attraction to a given steady state in the case of bi-stability, one could approach the same problem theoretically from the perspective of computing extinction probability within the framework of the CTMC model [200, 220]. The van Kampen's system size expansion could yield an expression for the power spectrum, which allows one to compute the peak frequency and amplification [208, 221, 222, 91]. From a practical perspective, future work could focus on validating theoretical results presented in this chapter using experimental measurements of the progress of autoimmune disease in animal hosts, with experimental autoimmune uveoretinitis (EAU), an autoimmune inflammation in the eyes, being one interesting possibility. In one such recent experiment, all animals were genetically identical C57BL/6 mice, but once the EAU was induced in them through inoculation, the autoimmune disease then progressed at slightly different rates [223, 94], and the measured variability in the numbers of infected cells and T cell responses could be compared to theoretical estimates of the variance as predicted by our model. From a clinical perspective, comparison of variance in the measured populations of different cells with the model conclusions will facilitate an efficient parameter identification and provide a set of prognostic criteria for the progress of autoimmunity, which can be used for risk stratification and assessment of patients with autoimmune disease. In terms of fundamental immunology, the model can be made more realistic by including additional effects, such as the control of IL-2 secretion by regulatory T cells [179], or the time delays associated with the processes of infection and mounting the immune response [224, 154, 113]. Therefore, in the next Chapter I present a time-delayed model which focuses on these features of the immune response.

Chapter 5

Effects of viral and cytokine delays on dynamics of autoimmunity

This chapter is based on the publication F. Fatehi, Y.N. Kyrychko, K.B. Blyuss, Effects of viral and cytokine delays on dynamics of autoimmunity, *Mathematics*, **6**, 66, 2018.

In this chapter I study an extension of the model (4.1) with particular focus on the role of time delays associated with the processes of infection and mounting the immune response, as well as an inhibiting effect of regulatory T cells on secretion of IL-2. In order to achieve this goal, first I introduce a time-delayed model and discuss its basic properties. Then, I propose a systematic analysis of all steady states, including conditions for their feasibility and stability, which allows us to identify parameter regions associated with different types of immune behaviour, such as, normal clearance of infection, chronic infection, and autoimmune dynamics. Later, a bifurcation analysis of the model and demonstration of various types of behaviour that the system exhibits depending on parameters and initial conditions are presented , which includes identification of attraction basins of various states.

5.1 Model derivation

In this chapter I consider a model illustrated in a diagram shown in Fig. 5.1, which is an extension of the model (4.1). I include in the model suppression of IL-2 by regulatory T cells at rate δ_2, in a manner similar to Burroughs et al. [179]. Moreover,

whilst the production of new virus particles by infected cells is assumed to be fast, I explicitly include in the model time delay τ_1 associated with the actual process of infection, which includes multiple stages of the *eclipse phase* of viral life cycle, such as virus attachment, cell penetration and uncoating [224, 154]. I also include the time delay τ_2 associated with stimulation and proliferation of T cells by IL-2, and for simplicity I assume this time delay is the same for all types of T cells, and the time delay τ_3 between antigen encounter and resulting T cell expansion [113].

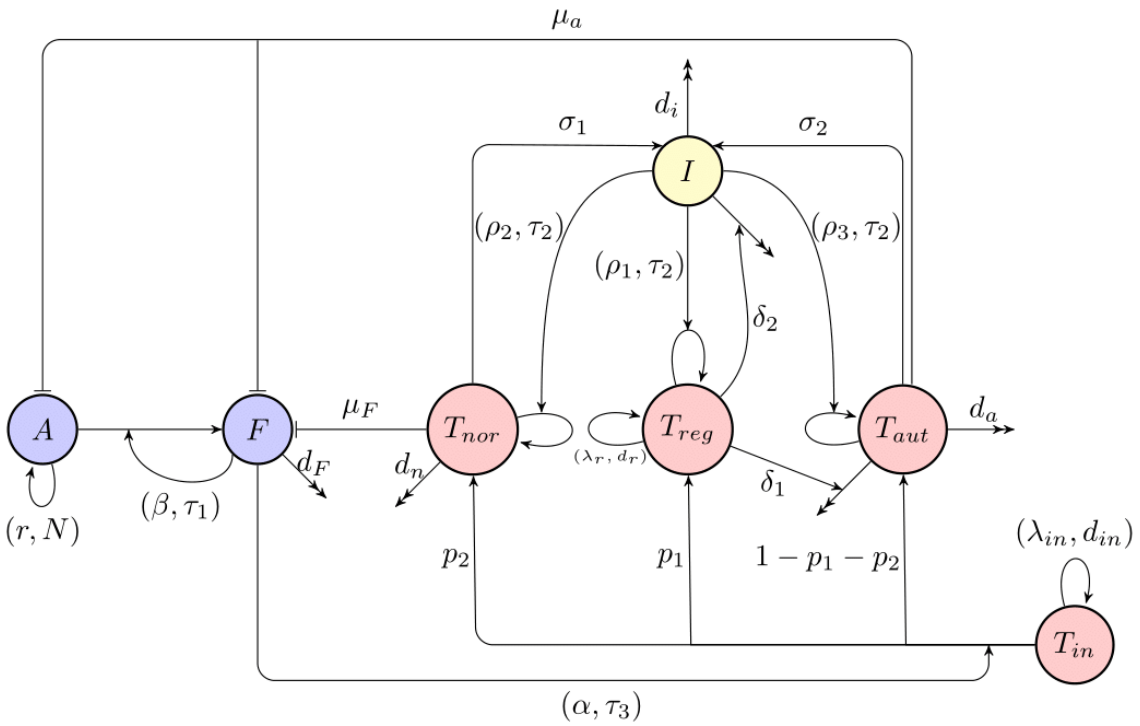

Figure 5.1: A schematic diagram of immune response to infection. Blue indicates host cells (susceptible and infected), red denotes different T cells (naïve, regulatory, normal activated, and autoreactive T cells), yellow shows cytokines (interleukin 2). τ_i inside each of the subnetworks shows the time delay associated with that process.

With the above assumptions, the complete model takes the form

$$\frac{dA}{dt} = rA\left(1 - \frac{A}{N}\right) - \beta AF - \mu_a T_{aut} A,$$

$$\frac{dF}{dt} = \beta A\left(t-\tau_1\right) F\left(t-\tau_1\right) - d_F F - \mu_F T_{nor} F - \mu_a T_{aut} F,$$

$$\frac{dT_{in}}{dt} = \lambda_{in} - d_{in} T_{in} - \alpha T_{in} F,$$

$$\frac{dT_{reg}}{dt} = \lambda_r - d_r T_{reg} + p_1 \alpha T_{in}\left(t-\tau_3\right) F\left(t-\tau_3\right) + \rho_1 I\left(t-\tau_2\right) T_{reg}\left(t-\tau_2\right),$$

$$\frac{dT_{nor}}{dt} = p_2 \alpha T_{in}\left(t-\tau_3\right) F\left(t-\tau_3\right) - d_n T_{nor} + \rho_2 I\left(t-\tau_2\right) T_{nor}\left(t-\tau_2\right),$$

$$\begin{aligned}\frac{dT_{aut}}{dt} = {} & (1-p_1-p_2)\alpha T_{in}\left(t-\tau_3\right) F\left(t-\tau_3\right) - d_a T_{aut} - \delta_1 T_{reg} T_{aut} \\ & + \rho_3 I\left(t-\tau_2\right) T_{aut}\left(t-\tau_2\right),\end{aligned}$$

$$\frac{dI}{dt} = \sigma_1 T_{nor} + \sigma_2 T_{aut} - \delta_2 T_{reg} I - d_i I.$$

Introducing non-dimensional variables

$$\begin{aligned}&T = rt, \quad A = N\hat{A}, \quad F = N\hat{F}, \quad T_{in} = \frac{\lambda_{in}}{d_{in}}\hat{T}_{in}, \quad T_{reg} = \frac{\lambda_{in}}{d_{in}}\hat{T}_{reg}, \\ &T_{nor} = \frac{\lambda_{in}}{d_{in}}\hat{T}_{nor}, \quad T_{aut} = \frac{\lambda_{in}}{d_{in}}\hat{T}_{aut}, \quad I = \frac{\lambda_{in}}{d_{in}}\hat{I},\end{aligned}$$

where

$$\begin{aligned}&\hat{\beta} = \frac{\beta N}{r}, \quad \hat{\mu}_a = \frac{\mu_a \lambda_{in}}{r d_{in}}, \quad \hat{d}_F = \frac{d_F}{r}, \quad \hat{\mu}_F = \frac{\mu_F \lambda_{in}}{r d_{in}}, \quad \hat{d}_{in} = \frac{d_{in}}{r}, \quad \hat{\alpha} = \frac{\alpha N}{r}, \\ &\hat{\lambda}_r = \frac{\lambda_r d_{in}}{\lambda_{in} r}, \quad \hat{d}_r = \frac{d_r}{r}, \quad \hat{d}_n = \frac{d_n}{r}, \quad \hat{d}_a = \frac{d_a}{r}, \quad \hat{\rho}_i = \frac{\rho_i \lambda_{in}}{r d_{in}}, \quad i = 1,2,3, \\ &\hat{\delta}_1 = \frac{\delta_1 \lambda_{in}}{r d_{in}}, \quad \hat{\delta}_2 = \frac{\delta_2 \lambda_{in}}{r d_{in}}, \quad \hat{\sigma}_1 = \frac{\sigma_1}{r}, \quad \hat{\sigma}_2 = \frac{\sigma_2}{r}, \quad \hat{d}_i = \frac{d_i}{r},\end{aligned}$$

yields a rescaled model

$$
\begin{aligned}
\frac{dA}{dT} &= A\left(1-A\right) - \beta AF - \mu_a T_{aut} A, \\
\frac{dF}{dT} &= \beta A\left(T-\tau_1\right) F\left(T-\tau_1\right) - d_F F - \mu_F T_{nor} F - \mu_a T_{aut} F, \\
\frac{dT_{in}}{dT} &= d_{in}\left(1-T_{in}\right) - \alpha T_{in} F, \\
\frac{dT_{reg}}{dT} &= \lambda_r - d_r T_{reg} + p_1 \alpha T_{in}\left(T-\tau_3\right) F\left(T-\tau_3\right) + \rho_1 I\left(T-\tau_2\right) T_{reg}\left(T-\tau_2\right), \\
\frac{dT_{nor}}{dT} &= p_2 \alpha T_{in}\left(T-\tau_3\right) F\left(T-\tau_3\right) - d_n T_{nor} + \rho_2 I\left(T-\tau_2\right) T_{nor}\left(T-\tau_2\right), \\
\frac{dT_{aut}}{dT} &= (1-p_1-p_2)\alpha T_{in}\left(T-\tau_3\right) F\left(T-\tau_3\right) - d_a T_{aut} - \delta_1 T_{reg} T_{aut} \\
&\quad + \rho_3 I\left(T-\tau_2\right) T_{aut}\left(T-\tau_2\right), \\
\frac{dI}{dT} &= \sigma_1 T_{nor} + \sigma_2 T_{aut} - \delta_2 T_{reg} I - d_i I,
\end{aligned}
\tag{5.1}
$$

where all hats in variables and parameters have been dropped for simplicity of notation, and all parameters are assumed to be positive. It is easy to show that this system is well-posed, i.e. solutions with non-negative initial conditions remain non-negative for all $t \geq 0$.

As a first step in the analysis of model (5.1), I look at its steady states

$$
S^* = \left(A^*, F^*, T_{in}^*, T_{reg}^*, T_{nor}^*, T_{aut}^*, I^*\right),
$$

that can be found by equating to zero the right-hand sides of equations (5.1) and solving the resulting system of algebraic equations, deferring the discussion of conditionally stable steady states to Section 5.2. First, I consider a situation where there are no infected cells at a steady state, i.e. $F^* = 0$, which immediately implies $T_{in}^* = 1$. In this case there are four possible combinations of steady states depending on whether T_{nor}^* and T_{aut}^* are each equal to zero or positive. If $T_{nor}^* = T_{aut}^* = 0$, there are two steady states

$$
S_1^* = \left(0, 0, 1, \frac{\lambda_r}{d_r}, 0, 0, 0\right), \quad S_2^* = \left(1, 0, 1, \frac{\lambda_r}{d_r}, 0, 0, 0\right),
$$

of which S_1^* is always unstable, and S_2^* is a disease-free conditionally stable steady

state, i.e. its stability depends on the values of parameters.

For $T^*_{nor} \neq 0$ and $T^*_{aut} = 0$, we again have two steady states

$$S^*_3 = \left(0, 0, 1, \frac{\lambda_r \rho_2}{\rho_2 d_r - \rho_1 d_n}, T^*_{nor}, 0, \frac{d_n}{\rho_2}\right), \quad S^*_4 = \left(1, 0, 1, \frac{\lambda_r \rho_2}{\rho_2 d_r - \rho_1 d_n}, T^*_{nor}, 0, \frac{d_n}{\rho_2}\right),$$

where $T^*_{nor} = \dfrac{d_n\left(\lambda_r \delta_2 \rho_2 + d_i d_r \rho_2 - d_i d_n \rho_1\right)}{\rho_2 \sigma_1 (\rho_2 d_r - \rho_1 d_n)}$, but they are both unstable for any values of parameters. In the case when $T^*_{nor} = 0$ and $T^*_{aut} \neq 0$, we have two further steady states S^*_5 and S^*_6,

$$S^*_5 = \left(0, 0, 1, T^*_{reg}, 0, \frac{\left(d_i + \delta_2 T^*_{reg}\right)\left(d_a + \delta_1 T^*_{reg}\right)}{\rho_3 \sigma_2}, \frac{d_a + \delta_1 T^*_{reg}}{\rho_3}\right),$$

$$S^*_6 = \left(A^*, 0, 1, T^*_{reg}, 0, \frac{\left(d_i + \delta_2 T^*_{reg}\right)\left(d_a + \delta_1 T^*_{reg}\right)}{\rho_3 \sigma_2}, \frac{d_a + \delta_1 T^*_{reg}}{\rho_3}\right),$$

where $A^* = 1 - \dfrac{\mu_a\left(d_i + \delta_2 T^*_{reg}\right)\left(d_a + \delta_1 T^*_{reg}\right)}{\rho_3 \sigma_2}$, and

$$T^*_{reg} = \frac{d_r \rho_3 - \rho_1 d_a \pm \sqrt{\left(d_r \rho_3 - \rho_1 d_a\right)^2 - 4\rho_1 \delta_1 \lambda_r \rho_3}}{2\rho_1 \delta}.$$

The steady state S^*_5 has $A^* = 0$, which implies the death of host cells, whereas the steady state S^*_6 corresponds to an autoimmune regime. The steady state S^*_7 with $T^*_{nor} \neq 0$ and $T^*_{aut} \neq 0$ exists only for a particular combination of parameters, namely, when

$$\delta_1 \rho_2^2 \lambda_r = (\rho_3 d_n - \rho_2 d_a)(\rho_2 d_r - \rho_1 d_n),$$

and is always unstable. Finally, when $F^* \neq 0$, the system (5.1) can have a steady state S^*_8 with all of its components being positive, but it does not appear possible to find a closed form expression for this state.

In summary, besides the unconditionally unstable steady states, i.e. steady states that are unstable for any values of parameters, the model (5.1) has at most four conditionally stable steady states: the *disease-free steady state* S^*_2, the *steady state with the death of host cells* S^*_5, the *autoimmune steady state* S^*_6, and the *persistent or chronic steady state* S^*_8. This implies that the new model has the same steady

states as the model (3.2).

5.2 Stability analysis of the steady states

5.2.1 Stability analysis of the disease-free steady state

Linearising the system (5.1) near the disease-free steady state S_2^* yields the following equation for characteristic roots λ

$$\lambda + d_F - \beta e^{-\lambda\tau_1} = 0. \tag{5.2}$$

If $d_F < \beta$, the above equation always has a real positive root for any value $\tau_1 \geq 0$, implying that the disease-free steady state is always unstable for any value of the time delays. If, however, the condition $d_F > \beta$ holds, the disease-free steady state is stable for $\tau_1 = 0$. To find out whether it can lose stability for $\tau_1 > 0$, I look for solutions of equation (5.2) in the form $\lambda = i\omega$. Separating real and imaginary parts yields

$$d_F = \beta \cos(\omega\tau_1),$$

$$\omega = -\beta \sin(\omega\tau_1).$$

Squaring and adding these two equations gives the following equation for potential Hopf frequency ω

$$\omega^2 + d_F^2 - \beta^2 = 0.$$

Since $d_F > \beta$, this equation does not have real roots for ω, suggesting that there can be no roots of the form $\lambda = i\omega$ of the characteristic equation (5.2). This implies that in the case $d_F > \beta$ the disease-free steady state S_2^* is stable for all values of the time delay $\tau_1 \geq 0$.

5.2.2 Stability analysis of the death, autoimmune and chronic steady states

The steady state S_5^* (respectively, S_6^*) is stable if

$$P < \frac{d_a + \delta_1 T_{reg}^*}{\rho_3} < \frac{d_n}{\rho_2}, \tag{5.3}$$

and all roots of the following equation have negative real part

$$\Delta(\tau_2, \lambda) = p_2(\lambda)e^{-2\lambda\tau_2} + p_1(\lambda)e^{-\lambda\tau_2} + p_0(\lambda) = 0, \tag{5.4}$$

where

$$\begin{aligned}
p_2(\lambda) =& \frac{\rho_1 \left(d_a + \delta_1 T_{reg}^*\right)^2}{\rho_3} \left(\lambda + 2d_i + \delta_2 T_{reg}^*\right), \\
p_1(\lambda) =& -\frac{\left(d_a + \delta_1 T_{reg}^*\right)}{\rho_3} \Big\{ (\rho_1 + \rho_3)\lambda^2 \\
&+ \left[\rho_1 \left(d_i + d_a + \delta_1 T_{reg}^*\right) + \rho_3 \left(d_r + 2d_i + 2\delta_2 T_{reg}^*\right)\right] \lambda \\
&+ d_i(\rho_1 d_a + 2d_r\rho_3) + \delta_2 T_{reg}^* \left(-\rho_1\delta_1 T_{reg}^* + 2d_r\rho_3\right) \Big\}, \\
p_0(\lambda) =& (\lambda + d_r) \left(\lambda + d_i + \delta_2 T_{reg}^*\right) \left(\lambda + d_a + \delta_1 T_{reg}^*\right),
\end{aligned}$$

and

$$P = \begin{cases} \dfrac{\sigma_2}{\mu_a \left(d_i + \delta_2 T_{reg}^*\right)}, & \text{for } S_5^*, \\ \\ \dfrac{\sigma_2 \left(\beta - d_F\right)}{\mu_a \left(1 + \beta\right) \left(d_i + \delta_2 T_{reg}^*\right)}, & \text{for } S_6^*. \end{cases}$$

This steady state undergoes a steady-state bifurcation if

$$\frac{d_a + \delta_1 T_{reg}^*}{\rho_3} = P, \quad \text{or} \quad \frac{d_a + \delta_1 T_{reg}^*}{\rho_3} = \frac{d_n}{\rho_2}, \quad \text{or} \quad \delta_1\rho_1 \left(T_{reg}^*\right)^2 = \lambda_r\rho_3. \tag{5.5}$$

For $\tau_2 = 0$ these steady states are stable if T_{reg}^* satisfies (5.3) and

$$\begin{aligned}
&\delta_1\rho_1 \left(T_{reg}^*\right)^2 > \lambda_r\rho_3, \\
&a_5 \left(T_{reg}^*\right)^5 + a_4 \left(T_{reg}^*\right)^4 + a_3 \left(T_{reg}^*\right)^3 + a_2 \left(T_{reg}^*\right)^2 + a_1 T_{reg}^* + a_0 > 0,
\end{aligned} \tag{5.6}$$

where

$$
\begin{aligned}
a_5 &= -\delta_1\delta_2(\delta_1\rho_1 - \delta_2\rho_1 + \delta_2\rho_3),\\
a_4 &= d_a\delta_2(\delta_2\rho_2 - \delta_1\rho_1 - \delta_2\rho_3) - d_i\delta_1(\delta_1\rho_1 - \delta_2\rho_1 + 2\delta_2\rho_3),\\
a_3 &= -d_i\delta_1(d_a\rho_1 + d_i\rho_3) + d_a d_i\delta_2(\rho_1 - 2\rho_3) + \lambda_r\delta_2(\delta_1\rho_1 + \delta_2\rho_3),\\
a_2 &= -d_a d_i^2\rho_3 + \lambda_r\delta_2(d_a\rho_1 + 2d_i\rho_3), \quad a_1 = \lambda_r\rho_3(d_i^2 + \delta_2\lambda_r), \quad a_0 = d_i\rho_3\lambda_r^2.
\end{aligned}
$$

To investigate whether stability can be lost for $\tau_2 > 0$, I use an iterative procedure described in [225, 226] to determine a function $F(\omega)$, whose roots give the Hopf frequency associated with purely imaginary roots of equation (5.4). Substituting $\lambda = i\omega$ into equation (5.4), I define $\Delta^{(1)}(\tau_2, \lambda)$ as

$$
\Delta^{(1)}(\tau_2, \lambda) = \overline{p_0(i\omega)}\Delta(\tau_2, i\omega) - p_2(i\omega)e^{-2i\omega\tau_2}\overline{\Delta(\tau_2, i\omega)} = p_0^{(1)}(i\omega) + p_1^{(1)}(i\omega)e^{-i\omega\tau_2},
$$

where

$$
\begin{aligned}
p_0^{(1)}(i\omega) =& |p_0(i\omega)|^2 - |p_2(i\omega)|^2,\\
p_1^{(1)}(i\omega) =& \overline{p_0(i\omega)}p_1(i\omega) - \overline{p_1(i\omega)}p_2(i\omega),
\end{aligned}
$$

and the bar denotes the complex conjugate. If we define

$$
F(\omega) = \left|p_0^{(1)}(i\omega)\right|^2 - \left|p_1^{(1)}(i\omega)\right|^2,
$$

then $\Delta(\tau_2, i\omega) = 0$ whenever ω is a root of $F(\omega) = 0$. The function $F(\omega)$ has the explicit form

$$
F(\omega) = \omega^{12} + b_{10}\omega^{10} + b_8\omega^8 + b_6\omega^6 + b_4\omega^4 + b_2\omega^2 + b_0,
$$

with

$$b_0 = \frac{\left(\delta_1 d_a + T^*_{reg}\right)^4}{{\rho_3}^4}\left(d_i + \delta_2 T^*_{reg}\right)\left(2T^*_{reg}\delta_1\rho_1 + d_a\rho_1 - d_r\rho_3\right)$$
$$\left[\left(d_i + \delta_2 T^*_{reg}\right)\left(d_a\rho_1 + 3d_r\rho_3\right) + 2d_i\rho_1\left(d_a + \delta_1 T^*_{reg}\right)\right]$$
$$\left[\rho_1\left(d_a + \delta_1 T^*_{reg}\right)\left(2d_i + \delta_2 T^*_{reg}\right) - d_r\rho_3\left(d_i + \delta_2 T^*_{reg}\right)\right]^2.$$

The explicit formulae for other coefficients of $F(\omega)$ can be found in Appendix A. Introducing $s = \omega^2$, the equation $F(\omega) = 0$ can be equivalently rewritten as follows,

$$h(s) = s^6 + b_{10}s^5 + b_8 s^4 + b_6 s^3 + b_4 s^2 + b_2 s + b_0 = 0. \tag{5.7}$$

Without loss of generality, suppose that equation (5.7) has six distinct positive roots denoted by s_1, s_2, ... , s_6, which means that the equation $F(\omega) = 0$ has six positive roots

$$\omega_i = \sqrt{s_i}, \quad i = 1, 2, ..., 6.$$

Substituting $\lambda_k = i\omega_k$ into equation (5.4) gives

$$\tau_{k,j} = \frac{1}{\omega_k}\left[\arctan\left(\frac{\omega_k\left((\rho_1+\rho_3)\omega_k^4 + f_2\omega_k^2 + f_0\right)}{\left(\rho_3 Z - d_r\rho_1 - \rho_3^2 I^* - \rho_1\delta_2 T^*_{reg}\right)\omega_k^4 + g_2\omega_k^2 + g_0}\right) + j\pi\right],$$

for $k = 1, 2, ..., 6$, $j = 0, 1, 2, ...,$ where

$$\begin{aligned}
f_0 =& -{\rho_1}^2\rho_3{}^2 I^{*3} Z - \rho_1\rho_3\left(2\rho_1 + 3\rho_3\right) I^{*2} Z^2 + \rho_1\rho_3 T^*_{reg}\left(-\delta_1\rho_1 + 3\delta_2\rho_1 + \delta_2\rho_3\right) I^{*2} Z \\
& - {T^*_{reg}}^2{\delta_2}^2{\rho_1}^2\rho_3 I^{*2} - T^*_{reg}\delta_1\rho_1\rho_3 I^* Z^2 + d_r\rho_3\left(-\delta_1\rho_1 T^*_{reg} + d_r\rho_3\right) I^* Z \\
& + d_r\left(-T^*_{reg}\delta_1\rho_1 + 2d_r\rho_3\right) Z^2, \\
f_2 =& -{\rho_1}^2\rho_3 I^{*2} + {\rho_3}^2 I^* Z + \left(\rho_1 + 2\rho_3\right) Z^2 + \rho_1 T^*_{reg}\left(\delta_1 - \delta_2\right) Z \\
& - d_r\left(T^*_{reg}\delta_2\rho_1 - d_r\rho_3\right), \\
g_0 =& {\rho_1}^2{\rho_3}^2 I^{*3}\left(2Z^2 - 3T^*_{reg}\delta_2 Z + {T^*_{reg}}^2{\delta_2}^2\right) + \rho_1\rho_3\left(-2T^*_{reg}\delta_1\rho_1 + 3d_r\rho_3\right) I^{*2} Z^2 \\
& + \rho_1\rho_3\delta_2 T^*_{reg}\left(T^*_{reg}\delta_1\rho_1 - d_r\rho_3\right) I^{*2} Z + d_r\rho_3\left(T^*_{reg}\delta_1\rho_1 - 2d_r\rho_3\right) I^* Z^2, \\
g_2 =& \rho_3 I^*\left({\rho_1}^2\rho_3 I^{*2} - {\rho_1}^2 I^* Z - 2\rho_3 Z^2 - T^*_{reg}\delta_1\rho_1 Z - {d_r}^2\rho_3\right) - \rho_1\left(d_r + \delta_1 T^*_{reg}\right) Z^2 \\
& + d_r\left(-T^*_{reg}\delta_1\rho_1 + T^*_{reg}\delta_2\rho_1 + d_r\rho_3\right) Z,
\end{aligned}$$

and

$$I^* = \frac{d_a + \delta_1 T^*_{reg}}{\rho_3}, \quad Z = d_i + \delta_2 T^*_{reg}.$$

This allows us to find

$$\tau^* = \tau_{k_0,0} = \min_{1\le k\le 6}\{\tau_{k,0}\}, \quad \omega_0 = \omega_{k_0},$$

as the first time delay for which the roots of the characteristic equation (5.4) cross the imaginary axis. To determine whether these steady states actually undergo a Hopf bifurcation at $\tau_2 = \tau^*$, we have to compute the sign of $d\mathrm{Re}[\lambda(\tau^*)]/d\tau_2$. For $\tau = \tau^*$, $\lambda(\tau^*) = i\omega_0$, and I also define $s_0 = \omega_0^2$.

Lemma 5.1. *Suppose $h'(s_0) \neq 0$ and $p_0^{(1)}(i\omega_0) \neq 0$. Then the following transversality condition holds*

$$\mathrm{sgn}\left\{\frac{d\,\mathrm{Re}(\lambda)}{d\,\tau_2}\bigg|_{\tau_2=\tau^*}\right\} = \mathrm{sgn}[p_0^{(1)}(i\omega_0)h'(s_0)].$$

Proof. Considering $p_j(i\omega_0) = x_j(\omega_0) + iy_j(\omega_0)$ for $j = 0, 1, 2$, we have

$$\begin{aligned}
p_0^{(1)}(i\omega_0) =& x_0^2 + y_0^2 - x_2^2 - y_2^2,\\
p_1^{(1)}(i\omega_0) =& (x_0x_1 + y_0y_1 - x_1x_2 - y_1y_2) + (x_0y_1 + x_2y_1 - x_1y_0 - x_1y_2)i,
\end{aligned}$$

where all x_j and y_j are expressed in terms of system parameters and steady state values of the variables. Substituting these expressions into $\Delta(\tau_2, i\omega_0) = 0$ and $\Delta^{(1)}(\tau_2, i\omega_0) = 0$, and then separating real and imaginary parts gives

$$\begin{cases}
x_2\cos(2\omega_0\tau^*) + y_2\sin(2\omega_0\tau^*) + x_1\cos(\omega_0\tau^*) + y_1\sin(\omega_0\tau^*) = -x_0,\\
y_2\cos(2\omega_0\tau^*) - x_2\sin(2\omega_0\tau^*) + y_1\cos(\omega_0\tau^*) - x_1\sin(\omega_0\tau^*) = -y_0,\\
(x_0x_1 + y_0y_1 - x_1x_2 - y_1y_2)\cos(\omega_0\tau^*) + (x_0y_1 + x_2y_1 - x_1y_0 - x_1y_2)\sin(\omega_0\tau^*)\\
\qquad = -x_0^2 - y_0^2 + x_2^2 + y_2^2,\\
(x_0y_1 + x_2y_1 - x_1y_0 - x_1y_2)\cos(\omega_0\tau^*) - (x_0x_1 + y_0y_1 - x_1x_2 - y_1y_2)\sin(\omega_0\tau^*) = 0.
\end{cases}$$

Solving this system of equations provides the values of $\sin(\omega_0\tau^*)$, $\cos(\omega_0\tau^*)$, $\sin(2\omega_0\tau^*)$, and $\cos(2\omega_0\tau^*)$. Taking the derivative of equation (5.4) with respect to

τ_2, one finds

$$\left(\frac{d\,\lambda}{d\,\tau_2}\right)^{-1} = \frac{p_2'(\lambda)e^{-2\lambda\tau_2} + p_1'(\lambda)e^{-\lambda\tau_2} + p_0'(\lambda)}{\lambda\,(2p_2(\lambda)e^{-2\lambda\tau_2} + p_1(\lambda)e^{-\lambda\tau_2})} - \frac{\tau_2}{\lambda}.$$

Hence,

$$\begin{aligned}
&\left(\frac{d\,\mathrm{Re}(\lambda)}{d\,\tau_2}\bigg|_{\tau_2=\tau^*}\right)^{-1} = \mathrm{Re}\left\{\frac{p_2'(\lambda)e^{-2\lambda\tau_2} + p_1'(\lambda)e^{-\lambda\tau_2} + p_0'(\lambda)}{\lambda\,(2p_2(\lambda)e^{-2\lambda\tau_2} + p_1(\lambda)e^{-\lambda\tau_2})}\right\}_{\tau_2=\tau^*} - \mathrm{Re}\left\{\frac{\tau_2}{\lambda}\right\}_{\tau_2=\tau^*} \\
&= \mathrm{Re}\left\{\frac{p_2'(i\omega_0)e^{-2i\omega_0\tau_2} + p_1'(i\omega_0)e^{-i\omega_0\tau_2} + p_0'(i\omega_0)}{i\omega_0\,(2p_2(i\omega_0)e^{-2i\omega_0\tau_2} + p_1(i\omega_0)e^{-i\omega_0\tau_2})}\right\} \\
&= \frac{1}{\omega_0}\,\mathrm{Im}\left\{\frac{p_2'(i\omega_0)e^{-2i\omega_0\tau_2} + p_1'(i\omega_0)e^{-i\omega_0\tau_2} + p_0'(i\omega_0)}{2p_2(i\omega_0)e^{-2i\omega_0\tau_2} + p_1(i\omega_0)e^{-i\omega_0\tau_2}}\right\} \\
&= \frac{1}{\Lambda\omega_0}\Big[- x_2x_2' - y_2y_2' + x_0x_0' + y_0y_0' + (x_2y_1' - y_2x_1' + x_0y_1' - x_1'y_0)\sin(\omega_0\tau^*) \\
&\qquad + (x_0x_1' + y_0y_1' - x_1'x_2 - y_1'y_2)\cos(\omega_0\tau^*) \\
&\qquad + (x_2y_0' - x_0'y_2 + x_0y_2' - x_2'y_0)\sin(2\omega_0\tau^*) \\
&\qquad + (x_0x_2' + y_0y_2' - x_0'x_2 - y_0'y_2)\cos(2\omega_0\tau^*)\Big],
\end{aligned}$$

where

$$\Lambda = \left|2p_2(i\omega_0)e^{-2i\omega_0\tau_2} + p_1(i\omega_0)e^{-i\omega_0\tau_2}\right|^2.$$

Substituting the values of $\sin(\omega_0\tau^*)$, $\cos(\omega_0\tau^*)$, $\sin(2\omega_0\tau^*)$, and $\cos(2\omega_0\tau^*)$ found earlier gives

$$\left(\frac{d\,\mathrm{Re}(\lambda)}{d\,\tau_2}\bigg|_{\tau_2=\tau^*}\right)^{-1} = \frac{1}{\Lambda\omega_0}\,\frac{F'(\omega_0)}{2\,p_0^{(1)}(i\omega_0)} = \frac{h'(s_0)}{\Lambda\,p_0^{(1)}(i\omega_0)}.$$

Therefore

$$\begin{aligned}
\mathrm{sgn}\left\{\frac{d\,\mathrm{Re}(\lambda)}{d\,\tau_2}\bigg|_{\tau_2=\tau^*}\right\} &= \mathrm{sgn}\left\{\left(\frac{d\,\mathrm{Re}(\lambda)}{d\,\tau_2}\bigg|_{\tau_2=\tau^*}\right)^{-1}\right\} = \mathrm{sgn}\left\{\frac{h'(s_0)}{\Lambda\,p_0^{(1)}(i\omega_0)}\right\} \\
&= \mathrm{sgn}[p_0^{(1)}(i\omega_0)h'(s_0)],
\end{aligned}$$

which completes the proof. □

We can now formulate the main result concerning stability of the steady states S_5^* and S_6^*.

Theorem 5.2. *Suppose the value of T^*_{reg} satisfies conditions (5.3) and (5.6). If equation (5.7) has at least one positive root s_0, and $p_0^{(1)}(i\omega_0)h'(s_0) > 0$ with $\omega_0 = \sqrt{s_0}$, then the steady state S^*_5 (respectively, S^*_6) is stable for $0 \leq \tau_2 < \tau^*$, unstable for $\tau_2 > \tau^*$, and undergoes a Hopf bifurcation at $\tau_2 = \tau^*$.*

Since T^*_{reg} satisfies conditions (5.3) and (5.6), the steady state S^*_5/S^*_6 is stable for $\tau_2 = 0$. Lemma 5.1 then ensures that τ^* is the first positive value of the time delay τ_2, for which the roots of the characteristic equation (5.4) cross the imaginary axis with positive speed. Hence, the steady state S^*_5/S^*_6 is stable for $0 \leq \tau_2 < \tau^*$, unstable for $\tau_2 > \tau^*$, and undergoes a Hopf bifurcation at $\tau_2 = \tau^*$.

Remark 5.3. A similar result can be formulated for a (reverse) supercritical Hopf bifurcation of the steady state S^*_5/S^*_6 at some higher value of τ_2.

The only remaining steady state is the persistent (chronic) equilibrium S^*_8 with all of its components being positive. Since it did not prove possible to find a closed form expression for this steady state, its stability also has to be studied numerically.

5.3 Numerical stability analysis and simulations

To investigate the role of different parameters in the dynamics of model (5.1), in this section I perform a detailed numerical bifurcation analysis and simulations of this model. Stability of different steady states is determined numerically by computing the largest real part of the characteristic eigenvalues, which is achieved by using a pseudospectral method implemented in a traceDDE suite in MATLAB, which is a tool for robust analysis and solving characteristic equations for delay differential equations [227].

Table 5.1: Table of parameter values

Parameter	Value	Parameter	Value
β	1	ρ_3	2
μ_a	20	d_n	1
d_F	1.1	d_a	0.001
μ_F	6	δ_1	0.0025
d_{in}	1	δ_2	0.001
α	0.4	σ_1	0.15
λ_r	3	σ_2	0.33
d_r	0.4	d_i	0.6
p_1	0.4	τ_1	1.4
p_2	0.4	τ_2	0.6
ρ_1	10	τ_3	0.6
ρ_2	0.8		

Analytical results from the previous section suggest that at $\beta = d_F$, the disease-free steady state S_2^* undergoes a transcritical bifurcation. For $\beta < d_F$, the disease-free steady state S_2^* is stable, and the chronic steady state is infeasible. On the contrary, when $\beta > d_F$, the disease-free steady state S_2^* is unstable, and in this case it makes sense to investigate stability of the chronic steady state. Therefore, these two cases are considered separately, and as a first step I fix the baseline values as given in Table 5.1. For this choice of parameters, we have $d_F - \beta > 0$, implying that S_2^* is always stable, and Figure 5.2 illustrates how the stability of S_5^* and S_6^* is affected by parameters. This figure indicates that the steady states S_5^* and S_6^* are only biologically feasible if the regulatory T cells do not grow too rapidly and do not clear autoreactive T cells too quickly. Importantly, Figure 5.2 shows that the value of the rate δ_2 of clearance of IL-2 by regulatory T cells does not have any effect on the thresholds of λ_r and δ_1, where the steady states S_5^* and S_6^* lose their feasibility. Moreover, if λ_r and δ_1 are small, then increasing the rate δ_2 at which Tregs inhibit the production of IL-2 makes S_6^* become unfeasible, resulting in a stable steady state S_5^*, which has the zero population of host cells A. On the other hand, the steady state S_6^* associated with autoimmune responses is favoured for higher values of δ_1 and λ_r. In the case stable periodic solutions around these steady states, increasing δ_2 results in the disappearance of oscillations and stabilisation of the associated steady state. At the intersection of the lines of Hopf bifurcation and the steady-state bifurcation, as determined by Theorem 5.2 and conditions (5.5), one has the co-dimension two fold-Hopf (also known as zero-Hopf or saddle-node

Hopf) bifurcation [191].

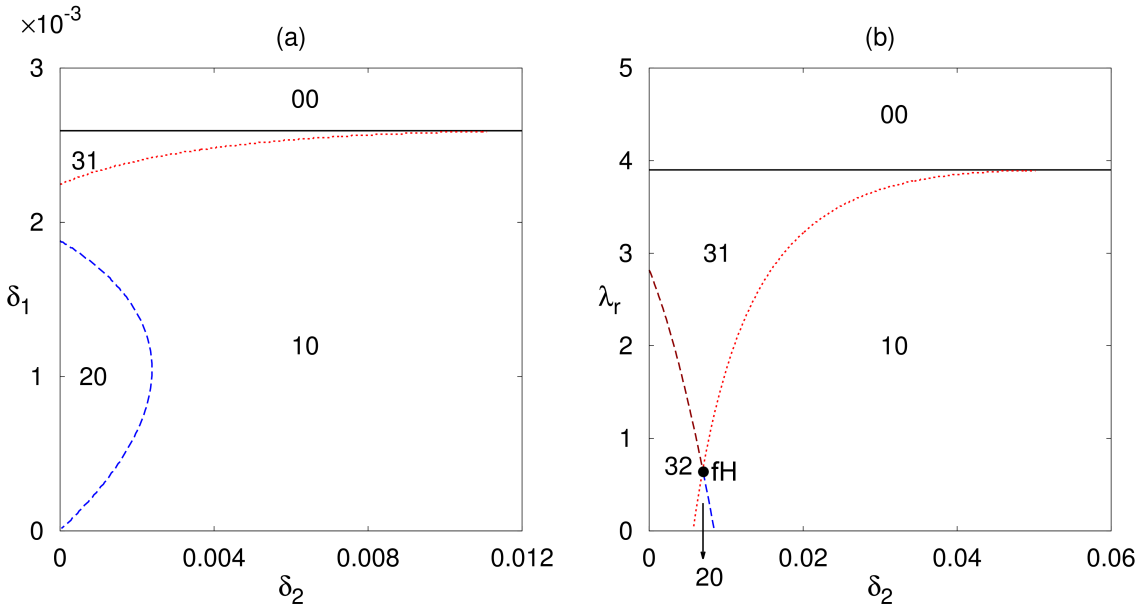

Figure 5.2: Regions of feasibility and stability of the steady states S_5^* and S_6^* with parameter values from Table 5.1, but in (b) $\mu_a = 10$. Black and red curves indicate the boundaries of feasibility and the steady-state bifurcation, whereas dashed lines (blue/brown) show the boundaries of Hopf bifurcation of the steady states S_5^* and S_6^*, respectively, with 'fH' indicating the fold-Hopf bifurcation. The first digit of the index refers to S_5^*, while the second corresponds to S_6^*, and they indicate that in that parameter region the respective steady state is unfeasible (index is '0'), stable (index is '1'), unstable via Hopf bifurcation with a periodic solution around this steady state (index is '2'), or unstable via a steady-state bifurcation (index is '3'). In all plots, the condition $\beta < d_F$ holds, so the disease-free steady state S_2^* is also stable.

Since our earlier analysis showed that stability of the steady states S_5^*/S_6^* is affected by the time delay τ_2, in Fig. 5.3 I consider stability of these equilibria depending on τ_2 and the rate δ_2. For the steady state S_5^*, if the effect of IL-2 on promoting proliferation of T cells is fast (i.e. τ_2 is small), there is a large range of δ_2, starting with some very low values, for which S_5^* is stable. Increasing the time delay τ_2 results in the Hopf bifurcation of this steady state as described in Theorem 5.2. One should note that for intermediate values of δ_2, the steady state S_5^* undergoes stability switches, whereby increasing the delay τ_2 further results in a subcritical Hopf bifurcation, which stabilises S_5^*, but after some number of such stability switches eventually the steady state S_5^* is unstable. For higher still values of δ_2, the steady state S_5^* remains stable for an entire range of τ_2 values, and the only way to lose its stability is via a steady state bifurcation as given by (5.5). In the case of autoimmune steady state S_6^*, the situation is somewhat different in

that increasing δ_2 beyond some critical values makes this steady state biologically infeasible. At the same time, for an entire range of δ_2 values where it is feasible, this steady state exhibits a single loss of stability through a Hopf bifurcation for some critical value of the time delay τ_2, in agreement with Theorem 5.2.

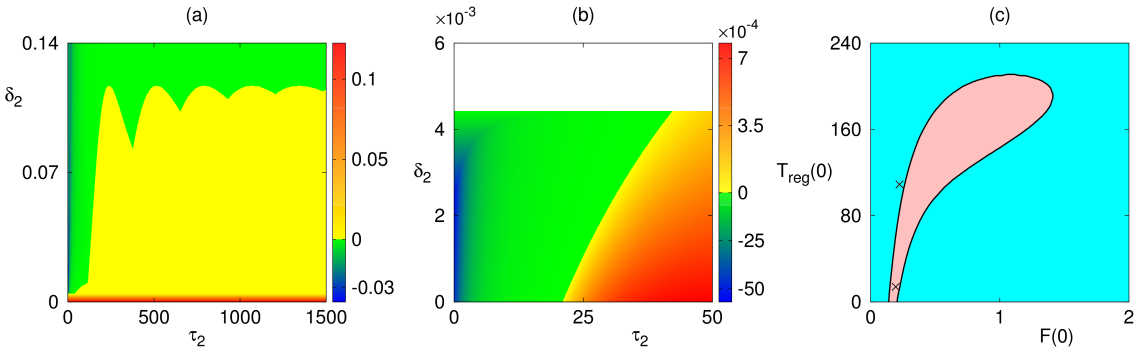

Figure 5.3: Stability of the steady states S_5^* (a), and S_6^* (b) with parameter values from Table 5.1. White area shows the region where the steady state S_6^* is infeasible. Colour code denotes max[Re(λ)] for the steady states when they are feasible. In all plots the condition $d_F > \beta$ holds, so the disease-free steady state S_2^* is stable. Basins of attraction of different steady states depending on the initial conditions (c), with other initial conditions specified in (5.8), and parameter values from Table 5.1, except for $\tau_2 = 18$. Cyan and pink areas are the basins of attraction of S_2^* and S_6^*, respectively.

As mentioned earlier, for parameter values used in Fig. 5.3, the disease-free steady state S_2^* is stable. Hence, the system exhibits a bi-stability between a disease-free state and either stable steady states S_5^*/S_6^*, or periodic solutions around these steady states. To investigate this bi-stability, I choose parameter values as in Table 5.1 except for $\tau_2 = 18$, which corresponds to a stable steady state S_6^*, and I fix initial conditions for state variables as follows,

$$(A(s), T_{in}(s), T_{nor}(s), T_{aut}(s), I(s)) = (0.9, 0.8, 0, 0, 0), \quad s \in [-\tau_{max}, 0], \tag{5.8}$$

and $\tau_{max} = \max\{\tau_1, \tau_2, \tau_3\}$, except for initial amounts of infected cells and regulatory T cells that are allowed to vary with a constant history. Figure 5.3(c) illustrates the bi-stability between S_2^* and S_6^* in terms of their basins of attraction. It is worth noting that recently significant research in approximation theory and meshless interpolation has focused on developing techniques for detection and analysis of attraction basins [228, 229, 230, 231, 232, 233]. Figure 5.3(c) suggests that for very large initial amounts of regulatory T cells, the system converges to the disease-free steady state. It also indicates that if the initial amount of infected cells is very small

or is bigger than some specific value, then the infection will be cleared.

Interestingly, increasing the initial amount of the regulatory T cells results in a larger range of initial amounts of infection, for which the system tends to a stable autoimmune state S_6^*. In Fig. 5.3(b) I discovered that increasing τ_2 makes the autoimmune steady state S_6^* undergo a Hopf bifurcation, in which case the system will exhibit a bi-stability between stable S_2^* and a periodic solution around S_6^*. Our numerical investigation suggests that the shape of basins of attraction in this case is qualitatively similar to that shown in Fig. 5.3(c), with the basin of attraction of the stable steady state S_6^* being replaced by the basin of attraction of the periodic solution around this steady state.

Figure 5.4 shows temporary evolution of the system (5.1) in the regime of bi-stability between a stable disease-free steady state and a stable autoimmune steady state S_6^* (similar pattern of behaviour is exhibited in the case of bi-stability between S_2^* and S_5^*). It also illustrates how the system develops a periodic solution around the steady state S_6^* for a higher value of τ_2. Periodic oscillations around the steady state S_6^* biologically correspond to a genuine autoimmune state: after the initial infection is cleared, the system exhibits sustained endogenous oscillations, characterised by periods of significant reduction in the number of organ cells through a negative action of autoreactive T cells, separated by periods of quiescence. This type of behaviour is often observed in clinical manifestations of autoimmune disease [77, 78, 79, 80]. This result has substantial biological significance as effectively it suggests that even for the same kinetic parameters of immune response, the ultimate state of the system, which can be either a successful clearance of infection without lasting consequences, or progression to autoimmunity, also depends on the strength of the initial infection and of the initial state of the immune system, as represented by the initial number of regulatory T cells.

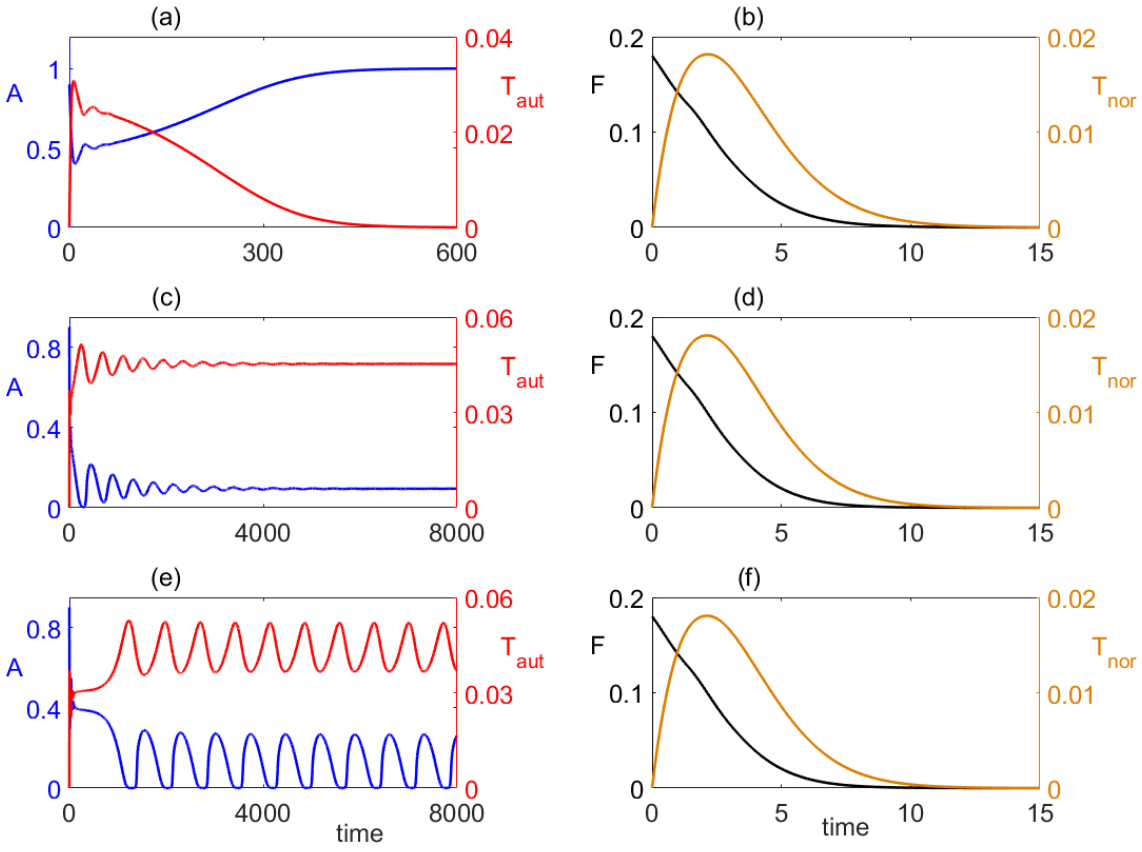

Figure 5.4: Numerical solutions of the model with parameters values from Table 5.1, except for $\tau_2 = 18$. (a) and (b) Stable disease-free steady state S_2^* for $F(0) = 0.18$, and $T_{reg}(0) = 100$. (c) and (d) Transient oscillations settling on a stable steady state S_6^* for $F(0) = 0.18$, and $T_{reg}(0) = 10$. (e) and (f) Autoimmune dynamics represented by periodic oscillations around the steady state S_6^* for $\tau_2 = 32$, $F(0) = 0.18$, and $T_{reg}(0) = 10$.

Next I consider a situation where $\beta > d_F$, so the disease-free steady state is unstable, and the system can have three steady states S_5^*, S_6^* and S_8^*. Our earlier results [234] suggest that in the case where regulatory T cells do not inhibit the production of IL-2, i.e. for $\delta_2 = 0$, the steady state S_6^* is stable. Figure 5.5 shows regions of feasibility and stability of these steady states depending on δ_2 and τ_2 in this case. One observes that S_5^* and S_6^*, whose stability boundaries are determined by Theorem 5.2, exhibit the same behaviour as in Fig. 5.3, namely, for S_5^* increasing τ_2 causes multiple stability switches for smaller values of δ_2, and the steady state is unstable for very small δ_2 and stable for large δ_2; in contrast, S_5^* exhibits a single loss of stability via Hopf bifurcation at some critical value of the time delay τ_2, which itself increases with δ_2.

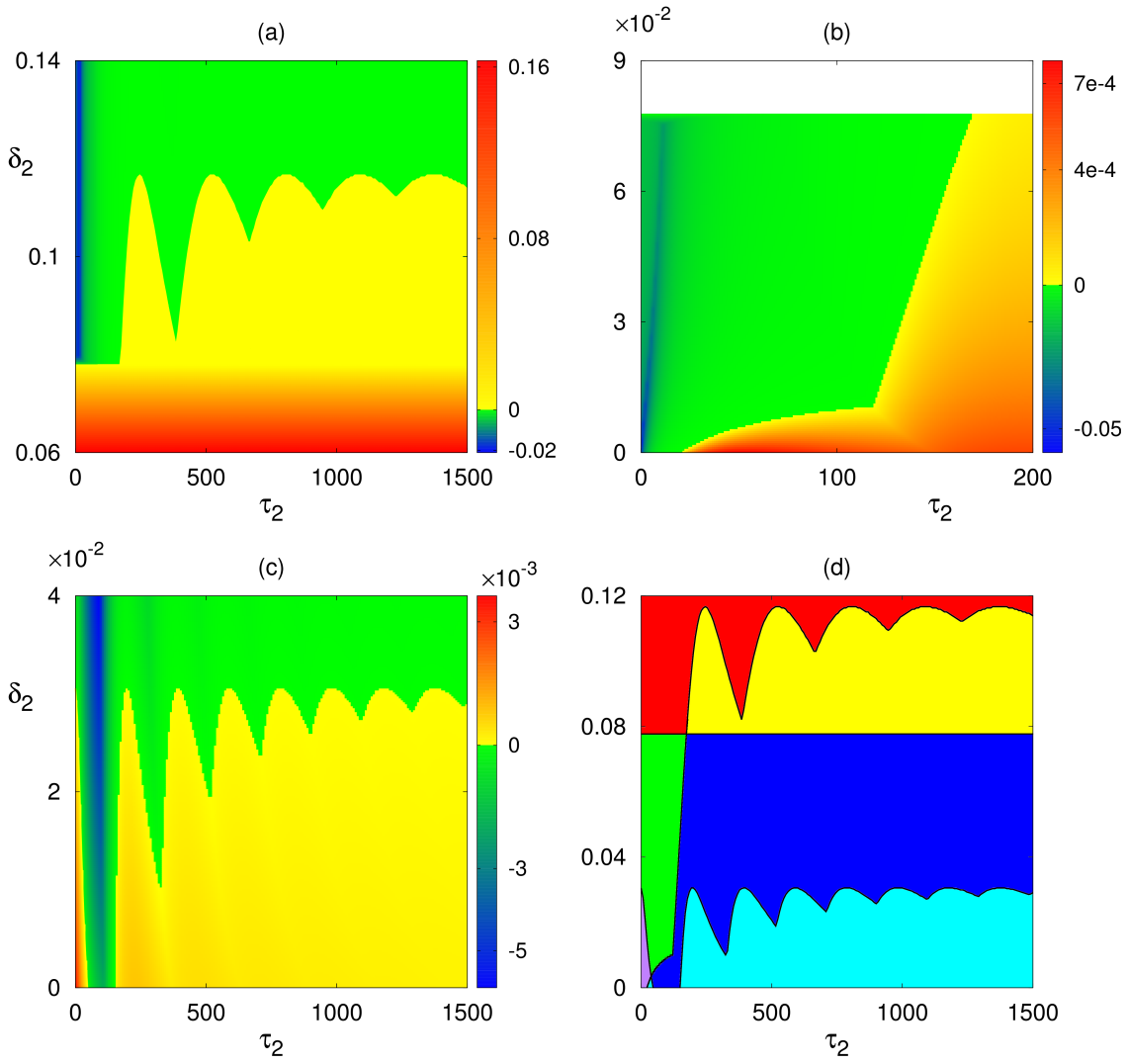

Figure 5.5: Stability of S_5^* (a), S_6^* (b), and S_8^* (c), with parameter values from Table 5.1, except for $\beta = 1.4$ and $\sigma_2 = 1$, so that $\beta > d_F$. White area shows the region where the steady state is infeasible. Colour code denotes max[Re(λ)] for each steady states when it is feasible. (d) Summary of stability results. Green indicates the region where S_6^* and S_8^* are stable, and S_5^* is unstable, whereas red is the area where S_5^* and S_8^* are stable, and S_6^* is infeasible. Yellow is where S_8^* is stable, S_5^* is unstable, and S_6^* is infeasible. Purple shows the region where S_6^* is stable, but S_5^* and S_8^* are unstable. Blue and cyan indicate the regions where S_5^* and S_6^* are unstable, but S_8^* is stable or unstable, respectively.

Behaviour of S_8^* is similar to that of S_5^* in that there are multiple stability switches for increasing value of τ_2 and small to intermediate values of δ_2, while for high values of δ_2, the chronic steady state S_8^* is stable for all values of τ_2. Figure 5.5(d) divides the δ_2-τ_2 plane into different regions based on feasibility and stability of these steady states and shows that increasing δ_2 makes the autoimmune steady state S_6^* infeasible. In other regions, the system can exhibit a bi-stability between a stable steady state S_8^* and either a stable steady state S_5^*, or a periodic solution around S_5^*.

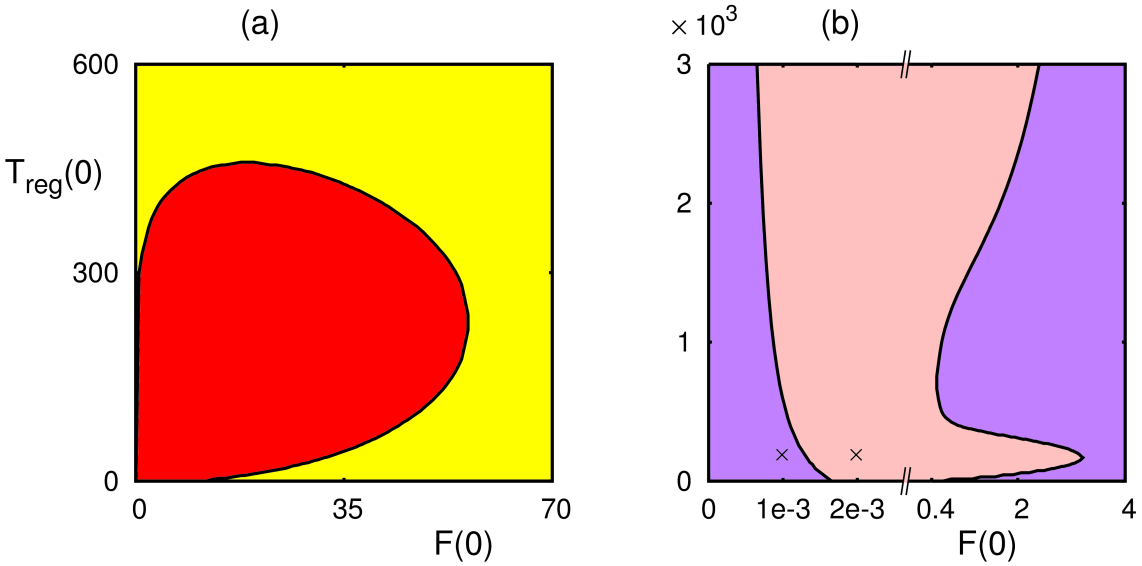

Figure 5.6: Bi-stability analysis of the steady states S_5^*, S_6^*, and S_8^* with the same parameter values as in Fig. 5.5, except for (a) $\delta_2 = 0.1$, (b) $\delta_2 = 0.02$, and the initial condition (5.8) with a constant history for the initial amount of Tregs and infected cells. Yellow indicates the basin of attraction of the chronic steady state S_8^*, purple is the basin of attraction of periodic solutions around S_8^*. Red and pink are the basins of attraction of the steady states S_5^* and S_6^*, respectively.

Figure 5.6 illustrates the basins of attraction of the steady states S_5^*, S_6^* and S_8^*, as well as periodic solutions around S_8^*. Figure 5.6 (a) shows the basins of attraction of the steady states S_5^* and S_8^* and demonstrates that if the initial number of regulatory T cells or infected cells is sufficiently high, or the initial amount of infected cells is very low, the immune response neither eliminates infection nor clears autoreactive T cells, and the system approaches the stable steady state S_5^*. Figure 5.6(b) illustrates bi-stability between the stable steady state S_6^* and a periodic solution around S_8^*, and has a different behaviour to than shown in Fig. 5.6(a). This figure suggests that for a specific range of $F(0)$ the system converges to a stable autoimmune state S_6^* for all values of $T_{reg}(0)$. However, if the initial number of infected cells is very high or very low, the system instead develops a periodic solution around the steady state S_8^* associated with chronic infection.

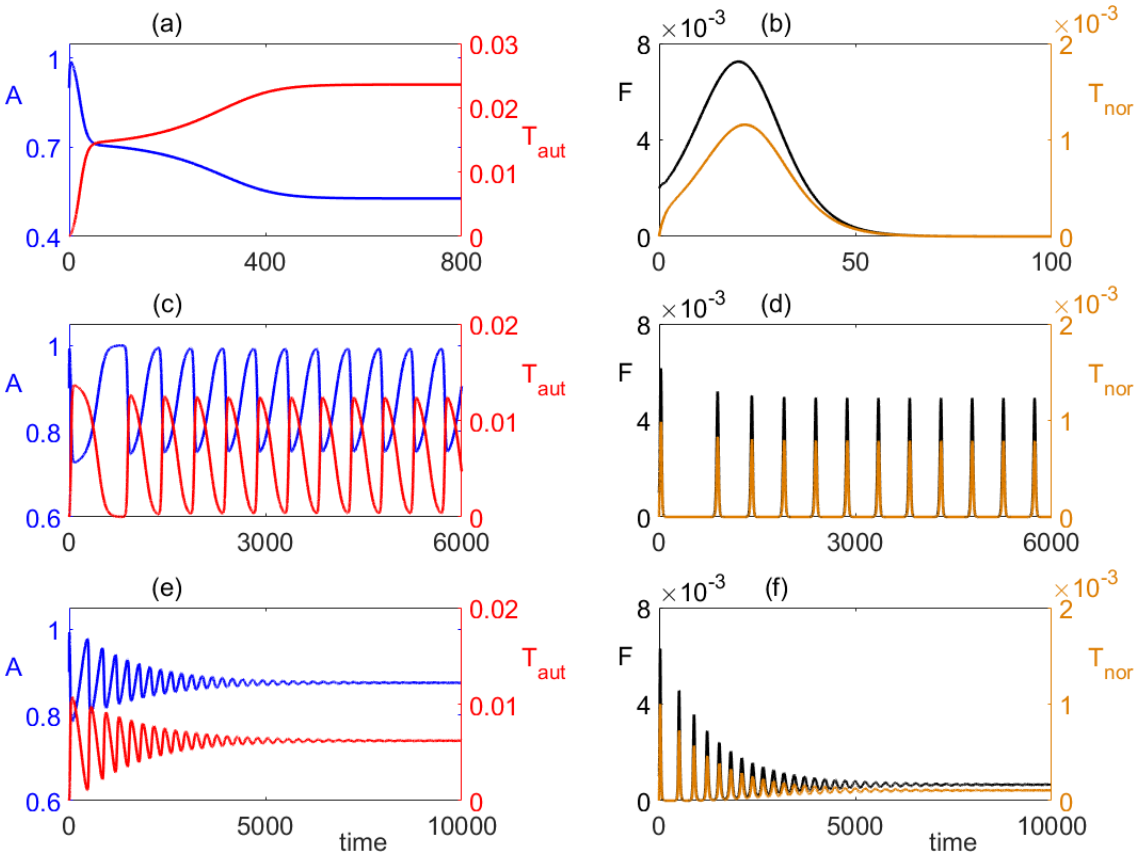

Figure 5.7: Numerical solutions of the model with same parameters values as Fig. 5.6 (b). (a) and (b) Stable steady state S_6^* for $F(0) = 0.002$ and $T_{reg}(0) = 200$. (c) and (d) Periodic oscillations around the steady state S_8^* for $F(0) = 0.001$ and $T_{reg}(0) = 200$. (e) and (f) Transient oscillations settling on a stable steady state S_8^* for $\tau_2 = 25$, $F(0) = 0.001$ and $T_{reg}(0) = 200$.

Figure 5.7 illustrates a regime of bi-stability between a stable steady state S_6^* and a periodic solution around S_8^* for combinations of initial conditions indicated by crossed in Fig. 5.6(b). It also illustrates how the system develops a stable solution around the steady state S_8^* for a higher value of τ_2. This figure shows that by increasing the initial number of infected cells the behaviour of the system changes, as it then approaches the autoimmune steady state S_6^*. Interestingly, one can observe that for high values of $F(0)$ the system can eliminate the infection, but it cannot clear the autoreactive T cells, in which case the system converges to S_6^*. On the other hand, for a smaller number of infected cells the system develops a periodic solution around the endemic steady state.

Figure 5.8 shows how the stability of the chronic infection steady state S_8^* changes with respect to time delays. Figure 5.8(a) indicates that for small values of τ_2 (i.e. when the influence of IL-2 on proliferation of T cells is occurring quite rapidly),

the steady state S_8^* is stable, and increasing the time delay τ_1 associated with viral eclipse phase does not have an effect on its stability. At the same time, if τ_2 exceeds some specific value, by increasing τ_1 the chronic steady state switches between being stable or unstable. Figure 5.8 (b) demonstrates a different behaviour, suggesting that for each value of τ_1, there is small range of τ_3 values where S_8^* is stable, but for smaller and larger values of τ_3 it is unstable. For intermediate values of the eclipse phase delay τ_1, there is an additional narrow range of τ_3 values where S_8^* is stable. Figure 5.8(c) illustrates that for very small, respectively very large, values of τ_3, the chronic infection steady state is stable, respectively unstable for any value of τ_2; for intermediate values of τ_3, this steady state undergoes a finite number of stability switches for increasing values of τ_2 and eventually becomes unstable.

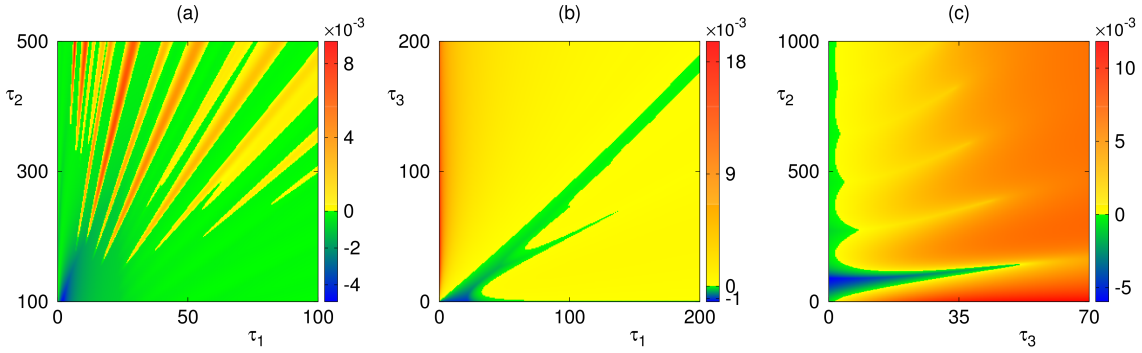

Figure 5.8: Colour code denotes max[Re(λ)] for the endemic steady state S_8^* depending on different time delays, with the parameter values taken from Table 5.1, except for $\beta = 1.4$, $\sigma_2 = 1$, and $\delta_2 = 0.04$.

It should be noted Fig. 5.8 shows that unlike τ_1 and τ_2, once the steady state S_8^* loses stability via Hopf bifurcation due to increasing τ_3, it cannot regain stability for higher values of τ_3.

5.4 Discussion

In this chapter I have developed and analysed a time-delayed model of immune response to a viral infection, which accounts for T cells with different activation thresholds, a cytokine mediating T cell proliferation, as well as regulatory T cells. Particular attention is payed to the dual suppressive role of regulatory T cells in terms of reducing the amount of autoreactive T cells, and also inhibiting IL-2. To achieve better biological realism of the model, I have explicitly included time delays

associated with the eclipse phase of the virus life cycle, stimulation/proliferation of T cells by IL-2, and suppression of IL-2 by regulatory T cells. Depending on the values of parameters, the system can have four steady states: the disease-free state, the state characterised by the death of host cells, the autoimmune state, and a state of chronic infection. We have established conditions for stability and steady-state or Hopf bifurcations of these steady states in terms of system parameters.

In the case when the natural death rate of infected cells exceeds the infection rate, the immune system is able to clear the infection, and the disease-fee steady state is stable. In this regime, the system can also support the autoimmune steady state or the steady state with the death of host cells, either of which can be stable, or give rise to a periodic solution emerging via Hopf bifurcation. In the opposite case, when the natural death rate of infected cells is smaller than the infection rate, the disease-fee steady state is unstable, but it is possible to have a bi-stability between the other three steady states or periodic solutions around them. To better understand bi-stability between different dynamical regimes, I have used numerical simulations to identify basins of attraction of different steady states and periodic solutions depending on the initial level of infection and the initial number of regulatory T cells. The fact that for the same parameter values the system can exhibit bi-stability between a disease-free steady state and an autoimmune state, represented by sustained periodic oscillations following the clearance of infection, is very important from a clinical point of view, as effectively it suggests that the progress and eventual outcome of viral infection is also determined by the strength of infection and the initial state of the immune system. One counter-intuitive observation is that in the case of bi-stability with a disease-free steady state, for higher initial numbers of regulatory T cells, the autoimmune steady state is actually stable for a wider range of initial levels of infection. In this regime of bi-stability, increasing the time delay associated with the positive impact of IL-2 on proliferation of T cells results in the loss of stability of autoimmune steady state and emergence of autoimmune dynamics, characterised by stable periodic oscillations. On the contrary, in the case where the disease-free steady state is unstable, increasing this time delay results in stabilisation of the chronic infection.

There are several directions in which the work presented in this chapter can

be extended. One direction is exploration of the contributions from other components of immune response, more specifically, antibodies to the onset and progress of autoimmunity [194, 195]. Whilst this model has focused on one specific growth cytokine IL-2, a number of other cytokines, such as IL-7 [235], TNF-β and IL-10 [58], are known to significantly affect homeostasis and proliferation of different types of T cells, as well as mediate their efficiency in eliminating the infection. Including these immune mediators explicitly in the model can provide further significant insights into the dynamics of immune response, as has been recently demonstrated on the example of a detailed model of immune response to hepatitis B [236]. Another biologically relevant and mathematically challenging problem is the investigation of the interplay between stochasticity, which is known to be an intrinsic feature of immune response [22, 189], and effects of time delays associated with various aspects of immune dynamics. Hence, In the next Chapter I investigate stochastic effects in a time-delayed model for autoimmunity.

Chapter 6

Stochastic dynamics in a time-delayed model for autoimmunity

This chapter is based on the publication F. Fatehi, Y.N. Kyrychko, K.B. Blyuss, Stochastic dynamics in a time-delayed model for autoimmunity, 2019, submitted.

In this chapter I discuss stochastic effects in a time-delayed model for autoimmunity which allows us to investigate the role of stochastic effects in facilitating possible oscillatory dynamics in a deterministic model. Starting with a delay differential equations system, I use the discrete stochastic simulation method to derive a delay chemical master equation (DCME) which illustrates the probability density function of the model. To do stochastic simulations I derive an Itô SDDE model which provides similar trajectories to delay stochastic simulation algorithms (DSSAs), but faster. As follows, I apply the linear noise approximation (LNA) methodology to find the magnitude of stochastic fluctuations around *stable* deterministic steady states. This method also provides insights into how the coherence of stochastic oscillations around deterministically stable steady states depends on parameters.

6.1 Stochastic model: a delayed chemical master equation

In order to understand how stochasticity interacts with time-delayed effects in immune dynamics, I use the model (5.1), but in this chapter I assume that suppression of IL-2 by regulatory T cells is negligible ($\delta_2 = 0$) [237] because adding this parameter does not change the dynamical behaviour of the model and increasing this parameter is not effective in controlling of autoimmune response. The diagram of the model is shown in Fig. 6.1 and it has the form

$$\begin{aligned}
\frac{dA}{dt} &= rA\left(1-\frac{A}{N}\right) - \beta AF - \mu_a T_{aut} A,\\
\frac{dF}{dt} &= \beta A(t-\tau_1)F(t-\tau_1) - d_F F - \mu_F T_{nor} F - \mu_a T_{aut} F,\\
\frac{dT_{in}}{dt} &= \lambda_{in} - d_{in} T_{in} - \alpha T_{in} F,\\
\frac{dT_{reg}}{dt} &= \lambda_r - d_r T_{reg} + p_1 \alpha T_{in}(t-\tau_3)F(t-\tau_3) + \rho_1 I(t-\tau_2)T_{reg}(t-\tau_2),\\
\frac{dT_{nor}}{dt} &= p_2 \alpha T_{in}(t-\tau_3)F(t-\tau_3) - d_n T_{nor} + \rho_2 I(t-\tau_2)T_{nor}(t-\tau_2),\\
\frac{dT_{aut}}{dt} &= (1-p_1-p_2)\alpha T_{in}(t-\tau_3)F(t-\tau_3) - d_a T_{aut} - \delta T_{reg} T_{aut} + \rho_3 I(t-\tau_2)T_{aut}(t-\tau_2),\\
\frac{dI}{dt} &= \sigma_1 T_{nor} + \sigma_2 T_{aut} - d_i I.
\end{aligned} \tag{6.1}$$

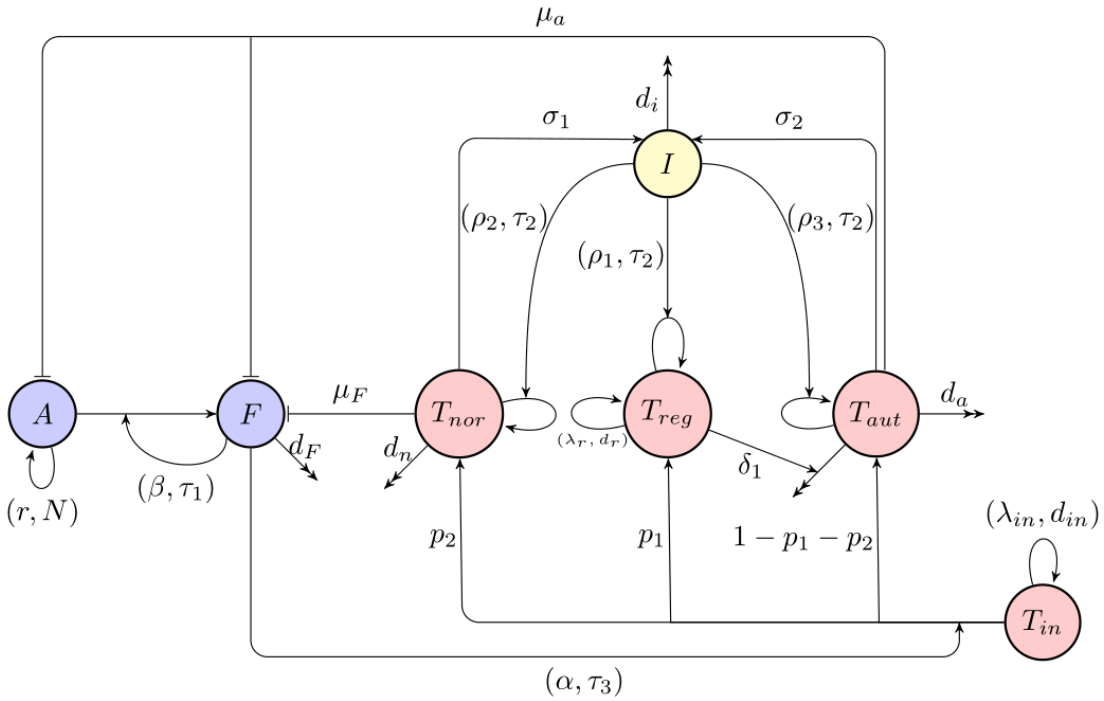

Figure 6.1: A diagram of immune response to an infection. Blue circles indicate host cells (uninfected and infected cells), red circles denote different T cells (naïve, regulatory, normal activated, and autoreactive T cells), yellow circle show cytokines (interleukin-2). τ_i's inside each of the subnetworks indicate the time delay in the respective processes.

To develop a stochastic version of this model, we introduce variables $X_1(t), \ldots,$ $X_7(t) \in \{0, 1, 2, \ldots\}$ as discrete random variables representing, respectively, the numbers of uninfected cells, infected cells, naïve T cells, regulatory T cells, normal activated T cells, autoreactive T cells, and interleukin 2 (IL-2) at time t, with the initial condition $\mathbf{X}(t) = \boldsymbol{\varphi}(t)$ for $t \in [-\tau, 0]$, where $\tau = \max\{\tau_1, \tau_2, \tau_3\}$. It is assumed that all these cells interact within some fixed volume Ω. The state change vector characterising each specific interaction between different cells R_j is denoted by $\mathbf{v}_j$, and its propensity function is given by $a_j(\mathbf{X}(t))$ in any given state $\mathbf{X}(t) = (X_1(t), X_2(t), \ldots, X_7(t))$. The propensity functions corresponding to interactions and transitions illustrated in Fig. 6.1 are given by [114, 117]

$$a_j(\mathbf{X}) = \begin{cases} b_1 X_1(t) + \dfrac{b_2}{\Omega} X_1(t)^2, & \mathbf{v}_1 = (1,0,0,0,0,0,0), \\ X_1(t)\left(d_1 + \dfrac{d_2}{\Omega} X_1(t) + \dfrac{\mu_a}{\Omega} X_6(t)\right), & \mathbf{v}_2 = (-1,0,0,0,0,0,0), \\ \dfrac{\beta}{\Omega} X_1(t-\tau_1) X_2(t-\tau_1), & \mathbf{v}_3 = (-1,1,0,0,0,0,0), \\ X_2(t)\left(d_F + \dfrac{\mu_F}{\Omega} X_5(t) + \dfrac{\mu_a}{\Omega} X_6(t)\right), & \mathbf{v}_4 = (0,-1,0,0,0,0,0), \\ \lambda_{in}\Omega, & \mathbf{v}_5 = (0,0,1,0,0,0,0), \\ d_{in} X_3(t), & \mathbf{v}_6 = (0,0,-1,0,0,0,0), \\ p_1 \dfrac{\alpha}{\Omega} X_2(t-\tau_3) X_3(t-\tau_3), & \mathbf{v}_7 = (0,0,-1,1,0,0,0), \\ p_2 \dfrac{\alpha}{\Omega} X_2(t-\tau_3) X_3(t-\tau_3), & \mathbf{v}_8 = (0,0,-1,0,1,0,0), \\ (1-p_1-p_2) \dfrac{\alpha}{\Omega} X_2(t-\tau_3) X_3(t-\tau_3), & \mathbf{v}_9 = (0,0,-1,0,0,1,0), \\ \lambda_r \Omega, & \mathbf{v}_{10} = (0,0,0,1,0,0,0), \\ \dfrac{\rho_1}{\Omega} X_4(t-\tau_2) X_7(t-\tau_2), & \mathbf{v}_{11} = (0,0,0,1,0,0,0), \\ d_r X_4(t), & \mathbf{v}_{12} = (0,0,0,-1,0,0,0), \\ \dfrac{\rho_2}{\Omega} X_5(t-\tau_2) X_7(t-\tau_2), & \mathbf{v}_{13} = (0,0,0,0,1,0,0), \\ d_n X_5(t), & \mathbf{v}_{14} = (0,0,0,0,-1,0,0), \\ \dfrac{\rho_3}{\Omega} X_6(t-\tau_2) X_7(t-\tau_2), & \mathbf{v}_{15} = (0,0,0,0,0,1,0), \\ X_6(t)\left(d_a + \dfrac{\delta}{\Omega} X_4(t)\right), & \mathbf{v}_{16} = (0,0,0,0,0,-1,0), \\ \sigma_1 X_5(t) + \sigma_2 X_6(t), & \mathbf{v}_{17} = (0,0,0,0,0,0,1), \\ d_i X_7(t), & \mathbf{v}_{18} = (0,0,0,0,0,0,-1), \end{cases} \tag{6.2}$$

where $b_1 X_1(t) + b_2 X_1(t)^2$ and $d_1 X_1(t) + d_2 X_1(t)^2$ are natural birth and death rates for uninfected cells at time t with $b_1 - d_1 = r$ and $d_2 - b_2 = \dfrac{r}{N}$ [196, 189]. In this model for numerical simulations I used $b_2 = 0$. Although vectors $\mathbf{v}_{10}$ and $\mathbf{v}_{11}$ show

the same change in state variables, it is important to explicitly separate them, since one of them happens with a time delay [114].

In order to derive the *delay chemical master equation* (DCME), one has to carefully account for delayed transitions/interactions. A convenient approach for handling time-delayed interactions has been proposed by Barrio et al. [115] in the context of an exact delay stochastic simulations algorithms. This methodology, when applied to chemical reactions (and for our model, individual cell populations can be interpreted and chemical reactants, and interactions between them as reaction), divides all reactions into three types: non-delayed reactions, non-consuming delayed reactions, and consuming delayed reactions. The distinction is that in consuming reactions, the reactants of an unfinished reaction cannot participate in a new reaction, On the other hand, in non-consuming reactions, the reactants of an unfinished reaction can participate in another reaction [115, 116]. This then translates into when the associated update of the state of the system takes place, and what the corresponding state change vector is. In non-delayed and delayed non-consuming reactions, there is a single time point where the update of the system happens both for original reactants and the resulting products - it happens either immediately in the case of non-delayed reactions, or, respectively, after the end of delay for delayed non-consuming reactions. In contrast, for delayed consuming reactions, there are two update points: original reactants are updated at the initiation of reaction, while the products are updated at the end of time delay. Based on the deterministic model (6.1), the stimulation and proliferation of activated T cells with a positive growth signal (IL-2) is a non-consuming reaction. In contrast, activation of naïve T cells, and production of infected cells from uninfected cells are consuming delay reactions. Therefore, the state change vector for these reactions should be split into two vectors, with one of them indicating the state change in the absence of delays, and the other one showing the state change of products which occurs with a delay [120].

If we denote the probability of finding the system in the state $\mathbf{n} = (n_1, n_2, n_3, n_4, n_5, n_6, n_7)$ with $n_i \in \{0, 1, 2, ...\}$ at time t by

$$P(\mathbf{n}, t) = \text{Prob}\{\mathbf{X}(t) = \mathbf{n} | \boldsymbol{\varphi}(t)\}.$$

it then satisfies the following DCME [114, 115, 120]

$$\frac{\partial P(\mathbf{n},t)}{\partial t} = \Big\{(\varepsilon_1^- - 1)a_1(\mathbf{n}) + (\varepsilon_1^+ - 1)\Big[a_2(\mathbf{n}) + a_3(\mathbf{n})\Big] + (\varepsilon_2^+ - 1)a_4(\mathbf{n})$$

$$+(\varepsilon_3^- - 1)a_5(\mathbf{n}) + (\varepsilon_3^+ - 1)\Big[a_6(\mathbf{n}) + a_7(\mathbf{n}) + a_8(\mathbf{n}) + a_9(\mathbf{n})\Big] + (\varepsilon_4^- - 1)a_{10}(\mathbf{n})$$

$$+(\varepsilon_4^+ - 1)a_{12}(\mathbf{n}) + (\varepsilon_5^+ - 1)a_{14}(\mathbf{n}) + (\varepsilon_6^+ - 1)a_{16}(\mathbf{n}) + (\varepsilon_7^- - 1)a_{17}(\mathbf{n})$$

$$+(\varepsilon_7^+ - 1)a_{18}(\mathbf{n})\Big\}P(\mathbf{n},t) + \sum_{\mathbf{m}\in I(\mathbf{n})}\Big[a_3(\mathbf{m})(\varepsilon_2^- - 1)P(\mathbf{n},t;\mathbf{m},t-\tau_1)\Big]$$

$$+\sum_{\mathbf{m}\in I(\mathbf{n})}\Big[\Big\{a_{11}(\mathbf{m})(\varepsilon_4^- - 1) + a_{13}(\mathbf{m})(\varepsilon_5^- - 1) + a_{15}(\mathbf{m})(\varepsilon_6^- - 1)\Big\}P(\mathbf{n},t;\mathbf{m},t-\tau_2)\Big]$$

$$+\sum_{\mathbf{m}\in I(\mathbf{n})}\Big[\Big\{a_7(\mathbf{m})(\varepsilon_4^- - 1) + a_8(\mathbf{m})(\varepsilon_5^- - 1) + a_9(\mathbf{m})(\varepsilon_6^- - 1)\Big\}P(\mathbf{n},t;\mathbf{m},t-\tau_3)\Big], \tag{6.3}$$

where $I(\mathbf{n})$ is the set of all possible system states in the past, from which the state $\mathbf{n}$ is able to follow via a chain of transitions, an operator $\varepsilon_i^{\pm}$ is defined as follows,

$$\varepsilon_i^{\pm} f(n_1,n_2,n_3,n_4,n_5,n_6,n_7,t) = f(n_1,...,n_i \pm 1,...,n_7,t), \text{ for each } 1 \le i \le 7,$$

and if $n_i < 0$ for any $1 \le i \le 7$, then $P(\mathbf{n},t) = 0$.

To simulate the above model, one can use delay stochastic simulation algorithms (DSSA), which describe the evolution of this delay discrete process over time, and also solve the DCME (6.3) to obtain the probability density function of the model. However, the discrete stochastic simulation methods are very computationally expensive [121, 201, 122], and solving the DCME is also a very challenging task. To deal with this problem, we will use delay chemical Langevin equation models which are more computationally efficient [122], and since we want to derive a continuous approximation of a delay discrete stochastic model, in which the jump probability is proportional to the number of available cells before the jump, it is better to use the Itô formulation [199]. Therefore, we will use Itô stochastic delay differential equation (SDDE) models which are based on the Langevin approach when the propensity

functions associated with the reactions are relatively large [121].

6.2 Itô SDDE model

To derive a computationally convenient form of SDDE, we will proceed in several steps. First, we will follow the methodology of Tian et al. [121] to obtain one possible formulation of SDDE directly from the DCME. Then we will use an approach similar to that of Allen et al. [206] for non-delayed stochastic equations to prove that another formulation of the SDDE is possible, which is equivalent both in distribution, and in sample paths. This is an important result as it addresses an issue mentioned in Tian et al. [121], where two different formulations of an SDDE gave slightly different results. Finally, we will formulate an equivalent but simplified form of SDDE and apply to our model.

As a starting point, drawing an analogy between cell interactions and chemical reactions, we consider a system of N molecular species $S = \{S_1, \ldots, S_N\}$, whose state at time t is described by a vector $\mathbf{X}(t) = (X_1(t), \ldots, X_N(t))$, and these species react through reactions $\{R_1, \ldots, R_m\}$. Each reaction R_j is characterised by a state change vector $\mathbf{v}_j = (v_{1j}, v_{2j}, \ldots, v_{Nj})^T$, and the associated propensity function a_j. As mentioned earlier, non-delayed and delayed non-consuming reactions have a single update vector $\mathbf{v}$, whereas for delayed consuming reactions, $\mathbf{v}_j^r$ and $\mathbf{v}_j^p$ are the update vectors for reactants at the start of reaction, and for products at the end of the time delay associated with reaction R_j, respectively, so $\mathbf{v}_j^r + \mathbf{v}_j^p = \mathbf{v}_j$. Assuming the first m_1 reactions to be non-delayed, the reactions $m_1 + 1$ to m_2 to be delayed non-consuming reactions with corresponding time delays $\tau_{m_1+1}, \ldots, \tau_{m_2}$, and the rest to be consuming delayed reactions with time delays $\tau_{m_2+1}, \ldots, \tau_m$, the DCME accounting for all non-consuming and consuming reactions is then given by [120]

$$\begin{aligned}\frac{\partial}{\partial t}P(\mathbf{X},t) =& -\sum_{j=1}^{m_1} a_j(\mathbf{X})P(\mathbf{X},t) + \sum_{j=1}^{m_1} a_j(\mathbf{X}-\mathbf{v}_j)P(\mathbf{X}-\mathbf{v}_j,t)\\ &- \sum_{j=m_1+1}^{m_2}\sum_{\mathbf{X}_i\in I(\mathbf{X})} a_j(\mathbf{X}_i)P(\mathbf{X},t;\mathbf{X}_i,t-\tau_j)\\ &+ \sum_{j=m_1+1}^{m_2}\sum_{\mathbf{X}_i\in I(\mathbf{X})} a_j(\mathbf{X}_i)P(\mathbf{X}-\mathbf{v}_j,t;\mathbf{X}_i,t-\tau_j)\\ &- \sum_{j=m_2+1}^{m}\sum_{\mathbf{X}_i\in I(\mathbf{X})} a_j(\mathbf{X}_i)P(\mathbf{X},t;\mathbf{X}_i,t-\tau_j)\\ &+ \sum_{j=m_2+1}^{m}\sum_{\mathbf{X}_i\in I(\mathbf{X})} a_j(\mathbf{X}_i)P(\mathbf{X}-\mathbf{v}_j^p,t;\mathbf{X}_i,t-\tau_j)\\ &- \sum_{j=m_2+1}^{m} a_j(\mathbf{X})P(\mathbf{X},t) + \sum_{j=m_2+1}^{m} a_j(\mathbf{X}-\mathbf{v}_j^r)P(\mathbf{X}-\mathbf{v}_j,t), \end{aligned} \tag{6.4}$$

where $I(\mathbf{X})$ is the set of all possible system states in the past, from which the given state $\mathbf{X}$ can follow via a chain of reactions. Applying the same method as in Tian et al. [121], the corresponding SDDE model which faithfully represents the intrinsic noise associated with all those delayed reaction, has the form

$$\begin{aligned} d\mathbf{X} =& \sum_{j=1}^{m_1}\mathbf{v}_j a_j(\mathbf{X}(t))dt + \sum_{j=m_1+1}^{m_2}\mathbf{v}_j a_j(\mathbf{X}(t-\tau_j))dt\\ &+ \sum_{j=m_2+1}^{m}\mathbf{v}_j^r a_j(\mathbf{X}(t))dt + \sum_{j=m_2+1}^{m}\mathbf{v}_j^p a_j(\mathbf{X}(t-\tau_j))dt\\ &+ \sum_{j=1}^{m_1}\mathbf{v}_j\sqrt{a_j(\mathbf{X}(t))}dW_j(t) + \sum_{j=m_1+1}^{m_2}\mathbf{v}_j\sqrt{a_j(\mathbf{X}(t-\tau_j))}dW_j(t)\\ &+ \sum_{j=m_2+1}^{m}\mathbf{v}_j^r\sqrt{a_j(\mathbf{X}(t))}dW_j(t) + \sum_{j=m_2+1}^{m}\mathbf{v}_j^p\sqrt{a_j(\mathbf{X}(t-\tau_j))}dW_{j-m_2+m}(t)\\ =& f\left(\mathbf{X}(t),\mathbf{X}(t-\tau_{m_1+1}),\ldots,\mathbf{X}(t-\tau_m)\right)dt + Hd\mathbf{W}(t), \end{aligned} \tag{6.5}$$

where $\mathbf{W}(t) = (W_1(t), W_2(t), \ldots, W_{2m-m_2})$ is a vector of independent Wiener processes, and $H = \begin{pmatrix} H_1 & H_2 & H_3 & H_4 \end{pmatrix}$ is a $N \times (2m - m_2)$ matrix which

$$H_1 = \begin{pmatrix} v_{11}\sqrt{a_1(\mathbf{X}(t))} & v_{12}\sqrt{a_2(\mathbf{X}(t))} & \cdots & v_{1m_1}\sqrt{a_{m_1}(\mathbf{X}(t))}\\ v_{21}\sqrt{a_1(\mathbf{X}(t))} & v_{22}\sqrt{a_2(\mathbf{X}(t))} & \cdots & v_{2m_1}\sqrt{a_{m_1}(\mathbf{X}(t))}\\ \vdots & \vdots & \ddots & \vdots\\ v_{N1}\sqrt{a_1(\mathbf{X}(t))} & v_{N2}\sqrt{a_2(\mathbf{X}(t))} & \cdots & v_{Nm_1}\sqrt{a_{m_1}(\mathbf{X}(t))} \end{pmatrix}_{N\times m_1},$$

$$H_2 = \begin{pmatrix} v_{1(m_1+1)}\sqrt{a_{m_1+1}(\mathbf{X}(t-\tau_{m_1+1}))} & \cdots & v_{1m_2}\sqrt{a_{m_2}(\mathbf{X}(t-\tau_{m_2}))} \\ v_{2(m_1+1)}\sqrt{a_{m_1+1}(\mathbf{X}(t-\tau_{m_1+1}))} & \cdots & v_{2m_2}\sqrt{a_{m_2}(\mathbf{X}(t-\tau_{m_2}))} \\ \vdots & \ddots & \vdots \\ v_{N(m_1+1)}\sqrt{a_{m_1+1}(\mathbf{X}(t-\tau_{m_1+1}))} & \cdots & v_{Nm_2}\sqrt{a_{m_2}(\mathbf{X}(t-\tau_{m_2}))} \end{pmatrix}_{N\times(m_2-m_1)},$$

$$H_3 = \begin{pmatrix} v^r_{1(m_2+1)}\sqrt{a_{m_2+1}(\mathbf{X}(t))} & v^r_{1(m_2+2)}\sqrt{a_{m_2+2}(\mathbf{X}(t))} & \cdots & v^r_{1m}\sqrt{a_m(\mathbf{X}(t))} \\ v^r_{2(m_2+1)}\sqrt{a_{m_2+1}(\mathbf{X}(t))} & v^r_{2(m_2+2)}\sqrt{a_{m_2+2}(\mathbf{X}(t))} & \cdots & v^r_{2m}\sqrt{a_m(\mathbf{X}(t))} \\ \vdots & \vdots & \ddots & \vdots \\ v^r_{N(m_2+1)}\sqrt{a_{m_2+1}(\mathbf{X}(t))} & v^r_{N(m_2+2)}\sqrt{a_{m_2+2}(\mathbf{X}(t))} & \cdots & v^r_{Nm}\sqrt{a_m(\mathbf{X}(t))} \end{pmatrix}_{N\times(m-m_2)},$$

$$H_4 = \begin{pmatrix} v^p_{1(m_2+1)}\sqrt{a_{m_2+1}(\mathbf{X}(t-\tau_{m_2+1}))} & \cdots & v^p_{1m}\sqrt{a_m(\mathbf{X}(t-\tau_m))} \\ v^p_{2(m_2+1)}\sqrt{a_{m_2+1}(\mathbf{X}(t-\tau_{m_2+1}))} & \cdots & v^p_{2m}\sqrt{a_m(\mathbf{X}(t-\tau_m))} \\ \vdots & \ddots & \vdots \\ v^p_{N(m_2+1)}\sqrt{a_{m_2+1}(\mathbf{X}(t-\tau_{m_2+1}))} & \cdots & v^p_{Nm}\sqrt{a_m(\mathbf{X}(t-\tau_m))} \end{pmatrix}_{N\times(m-m_2)}.$$

Tian et al. [121] have also considered an alternative formulation of the model in the form

$$\begin{aligned} d\mathbf{X}^*(t) =& \mathbf{f}\left(\mathbf{X}^*(t), \mathbf{X}^*(t-\tau_1), \ldots, \mathbf{X}^*(t-\tau_r), t\right) dt \\ &+ G\left(\mathbf{X}^*(t), \mathbf{X}^*(t-\tau_1), \ldots, \mathbf{X}^*(t-\tau_r), t\right) d\mathbf{W}^*(t), \end{aligned} \tag{6.6}$$

where $\mathbf{X}^*(t) = [X_1^*(t), X_2^*(t), \ldots, X_N^*(t)]^T$, $\mathbf{W}^*(t) = [W_1^*(t), W_2^*(t), \ldots, W_N^*(t)]^T$, with W_j^*, $1 \le j \le N$, being independent Wiener processes, and G being an $N \times N$ symmetric positive semidefinite matrices related to H through an $N \times N$ matrix V, where $V = HH^T$ and $G = V^{1/2}$, which also implies $V = GG^T$. For convenience, we have also renumbered time delays from τ_{m_1+1} to τ_m into τ_1 to τ_r. By considering a particular example of a model for gene regulatory networks, Tian et al. have shown using 10000 simulations that there is little difference between means and variances of the above two stochastic models, while also noting that "*more work is needed to compare the difference between the two types of the Langevin approach*" [121].

To address this problem, we will now extend the methodology used by Allen et al. [206] for systems without delays to show that the above two models are actually equivalent in the sense that their solutions have the same probability distribution, as well as the same sample path solutions.

To show that systems (6.5) and (6.6) are equivalent in distribution, i.e. their solutions have the same probability distribution, it suffice to show that the probability density function for both of these systems satisfies the same forward Kolmogorov or Fokker-Planck equation. This is established by the following result, which generalises earlier work in [128, 238] to the case of multiple time delays and multi-dimensional stochastic system.

Theorem 6.1. *Consider the following Itô SDDE model*

$$\begin{aligned} dX_i(t) =& f_i\left(\boldsymbol{X}(t), \boldsymbol{X}(t-\tau_1), \ldots, \boldsymbol{X}(t-\tau_r), t\right) dt \\ &+ \sum_{j=1}^{m} g_{ij}\left(\boldsymbol{X}(t), \boldsymbol{X}(t-\tau_1), \ldots, \boldsymbol{X}(t-\tau_r), t\right) dW^j(t), \end{aligned}$$

where $W^j(t)$ are independent Wiener processes, and

$$f_i : \underbrace{\mathbb{R}^N \times \mathbb{R}^N \times \cdots \times \mathbb{R}^N}_{(r+1)\text{-times}} \times \mathbb{R} \to \mathbb{R}, \quad g_{ij} : \underbrace{\mathbb{R}^N \times \mathbb{R}^n \times \cdots \times \mathbb{R}^N}_{(r+1)\text{-times}} \times \mathbb{R} \to \mathbb{R},$$

for every $1 \leq i \leq N$ and $1 \leq j \leq m$, with the initial condition $\boldsymbol{X}(t) = \boldsymbol{\varphi}(t)$ for $t \in [-\tau, 0]$, where $\tau = \max\{\tau_1, \ldots, \tau_r\}$. The corresponding delay Fokker-Planck equation has the form

$$\begin{aligned} \frac{\partial}{\partial t} P(\boldsymbol{x}, t \mid \boldsymbol{\varphi}) = & \\ & - \sum_{i=1}^{N} \frac{\partial}{\partial x_i} \underbrace{\int \cdots \int}_{r} f_i(\boldsymbol{x}, \boldsymbol{x}_{\tau_1}, \ldots, \boldsymbol{x}_{\tau_r}, t) P(\boldsymbol{x}, t; \boldsymbol{x}_{\tau_1}, t-\tau_1; \ldots; \boldsymbol{x}_{\tau_r}, t-\tau_r \mid \boldsymbol{\varphi}) dV \\ & + \frac{1}{2} \sum_{i,j} \frac{\partial^2}{\partial x_i \partial x_j} \underbrace{\int \cdots \int}_{r} \left(GG^T\right)_{ij} P(\boldsymbol{x}, t; \boldsymbol{x}_{\tau_1}, t-\tau_1; \ldots; \boldsymbol{x}_{\tau_r}, t-\tau_r \mid \boldsymbol{\varphi}) dV, \end{aligned}$$

where $dV = d\boldsymbol{x}_{\tau_1} d\boldsymbol{x}_{\tau_2} \ldots d\boldsymbol{x}_{\tau_r}$, and G is an $n \times m$ matrix with $G_{ij} = g_{ij}(\boldsymbol{x}, \boldsymbol{x}_{\tau_1}, \ldots, \boldsymbol{x}_{\tau_r}, t)$, for every $1 \leq i \leq N$ and $1 \leq j \leq m$.

Proof. Let us consider the joint probability density

$$P(\mathbf{x},t;\mathbf{x}',t';\mathbf{x}_{\tau_1},t'-\tau_1;\ldots;\mathbf{x}_{\tau_r},t'-\tau_r \mid \boldsymbol{\varphi}) = \left\langle \delta\big(\mathbf{x}-\mathbf{X}(t)\big)\delta\big(\mathbf{x}'-\mathbf{X}(t')\big)\prod_{k=1}^{r}\delta\big(\mathbf{x}_{\tau_k}-\mathbf{X}(t'-\tau_k)\big)\right\rangle$$

for $t \geq t'$, where $\langle \ldots \rangle$ denotes ensemble average, and $\delta(\cdot)$ is the Dirac delta function. Expressing the single time-point probability density $P(\mathbf{x},t \mid \boldsymbol{\varphi})$ through the conditional probability density and utilising the generalized Kramers-Moyal expansion [128, 238] yields the following PDE

$$\frac{\partial}{\partial t}P(\mathbf{x},t \mid \boldsymbol{\varphi}) = \sum_{\upsilon=1}^{\infty}\sum_{j_1,j_2,\ldots,j_\upsilon}\frac{(-\partial)^\upsilon}{\partial x_{j_1}\ldots\partial x_{j_\upsilon}}\underbrace{\int\cdots\int}_{r}D^{(\upsilon)}_{j_1\ldots j_\upsilon}P(\mathbf{x},t;\mathbf{x}_{\tau_1},t-\tau_1;\ldots;\mathbf{x}_{\tau_r},t-\tau_r \mid \boldsymbol{\varphi})dV,$$

where $dV = d\mathbf{x}_{\tau_1}d\mathbf{x}_{\tau_2}\ldots d\mathbf{x}_{\tau_r}$, and $D^{(\upsilon)}_{j_1\ldots j_\upsilon}(\cdot)$ are given by

$$D^{(\upsilon)}_{j_1\ldots j_\upsilon}(\mathbf{x},\mathbf{x}_{\tau_1},\ldots,\mathbf{x}_{\tau_r},t) = \lim_{h\to 0}\frac{1}{h}\int\frac{\prod_{k=1}^{\upsilon}(y_{j_k}-x_{j_k})}{\upsilon!}P(\mathbf{y},t+h \mid \mathbf{x},t;\mathbf{x}_{\tau_1},t-\tau_1;\ldots;\mathbf{x}_{\tau_r},t-\tau_r;\boldsymbol{\varphi})d\mathbf{y}.$$

Since we are working with an Itô SDDE, it is possible to reformulate the problem in the form of Langevin equation similar to the case of Markov process [128]. If we then rewrite coefficients $D^{(\upsilon)}_{j_1\ldots j_\upsilon}$ in the form

$$D^{(\upsilon)}_{j_1\ldots j_\upsilon}(\mathbf{x},\mathbf{x}_{\tau_1},\ldots,\mathbf{x}_{\tau_r},t) = \lim_{h\to 0}\frac{1}{h}\left.\frac{\left\langle\prod_{k=1}^{\upsilon}\big(X_{j_k}(t+h)-X_{j_k}(t)\big)\right\rangle}{\upsilon!}\right|_{\mathbf{X}(t)=\mathbf{x},\mathbf{X}(t-\tau_1)=\mathbf{x}_{\tau_1},\ldots,\mathbf{X}(t-\tau_r)=\mathbf{x}_{\tau_r}}, \quad (6.7)$$

we can use the time-discrete version of the SDDE model [128, 238] to obtain the following expressions for these coefficients

$$\begin{aligned}
D^{(1)}_i(\mathbf{x},\mathbf{x}_{\tau_1},\ldots,\mathbf{x}_{\tau_r},t) &= f_i(\mathbf{x},\mathbf{x}_{\tau_1},\ldots,\mathbf{x}_{\tau_r},t),\\
D^{(2)}_{ij}(\mathbf{x},\mathbf{x}_{\tau_1},\ldots,\mathbf{x}_{\tau_r},t) &= \frac{1}{2}\sum_{k=1}^{m}g_{ik}(\mathbf{x},\mathbf{x}_{\tau_1},\ldots,\mathbf{x}_{\tau_r},t)g_{jk}(\mathbf{x},\mathbf{x}_{\tau_1},\ldots,\mathbf{x}_{\tau_r},t),\\
D^{(\upsilon)}_{j_1\ldots j_\upsilon}(\mathbf{x},\mathbf{x}_{\tau_1},\ldots,\mathbf{x}_{\tau_r},t) &= 0, \quad \text{for every } \upsilon \geq 3,
\end{aligned}$$

which completes the proof. □

Due to the relation $V = GG^T = HH^T$, Theorem 6.1 implies that solutions to (6.5) and (6.6) do indeed have the same probability distribution. Using a minor modification of methodology of Allen et al. [206], it is straightforward to show that a sample path solution of one of these systems is also a sample path of the second one, i.e. given a Wiener trajectory $\mathbf{W}(t)$ with the sample path solution $\mathbf{X}(t)$ to (6.5), there exist a Wiener trajectory $\mathbf{W}^*(t)$ with the sample path solution $\mathbf{X}^*(t) = \mathbf{X}(t)$ to (6.6), and vice versa (see Appendix B for details). Taken together, these two results confirm the systems (6.5) and (6.6) are indeed equivalent both in distribution, and in sample paths. Effectively, this means that the dynamics of model (6.5) is equivalent to the dynamics of any other similar model (6.6) which has the same function $\mathbf{f}$, and as long as $GG^T = V$. The importance of this result is that since normally there is a larger number of reactions involved, by allowing one to replace an $N \times (2m - m_2)$ matrix by an $N \times N$ matrix with $2m - m_2 \gg N$, this equivalence can significantly reduce computational complexity of the resulting SDDE model.

Now that the equivalence of systems (6.5) and (6.6) has been established, let us present an alternative approach for finding the function $\mathbf{f}(\mathbf{X}(t), \mathbf{X}(t-\tau_1), \ldots, \mathbf{X}(t-\tau_r))$ and the matrix H, such that $HH^T = V$, which is similar to the method presented earlier in [189, 205] for systems without time delays. Using again the terminology of chemical reactions, let $\mathbf{Y}(t) = (Y_1(t), Y_2(t), \ldots, Y_N(t))$ be a vector of continuous random variables representing the amounts of molecular species at time t.

Table 6.1: State changes $\Delta\mathbf{Y}$ in a small time interval Δt

i	$(\Delta\mathbf{Y})_i$	Probability $P_i\Delta t$
1	$\mathbf{v}_1$	$a_1(\mathbf{Y})\Delta t$
$\vdots$	$\vdots$	$\vdots$
m_1	$\mathbf{v}_{m_1}$	$a_{m_1}(\mathbf{Y})\Delta t$
m_1+1	$\mathbf{v}_{m_1+1}$	$a_{m_1+1}(\mathbf{Y})\Delta t$
$\vdots$	$\vdots$	$\vdots$
m_2	$\mathbf{v}_{m_2}$	$a_{m_2}(\mathbf{Y})\Delta t$
m_2+1	$\mathbf{v}^r_{m_2+1}$	$a_{m_2+1}(\mathbf{Y})\Delta t$
$\vdots$	$\vdots$	$\vdots$
m	$\mathbf{v}^r_m$	$a_m(\mathbf{Y})\Delta t$
$m+1$	$\mathbf{v}^p_{m_2+1}$	$a_{m_2+1}(\mathbf{Y})\Delta t$
$\vdots$	$\vdots$	$\vdots$
$2m-m_2$	$\mathbf{v}^p_m$	$a_m(\mathbf{Y})\Delta t$
$2m-m_2+1$	$\mathbf{0}$	$1-\sum_{i=1}^{2m-m_2} P_i\Delta t$

As before, it is assumed that these species are well-mixed and interact in such as way that the first m_1 reactions are non-delayed, reactions m_1+1 to m_2 are delayed non-consuming reactions, and the remaining reactions are delayed consuming reactions. We assume that Δt is small enough, so that during this time interval at most one change can occur in state variables as represented by the state change vectors, and if it is a consuming delay reaction, then we split its state change vector into two vectors in a similar way to how it was done for the DCME (6.4). These state changes together with corresponding probabilities are listed in Table 6.1. Using this table of possible state changes, one can compute the expectation vector and covariance matrix of $\Delta\mathbf{Y}$ for sufficiently small Δt.

The expectation vector to order Δt is given by

$$\mathbb{E}(\Delta\mathbf{Y}) \approx \sum_{i=1}^{2m-m_2} P_i(\Delta\mathbf{Y})_i\Delta t = \mathbf{f}\left(\mathbf{Y}(t), \mathbf{Y}(t-\tau_{m_1+1}), \ldots, \mathbf{Y}(t-\tau_m)\right)\Delta t = \boldsymbol{\mu}\Delta t,$$

and the covariance matrix is obtained by only keeping terms of order Δt, i.e.

$$\begin{aligned}\operatorname{cov}(\Delta\mathbf{Y}) &= \mathbb{E}\left[(\Delta\mathbf{Y})(\Delta\mathbf{Y})^T\right] - \mathbb{E}\left[\Delta\mathbf{Y}\right]\left(\mathbb{E}\left[\Delta\mathbf{Y}\right]\right)^T \approx \mathbb{E}\left[(\Delta\mathbf{Y})(\Delta\mathbf{Y})^T\right] \\ &= \sum_{i=1}^{2m-m_2} P_i(\Delta\mathbf{Y})_i(\Delta\mathbf{Y}_i)^T\Delta t = \Sigma\Delta t,\end{aligned}$$

where it can be easily shown that replacing $\mathbf{X}$ with $\mathbf{Y}$ in the matrix H in (6.5) would give $HH^T = \Sigma$.

In summary, to derive a SDDE model for a discrete delay process with delays $\{\tau_1, \tau_2, \ldots, \tau_r\}$, first we have to find the possible state changes table, then we have to find the expectation vector $\boldsymbol{\mu}$ which is called the drift vector, and covariance matrix Σ also known as the diffusion matrix, from which we will find an $N \times N$ matrix H satisfying $HH^T = \Sigma$. One should note that the order of the entries in the table of state changes is irrelevant, since all entries come with their respective probabilities. Moreover, if any two (or more) entries have the same vectors representing a state change, these entries can be combined into one, with the associated probability being the sum of individual probabilities of those entries. This would reduce the size of the tables of state changes, but would not affect the drift vector of the diffusion matrix. The resulting Itô SDDE model has the form

$$\begin{cases} d\mathbf{Y}(t) = \boldsymbol{\mu}dt + Hd\mathbf{W}(t), \\ \mathbf{Y}(t) = \boldsymbol{\varphi}(t) \quad \text{for} \quad t \in [-\tau, 0], \end{cases} \tag{6.8}$$

where $\tau = \max\{\tau_1, \ldots, \tau_r\}$, and $\mathbf{W}(t)$ is an N-dimensional vector of independent Wiener processes.

Table 6.2: Possible state changes $\Delta\mathbf{Y}$ during a small time interval Δt

i	$(\Delta\mathbf{Y})_i^T$	Probability $P_i\Delta t$
1	$(1,0,0,0,0,0,0)$	$\left(b_1Y_1(t)+\frac{b_2}{\Omega}Y_1(t)^2\right)\Delta t$
2	$(-1,0,0,0,0,0,0)$	$\left(d_1Y_1(t)+\frac{d_2}{\Omega}Y_1(t)^2+\frac{\mu_a}{\Omega}Y_6(t)Y_1(t)+\frac{\beta}{\Omega}Y_1(t)Y_2(t)\right)\Delta t$
3	$(0,1,0,0,0,0,0)$	$\frac{\beta}{\Omega}Y_1(t-\tau_1)Y_2(t-\tau_1)\Delta t$
4	$(0,-1,0,0,0,0,0)$	$\left[d_F+\frac{\mu_F}{\Omega}Y_5(t)+\frac{\mu_a}{\Omega}Y_6(t)\right]Y_2(t)\Delta t$
5	$(0,0,1,0,0,0,0)$	$\lambda_{in}\Omega\Delta t$
6	$(0,0,-1,0,0,0,0)$	$\left[d_{in}Y_3(t)+\frac{\alpha}{\Omega}Y_3(t)Y_2(t)\right]\Delta t$
7	$(0,0,0,1,0,0,0)$	$p_1\frac{\alpha}{\Omega}Y_3(t-\tau_3)Y_2(t-\tau_3)\Delta t$
8	$(0,0,0,0,1,0,0)$	$p_2\frac{\alpha}{\Omega}Y_3(t-\tau_3)Y_2(t-\tau_3)\Delta t$
9	$(0,0,0,0,0,1,0)$	$(1-p_1-p_2)\frac{\alpha}{\Omega}Y_3(t-\tau_3)Y_2(t-\tau_3)\Delta t$
10	$(0,0,0,1,0,0,0)$	$\lambda_r\Omega\Delta t$
11	$(0,0,0,1,0,0,0)$	$\frac{\rho_1}{\Omega}Y_7(t-\tau_2)Y_4(t-\tau_2)\Delta t$
12	$(0,0,0,-1,0,0,0)$	$d_rY_4(t)\Delta t$
13	$(0,0,0,0,1,0,0)$	$\frac{\rho_2}{\Omega}Y_7(t-\tau_2)Y_5(t-\tau_2)\Delta t$
14	$(0,0,0,0,-1,0,0)$	$d_nY_5(t)\Delta t$
15	$(0,0,0,0,0,1,0)$	$\frac{\rho_3}{\Omega}Y_7(t-\tau_2)Y_6(t-\tau_2)\Delta t$
16	$(0,0,0,0,0,-1,0)$	$\left[d_a+\frac{\delta}{\Omega}Y_4(t)\right]Y_6(t)\Delta t$
17	$(0,0,0,0,0,0,1)$	$\left[\sigma_1Y_5(t)+\sigma_2Y_6(t)\right]\Delta t$
18	$(0,0,0,0,0,0,-1)$	$d_iY_7(t)\Delta t$
19	$(0,0,0,0,0,0,0)$	$1-\sum_{i=1}^{18}P_i\Delta t$

Using the above method, we can now derive an SDDE model associated with the model (6.2). Let $\mathbf{Y}(t)=(Y_1(t),Y_2(t),Y_3(t),Y_4(t),Y_5(t),Y_6(t),Y_7(t))$ be a continuous random vector for the sizes of various cell compartments at time t, and Δt be small enough so that during this time interval at most one change can occur in state variables. These changes together with their probabilities are listed in Table 6.2. Using this table of possible state changes, one can compute the expectation vector and covariance matrix of $\Delta\mathbf{Y}$ for sufficiently small Δt.

The expectation vector to order Δt is now given by

$$\mathbb{E}(\Delta \mathbf{Y}) \approx \sum_{i=1}^{18} P_i (\Delta \mathbf{Y})_i \Delta t = \boldsymbol{\mu} \Delta t,$$

where

$$\boldsymbol{\mu} = \begin{pmatrix} P_1 - P_2 \\ P_3 - P_4 \\ P_5 - P_6 \\ P_7 + P_{10} + P_{11} - P_{12} \\ P_8 + P_{13} - P_{14} \\ P_9 + P_{15} - P_{16} \\ P_{17} - P_{18} \end{pmatrix}$$

is the drift vector, which is identical to the right-hand side of the deterministic model (6.1). The covariance matrix is obtained by only keeping terms of order Δt, i.e.

$$\mathrm{cov}(\Delta \mathbf{Y}) \approx \sum_{i=1}^{18} P_i (\Delta \mathbf{Y})_i (\Delta \mathbf{Y}_i)^T \Delta t = \Sigma \Delta t,$$

where

$$\Sigma = \begin{pmatrix} P_1 + P_2 & 0 & 0 & 0 & 0 & 0 & 0 \\ 0 & P_3 + P_4 & 0 & 0 & 0 & 0 & 0 \\ 0 & 0 & P_5 + P_6 & 0 & 0 & 0 & 0 \\ 0 & 0 & 0 & P_7 + P_{10} + P_{11} + P_{12} & 0 & 0 & 0 \\ 0 & 0 & 0 & 0 & P_8 + P_{13} + P_{14} & 0 & 0 \\ 0 & 0 & 0 & 0 & 0 & P_9 + P_{15} + P_{16} & 0 \\ 0 & 0 & 0 & 0 & 0 & 0 & P_{17} + P_{18} \end{pmatrix}$$

is a 7×7 diffusion matrix. Since Σ is a diagonal matrix, the matrix H is also a diagonal matrix with $H_{ii} = \sqrt{\Sigma_{ii}}$ for $1 \leq i \leq 7$. The Itô SDDE model thus has the form

$$\begin{cases} d\mathbf{Y}(t) = \boldsymbol{\mu} dt + H d\mathbf{W}(t), \\ \mathbf{Y}(t) = \boldsymbol{\varphi}(t) \quad \text{for} \quad t \in [-\tau, 0], \end{cases} \tag{6.9}$$

where $\tau = \max\{\tau_1, \tau_2, \tau_3\}$, and $\mathbf{W}(t) = [W_1(t), W_2(t), \ldots, W_7(t)]^T$ is a vector of seven independent Wiener processes, and $\boldsymbol{\varphi}(t)$ is the vector of initial conditions. This form of SDDE is amenable to direct numerical simulations, which will be

performed in Section 6.4 to illustrate various dynamical behaviours of the model.

6.3 System size expansion and fluctuations

In principle, one could try to find an approximate probability density function for the above model (6.9) as a solution of the Fokker-Planck equation derived as an approximation of the master equation [205, 207]. However, since this equation would be a linear high-dimensional PDE, solving it analytically is impossible. Therefore, we will instead use a so-called system size expansion, or van Kampen's expansion [199], of the DCME to construct a continuous approximation for discrete stochastic models [88, 89, 122]. This will allow us to decompose the time evolution of each cell population into deterministic and stochastic components, thus providing a methodology for analytically studying fluctuations around deterministic attractors [122, 129].

In order to apply the system size expansion to the DCME (6.3), we consider each n_i to be of order Ω, with fluctuations of order $\Omega^{1/2}$, which can be written as follows,

$$n_i(t) = \Omega x_i(t) + \Omega^{1/2}\xi_i(t), \quad i = 1, 2, \ldots, 7,$$

where $x_i(t)$ are determined by the deterministic rate equations, and $\xi_i(t)$ describe random fluctuations around the deterministic solution. Similarly, for delayed variables we write

$$m_i = \Omega x_i(t - \tau_j) + \Omega^{1/2}\eta_i(t), \quad i = 1, \ldots, 7, \ j = 1, 2, 3,$$

where the index j is chosen depending on the delayed reaction being considered. For example, if it is the reaction of production of infected cells from uninfected cells, then $m_i = \Omega x_i(t - \tau_1) + \Omega^{1/2}\eta_i(t), \quad i = 1, 2, \ldots, 7.$

The probability distributions $P(\mathbf{n}, t)$ and $P(\mathbf{n}, t; \mathbf{m}, t - \tau_j)$ can be written as functions of $\boldsymbol{\xi}$, i.e.

$$\begin{aligned} P(\mathbf{n}, t) &= P(\Omega\mathbf{x} + \Omega^{1/2}\boldsymbol{\xi}, t) = \Pi(\boldsymbol{\xi}, t), \\ P(\mathbf{n}, t; \mathbf{m}, t - \tau_j) &= \Pi(\boldsymbol{\xi}, t; \boldsymbol{\eta}, t - \tau_j), \quad j = 1, 2, 3, \end{aligned}$$

which implies

$$\frac{dP(\mathbf{n},t)}{dt} = \frac{\partial \Pi}{\partial t} - \sum_{i=1}^{7} \Omega^{1/2} \frac{dx_i}{dt} \frac{\partial \Pi}{\partial \xi_i}. \tag{6.10}$$

To expand the master equation in a power series in $\Omega^{-1/2}$, we use the following expansions for step operators $\varepsilon_i^{\pm}$

$$\varepsilon_i^{\pm} = 1 \pm \Omega^{-1/2} \frac{\partial}{\partial \xi_i} + \frac{1}{2}\Omega^{-1} \frac{\partial^2}{\partial \xi_i^2} \pm \cdots . \tag{6.11}$$

Similar expansions can be obtained for propensity functions a_i. For non-delayed reactions we have

$$a_1(\mathbf{n}) = b_2\xi_1^2 + (b_1\xi_1 + 2b_2x_1\xi_1)\Omega^{1/2} + \left(b_1x_1 + b_2x_1^2\right)\Omega,$$

$$\begin{aligned} a_2(\mathbf{n}) + a_3(\mathbf{n}) =& d_2\xi_1^2 + \mu_a\xi_1\xi_6 + \beta\xi_1\xi_2 + (d_1\xi_1 + 2d_2x_1\xi_1 + \mu_a x_1\xi_6 + \mu_a x_6\xi_1 \\ &+ \beta x_1\xi_2 + \beta x_2\xi_1)\Omega^{1/2} + \left(d_1x_1 + d_2x_1^2 + \mu_a x_1x_6 + \beta x_1x_2\right)\Omega, \end{aligned}$$

$$\begin{aligned} a_4(\mathbf{n}) =& \mu_F\xi_2\xi_5 + \mu_a\xi_2\xi_6 + (d_F\xi_2 + \mu_F x_2\xi_5 + \mu_F x_5\xi_2 + \mu_a x_2\xi_6 + \mu_a x_6\xi_2)\Omega^{1/2} \\ &+ (d_F x_2 + \mu_F x_2x_5 + \mu_a x_2x_6)\Omega, \end{aligned}$$

$$a_5(\mathbf{n}) = \lambda_{in}\Omega, \quad a_{10}(\mathbf{n}) = \lambda_r\Omega, \quad a_{12}(\mathbf{n}) = d_r\xi_4\Omega^{1/2} + d_rx_4\Omega,$$

$$a_{14}(\mathbf{n}) = d_n\xi_5\Omega^{1/2} + d_nx_5\Omega,$$

$$\begin{aligned} a_6(\mathbf{n}) + a_7(\mathbf{n}) + a_8(\mathbf{n}) + a_9(\mathbf{n}) =& \alpha\xi_2\xi_3 + (d_{in}\xi_3 + \alpha x_2\xi_3 + \alpha x_3\xi_2)\Omega^{1/2} \\ &+ (d_{in}x_3 + \alpha x_2x_3)\Omega, \end{aligned}$$

$$a_{16}(\mathbf{n}) = \delta\xi_4\xi_6 + (d_a\xi_6 + \delta x_4\xi_6 + \delta x_6\xi_4)\Omega^{1/2} + (d_ax_6 + \delta x_4x_6)\Omega,$$

$$a_{17}(\mathbf{n}) = (\sigma_1\xi_5 + \sigma_2\xi_6)\Omega^{1/2} + (\sigma_1 x_5 + \sigma_2 x_6)\Omega, \quad a_{18}(\mathbf{n}) = d_i\xi_7\Omega^{1/2} + d_i x_7\Omega.$$

The propensity functions of delayed reactions can be obtained in a similar way:

$$a_3(\mathbf{m}) = \beta\eta_1\eta_2 + \Big(\beta x_1(t-\tau_1)\eta_2 + \beta x_2(t-\tau_1)\eta_1\Big)\Omega^{1/2} + \beta x_1(t-\tau_1)x_2(t-\tau_1)\Omega,$$

$$\begin{aligned} a_7(\mathbf{m}) =& p_1\alpha\eta_2\eta_3 + \Big(p_1\alpha x_2(t-\tau_3)\eta_3 + p_1\alpha x_3(t-\tau_3)\eta_2\Big)\Omega^{1/2} \\ &+ p_1\alpha x_2(t-\tau_3)x_3(t-\tau_3)\Omega, \end{aligned}$$

$$\begin{aligned} a_8(\mathbf{m}) =& p_2\alpha\eta_2\eta_3 + \Big(p_2\alpha x_2(t-\tau_3)\eta_3 + p_2\alpha x_3(t-\tau_3)\eta_2\Big)\Omega^{1/2} \\ &+ p_2\alpha x_2(t-\tau_3)x_3(t-\tau_3)\Omega, \end{aligned}$$

$$\begin{aligned} a_9(\mathbf{m}) =& (1-p_1-p_2)\alpha\eta_2\eta_3 + (1-p_1-p_2)\Big(\alpha x_2(t-\tau_3)\eta_3 + \alpha x_3(t-\tau_3)\eta_2\Big)\Omega^{1/2} \\ &+ (1-p_1-p_2)\alpha x_2(t-\tau_3)x_3(t-\tau_3)\Omega, \end{aligned}$$

$$a_{11}(\mathbf{m}) = \rho_1\eta_4\eta_7 + \Big(\rho_1 x_4(t-\tau_2)\eta_7 + \rho_1 x_7(t-\tau_2)\eta_4\Big)\Omega^{1/2} + \rho_1 x_4(t-\tau_2)x_7(t-\tau_2)\Omega,$$

$$a_{13}(\mathbf{m}) = \rho_2\eta_5\eta_7 + \Big(\rho_2 x_5(t-\tau_2)\eta_7 + \rho_2 x_7(t-\tau_2)\eta_5\Big)\Omega^{1/2} + \rho_2 x_5(t-\tau_2)x_7(t-\tau_2)\Omega,$$

$$a_{15}(\mathbf{m}) = \rho_3\eta_6\eta_7 + \Big(\rho_3 x_6(t-\tau_2)\eta_7 + \rho_3 x_7(t-\tau_2)\eta_6\Big)\Omega^{1/2} + \rho_3 x_6(t-\tau_2)x_7(t-\tau_2)\Omega.$$

Substituting expressions (6.10) and (6.11), together with the expansions for propensity functions, into the DCME (6.3) shows that the left-hand side of the equation only contains terms of the order $\Omega^{1/2}$ and Ω^0, while the right-hand side has terms of the order $\Omega^{1/2}$, Ω^0, and $\Omega^{-n/2}$, for $n \in \mathbb{N}$, and we will ignore the terms of order $\Omega^{-n/2}$. To show how the process of substitution works, let us illustrate

expansions for one non-delayed term of of the DCME (6.3)

$$
\begin{aligned}
(\varepsilon_1^- - 1)a_1(\mathbf{n})P(\mathbf{n},t) = \\
&\left(-\Omega^{-1/2}\frac{\partial}{\partial\xi_1} + \frac{1}{2}\Omega^{-1}\frac{\partial^2}{\partial\xi_1^2}\right)\Big[(b_1\xi_1 + 2b_2x_1\xi_1)\Omega^{1/2} + \left(b_1x_1 + b_2x_1^2\right)\Omega\Big]\Pi(\boldsymbol{\xi},t) \\
&= -\left(b_1x_1 + b_2x_1^2\right)\Omega^{1/2}\frac{\partial\Pi(\boldsymbol{\xi},t)}{\partial\xi_1} - \frac{\partial}{\partial\xi_1}\Big[(b_1\xi_1 + 2b_2x_1\xi_1)\Pi\Big]\Omega^0 \\
&\quad + \frac{1}{2}\left(b_1x_1 + b_2x_1^2\right)\frac{\partial^2\Pi(\boldsymbol{\xi},t)}{\partial\xi_1^2}\Omega^0.
\end{aligned}
$$

and one delayed term

$$
\begin{aligned}
&\sum_{\mathbf{m}\in I(\mathbf{n})}\Big[a_3(\mathbf{m})(\varepsilon_2^- - 1)P(\mathbf{n},t;\mathbf{m},t-\tau_1)\Big] = \\
&\int_{\boldsymbol{\eta}}\left(-\Omega^{-1/2}\frac{\partial}{\partial\xi_2} + \frac{1}{2}\Omega^{-1}\frac{\partial^2}{\partial\xi_2^2}\right)\Big[\Big(\beta x_1(t-\tau_1)\eta_2 + \beta x_2(t-\tau_1)\eta_1\Big)\Omega^{1/2} + \beta x_1(t-\tau_1)x_2(t-\tau_1)\Omega\Big] \\
&\quad \Pi(\boldsymbol{\xi},t;\boldsymbol{\eta},t-\tau_1)d\boldsymbol{\eta} \\
&= -\beta x_1(t-\tau_1)x_2(t-\tau_1)\Omega^{1/2}\frac{\partial\Pi(\boldsymbol{\xi},t)}{\partial\xi_2} \\
&\quad - \frac{\partial}{\partial\xi_2}\int_{\boldsymbol{\eta}}\Big(\beta x_1(t-\tau_1)\eta_2 + \beta x_2(t-\tau_1)\eta_1\Big)\Pi(\boldsymbol{\xi},t;\boldsymbol{\eta},t-\tau_1)d\boldsymbol{\eta}\Omega^0 \\
&\quad + \frac{1}{2}\beta x_1(t-\tau_1)x_2(t-\tau_1)\frac{\partial^2\Pi(\boldsymbol{\xi},t)}{\partial\xi_2^2}\Omega^0.
\end{aligned}
$$

with all other terms being computed in the same way. After substitution, collecting terms of order $\Omega^{1/2}$ yields the following system of equations describing macroscopic

behaviour of the model

$$\begin{aligned}
\frac{dx_1}{dt} &= b_1x_1 + b_2x_1^2 - d_1x_1 - d_2x_1^2 - \beta x_1x_2 - \mu_a x_1x_6,\\
\frac{dx_2}{dt} &= \beta x_1(t-\tau_1)x_2(t-\tau_1) - d_Fx_2 - \mu_F x_2x_5 - \mu_a x_2x_6,\\
\frac{dx_3}{dt} &= \lambda_{in} - d_{in}x_3 - \alpha x_2x_3,\\
\frac{dx_4}{dt} &= \lambda_r - d_rx_4 + p_1\alpha x_2(t-\tau_3)x_3(t-\tau_3) + \rho_1x_4(t-\tau_2)x_7(t-\tau_2),\\
\frac{dx_5}{dt} &= p_2\alpha x_2(t-\tau_3)x_3(t-\tau_3) - d_nx_5 + \rho_2x_5(t-\tau_2)x_7(t-\tau_2),\\
\frac{dx_6}{dt} &= (1-p_1-p_2)\alpha x_2(t-\tau_3)x_3(t-\tau_3) - d_ax_6 - \delta x_4x_6 + \rho_3x_6(t-\tau_2)x_7(t-\tau_2),\\
\frac{dx_7}{dt} &= \sigma_1x_5 + \sigma_2x_6 - d_ix_7.
\end{aligned} \tag{6.12}$$

This model has been analysed earlier in Fatehi et al. [190, 236], who have shown that it has at most four biologically feasible steady states. The first one, a *disease-free steady state*, is given by

$$S_1^* = \left(\frac{b_1-d_1}{d_2-b_2}, 0, \frac{\lambda_{in}}{d_{in}}, \frac{\lambda_r}{d_r}, 0, 0, 0\right),$$

and it is stable if $d_F > \widetilde{\beta}$, irrespective of the values of time delays. The second and third steady states can be found as

$$S_2^* = \left(0, 0, \frac{\lambda_{in}}{d_{in}}, x_4^*, 0, \frac{d_i\left(d_a+\delta x_4^*\right)}{\rho_3\sigma_2}, \frac{d_a+\delta x_4^*}{\rho_3}\right),$$

and

$$S_3^* = \left(\frac{\rho_3\sigma_2(b_1-d_1) - \mu_a d_i\left(d_a+\delta x_4^*\right)}{\rho_3\sigma_2\left(d_2-b_2\right)}, 0, \frac{\lambda_{in}}{d_{in}}, x_4^*, 0, \frac{d_i\left(d_a+\delta x_4^*\right)}{\rho_3\sigma_2}, \frac{d_a+\delta x_4^*}{\rho_3}\right),$$

where x_4^* satisfies the following quadratic equation

$$\rho_1\delta\left(x_4^*\right)^2 + \left(\rho_1d_a - \rho_3d_r\right)x_4^* + \rho_3\lambda_r = 0. \tag{6.13}$$

These steady states are stable, provided

$$\frac{\sigma_2}{\mu_a d_i} K < \frac{d_a + \delta x_4^*}{\rho_3} < \frac{d_n}{\rho_2},$$

where $K = 1$ for S_2^*, and $K = (\beta - d_F)/(1 + \beta)$ for S_3^*, and the following equation

$$\Delta(\tau_2, \lambda) = p_2(\lambda) e^{-2\lambda\tau_2} + p_1(\lambda) e^{-\lambda\tau_2} + p_0(\lambda) = 0, \tag{6.14}$$

where

$$\begin{aligned}
p_2(\lambda) =& \frac{\rho_1 \left(d_a + \delta x_4^*\right)^2}{\rho_3} \left(\lambda + 2d_i\right), \\
p_1(\lambda) =& \frac{-\left(d_a + \delta x_4^*\right)}{\rho_3} \Big\{ (\rho_1 + \rho_3)\lambda^2 + \left[\rho_1 \left(d_a + \delta x_4^*\right) + d_i\rho_1 + 2d_i\rho_3 + d_r\rho_3\right] \lambda \\
& \qquad + d_i(\rho_1 d_a + 2d_r\rho_3) \Big\}, \\
p_0(\lambda) =& \lambda^3 + \left(d_i + d_r + d_a + \delta x_4^*\right) \lambda^2 + \left[d_i \left(d_a + \delta x_4^*\right) + d_r \left(d_a + \delta x_4^*\right) + d_i d_r\right] \lambda \\
& + d_i d_r \left(d_a + \delta x_4^*\right),
\end{aligned}$$

only has roots with negative real part. Biologically, the steady state S_2^* represents the death of host cells, while S_3^* corresponds to an autoimmune state. The final steady state S_4^* has all of its components positive and corresponds to the state of chronic infection.

At the next order, i.e. at order Ω^0, we obtain the following linear delayed Fokker-Planck equation, known as the linear noise approximation (LNA), that describes stochastic fluctuations around the deterministic trajectory

$$
\begin{aligned}
\frac{\partial \Pi}{\partial t} &= -\frac{\partial}{\partial \xi_1}\Big[(b_1\xi_1 + 2b_2x_1\xi_1 - d_1\xi_1 - 2d_2x_1\xi_1 - \mu_a x_1\xi_6 - \mu_a x_6\xi_1 - \beta x_1\xi_2 - \beta x_2\xi_1)\Pi\Big] \\
&- \frac{\partial}{\partial \xi_2}\Big[- (d_F\xi_2 + \mu_F x_2\xi_5 + \mu_F x_5\xi_2 + \mu_a x_2\xi_6 + \mu_a x_6\xi_2)\Pi\Big] \\
&- \frac{\partial}{\partial \xi_2}\int_{\boldsymbol{\eta}} \Big(\beta x_1(t-\tau_1)\eta_2 + \beta x_2(t-\tau_1)\eta_1\Big)\Pi(\boldsymbol{\xi}, t; \boldsymbol{\eta}, t-\tau_1)d\boldsymbol{\eta} \\
&- \frac{\partial}{\partial \xi_3}\Big[- (d_{in}\xi_3 + \alpha x_2\xi_3 + \alpha x_3\xi_2)\Pi\Big] - \frac{\partial}{\partial \xi_4}(-d_r\xi_4\Pi) \\
&- \frac{\partial}{\partial \xi_4}\int_{\boldsymbol{\eta}} \Big(\rho_1 x_4(t-\tau_2)\eta_7 + \rho_1 x_7(t-\tau_2)\eta_4\Big)\Pi(\boldsymbol{\xi}, t; \boldsymbol{\eta}, t-\tau_2)d\boldsymbol{\eta} \\
&- \frac{\partial}{\partial \xi_4}\int_{\boldsymbol{\eta}} \Big(p_1\alpha x_2(t-\tau_3)\eta_3 + p_1\alpha x_3(t-\tau_3)\eta_2\Big)\Pi(\boldsymbol{\xi}, t; \boldsymbol{\eta}, t-\tau_3)d\boldsymbol{\eta} \\
&- \frac{\partial}{\partial \xi_5}(-d_n\xi_5\Pi) - \frac{\partial}{\partial \xi_5}\int_{\boldsymbol{\eta}} \Big(\rho_2 x_5(t-\tau_2)\eta_7 + \rho_2 x_7(t-\tau_2)\eta_5\Big)\Pi(\boldsymbol{\xi}, t; \boldsymbol{\eta}, t-\tau_2)d\boldsymbol{\eta} \\
&- \frac{\partial}{\partial \xi_5}\int_{\boldsymbol{\eta}} \Big(p_2\alpha x_2(t-\tau_3)\eta_3 + p_2\alpha x_3(t-\tau_3)\eta_2\Big)\Pi(\boldsymbol{\xi}, t; \boldsymbol{\eta}, t-\tau_3)d\boldsymbol{\eta} \\
&- \frac{\partial}{\partial \xi_6}\Big[- (d_a\xi_6 + \delta x_4\xi_6 + \delta x_6\xi_4)\Pi\Big] \\
&- \frac{\partial}{\partial \xi_6}\int_{\boldsymbol{\eta}} \Big(\rho_3 x_6(t-\tau_2)\eta_7 + \rho_3 x_7(t-\tau_2)\eta_6\Big)\Pi(\boldsymbol{\xi}, t; \boldsymbol{\eta}, t-\tau_2)d\boldsymbol{\eta} \\
&- \frac{\partial}{\partial \xi_6}\int_{\boldsymbol{\eta}} (1-p_1-p_2)\Big(\alpha x_2(t-\tau_3)\eta_3 + \alpha x_3(t-\tau_3)\eta_2\Big)\Pi(\boldsymbol{\xi}, t; \boldsymbol{\eta}, t-\tau_3)d\boldsymbol{\eta} \\
&- \frac{\partial}{\partial \xi_7}\Big[(\sigma_1\xi_5 + \sigma_2\xi_6 - d_i\xi_7)\Pi\Big] + \frac{1}{2}\Bigg\{ \Big(b_1x_1 + b_2x_1^2 + d_1x_1 + d_2x_1^2 + \mu_a x_1x_6 + \beta x_1x_2\Big)\frac{\partial^2\Pi}{\partial \xi_1^2} \\
&+ \Big(\beta x_1(t-\tau_1)x_2(t-\tau_1) + d_F x_2 + \mu_F x_2x_5 + \mu_a x_2x_6\Big)\frac{\partial^2\Pi}{\partial \xi_2^2} + (\lambda_{in} + d_{in}x_3 + \alpha x_2x_3)\frac{\partial^2\Pi}{\partial \xi_3^2} \\
&+ \Big(\lambda_r + d_r x_4 + p_1\alpha x_2(t-\tau_3)x_3(t-\tau_3) + \rho_1 x_4(t-\tau_2)x_7(t-\tau_2)\Big)\frac{\partial^2\Pi}{\partial \xi_4^2} \\
&+ \Big(d_n x_5 + p_2\alpha x_2(t-\tau_3)x_3(t-\tau_3) + \rho_2 x_5(t-\tau_2)x_7(t-\tau_2)\Big)\frac{\partial^2\Pi}{\partial \xi_5^2} \\
&+ \Big(d_a x_6 + \delta x_4x_6 + (1-p_1-p_2)\alpha x_2(t-\tau_3)x_3(t-\tau_3) + \rho_3 x_6(t-\tau_2)x_7(t-\tau_2)\Big)\frac{\partial^2\Pi}{\partial \xi_6^2} \\
&+ (\sigma_1x_5 + \sigma_2x_6 + d_i x_7)\frac{\partial^2\Pi}{\partial \xi_7^2}\Bigg\}.
\end{aligned}
$$

Following Phillips et al. [122], we use the structure of this equation to derive a system of equations that describes the delayed Langevin dynamics of fluctuations around any deterministic steady states $S^* = (x_1^*, x_2^*, \ldots, x_7^*)$ of the model (6.12). This system has the form

$$
\begin{aligned}
\dot{\xi_1} &= (b_1 + 2b_2x_1^* - d_1 - 2d_2x_1^* - \beta x_2^* - \mu_a x_6^*)\xi_1 - \beta x_1^*\xi_2 - \mu_a x_1^*\xi_6 + \zeta_1,\\
\dot{\xi_2} &= \beta x_2^*\xi_1(t-\tau_1) + \beta x_1^*\xi_2(t-\tau_1) - (d_F + \mu_F x_5^* + \mu_a x_6^*)\xi_2 - \mu_F x_2^*\xi_5 - \mu_a x_2^*\xi_6 + \zeta_2,\\
\dot{\xi_3} &= -\alpha x_3^*\xi_2 - (d_{in} + \alpha x_2^*)\xi_3 + \zeta_3,\\
\dot{\xi_4} &= -d_r\xi_4 + p_1\alpha x_3^*\xi_2(t-\tau_3) + p_1\alpha x_2^*\xi_3(t-\tau_3) + \rho_1 x_7^*\xi_4(t-\tau_2) + \rho_1 x_4^*\xi_7(t-\tau_2) + \zeta_4,\\
\dot{\xi_5} &= -d_n\xi_5 + p_2\alpha x_3^*\xi_2(t-\tau_3) + p_2\alpha x_2^*\xi_3(t-\tau_3) + \rho_2 x_7^*\xi_5(t-\tau_2) + \rho_2 x_5^*\xi_7(t-\tau_2) + \zeta_5,\\
\dot{\xi_6} &= -\delta x_6^*\xi_4 - (d_a + \delta x_4^*)\xi_6 + (1-p_1-p_2)\alpha x_3^*\xi_2(t-\tau_3) + (1-p_1-p_2)\alpha x_2^*\xi_3(t-\tau_3)\\
&\quad + \rho_3 x_7^*\xi_6(t-\tau_2) + \rho_3 x_6^*\xi_7(t-\tau_2) + \zeta_6,\\
\dot{\xi_7} &= \sigma_1\xi_5 + \sigma_2\xi_6 - d_i\xi_7 + \zeta_7,
\end{aligned}
\tag{6.15}
$$

where $\boldsymbol{\zeta}(t) = (\zeta_1(t), \zeta_2(t), \ldots, \zeta_7(t))$ is a vector of seven independent Gaussian white noise variables with zero mean and the noise correlators given by

$$
\begin{aligned}
\langle\zeta_1(t)\zeta_1(t')\rangle &= (b_1x_1^* + b_2x_1^{*2} + d_1x_1^* + d_2x_1^{*2} + \beta x_1^*x_2^* + \mu_a x_1^*x_6^*)\delta(t-t'),\\
\langle\zeta_2(t)\zeta_2(t')\rangle &= (\beta x_1^*x_2^* + d_F x_2^* + \mu_F x_2^*x_5^* + \mu_a x_2^*x_6^*)\delta(t-t'),\\
\langle\zeta_3(t)\zeta_3(t')\rangle &= (\lambda_{in} + d_{in}x_3^* + \alpha x_2^*x_3^*)\delta(t-t'),\\
\langle\zeta_4(t)\zeta_4(t')\rangle &= (\lambda_r + d_r x_4^* + p_1\alpha x_2^*x_3^* + \rho_1 x_4^*x_7^*)\delta(t-t'),\\
\langle\zeta_5(t)\zeta_5(t')\rangle &= (p_2\alpha x_2^*x_3^* + d_n x_5^* + \rho_2 x_5^*x_7^*)\delta(t-t'),\\
\langle\zeta_6(t)\zeta_6(t')\rangle &= \Big((1-p_1-p_2)\alpha x_2^*x_3^* + d_a x_6^* + \delta x_4^*x_6^* + \rho_3 x_6^*x_7^*\Big)\delta(t-t'),\\
\langle\zeta_7(t)\zeta_7(t')\rangle &= (\sigma_1 x_5^* + \sigma_2 x_6^* + d_i x_7^*)\delta(t-t'),\\
\langle\zeta_i(t)\zeta_j(t')\rangle &= 0, \quad \forall\ i \neq j.
\end{aligned}
$$

Using a Fourier transformation of the model (6.15), one can find the power spectral density (PSD) of the fluctuations, which can be used to determine the variance and coherence of the stochastic oscillations. Fourier transform of the model (6.15) gives

$$
M(\omega)\tilde{\boldsymbol{\xi}}(\omega) = \tilde{\boldsymbol{\zeta}}(\omega),
$$

where $M(\omega) = i\omega I - M_1 - e^{-i\omega\tau_1}M_2 - e^{-i\omega\tau_2}M_3 - e^{-i\omega\tau_3}M_4$, and

$$M_1 = \begin{pmatrix} b_1 + 2b_2x_1^* - d_1 - 2d_2x_1^* - \mu_a x_6^* - \beta x_2^* & -\beta x_1^* & 0 & 0 & 0 & -\mu_a x_1^* & 0 \\ 0 & -d_F - \mu_F x_5^* - \mu_a x_6^* & 0 & 0 & -\mu_F x_2^* & \mu_a x_2^* & 0 \\ 0 & -\alpha x_3^* & -d_{in} - \alpha x_2^* & 0 & 0 & 0 & 0 \\ 0 & 0 & 0 & -d_r & 0 & 0 & 0 \\ 0 & 0 & 0 & 0 & -d_n & 0 & 0 \\ 0 & 0 & 0 & -\delta x_6^* & 0 & -d_a - \delta x_4^* & 0 \\ 0 & 0 & 0 & 0 & \sigma_1 & \sigma_2 & -d_i \end{pmatrix},$$

$$(M_2)_{ij} = \begin{cases} \beta x_2^*, & \text{if } (i,j) = (1,2), \\ \beta x_1^*, & \text{if } (i,j) = (2,2), \\ 0, & \text{otherwise,} \end{cases}$$

$$(M_3)_{ij} = \begin{cases} \rho_1 x_7^*, & \text{if } (i,j) = (4,4), \\ \rho_1 x_4^*, & \text{if } (i,j) = (4,7), \\ \rho_2 x_7^*, & \text{if } (i,j) = (5,5), \\ \rho_2 x_5^*, & \text{if } (i,j) = (5,7), \\ \rho_3 x_7^*, & \text{if } (i,j) = (6,6), \\ \rho_3 x_6^*, & \text{if } (i,j) = (6,7), \\ 0, & \text{otherwise,} \end{cases} \quad (M_4)_{ij} = \begin{cases} p_1\alpha x_3^*, & \text{if } (i,j) = (4,2), \\ p_1\alpha x_2^*, & \text{if } (i,j) = (4,3), \\ p_2\alpha x_3^*, & \text{if } (i,j) = (5,2), \\ p_2\alpha x_2^*, & \text{if } (i,j) = (5,3), \\ (1-p_1-p_2)\alpha x_3^*, & \text{if } (i,j) = (6,2), \\ (1-p_1-p_2)\alpha x_2^*, & \text{if } (i,j) = (6,3), \\ 0, & \text{otherwise.} \end{cases}$$

Using this formulation, it can be easily shows that in the case where the model (6.12) converges to either of the steady states S_2^* or S_3^*, the power spectrum for the number of regulatory T cells, $P_r(\omega)$, is given by

$$P_r(\omega) = \frac{a_4|L|^2 + a_6\sigma_2^2\rho_1^2{x_4^*}^2 + a_7\rho_1^2{x_4^*}^2\left|i\omega + d_a + \delta x_4^* - \rho_3 e^{-i\omega\tau_2}x_7^*\right|^2}{|\det(D)|^2},$$

where $L = (i\omega + d_i)\left(i\omega + d_a + \delta x_4^* - \rho_3 e^{-i\omega\tau_2}x_7^*\right) - \rho_3\sigma_2 e^{-i\omega\tau_2}x_6^*$, and

$$D = \begin{pmatrix} i\omega + d_r - \rho_1 e^{-i\omega\tau_2}x_7^* & 0 & -\rho_1 e^{-i\omega\tau_2}x_4^* \\ \delta x_6^* & i\omega + d_a + \delta x^* - \rho_3 e^{-i\omega\tau_2}x_7^* & -\rho_3 e^{-i\omega\tau_2}x_7^* \\ 0 & -\sigma_2 & i\omega + d_i \end{pmatrix},$$

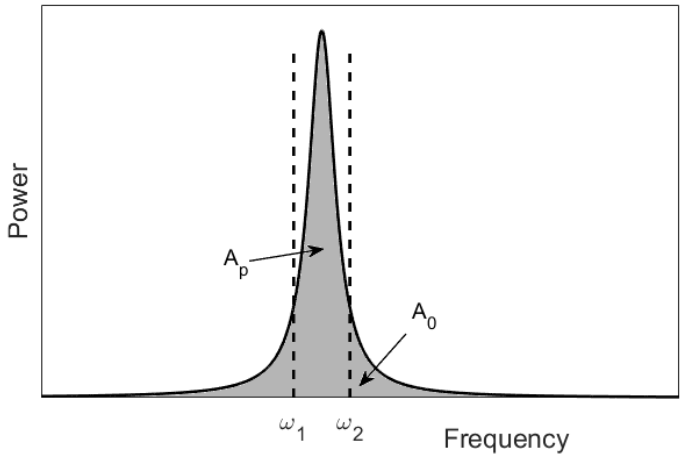

Figure 6.2: Coherence of stochastic oscillations c defined as the spectral power associated with a range of frequencies around the peak A_p relative to the total area under the PSD curve A_0 [122, 91].

and similar results can be obtained the PSDs of other state variables.

Introducing the matrix of spectra $S(\omega)$ as $S_{ij}(\omega) = \langle \xi_i(\omega)\xi_j(\omega)^\dagger \rangle$ [122], we then have

$$S(\omega) = M(\omega)^{-1}\Big\langle \tilde{\boldsymbol{\zeta}}(\omega)\tilde{\boldsymbol{\zeta}}(\omega)^\dagger \Big\rangle \Big(M(\omega)^\dagger\Big)^{-1},$$

where

$$\Big\langle \tilde{\boldsymbol{\zeta}}(\omega)\tilde{\boldsymbol{\zeta}}(\omega')^\dagger \Big\rangle = \mathrm{diag}\{a_1, a_2, \ldots, a_7\}\delta(\omega + \omega'),$$

and

$$a_i = \begin{cases} b_1 x_1^* + b_2 x_1^{*2} + d_1 x_1^* + d_2 x_1^{*2} + \beta x_1^* x_2^* + \mu_a x_1^* x_6^*, & \text{if } i = 1, \\ \beta x_1^* x_2^* + d_F x_2^* + \mu_F x_2^* x_5^* + \mu_a x_2^* x_6^*, & \text{if } i = 2, \\ \lambda_{in} + d_{in} x_3^* + \alpha x_2^* x_3^*, & \text{if } i = 3, \\ \lambda_r + d_r x_4^* + p_1 \alpha x_2^* x_3^* + \rho_1 x_4^* x_7^*, & \text{if } i = 4, \\ p_2 \alpha x_2^* x_3^* + d_n x_5^* + \rho_2 x_5^* x_7^*, & \text{if } i = 5, \\ (1 - p_1 - p_2)\alpha x_2^* x_3^* + d_a x_6^* + \delta x_4^* x_6^* + \rho_3 x_6^* x_7^*, & \text{if } i = 6, \\ \sigma_1 x_5^* + \sigma_2 x_6^* + d_i x_7^*, & \text{if } i = 7. \end{cases}$$

At any steady state, the covariance matrix Ξ with $\Xi_{ij} = \langle \xi_i(t)\xi_j(t) \rangle - \langle \xi_i(t) \rangle \langle \xi_j(t) \rangle$ $= \langle \xi_i(t)\xi_j(t) \rangle$ is independent of time, and is given by [130]

$$\Xi = \frac{1}{2\pi} \int_{-\infty}^{+\infty} S(\omega) d\omega = \frac{1}{\pi} \int_{0}^{+\infty} S(\omega) d\omega. \tag{6.16}$$

To relate the results of this analysis to the outcome of direct numerical simulations of the SDDE, it is instructive to express the covariance matrix in terms of actual numbers of cells in each compartment, rather than deviations from stationary values. This can be achieved by defining the covariance matrix C as $C_{ij} = \langle (n_i - \langle n_i \rangle)(n_j - \langle n_j \rangle) \rangle$, which is related to Ξ through $C_{ij} = \Omega \Xi_{ij}$. It is worth noting that when there is no delay, as an alternative to numerical computation of matrices Ξ and C by evaluation of the matrix of spectra $S(\omega)$ and its subsequent numerical integration, one could also determine these matrices by solving the corresponding Lyapunov equation [189, 211]. Either of those approaches allows one to compute the value of variance of fluctuations around any steady state of the deterministic model.

In order to quantify how well-structured stochastic oscillations are around the dominant spectral frequency for any of the relevant state variables, we can use the notion of coherence [122, 130, 91]. Choosing a particular state variable $X(t)$, we can consider the power spectral density $P(\omega)$ of stochastic oscillations of this variable around its steady state value X^*. The overall level of fluctuations can be measured by the mean-square variance

$$A_0 = \lim_{T \to \infty} \int_{-T}^{+T} [X(t) - X^*]^2 \, dt = \int_0^{+\infty} P(\omega) d\omega.$$

Focusing on the particular interval of frequencies $[\omega_1, \omega_2]$ around the peak frequency in the distribution $P(\omega)$, as shown in Fig. 6.2, one can compute the quantity

$$A_p = \int_{\omega_1}^{\omega_2} P(\omega) d\omega,$$

and then define *coherence of stochastic oscillations* as $c = A_p / A_0$ [122, 91].

6.4 Numerical stability analysis and simulations

In order to perform numerical simulations of the model (6.9), we use the strong predictor-corrector method with the degree of implicitness in the drift coefficient chosen to be equal to 1/7, since for this value the method has the largest stability region [123, 124]. It has been previously shown [190, 237] that in the model (6.12),

the disease-free steady state S_1^* undergoes a transcritical bifurcation at $\beta = d_F$. For $\beta < d_F$, the disease-free steady state is stable, while the chronic infection steady state S_4^* is infeasible. On the contrary, for $\beta > d_F$, the disease-free steady state is unstable, and in this case we can study the stability of the chronic infection steady state [190, 237]. This qualitative distinction between different regimes suggests that it is feasible to consider the two cases separately. First, we consider consider a situation corresponding to the parameter regime $\beta < d_F$, with the values of parameters given in Table 6.3. The initial condition is chosen to be

$$(x_1(s), x_3(s), x_4(s), x_5(s), x_6(s), x_7(s)) = (18, 7.2, 6.3, 0, 0, 0), \quad s \in [-\tau_{max}, 0], \tag{6.17}$$

and $\tau_{max} = \max\{\tau_1, \tau_2, \tau_3\}$, except for the initial number of infected cells being allowed to vary with a constant history between different simulations.

Table 6.3: Table of parameters

parameter	value	parameter	value
b_1	2.5	p_2	0.4
b_2	0	ρ_1	20/9
d_1	0.5	ρ_2	8/45
d_2	0.1	ρ_3	4/9
β	0.1	d_n	2
μ_a	40/9	d_a	0.002
d_F	2.2	δ	2/4500
μ_F	4/3	σ_1	0.3
λ_{in}	18	σ_2	0.4
d_{in}	2	d_i	1.2
α	0.04	τ_1	0.7
λ_r	54	τ_2	0.5
d_r	0.8	τ_3	0.3
p_1	0.4	Ω	1000

Figure 6.3 shows the result of 20000 simulations with the initial condition (6.17) and $x_2(0) = 2$ and $\mu_a = 2$. In this case, in the deterministic model (6.12) the steady states S_1^* and S_3^* are both stable, but based on the chosen initial condition, the system is in the attraction basin of S_3^*. As can be seen from Fig. 6.3, in the stochastic model (6.9), the majority of paths go into the basin of attraction of S_3^*, and a small proportion of them enter the basin of attraction of S_1^*. This figure also shows single stochastic trajectories around S_1^* and S_3^*, as well as areas of one

standard deviation from the mean in the basins of attraction of these steady states, where trajectories show sustained stochastic oscillations [212, 90].

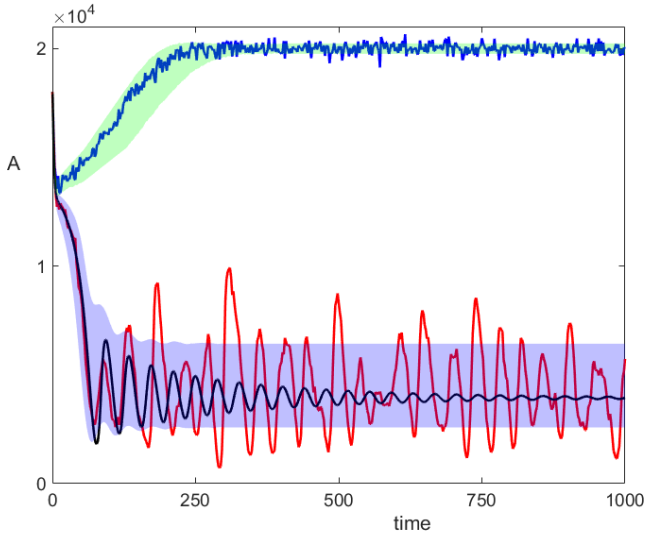

Figure 6.3: Numerical simulation of the model (6.9) with parameter values from Table 6.3, with $\mu_a = 2$, $x_2(0) = 2$, and the initial condition (6.17). Red and blue curves represent two sample trajectories that have entered the basins of attraction of steady states S_3^* and S_1^*, respectively. Black curve is the deterministic trajectory of the model (6.12), and the shaded areas indicate the regions of one standard deviation from the mean.

One observes that taking an average of a large number of simulations that enter the basin of attraction of S_3^* would show a decaying oscillations around S_3^*, which is similar to a deterministic trajectory, while single stochastic trajectories exhibit sustained stochastic oscillations [92]. Furthermore, this figure also shows that although deterministically the system is in the attraction basin of the autoimmune steady state S_3^*, it is still possible for a small number of realisations to successfully clear the infection and reach a disease-free steady state, which corresponds to a spontaneous recovery. It should be noted, however, that this only occurred in around 1.5% of simulations, suggesting that while recovery from a pathogen-induced autoimmune disease is theoretically possible, substantial caution would have to be used when relying on this result in the clinical practice.

Figure 6.4(a) illustrates temporal evolution of the probability distribution for the same set of parameters and initial condition as in Fig. 6.3. The bi-stability between steady states S_1^* and S_3^* results in the system reaching a bimodal stationary distribution after some initial transient, as shown in Fig. 6.4(b). Increase the value of the rate μ_a, at which autoreactive T cells are destroying infected and healthy host

cells, from 2 to 10/3 shift dynamical behaviour for the deterministic model (6.12) to a regime of bi-stability between steady states S_1^* and S_2^*. In this case, with the same initial condition (6.17) and $x_2(0) = 2.2$, the system is in the basin of attraction of S_2^*. Figures 6.4(c) and (d) show the evolution of the probability distribution, as well as the final bimodal distribution in this case. One should note that since the size of fluctuations around deterministic solutions scales as $\Omega^{-1/2}$, increasing the size of system Ω would result in these bimodal distributions becoming unimodal [189, 129].

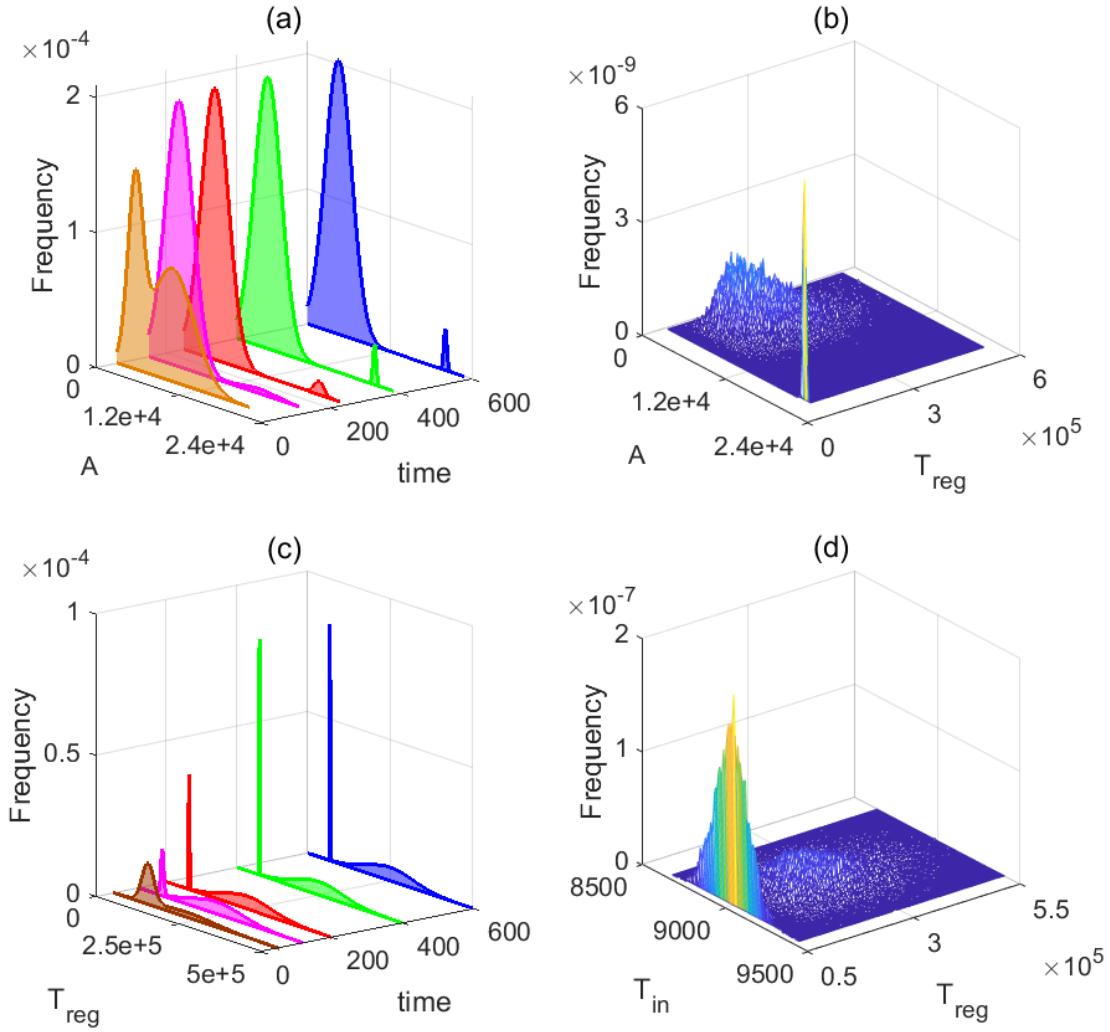

Figure 6.4: Probability distribution of solutions out of 20000 simulations. (a) and (b) with parameters from Table 6.3 except for $\mu_a = 2$, and the initial condition (6.17) with $x_2(0) = 2$. (c) and (d) with parameters from Table 6.3 except for $\mu_a = 10/3$, and the initial condition (6.17) with $x_2(0) = 2.2$. In (a) and (c), the probability histogram is fit to a bimodal normal distribution at different times. (b) and (d) illustrate stationary joint probability histograms.

Figure 6.5 highlights the main difference between deterministic and stochastic models by illustrating how the coherence of stochastic oscillations changes in the

region where S_2^* and S_3^* are deterministically stable, i.e. the deterministic solution exhibits damped oscillations that eventually reach a steady state. This figure indicates that by increasing time delay τ_2 associated with the effects of IL-2 on proliferation of T cells, we approach the boundary of the Hopf bifurcation, and the coherence also increases, while in the region where deterministically the model has a periodic solution around these steady states, the value of coherence is equal to one.

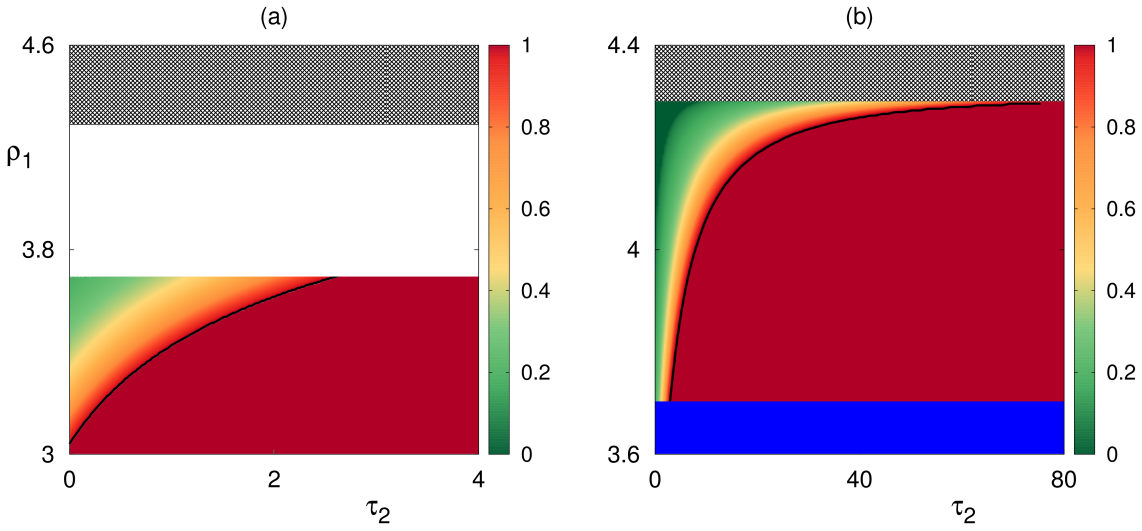

Figure 6.5: Coherence of oscillations in the stability regions of S_2^* (a) and S_3^* (b) with parameter values from Table 6.3, except for $\rho_3 = 2/3$. Black curves show deterministic boundaries of Hopf bifurcation for respective steady states. In the white region, the steady state S_2^* is infeasible, in the blue region the steady state S_3^* is infeasible, and in the region indicated by the black grid both steady states S_2^* and S_3^* are infeasible.

Using equation (6.16), we can determine the covariance matrix C, which provides the variance of individual state variables, when the deterministic model is at one of its steady states. One should note that in this method the variance goes to infinity as one approaches a bifurcation. Therefore, this method can only be applied when a steady state is stable, and we are not close to bifurcation boundaries. Figure 6.6 illustrates how variance in the number of regulatory T cells T_{reg}, as determined by $C_{4,4}$, varies with system parameters in the parameter regions where S_3^* is deterministically stable. One can observe that as one gets closer to the border between the area, where S_3^* is stable, and the area, where the deterministic model can have a periodic solution around S_3^*, the variance of stochastic oscillations in Tregs increases. Moreover, this variance increases with the rate σ_2 of production of IL-2 by autoreactive T cells, as well as with the time delay τ_2 associated with simulation and proliferation of T cells by IL-2. In contrast, Figure 6.6(b) suggests

that the variance of stochastic oscillations in Tregs is insensitive to changes in the rate μ_a of destruction of infected and healthy host cells by autoreactive T cells.

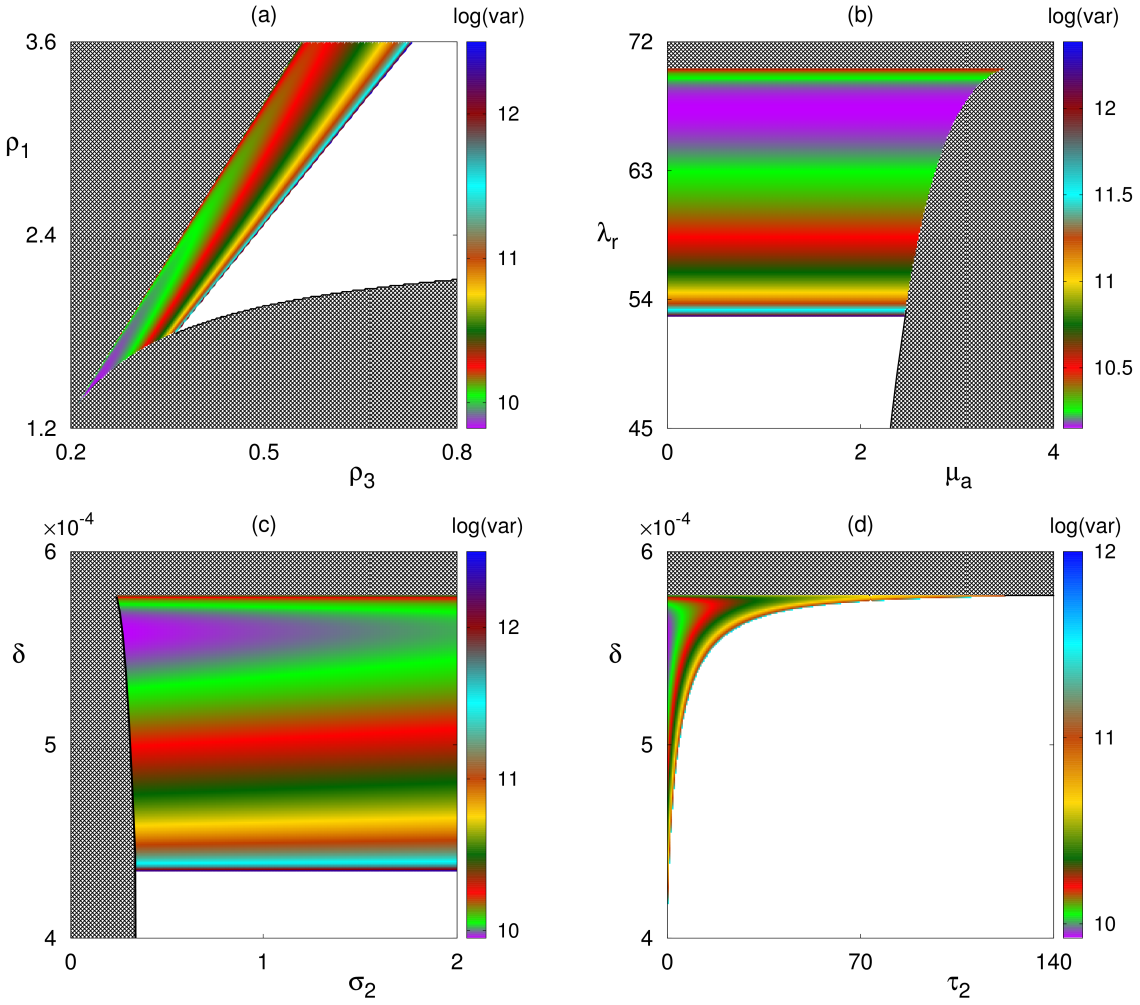

Figure 6.6: Variance of the number of regulatory T cells with parameter values from Table 6.3, but $\mu_a = 2$. Colored regions indicate areas in respective parameter planes where the autoimmune steady state S_3^* is deterministically stable. Black grid area indicates the region where S_3^* is infeasible, and in the white region it is feasible but unstable.

Now we consider a situation where $\beta > d_F$, in which case deterministically the disease-free steady state S_1^* is unstable, and we can investigate stability of the chronic steady state S_4^*. Earlier results by Fatehi et al. [190, 237] indicate that for parameter values from Table 6.3, but with $\delta = 8/15000$, $\sigma_2 = 0.66$ and $\beta = 0.14$, the steady states S_3^* and S_4^* are both deterministically stable, and for the initial condition (6.17) with $x(2) = 0.6$ and $x(4) = 36$, the model (6.12) is in the basin of attraction of the chronic steady state S_4^*. Figure 6.7 shows the results of 20000 stochastic simulations with these parameter values and initial conditions. Since deterministically S_4^* is stable, and the system is in its basin of attraction for the

specific chosen initial conditions, the majority of stochastic trajectories also enter the basin of attraction of S_4^*. Due to bi-stability, a proportion of these trajectories (about 17.5%) go to S_3^*. Interestingly, Figure 6.7(a) indicates that although the disease-free steady state is deterministically unstable, a less than two percent of trajectories approach S_1^* and exhibit stochastic oscillations around it. The impact of these trajectories can be observed in Fig. 6.7(b), which shows temporal evolution of the probability distribution of the solutions. In this figure, initially one observes a trimodal probability distribution, where the middle peak corresponds to trajectories approaching S_1^*. Over time, this peak disappears, while the peak at S_3^* becomes more pronounced. Since the proportion of trajectories going to S_1^* is very small, and the amounts of healthy cells A in the steady states S_4^* and S_1^* are close, the stationary probability distribution is effectively bimodal with peaks at S_3^* and S_4^*. However, the presence of a small number of trajectories approaching the steady state S_1^* results in a small reduction of the peak associated with the chronic steady state S_4^*.

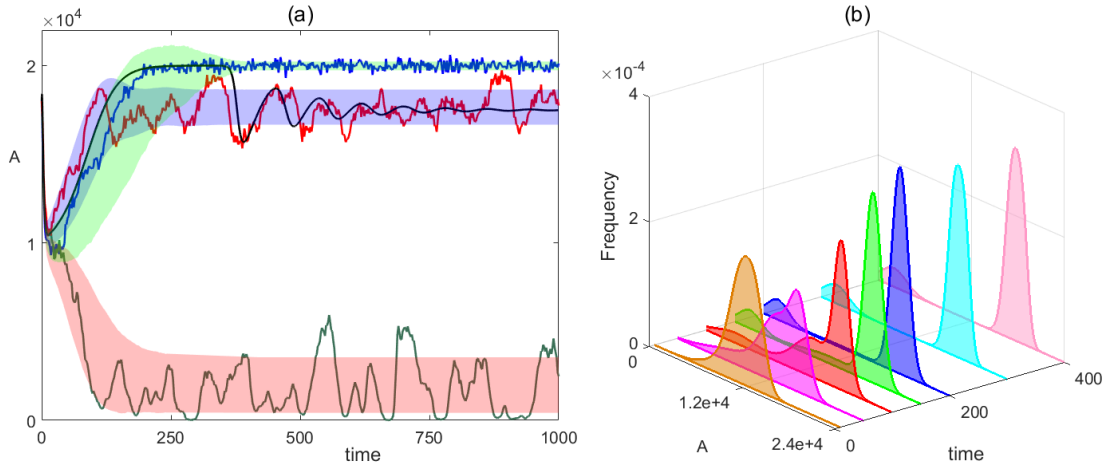

Figure 6.7: Numerical simulations (a) and probability distribution (b) out of 20000 simulations with parameter values from Table 6.3, except for $\delta = 8/15000$, $\sigma_2 = 0.66$ and $\beta = 0.14$, and the initial condition (6.17) with $x(2) = 0.6$ and $x(4) = 36$. In (a) blue, red and green are sample trajectories, which have entered the basins of attraction of S_1^*, S_4^* and S_3^*, respectively. Black curve is the deterministic trajectory of the model (6.12), and the shaded areas indicate the regions of one standard deviation from the mean. In (b) the probability histogram is fit to a multimodal normal distribution at different times.

Figure 6.8 illustrates how the coherence of stochastic oscillations around the chronic steady state S_4^* changes with parameters. We observe that the general trend is similar to that shown earlier in Fig. 6.5 for steady states S_2^*/S_3^* in that

approaching the deterministic boundary of the Hopf bifurcation results in the increase of coherence, while increasing the rate δ at which regulatory T cells suppress autoreactive T cells reduces the coherence of stochastic oscillations. When this rate is very small, the chronic steady state S_4^* is infeasible, and once δ increases past some minimum threshold, the steady state S_4^* becomes feasible but unstable, with a deterministic periodic orbit around it, which corresponds to the maximum level of coherence. Increasing δ further results in stabilisation of the steady state S_4^* and a reduced coherence of stochastic oscillations around the stable steady state. It is worth noting that there is a major difference in behaviour with regards to effects of time delays. For the time delay τ_2, associated with stimulation and proliferation of T cells by IL-2, there are multiple stability switches in the stability of S_4^* for intermediate values of δ, which leads to successive growth and reduction in the level of coherence. In contrast, increasing time delay τ_3, which characterises a lag in proliferation and differentiation of naïve T cells, there is a single stability switch, with coherence being low for small values of this time delay, then increasing all the way up to the boundary of Hopf bifurcation, and being at its maximum value subsequently.

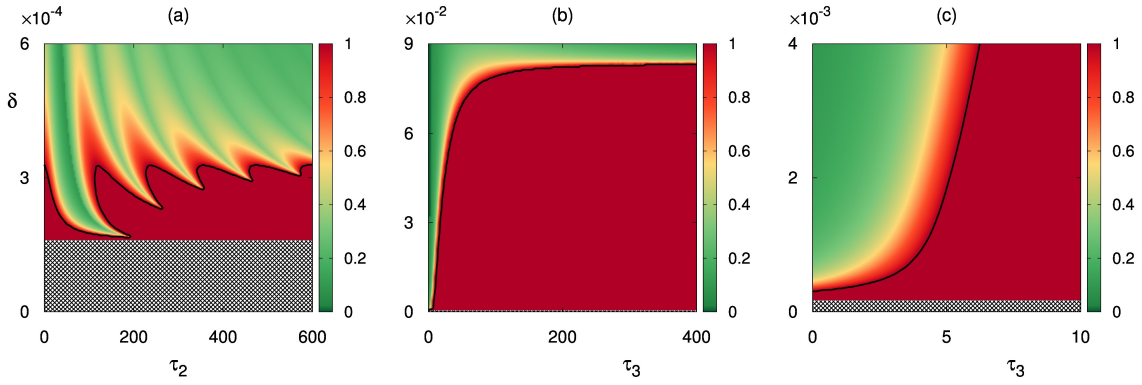

Figure 6.8: Coherence of oscillations in the region of stability of S_4^* with parameters from Table 6.3, except for $\sigma_2 = 0.66$ and $\beta = 0.14$. Black curves show the boundary of Hopf bifurcation. The steady state S_4^* is infeasible in the region indicated with a black grid.

In Fig. 6.9 we illustrate how the variance in the number of regulatory T cells T_{reg} for the steady states S_3^* or S_4^* changes with parameters in the region where these states are deterministically stable.

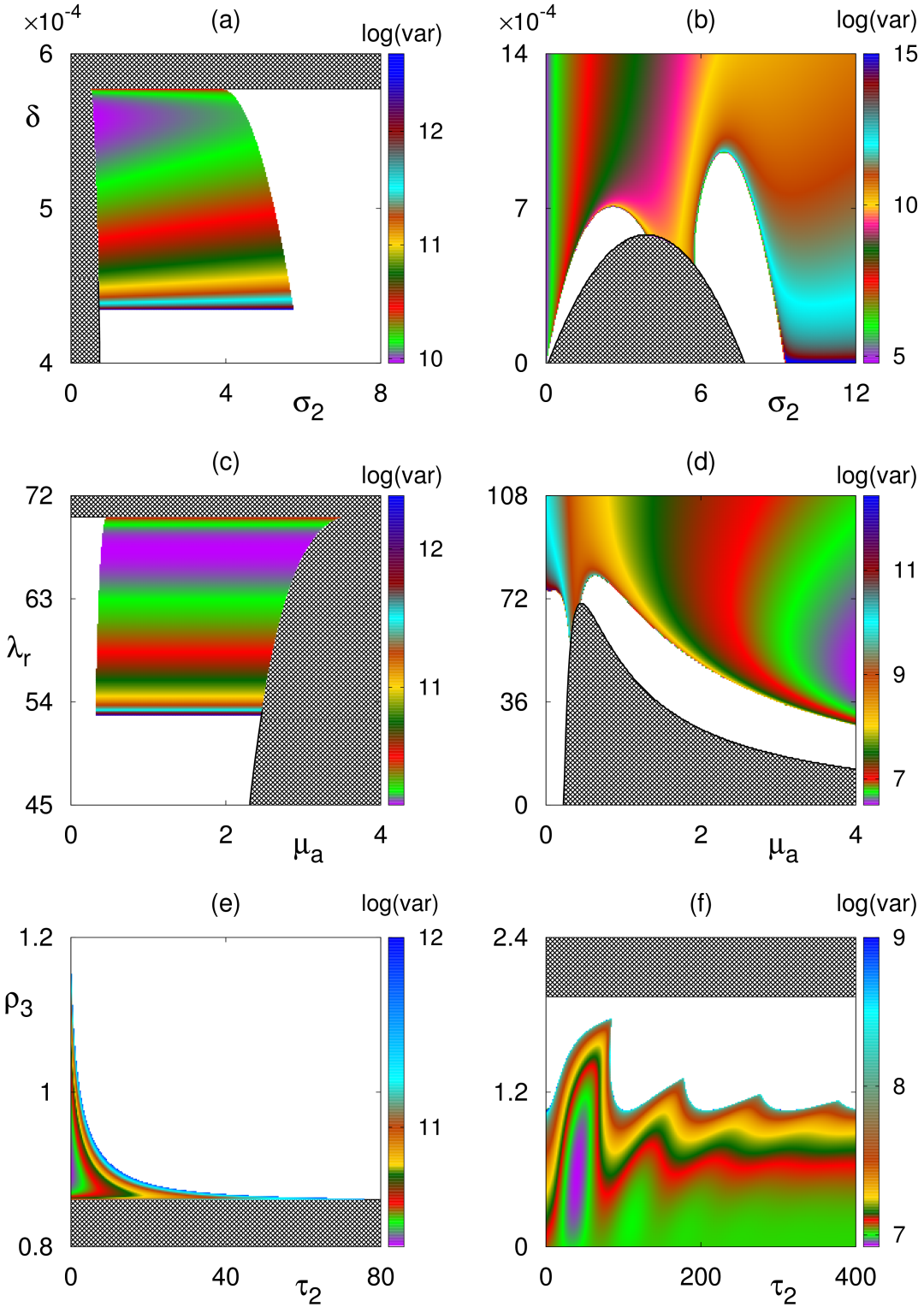

Figure 6.9: Variance of the number of regulatory T cells with parameter values from Table 6.3 and $\beta = 0.14$, but in (e) and (f) $\rho_1 = 50/9$. In the left (respectively, right) column, coloured regions indicate areas of respective parameter planes where the autoimmune (respectively, chronic) steady state S_3^* (respectively, S_4^*) is deterministically stable, white areas are regions where the steady state is feasible but unstable, and the black grid area indicates the region where the steady state is infeasible.

One observes some notable differences in the behaviour of variance for these two

steady states. For example, while for the steady state S_3^* the variance appears to be almost completely independent on the rate μ_a, at which autoreative T cells are destroying healthy host cells, for the steady state S_4^* the variance substantially decreases with the increase of this rate. Also, due to the difference in that there is a single loss of stability of S_3^* depending on the time delay τ_2 compared to several stability switches for S_4^*, one observes a monotonic increase of variance for increasing values of τ_2 for S_3^*, whereas in the case of S_4^*, periods of increased variance are followed by periods of decreased variance until it settles on some steady level.

6.5 Discussion

In this chapter I have analysed stochastic aspects of immune response against a viral infection with account for T cells with different activation thresholds, regulatory T cells, as well as the cytokine mediating T cell activity, while paying particular attention to viral and cytokine delays. Using the framework of delayed chemical reactions, I have carefully reinterpreted various transitions and interactions in the model as discrete stochastic changes in the populations of state variables to derive a delayed chemical master equation that describes the dynamics of the probability distribution of finding the system in a particular state. To make further progress, I used the formalism of consuming and non-consuming delayed reactions to reformulate the DCME as an SDDE. I have proven the equivalence between different formulations of the resulting SDDE, which are identical in terms of probability distribution and sample paths. Using this equivalence, I have proposed an alternative formulation of the SDDE, which is much more amenable to direct numerical treatment. Applying system size expansion to the exact DCME, I have derived a linear Langevin model for our system that characterises stochastic fluctuations around deterministic trajectories, and used this information to derive expressions for the variance of stochastic fluctuations around deterministically stable steady states.

Numerical simulations of the model indicate an intricate interplay between bistability and stochasticity. While deterministically the system can be in a basin of attraction of one particular steady state for a chosen combination of parameters, due to stochasticity it rather has a bi-modal probability density distribution, with

a proportion of trajectories approaching another stable steady state. Moreover, we have observed that in a small number of realisations, solutions trajectories may exhibit oscillations around a disease-free steady state, which itself is unstable, suggesting theoretical possibility of a spontaneous clearance of infection. Qualitatively similar behaviour was observed in the case, where the disease-free steady state is unstable, and the system possesses a feasible chronic steady state. The effect of time delays consists in possibly destabilising some of the steady states, and in each case the computations indicate that the variance of stochastic oscillations around deterministically stable steady states increases as one approaches the stability boundary from the stable side. We have also observed that some parameters may have almost no effect on the variance of oscillations around one steady state, while having a significant effect on the variance of oscillations around another steady state for all other values of parameters being the same. Increasing the rates of homeostatic production of regulatory T cells λ_r or the rate of suppression of autoreactive T cells by regulatory T cells δ results in the reduction of variance of oscillations.

An important practical observation concerns the difference between mean, or averaged, dynamics and the behaviour of individual stochastic realisations [189]. Even in the case when deterministically, or as a result of averaging of a large number of simulations, the system can be settling on a stable steady state, individual realisations can still exhibit sustained stochastic oscillations around that steady state. Since the normal laboratory or clinical practice deals with single observations of individual patients, this result suggests the importance of properly accounting for stochastic effects when developing realistic models of immune dynamics. Numerical simulations of the SDDE model have illustrated the behaviour of individual stochastic trajectories, as well as the time evolution of the probability distribution of the solutions.

There is a number of interesting potential extensions of this work. In terms of more accurate representation of immune response, one could consider including in the model the effects of regulatory T cells on controlling IL-2 secretion [190, 179], as well as memory T cells [194, 195]. A related question to explore concern the role of other cytokines, such as IL-7 [235], TNF-β and IL-10 [58], which are also known to have a significant impact on proliferation of different T cells and mediating their

efficiency in eliminating the infection. Including different cytokines can provide a better insight into the dynamics of immune response, as has been recently shown in a detailed model of immune response to hepatitis B [236]. Another relevant aspect is the analysis of the dependence of basins of attraction of different dynamical states on system parameters in the case of bi-stability, which highlights an important role played by the initial state of the system in terms of initial level of infection, and initial immune status [189]. Having computed the variance of stochastic oscillations depending on parameters, it should now be possible to compare these results to experimental data on the progress and variation of autoimmune disease. One possibility for such a comparison is provided by the recent work on experimental autoimmune uveoretinitis (EAU), where it has been observed that in genetically identical C57BL/6 mice, once the EAU was induced in them through inoculation, the autoimmune disease then progressed at slightly different rates [223]. In this respect, comparing theoretical estimates of the variance in this model with the measured variability in the numbers of T cells and infected cells could provide really important insights and validation of the approach developed in this chapter.

Chapter 7

Discussion

7.1 Summary

In this thesis, I have considered two deterministic models of immune response to infection. The first model analysed the dynamics of a cytokine-mediated immune response to hepatitis B, which takes into account various innate and adaptive immune response, as well as cytokines. The second model studied immune response to a viral infection with the possibility of onset and progress of autoimmunity, and included different types of T cells and IL-2. Particular emphasis has been made on stochastic properties of immune response dynamics, as well as on the roles of time delays associated with various biological processes, such as viral replication and mounting of immune response. The first chapter presented an overview of biological aspects of the immune system, as well as earlier work and results on mathematical modelling of various aspects of immune dynamics, in particular, immune response to viral infections.

In Chapter 2, I presented and analysed a very comprehensive deterministic mathematical model of the dynamics of immune system during HBV infection, which explicitly accounts not only for innate and adaptive branches of immune response, but also for different types of cytokines known to mediate these responses. I have analytically studied the stability and bifurcations of all the steady states, and showed that this model has two conditionally stable steady states: a disease-free and an endemic steady state. I have also studied the effects of two main types of drugs that are routinely used to treat hepatitis B. Since analytical results indicate that stability

of disease-free steady state depends on the product of the infection rate and the rate of production of new virus particles, rather than on each of them individually, the total treatment effectiveness is considered as the product of the effects of treatments. This allows one to easily determine the critical drug efficacy. Numerical bifurcation analysis of the steady states suggests that for any values of parameters, if the rate of clearance of free viruses by antibodies is high enough, the immune system can successfully clear the infection. It also indicates that increasing the values of parameters describing the contribution of IFN-α/β cannot by itself result in the clearance of infection. In contrast, increasing the effect of IFN-γ can revert the system to a stable disease-free state. Numerical simulations of treatment show that when the total drug effectiveness is smaller than the critical value, it is possible to have a case where the virus is also strong enough to withstand treatment, and in such a case one has to analyse the distinct effects of treatments separately, rather than as some cumulative characteristic. Our results indicate this can happen if the efficacy of IFN-based therapy is not sufficient. We have also performed extensive numerical simulations to illustrate different dynamical regimes that can be exhibited by the model, and the impact of treatment on this dynamics.

In Chapter 3, a new mathematical model of cytokine-mediated autoimmunity caused by a viral infection was developed. Since T cells play an important role in the onset of autoimmunity, the model focused on four populations of T cells: naïve T cells, regulatory T cells, normal activated T cells, and autoreactive T cells, and it has also included cytokines mediating T cell activity. We have shown how inclusion of regulatory T cells and the cytokine mediating T cell activity can lead to the emergence of periodic oscillations in the model even when the amount of free virus and the number of infected cells are equal zero, thus overcoming a limitation of some earlier models of autoimmune dynamics. The model can exhibit bi-stability, which can explain clinical observations suggesting that patients with very similar parameters of immune response can have significantly different course and outcome of the infection. Therefore, the new model provides a more realistic representation of the immune response. This model has four conditionally stable steady states: the disease-free steady state, the steady state characterised by the death of host cells, the autoimmune steady state, and the persistent or chronic

steady state. Moreover, it displays a bi-stability between different states, as well as periodic solutions. I have found analytical boundaries of steady-state and Hopf bifurcations for all steady states except for the chronic steady state, for which stability was studied numerically. I have explored how these stability boundaries depend on different system parameters, and used numerical simulations to illustrate each of the corresponding dynamical regimes. These figures indicates how bi-stability between different dynamics is affected by the parameters.

The disease-free steady state is stable when the product of natural clearance rate of free virus and natural death rate of infected cells exceeds the product of infection rate and rate of production of free virus. This suggests that increasing speed and effectiveness of treatment of infection can reduce the possibility of developing an autoimmune reaction. In the case of bi-stability between a stable disease-free steady state and an autoimmune response, we have observed that increasing the rate at which normal activated T cells destroy infected cells does not directly affect the stability of these two states, but the basin of attraction basin of the autoimmune state decreases, and if this parameter is sufficiently large, that basin of attraction can completely disappear.

Chapter 4 investigates the effects of stochasticity on the dynamics of pathogen-induced autoimmunity. The CTMC formalism provides a chemical master equation, which describes the exact probability distribution of finding the system in a particular state, however, solving this equation directly is not possible. Therefore, using van Kampen's approach I analysed how stochasticity can result in sustained periodic oscillations around deterministically stable steady states, thus providing a possible explanation of experimentally observed variation in the progression of autoimmune disease. Moreover, this approach yields a Lyapunov equation, which determines the variance of oscillations around deterministically stable steady state. Computation of the magnitude of stochastic fluctuations from this equation can be used as a guide for new laboratory experiments aimed at comparing theoretical predictions with experimental data on variation in the observed numbers of T cells and organ cells affected by infection.

Numerical simulations of the stochastic model indicate that in the case of bi-stability between two steady states, the system reaches a stationary bimodal normal

distribution, when deterministically the initial condition is in the basin of attraction of one of these two states. These results show that when the autoimmune and disease-free steady state are both stable, and deterministically the system is in the basin of attraction of autoimmune state, due to stochastic oscillations a small proportion of stochastic realisations would still end up in the basin of attraction of the disease-free steady state, suggesting that in a clinical setting a patient can have a chance not to develop an autoimmune disease, but rather successfully clear the infection without any lasting consequences. We have also shown how probability of this scenario changes depending on the initial conditions, and one can observe that moving deeper into the basin of attraction of autoimmune state reduces the chance of this happening. Therefore, in a stochastic model there is no clear separation of the basins of attraction of deterministically stable steady states, but rather the probability of finding the system in a particular steady states varies smoothly across the deterministic boundary separating distinct basins of attraction.

In Chapter 5, I analysed the effects of time delays associated with the processes of infection and developing the immune response, as well as the control of secretion of IL-2 by Tregs, on the dynamics of autoimmunity. I have analytically studied the characteristic equation associated with each steady state and proved that stability of the disease-free steady state does not depend on the time delays, while for the autoimmune and death of host cells steady states it depends only on the time delay associated with simulation and proliferation of T cells by IL-2. Moreover, for each of these steady states, I have analytically found a critical value of that time delay, at which these steady states undergo a Hopf bifurcation. Numerical results suggest that increasing the rate of clearance of IL-2 by Tregs, unlike increasing the rate of clearance of autoreactive T cells by Tregs, is not effective in controlling of autoimmune response. At the same time, increasing this parameter, the autoimmune steady state can be made biologically infeasible by stabilising the steady state corresponding to the death of host cells.

An important observation from immunological studies suggests that reducing the burden of infection can actually increase the incidence of some autoimmune diseases. I have demonstrated that adding the lag phase of virus cycle dynamics to the model shows exactly this dual role of infection, where increasing the level of infections can

protect against the development of autoimmunity.

Chapter 6 is devoted to the analysis of stochastic effects in a time-delayed model for autoimmunity. Using delay stochastic simulation algorithms is very computationally expensive, and solving the delay chemical master equation, which describes the probability distribution of the model, is also a very challenging task. Hence, I developed a new methodology for deriving an Itô stochastic delay differential equation from delay discrete stochastic models, which is more computationally efficient than the previous method, while providing the same sample path trajectories. Moreover, I have used the linear noise approximation obtained through a system size expansion of the delay chemical master equation to find the magnitude of stochastic fluctuations around deterministic steady states, and to obtain insights into how the coherence of stochastic oscillations around deterministically stable steady states depends on system parameters.

We have observed that approaching the boundary of the Hopf bifurcation, the coherence and variance of stochastic oscillations increase. In the case of bi-stability between autoimmune and chronic steady states in the deterministic model, where the disease-free steady state is unstable, it has been observed that a small proportion of stochastic simulations will still enter the basin of attraction of the disease-free steady state, and the stationary probability distribution is still given by a bimodal distribution. However, one can observe the peak probability that is related to the steady state of chronic infection will decrease slightly due to the presence of those trajectories. This result highlights the importance of using stochastic rather than deterministic models for studying complex biological processes, such as the dynamics of immune response.

7.2 Future work

There are several directions in which the work presented in this thesis can be extended. In Chapter 2 I introduced an ODE model, but, as we know, the lag phase for HBV, and the lag between infection and recruitment of CTLs are non-negligible. Thus, including these as discrete or distributed time delays the model can provide a more realistic representation of the immune response. Moreover, due to the stochas-

tic nature of immune response, one can study this model as an individual-based model and use the methods that have been presented in Chapters 4 and 6. Furthermore, it is known that antibodies do not kill the virus particles directly, but rather stick to them, creating a virus-antibody complex [35]. These complexes are not stable forever and can experience some dissociation, hence, explicitly including them into the model can provide better insights into the dynamics.

The model of autoimmunity presented in Chapter 3 can be extended in several directions. An important question within the framework of T cells with tunable activation thresholds concerns an observation that during the process of immune response, activation thresholds themselves can also change [63, 66, 67], which can have a major effect on the progress of immune dynamics. Embedding activation thresholds as additional variables in a model similar to the one studied in that Chapter would provide a more comprehensive and accurate representation of T cell dynamics during immune response. Further realism can be added to the model by including other aspects of immune system, such as antibodies and memory T cells [194, 195]. Another aspect that is relevant for this model is the fact that besides IL-2 there are other cytokines which are known to significantly affect homeostasis and proliferation of different types of T cells, as well as mediate their efficiency in eliminating the infection, such as IL-7 [235], TNF-β and IL-10 [58]. Including these factors in the model can provide new insights into the dynamics of autoimmune diseases.

The work presented in Chapter 6 from a practical perspective can be used for comparing the computed variance of stochastic fluctuations to experimental data on the progress and variation of autoimmune disease such as, the recent work on experimental autoimmune uveoretinitis (EAU), where it has been observed that there is a variation in the way disease develops in the individual eyes of the same animals and also in genetically identical C57BL/6 mice [223, 94, 93]. Fitting this model with experimental data can provide really important and valuable insights, as well as a validation of the approach developed in this thesis.

Bibliography

[1] A. K. Abbas, A. H. Lichtman, and S. Pillai, *Cellular and molecular immunology*. Elsevier Health Sciences, 2014.

[2] L. G. Guidotti, R. Rochford, J. Chung, M. Shapiro, R. Purcell, and F. V. Chisari, "Viral clearance without destruction of infected cells during acute HBV infection," *Science*, vol. 284, pp. 825–829, 1999.

[3] L. G. Guidotti and F. V. Chisari, "Noncytolytic control of viral infections by the innate and adaptive immune response," *Ann. Rev. Immunol.*, vol. 19, no. 1, pp. 65–91, 2001.

[4] L. G. Guidotti, "The role of cytotoxic T cells and cytokines in the control of hepatitis B virus infection," *Vaccine*, vol. 20, no. Suppl 4, pp. A80–A82, 2002.

[5] K. Wing, Z. Fehervari, and S. Sakaguchi, "Emerging possibilities in the development and function of regulatory T cells," *Int. Immunol.*, vol. 18, no. 7, pp. 991–1000, 2006.

[6] D. Mason, "A very high level of crossreactivity is an essential feature of the T-cell receptor," *Immunol. Today*, vol. 19, no. 9, pp. 395–404, 1998.

[7] A. C. Anderson, H. P. Waldner, V. Turchin, C. Jabs, M. Prabhu Das, V. K. Kuchroo, *et al.*, "Autoantigen responsive T cell clones demonstrate unfocused TCR cross-reactivity towards multiple related ligands: implications for autoimmunity," *Cell. Immunol.*, vol. 202, no. 2, pp. 88–96, 2000.

[8] E. C. Kerr, D. A. Copland, A. D. Dick, and L. B. Nicholson, "The dynamics of leukocyte infiltration in experimental autoimmune uveoretinitis," *Prog. Retin. Eye Res.*, vol. 27, no. 5, pp. 527–535, 2008.

[9] E. Prat and R. Martin, "The immunopathogenesis of multiple sclerosis," *J. Rehabil. Res. Dev.*, vol. 39, no. 2, pp. 187–200, 2002.

[10] P. Santamaria, "The long and winding road to understanding and conquering type 1 diabetes," *Immunity*, vol. 32, no. 4, pp. 437–445, 2010.

[11] R. Root-Bernstein and D. Fairweather, "Unresolved issues in theories of autoimmune disease using myocarditis as a framework," *J. Theor. Biol.*, vol. 375, pp. 101–123, 2015.

[12] A. L. P. Caforio and S. Iliceto, "Genetically determined myocarditis: clinical presentation and immunological characteristics," *Curr. Opin. Cardiol.*, vol. 23, no. 3, pp. 219–226, 2008.

[13] H. S. Li, D. L. Ligons, and N. R. Rose, "Genetic complexity of autoimmune myocarditis," *Autoimmun. Rev.*, vol. 7, no. 3, pp. 168–173, 2008.

[14] L. Guilherme, K. F. Köhler, E. Postol, and J. Kalil, "Genes, autoimmunity and pathogenesis of rheumatic heart disease," *Ann. Pediatr. Cardiol.*, vol. 4, no. 1, pp. 13–21, 2011.

[15] D. Germolic, D. H. Kono, J. C. Pfau, and K. M. Pollard, "Animal models used to examine the role of environment in the development of autoimmune disease: findings from an NIEHS Expert Panel Workshop," *J. Autoimmun.*, vol. 39, no. 4, pp. 285–293, 2012.

[16] M. P. Mallampalli, E. Davies, D. Wood, H. Robertson, F. Polato, and C. L. Carter, "Role of environment and sex differences in the development of autoimmune disease: a roundtable meeting report," *J. Womens Health*, vol. 22, no. 7, pp. 578–586, 2013.

[17] S. Manfredo Vieira, M. Hiltensperger, V. Kumar, D. Zegarra-Ruiz, C. Dehner, N. Khan, *et al.*, "Translocation of a gut pathobiont drives autoimmunity in mice and humans," *Science*, vol. 359, pp. 1156–1161, 2018.

[18] R. S. Fujinami, "Can virus infections trigger autoimmune disease?," *J. Autoimmun.*, vol. 16, no. 3, pp. 229–234, 2001.

[19] M. G. von Herrath and M. B. A. Oldstone, "Virus-induced autoimmune disease," *Curr. Opin. Immunol.*, vol. 8, no. 6, pp. 878–885, 1996.

[20] A. M. Ercolini and S. D. Miller, "The role of infections in autoimmune disease," *Clin. Exp. Immunol.*, vol. 155, no. 1, pp. 1–15, 2009.

[21] M. A. Nowak and R. M. May, *Virus dynamics*. Oxford University Press, Oxford, 2000.

[22] A. S. Perelson and G. Weisbuch, "Immunology for physicists," *Rev. Mod. Phys.*, vol. 69, no. 4, pp. 1219–1267, 1997.

[23] G. A. Bocharov, "Modelling the dynamics of LCMV infection in mice: conventional and exhaustive CTL responses," *J. Theor. Biol.*, vol. 192, no. 3, pp. 283–308, 1998.

[24] D. Wodarz, *Killer cell dynamics*. Springer-Verlag, 2007.

[25] A. S. Perelson, "Modelling viral and immune system dynamics," *Nat. Rev. Immunol.*, vol. 2, pp. 28–36, 2002.

[26] G. I. Marchuk, R. V. Petrov, A. A. Romanyukha, and G. A. Bocharov, "Mathematical model of antiviral immune response. I. Data analysis, generalized picture construction and parameters evaluation for hepatitis B," *J. Theor. Biol.*, vol. 151, no. 1, pp. 1–40, 1991.

[27] G. A. Bocharov and A. A. Romanyukha, "Mathematical model of antiviral immune response III. Influenza A virus infection," *J. Theor. Biol.*, vol. 167, no. 4, pp. 323–360, 1994.

[28] M. A. Nowak and C. R. M. Bangham, "Population dynamics of immune responses to persistent viruses," *Science*, vol. 272, no. 5258, pp. 74–79, 1996.

[29] A. S. Perelson, D. E. Kirschner, and R. De Boer, "Dynamics of HIV infection of $CD4^+$ T cells," *Math. Biosci.*, vol. 114, no. 1, pp. 81–125, 1993.

[30] A. S. Perelson, A. U. Neumann, and M. Markowitz, "HIV-1 dynamics in vivo: Virion clearance rate, infected cell lifespan, and viral generation time," *Science*, vol. 271, no. 5255, pp. 1582–1586, 1996.

[31] A. U. Neumann, N. P. Lam, H. Dahari, D. R. Gretch, T. E. Wiley, T. J. Layden, *et al.*, "Hepatitis C viral dynamics in vivo and the antiviral efficacy of interferon-α therapy," *Science*, vol. 282, no. 5386, pp. 103–107, 1998.

[32] S. M. Andrew, C. T. H. Baker, and G. A. Bocharov, "Rival approaches to mathematical modelling in immunology," *J. Comput. Appl. Math.*, vol. 205, no. 2, pp. 669–686, 2007.

[33] S. M. Ciupe, R. M. Ribeiro, P. W. Nelson, G. Dusheiko, and A. S. Perelson, "The role of cells refractory to productive infection in acute hepatitis B viral dynamics," *Proc. Natl. Acad. Sci. USA*, vol. 104, no. 12, pp. 5050–5055, 2007.

[34] S. M. Ciupe, R. M. Ribeiro, P. W. Nelson, and A. S. Perelson, "Modeling the mechanisms of acute hepatitis B virus infection," *J. Theor. Biol.*, vol. 247, pp. 23–35, 2007.

[35] S. M. Ciupe, R. M. Ribeiro, and A. S. Perelson, "Antibody responses during hepatitis B viral infection," *PLoS Comp. Biol.*, vol. 10, no. 7, p. e1003730, 2014.

[36] L. Min, Y. Su, and Y. Kuang, "Mathematical analysis of a basic model of virus infection with application to HBV infection," *Rocky Mountain J. Math.*, vol. 38, no. 5, pp. 1573–1585, 2008.

[37] S. Gourley, Y. Kuang, and J. D. Nagy, "Dynamics of a delay differential model of hepatitis B virus," *J. Biol. Dyn.*, vol. 2, pp. 140–153, 2008.

[38] S. Hews, S. Eikenberry, J. D. Nagy, and Y. Kuang, "Rich dynamics of a hepatitis B viral infection model with logistic hepatocyte growth," *J. Math. Biol.*, vol. 60, pp. 573–590, 2010.

[39] N. Yousfi, K. Hattaf, and A. Tridane, "Modeling the adaptive immune response in HBV infection," *J. Math. Biol.*, vol. 63, no. 5, pp. 933–957, 2011.

[40] E. N. Wiah, I. K. Dontwi, and I. A. Adetunde, "Using mathematical model to depict the immune response to hepatitis B virus infection," *J. Math. Res.*, vol. 3, no. 2, pp. 157–167, 2011.

[41] H. Y. Kim, H. D. Kwon, T. S. Jang, J. Lim, and H. S. Lee, "Mathematical modeling of triphasic viral dynamics in patients with HBeAg-positive chronic hepatitis B showing response to 24-week clevudine therapy," *PLoS ONE*, vol. 7, p. e50377, 2012.

[42] H. Dahari, E. Shudo, R. M. Ribeiro, and A. S. Perelson, "Modeling complex decay profiles of hepatitis B virus during antiviral therapy," *Hepatology*, vol. 49, no. 1, pp. 32–38, 2009.

[43] S. R. Lewin, R. M. Ribeiro, T. Walters, G. K. Lau, S. Bowden, S. Locarnini, *et al.*, "Analysis of hepatitis B viral load decline under potent therapy: complex decay profiles observed," *Hepathology*, vol. 34, no. 5, pp. 1012–1020, 2001.

[44] V. A. Sypsa, K. Mimidis, N. C. Tassopoulous, D. Chrysagis, T. Vassiliadis, A. Moulakakis, *et al.*, "A viral kinetic study using pegylated interferon alfa-2b and/or lamivudine in patients with chronic hepatitis B/HBeAg negative," *Hepathology*, vol. 42, no. 1, pp. 77–85, 2005.

[45] L. A. Segel, E. Jäger, D. Elias, and I. R. Cohen, "A quantitative model of autoimmune disease and T-cell vaccination: does more mean less?," *Immunol. Today*, vol. 16, no. 2, pp. 80–84, 1995.

[46] J. A. M. Borghans and R. J. De Boer, "A minimal model for T-cell vaccination," *Proc. R. Soc. Lond. Ser. B Biol. sci.*, vol. 259, no. 1355, pp. 173–178, 1995.

[47] J. A. M. Borghans, R. J. De Boer, E. Sercarz, and V. Kumar, "T cell vaccination in experimental autoimmune encephalomyelitis: a mathematical model," *J. Immunol.*, vol. 161, no. 3, pp. 1087–1093, 1998.

[48] K. León, R. Perez, A. Lage, and J. Carneiro, "Modelling T-cell-mediated suppression dependent on interactions in multicellular conjugates," *J. Theor. Biol.*, vol. 207, no. 2, pp. 231–254, 2000.

[49] K. León, A. Lage, and J. Carneiro, "Tolerance and immunity in a mathematical model of T-cell mediated suppression," *J. Theor. Biol.*, vol. 225, no. 1, pp. 107–126, 2003.

[50] K. León, J. Faro, A. Lage, and J. Carneiro, "Inverse correlation between the incidences of autoimmune disease and infection predicted by a model of T cell mediated tolerance," *J. Autoimmun.*, vol. 22, no. 1, pp. 31–42, 2004.

[51] J. Carneiro, T. Paixão, D. Milutinovic, J. Sousa, K. León, R. Gardner, *et al.*, "Immunological self-tolerance: Lessons from mathematical modeling," *J. Comput. Appl. Math.*, vol. 184, no. 1, pp. 77–100, 2005.

[52] S. Iwami, Y. Takeuchi, Y. Miura, T. Sasaki, and T. Kajiwara, "Dynamical properties of autoimmune disease models: tolerance, flare-up, dormancy," *J. Theor. Biol.*, vol. 246, no. 4, pp. 646–659, 2007.

[53] S. Iwami, Y. Takeuchi, K. Iwamoto, Y. Naruo, and M. Yasukawa, "A mathematical design of vector vaccine against autoimmune disease," *J. Theor. Biol.*, vol. 256, no. 3, pp. 382–392, 2009.

[54] H. K. Alexander and L. M. Wahl, "Self-tolerance and autoimmunity in a regulatory T cell model," *Bull. Math. Biol.*, vol. 73, no. 1, pp. 33–71, 2011.

[55] N. J. Burroughs, M. Ferreira, B. M. P. M. Oliveira, and A. A. Pinto, "Autoimmunity arising from bystander proliferation of T cells in an immune response model," *Math. Comput. Model.*, vol. 53, no. 7, pp. 1389–1393, 2011.

[56] N. J. Burroughs, M. Ferreira, B. M. P. M. Oliveira, and A. A. Pinto, "A transcritical bifurcation in an immune response model," *J. Diff. Eqns. Appl.*, vol. 17, pp. 1101–1106, 2011.

[57] R. Root-Bernstein, "Theories and modeling of autoimmunity," *J. Theor. Biol.*, vol. 375, pp. 1–124, 2015.

[58] S. Sakaguchi, "Naturally arising $CD4^+$ regulatory T cells for immunologic self-tolerance and negative control of immune responses," *Ann. Rev. Immunol.*, vol. 22, pp. 531–562, 2004.

[59] S. Z. Josefowicz, L.-F. Lu, and A. Y. Rudensky, "Regulatory T cells: mechanisms of differentiation and function," *Ann. Rev. Immunol.*, vol. 30, pp. 531–564, 2012.

[60] A. Corthay, "How do regulatory T cells work?," *Scand. J. Immunol.*, vol. 70, no. 4, pp. 326–336, 2009.

[61] J. D. Fontenot, M. A. Gavin, and A. Y. Rudensky, "Foxp3 programs the development and function of $CD4^+CD25^+$ regulatory T cells," *Nat. Immunol.*, vol. 4, no. 4, pp. 330–336, 2003.

[62] R. Khattri, T. Cox, S.-A. Yasayko, and F. Ramsdell, "An essential role for Scurfin in $CD4^+CD25^+$ T regulatory cells," *Nat. Immunol.*, vol. 4, no. 4, pp. 337–342, 2003.

[63] Z. Grossman and A. Singer, "Tuning of activation thresholds explains flexibility in the selection and development of T cells in the thymus," *Proc. Natl. Acad. Sci. USA*, vol. 93, no. 25, pp. 14747–14752, 1996.

[64] Z. Grossman and W. E. Paul, "Adaptive cellular interactions in the immune system: the tunable activation threshold and the significance of subthreshold responses," *Proc. Natl. Acad. Sci. USA*, vol. 89, no. 21, pp. 10365–10369, 1992.

[65] Z. Grossman and W. E. Paul, "Self-tolerance: context dependent tuning of T cell antigen recognition," *Semin. Immunol.*, vol. 12, no. 3, pp. 197–203, 2000.

[66] G. Altan-Bonnet and R. N. Germain, "Modeling T cell antigen discrimination based on feedback control of digital ERK responses," *PLoS Biol.*, vol. 3, p. e356, 2005.

[67] H. A. van den Berg and D. A. Rand, "Dynamics of T cell activation threshold tuning," *J. Theor. Biol.*, vol. 228, no. 3, pp. 397–416, 2004.

[68] A. Scherer, A. Noest, and R. J. de Boer, "Activation-threshold tuning in an affinity model for the T-cell repertoire," *Proc. R. Soc. Lond. B Biol. Sci.*, vol. 271, no. 1539, pp. 609–616, 2004.

[69] O. Feinerman, R. N. Germain, and G. Altan-Bonnet, "Quantitative challenges in understanding ligand discrimination by αβ T cells," *Mol. Immunol.*, vol. 45, no. 3, pp. 619–631, 2008.

[70] A. J. T. George, J. Stark, and C. Chan, "Understanding specificity and sensitivity of T-cell recognition," *Trends Immunol.*, vol. 26, no. 12, pp. 653–659, 2005.

[71] A. D. Bitmansour, D. C. Douek, V. C. Maino, and L. J. Picker, "Direct ex vivo analysis of human $CD4^+$ memory T cell activation requirements at the single clonotype level," *J. Immunol.*, vol. 169, no. 3, pp. 1207–1218, 2002.

[72] L. B. Nicholson, A. C. Anderson, and V. K. Kuchroo, "Tuning T cell activation threshold and effector function with cross-reactive peptide ligands," *Int. Immunol.*, vol. 12, no. 2, pp. 205–213, 2000.

[73] P. S. Römer, S. Berr, E. Avota, S.-Y. Na, M. Battaglia, I. ten Berge, *et al.*, "Preculture of PBMC at high cell density increases sensitivity of T-cell responses, revealing cytokine release by CD28 superagonist TGN1412," *Blood*, vol. 118, no. 26, pp. 6772–6782, 2011.

[74] I. Stefanová, J. R. Dorfman, and R. N. Germain, "Self-recognition promotes the foreign antigen sensitivity of naive T lymphocytes," *Nature*, vol. 420, no. 6914, pp. 429–434, 2002.

[75] A. J. Noest, "Designing lymphocyte functional structure for optimal signal detection: *voilà*, T cells," *J. Theor. Biol.*, vol. 207, pp. 195–216, 2000.

[76] K. B. Blyuss and L. B. Nicholson, "The role of tunable activation thresholds in the dynamics of autoimmunity," *J. Theor. Biol.*, vol. 308, pp. 45–55, 2012.

[77] K. B. Blyuss and L. B. Nicholson, "Understanding the roles of activation threshold and infections in the dynamics of autoimmune disease," *J. Theor. Biol.*, vol. 375, pp. 13–20, 2015.

[78] D. Ben Ezra and J. V. Forrester, "Fundal white dots: the spectrum of a similar pathological process," *Brit. J. Ophthalmol.*, vol. 79, no. 9, pp. 856–860, 1995.

[79] T. F. Davies, D. C. Evered, B. Rees Smith, P. P. B. Yeo, F. Clark, and R. Hall, "Value of thyroid-stimulating-antibody determinations in predicting the short-term thyrotoxic relapse in Graves' disease," *Lancet*, vol. 309, no. 8023, pp. 1181–1182, 1977.

[80] A. Nylander and D. A. Hafler, "Multiple sclerosis," *J. Clin. Invest.*, vol. 122, no. 4, pp. 1180–1188, 2012.

[81] S. Roy, K. Shrinivas, and B. Bagchi, "A stochastic chemical dynamic approach to correlate autoimmunity and optimal vitamin-D range," *PloS ONE*, vol. 9, no. 6, p. e100635, 2014.

[82] M. Baker, S. Denman-Johnson, B. S. Brook, I. Gaywood, and M. R. Owen, "Mathematical modelling of cytokine-mediated inflammation in rheumatoid arthritis," *Math. Med. Biol.*, vol. 30, pp. 311–337, 2013.

[83] N. Rapin, E. Mosekilde, and O. Lund, "Bistability in autoimmune diseases," *Autoimmunity*, vol. 44, no. 4, pp. 256–260, 2011.

[84] E. K. Deenick, A. V. Gett, and P. D. Hodgkin, "Stochastic model of T cell proliferation: A calculus revealing IL-2 regulation of precursor frequencies, cell cycle time, and survival," *J. Immunol.*, vol. 170, pp. 4963–4972, 2003.

[85] J. N. Blattman, K. Sourdive D J D, Murali-Krishna, R. Ahmed, and J. D. Altman, "Evolution of the T cell repertoire during primary, memory, and recall response to viral infection," *J. Immunol.*, vol. 165, pp. 6081–6090, 2000.

[86] V. Detours and A. S. Perelson, "The paradox of alloreactivity and self MHC restriction: Quantitative analysis and statistics," *Proc. Natl. Acad. Sci. USA*, vol. 97, pp. 8479–8483, 2000.

[87] D. L. Chao, M. P. Davenport, S. Forrest, and A. S. Perelson, "A stochastic model of cytotoxic T cell responses," *J. Theor. Biol.*, vol. 228, pp. 227–240, 2004.

[88] E. R. Stirk, G. Lythe, H. A. van den Berg, G. A. D. Hurst, and C. Molina-París, "The limiting conditional probability distribution in a stochastic model of T cell repertoire maintenance," *Math. Biosci.*, vol. 224, pp. 74–86, 2010.

[89] E. R. Stirk, G. Lythe, H. A. Van den Berg, and C. Molina-París, "Stochastic competitive exclusion in the maintenance of the naïve T cell repertoire," *J. Theor. Biol.*, vol. 265, no. 3, pp. 396–410, 2010.

[90] J. Reynolds, M. Coles, G. Lythe, and C. Molina-París, "Deterministic and stochastic naïve T cell population dynamics: Symmetric and asymmetric cell division," *Dynamical Systems*, vol. 27, no. 1, pp. 75–103, 2012.

[91] D. Alonso, A. J. McKane, and M. Pascual, "Stochastic amplification in epidemics," *J. R. Soc. Interface*, vol. 4, no. 14, pp. 575–582, 2007.

[92] R. Kuske, L. F. Gordillo, and P. Greenwood, "Sustained oscillations via coherence resonance in SIR," *J. Theo. Biol.*, vol. 245, no. 3, pp. 459–469, 2007.

[93] J. Boldison, C. J. Chu, D. A. Copland, P. J. P. Lait, T. K. Khera, A. D. Dick, *et al.*, "Tissue-resident exhausted effector memory $CD8^+$ T cells accumulate in the retina during chronic experimental autoimmune uveoretinitis," *J. Immunol.*, vol. 192, no. 10, pp. 4541–4550, 2014.

[94] J. Boldison and L. B. Nicholson, "unpublished." 2015.

[95] J. Tam, "Delay effect in a model for virus replication," *IMA J. Math. Appl. Med. Biol.*, vol. 16, no. 1, pp. 29–37, 1999.

[96] R. V. Culshaw and S. Ruan, "A delay-differential equation model of HIV infection of $CD4^+$ T-cells," *Math. Biosci.*, vol. 165, no. 1, pp. 27–39, 2000.

[97] P. W. Nelson and A. S. Perelson, "Mathematical analysis of delay differential equation models of HIV-1 infection," *Math. Biosci.*, vol. 179, no. 1, pp. 73–94, 2002.

[98] X. Zhou, X. Song, and X. Shi, "Analysis of stability and Hopf bifurcation for an HIV infection model with time delay," *Appl. Math. Comput.*, vol. 199, no. 1, pp. 23–38, 2008.

[99] C. A. A. Beauchemin, J. J. McSharry, G. L. Drusano, J. T. Nguyen, G. T. Went, R. M. Ribeiro, *et al.*, "Modeling amantadine treatment of influenza A virus in vitro," *J. Theor. Biol.*, vol. 254, no. 2, pp. 439–451, 2008.

[100] C. A. A. Beauchemin and A. Handel, "A review of mathematical models of influenza A infections within a host or cell culture: lessons learned and challenges ahead," *BMC Public Health*, vol. 11 (Suppl 1), p. S7, 2011.

[101] A. S. Perelson, "Viral kinetics and mathematical models," *Am. J. Med.*, vol. 107(Suppl 2), no. 6, pp. 49–52, 1999.

[102] B. Krone and J. M. Grange, "Multiple sclerosis: are protective immune mechanisms compromised by a complex infectious background?," *Autoimmune Dis.*, vol. 2011, 2010.

[103] M. Ohashi, N. Orlova, C. Quink, and F. Wang, "Cloning of the Epstein-Barr virus-related rhesus lymphocryptovirus as a bacterial artificial chromosome: a loss-of-function mutation of the rhBARF1 immune evasion gene," *J. Virol.*, vol. 85, no. 3, pp. 1330–1339, 2011.

[104] D. Hober and P. Sauter, "Pathogenesis of type 1 diabetes mellitus: interplay between enterovirus and host," *Nat. Rev. Endocrinol.*, vol. 6, no. 5, pp. 279–289, 2010.

[105] S. E. Myers, L. Brewer, D. P. Shaw, W. H. Greene, B. C. Love, B. Hering, *et al.*, "Prevalent human coxsackie B-5 virus infects porcine islet cells primarily using the coxsackie-adenovirus receptor," *Xenotransplantation*, vol. 11, no. 6, pp. 536–546, 2004.

[106] K. Döhner, K. Radtke, S. Schmidt, and B. Sodeik, "Eclipse phase of herpes simplex virus type 1 infection: Efficient dynein-mediated capsid transport without the small capsid protein VP26," *J. Virol.*, vol. 80, no. 16, pp. 8211–8224, 2006.

[107] U. Maurer, B. Sodeik, and K. Gruenewald, "Native 3D intermediates of membrane fusion in herpes simplex virus 1 entry," *Proc. Natl. Acad. Sci. USA*, vol. 105, no. 30, pp. 10559–10564, 2008.

[108] A. J. Yates, M. Van Baalen, and R. Antia, "Virus replication strategies and the critical CTL numbers required for the control of infection," *PLoS Comput. Biol.*, vol. 7, no. 11, p. e1002274, 2011.

[109] G. J. M. Webster, S. Reignat, M. K. Maini, S. A. Whalley, G. S. Ogg, A. King, *et al.*, "Incubation phase of acute hepatitis B in man: dynamic of cellular immune mechanisms," *Hepatology*, vol. 32, no. 5, pp. 1117–1124, 2000.

[110] M. S. Ciupe, B. L. Bivort, D. M. Bortz, and P. W. Nelson, "Estimating kinetic parameters from HIV primary infection data through the eyes of three different mathematical models," *Math. Biosci.*, vol. 200, no. 1, pp. 1–27, 2006.

[111] M. P. Davenport, R. M. Ribeiro, and A. S. Perelson, "Kinetics of virus-specific $CD8^+$ T cells and the control of human immunodeficiency virus infection," *J. Virol.*, vol. 78, no. 18, pp. 10096–10103, 2004.

[112] R. Thimme, J. Bukh, H. C. Spangenberg, S. Wieland, J. Pemberton, C. Steiger, *et al.*, "Viral and immunological determinants of hepatitis C virus clearance, persistence, and disease," *Proc. Natl. Acad. Sci. USA*, vol. 99, no. 24, pp. 15661–15668, 2002.

[113] P. S. Kim, P. P. Lee, and D. Levy, "Modeling regulation mechanisms in the immune system," *J. Theor. Biol.*, vol. 246, no. 1, pp. 33–69, 2007.

[114] D. Bratsun, D. Volfson, L. S. Tsimring, and J. Hasty, "Delay-induced stochastic oscillations in gene regulation," *Proc. Natl. Acad. Sci. USA*, vol. 102, no. 41, pp. 14593–14598, 2005.

[115] M. Barrio, K. Burrage, A. Leier, and T. Tian, "Oscillatory regulation of Hes1: discrete stochastic delay modelling and simulation," *PLoS Comput. Biol.*, vol. 2, no. 9, p. e117, 2006.

[116] X. Cai, "Exact stochastic simulation of coupled chemical reactions with delays," *J. Chem. Phys.*, vol. 126, no. 12, p. 124108, 2007.

[117] E. Zavala and T. T. Marquez-Lago, "Delays induce novel stochastic effects in negative feedback gene circuits," *Biophys. J.*, vol. 106, no. 2, pp. 467–478, 2014.

[118] V. H. Thanh, C. Priami, and R. Zunino, "Efficient rejection-based simulation of biochemical reactions with stochastic noise and delays," *J. Chem. Phys.*, vol. 141, no. 13, p. 134116, 2014.

[119] V. H. Thanh, R. Zunino, and C. Priami, "Efficient stochastic simulation of biochemical reactions with noise and delays," *J. Chem. Phys.*, vol. 146, no. 8, p. 084107, 2017.

[120] A. Leier and T. T. Marquez-Lago, "Delay chemical master equation: direct and closed-form solutions," *Proc. R. Soc. A*, vol. 471, no. 2179, p. 20150049, 2015.

[121] T. Tian, K. Burrage, P. M. Burrage, and M. Carletti, "Stochastic delay differential equations for genetic regulatory networks," *J. Comput. Appl. Math.*, vol. 205, no. 2, pp. 696–707, 2007.

[122] N. E. Phillips, C. S. Manning, T. Pettini, V. Biga, E. Marinopoulou, P. Stanley, *et al.*, "Stochasticity in the miR-9/Hes1 oscillatory network can account for clonal heterogeneity in the timing of differentiation," *Elife*, vol. 5, p. e16118, 2016.

[123] Y. Niu, C. Zhang, and K. Burrage, "Strong predictor-corrector approximation for stochastic delay differential equations," *J. Comput. Math.*, vol. 33, no. 6, pp. 587—605, 2015.

[124] Y. Niu, K. Burrage, and C. Zhang, "Multi-scale approach for simulating time-delay biochemical reaction systems," *IET Syst. Biol.*, vol. 9, no. 1, pp. 31–38, 2015.

[125] J. Yang, S. Zhong, and W. Luo, "Mean square stability analysis of impulsive stochastic differential equations with delays," *J. Comput. Appl. Math.*, vol. 216, no. 2, pp. 474–483, 2008.

[126] A. Lang, A. Petersson, and A. Thalhammer, "Mean-square stability analysis of approximations of stochastic differential equations in infinite dimensions," *BIT Numer. Math.*, vol. 57, no. 4, pp. 963–990, 2017.

[127] T. D. Frank, "Multivariate Markov processes for stochastic systems with delays: application to the stochastic Gompertz model with delay," *Phys. Rev. E*, vol. 66, no. 1, p. 011914, 2002.

[128] T. D. Frank, "Kramers–Moyal expansion for stochastic differential equations with single and multiple delays: Applications to financial physics and neurophysics," *Phys. Lett. A*, vol. 360, pp. 552–562, 2007.

[129] T. Galla, "Intrinsic fluctuations in stochastic delay systems: Theoretical description and application to a simple model of gene regulation," *Phys. Rev. E*, vol. 80, no. 2, p. 021909, 2009.

[130] S. Guillouzic, I. L'Heureux, and A. Longtin, "Small delay approximation of stochastic delay differential equations," *Phys. Rev. E*, vol. 59, no. 4, p. 3970, 1999.

[131] R. B. Takkenberg, C. J. Weegink, H. L. Zaaijer, and H. W. Reesink, "New developments in antiviral therapy for chronic hepatitis B," *Vox Sang.*, vol. 98, no. 4, pp. 481–494, 2009.

[132] WHO, "Hepatitis B," *WHO Fact Sheet*, vol. 117, 2016.

[133] T. Vos, R. M. Barber, B. Bell, A. Bertozzi-Villa, S. Biryukov, I. Bolliger, *et al.*, "Global, regional, and national incidence, prevalence, and years lived with disability for 301 acute and chronic diseases and injuries in 188 countries, 1990-2013: a systematic analysis for the Global Burden of Disease Study 2013," *Lancet*, vol. 386, no. 9995, pp. 743–800, 2015.

[134] M. Naghavi, H. Wang, R. Lozano, A. Davis, X. Liang, and M. Zhou, "GBD 2013 mortality and causes of death collaborators. Global, regional, and national age-sex specific all-cause and cause-specific mortality for 240 causes of death, 1990-2013: a systematic analysis for the Global Burden of Disease Study 2013," *Lancet*, vol. 385, no. 9963, pp. 117–171, 2015.

[135] C. Seeger and W. S. Mason, "Hepatitis B virus biology," *Microbiol. Mol. Biol. Rev.*, vol. 64, no. 1, pp. 51–68, 2000.

[136] T. J. Liang, "Hepatitis B: The virus and disease," *Hepatology*, vol. 49, no. 5 Suppl, pp. S13–S21, 2009.

[137] B. Rehermann and M. Nascimbeni, "Immunology of hepatitis B virus and hepatitis C virus infection," *Nat. Rev. Immunol.*, vol. 5, no. 3, pp. 215–229, 2014.

[138] A. Bertoletti and A. J. Gehring, "The immune response during hepatitis B virus infection," *J. Gen. Virol.*, vol. 87, pp. 1439–1449, 2006.

[139] S. F. Wieland and F. V. Chisari, "Stealth and cunning: hepatitis B and hepatitis C viruses," *J. Virol.*, vol. 79, no. 15, pp. 9369–9380, 2005.

[140] A. L. DeVico and R. C. Gallo, "Control of HIV-1 infection by soluble factors of the immune response," *Nat. Rev. Microbiol.*, vol. 2, no. 5, pp. 401–413, 2004.

[141] A. Isaacs and J. Lindeman, "Virus interference. I. the interferon," *Proc. R. Soc. Lond. B*, vol. 147, no. 927, pp. 258–267, 1957.

[142] D. V. Kalvakolanu and E. C. Borden, "An overview of the interferon system: signal transduction and mechanism of action," *Cancer Invest.*, vol. 14, no. 1, pp. 25–53, 1996.

[143] Z. O. E. Babiker, C. Hogan, A. Ustianowski, and E. Wilkins, "Does interferon-sparing tenofovir disoproxil fumarate-based therapy have a role in the management of severe acute hepatitis delta superinfection?," *J. Med. Microbiol.*, vol. 61, no. 12, pp. 1780–1783, 2012.

[144] S. Tamura, T. Tanimoto, and T. Kurata, "Mechanisms of broad cross protection provided by influenza virus infection and their application to vaccines," *Jpn. J. Infect. Dis.*, vol. 58, no. 4, pp. 195–207, 2005.

[145] A. J. Ramsay, J. Ruby, and I. A. Ramshaw, "A case for cytokines as effector molecules in the resolution of virus infection," *Immunol. Today*, vol. 14, no. 4, pp. 155–157, 1993.

[146] M. A. Nowak, S. Bonhoeffer, A. M. Hill, and R. Boehme, "Viral dynamics in hepatitis B virus infection," *Proc. Natl. Acad. Sci. USA*, vol. 93, no. 9, pp. 4398–4402, 1996.

[147] Y. Su, Y. Wen, and L. Min, "Analysis of a HBV infection model with ALT," in *2012 IEEE 6th International Conference on Systems Biology (ISB), China, August 18-20, 2012*, (New York, NY, USA), pp. 97–100, IEEE, 2012.

[148] A. Busca and A. Kumar, "Innate immune responses in hepatitis B virus (HBV) infection," *Virol. J.*, vol. 11, no. 1, p. 22, 2014.

[149] L. G. Guidotti, S. Guilhot, and F. V. Chisari, "Interleukin 2 and interferon α/β negatively regulates hepatitis B virus gene expression in vivo by tumor necrosis factor dependent and independent pathways," *J. Virol.*, vol. 68, no. 3, pp. 1265–1270, 1994.

[150] G. Herbein and W. A. O'Brien, "Tumor necrosis factor (TNF)-α and TNF receptors in viral pathogenesis," *Proc. Soc. Exp. Biol. Med.*, vol. 223, no. 3, pp. 241–257, 2000.

[151] I. Julkunen, T. Sareneva, J. Pirhonen, T. Ronni, and K. Melen, "Molecular pathogenesis of influenza A virus infection and virus-induced regulation of cytokine gene expression," *Cytokine Growth Factor Rev.*, vol. 12, no. 2, pp. 171–180, 2001.

[152] G. E. Price, A. Gaszewska-Mastarlarz, and D. Moskophidis, "The role of alpha/beta and gamma interferons in development of immunity to influenza A virus in mice," *J. Virol.*, vol. 74, no. 9, pp. 3996–4003, 2000.

[153] I. A. Ramshaw, A. J. Ramsay, G. Karupiah, M. S. Rolph, S. Mahalingam, and J. C. Ruby, "Cytokines and immunity to viral infections," *Immunol. Rev.*, vol. 159, no. 1, pp. 119–135, 1997.

[154] K. A. Pawelek, G. T. Huynh, M. Quinlivan, A. Cullinane, L. Rong, and A. S. Perelson, "Modeling within-host dynamics of influenza virus infection including immune responses," *PLoS Comput. Biol.*, vol. 8, no. 6, p. e1002588, 2012.

[155] Z. Abbas and R. Afzal, "Life cycle and pathogenesis of hepatitis D virus: A review," *World J. Hepatol.*, vol. 5, no. 12, pp. 666–675, 2013.

[156] K. Schroder, P. J. Hertzog, T. Ravasi, and D. A. Hume, "Interferon-γ: an overview of signals, mechanisms and functions," *J. Leukoc. Biol.*, vol. 75, no. 2, pp. 163–189, 2004.

[157] C. Carnaud, D. Lee, O. Donnars, S. H. Park, A. Beavis, Y. Koezuka, *et al.*, "Cutting edge: cross-talk between cells of the innate immune system: NKT cells rapidly activate NK cells," *J. Immunol.*, vol. 163, no. 9, pp. 4647–4650, 1999.

[158] C. A. Biron, K. B. Nguyen, G. C. Pien, L. P. Cousens, and T. P. Salazar-Mather, "Natural killer cells in antiviral defense: function and regulation by innate cytokines," *Ann. Rev. Immunol.*, vol. 17, no. 1, pp. 189–220, 1999.

[159] G. R. Stark, I. M. Kerr, B. R. Williams, R. H. Silverman, and R. D. Schreiber, "How cells respond to interferons," *Annu. Rev. Biochem.*, vol. 67, pp. 227–264, 1998.

[160] M. L. Chang and Y. F. Liaw, "Hepatitis B flares in chronic hepatitis B: pathogenesis, natural course and management," *J. Hepatol.*, vol. 61, no. 6, pp. 1407–1417, 2014.

[161] R. P. Perillo, "Acute flares in chronic hepatitis B: the natural and unnatural history of an immunology mediated liver disease," *Gastroenterology*, vol. 120, no. 4, pp. 1009–1022, 2001.

[162] Y. Lenbury, R. Ouncharoen, and N. Tumrasvin, "Higher-dimensional separation principle for the analysis of relaxation oscillations in nonlinear systems: application to a model of HTV infection," *IMA J. Math. Appl. Med. Biol.*, vol. 17, no. 3, pp. 243–261, 2000.

[163] S. J. Merrill, "A model of the stimulation of B-cells by replicating antigen–l," *Math. Biosci.*, vol. 41, pp. 125–141, 1978.

[164] A. Packer, J. Forde, S. Hews, and Y. Kuang, "Mathematical models of the interrelated dynamics of hepatitis D and B," *Math. Biosci.*, vol. 247, pp. 38–46, 2014.

[165] L. Min, W. Li, Y. Su, and Y. Kuang, "A mathematical model of the dynamics for anti-HBV infection treatment with Peginterferon Alfa-2a," in *Proceedings of ICCCAS 2008, China, 25-27 May 2008*, (New York, NY, USA), pp. 1295–1298, IEEE, 2008.

[166] P. Colombato, L. Civitano, R. Bizzari, F. Oliveri, S. Choudhury, R. Gieschke, *et al.*, "A multiphase model of the dynamics of HBV infection in HBeAg-negative patients during pegylated interferon-α2a, lamivudine and combination therapy," *Antivir. Ther.*, vol. 11, pp. 197–212, 2006.

[167] P. W. Nelson, J. D. Murray, and A. S. Perelson, "A model of HIV-1 pathogenesis that includes an intracellular delay," *Math. Biosci.*, vol. 163, pp. 201–215, 2000.

[168] A. R. McLean, "Modelling T cell memory," *J. Theor. Biol.*, vol. 170, no. 1, pp. 63–74, 1994.

[169] C. Utzny and N. J. Burroughs, "Perturbation theory analysis of competition in a heterogeneous population," *Physica D*, vol. 175, no. 1, pp. 109–126, 2003.

[170] A. L. DeFranco, R. M. Locksley, and M. Robertson, *Immunity: The immune response in infectious and inflammatory disease*. New Science Press Ltd., 2007.

[171] A. Toda and C. A. Piccirillo, "Development and function of naturally occurring $CD4^+CD25^+$ regulatory T cells," *J. Leukoc. Biol.*, vol. 80, no. 3, pp. 458–470, 2006.

[172] D. Wodarz and V. A. A. Jansen, "A dynamical perspective of CTL cross-priming and regulation: implications for cancer immunology," *Immunol. Lett.*, vol. 86, no. 3, pp. 213–227, 2003.

[173] S. D. Wolf, B. N. Dittel, F. Hardardottir, and C. A. Janeway Jr., "Experimental autoimmune encephalomyelitis induction in genetically B cell-deficient mice," *J. Exp. Med.*, vol. 184, no. 6, pp. 2271–2278, 1996.

[174] H.-J. Wu, I. I. Ivanov, J. Darce, K. Hattori, T. Shima, Y. Umesaki, *et al.*, "Gut-residing segmented filamentous bacteria drive autoimmune arthritis via T helper 17 cells," *Immunity*, vol. 32, no. 6, pp. 815–827, 2010.

[175] A. S. Perelson and P. W. Nelson, "Mathematical analysis of HIV-1 dynamics in vivo," *SIAM Rev.*, vol. 41, no. 1, pp. 3–44, 1999.

[176] S. Sakaguchi, N. Sakaguchi, M. Asano, M. Itoh, and M. Toda, "Immunologic self-tolerance maintained by activated T cells expressing IL-2 receptor α-chains (CD25). Breakdown of a single mechanism of self-tolerance causes various autoimmune diseases.," *J. Immunol.*, vol. 155, no. 3, pp. 1151–1164, 1995.

[177] C. A. Janeway, P. Travers, M. Walport, and M. J. Shlomchik, *Immunobiology: the immune system in health and disease*. New York: Garland Science, 6th ed., 2005.

[178] M. R. Walker, B. D. Carson, G. T. Nepom, S. F. Ziegler, and J. H. Buckner, "*De novo* generation of antigen-specific $CD4^+CD25^+$ regulatory T cells from human $CD4^+CD25^-$cells," *Proc. Natl. Acad. Sci. USA*, vol. 102, no. 11, pp. 4103–4108, 2005.

[179] N. J. Burroughs, B. M. P. M. de Oliveira, and A. A. Pinto, "Regulatory T cell adjustment of quorum growth thresholds and the control of local immune responses," *J. Theor. Biol.*, vol. 241, no. 1, pp. 134–141, 2006.

[180] N. A. Danke, D. M. Koelle, C. Yee, S. Beheray, and W. W. Kwok, "Autoreactive T cells in healthy individuals," *J. Immunol.*, vol. 172, no. 10, pp. 5967–5972, 2004.

[181] I. Baltcheva, L. Codarri, G. Pantaleo, and J.-Y. Le Boudec, "Lifelong dynamics of human $CD4^+CD25^+$ regulatory T cells: Insights from *in vivo* data and mathematical modeling," *J. Theor. Biol.*, vol. 266, no. 2, pp. 307–322, 2010.

[182] A. M. Thornton and E. M. Shevach, "$CD4^+CD25^+$ immunoregulatory T cells suppress polyclonal T cell activation in vitro by inhibiting interleukin 2 production," *J. Exp. Med.*, vol. 188, no. 2, pp. 287–296, 1998.

[183] E. M. Shevach, R. S. McHugh, C. A. Piccirillo, and A. M. Thornton, "Control of T-cell activation by $CD4^+CD25^+$ suppressor T cells," *Immunol. Rev.*, vol. 182, no. 1, pp. 58–67, 2001.

[184] P. Yu, R. K. Gregg, J. J. Bell, J. S. Ellis, R. Divekar, H.-H. Lee, *et al.*, "Specific T regulatory cells display broad suppressive functions against experimental allergic encephalomyelitis upon activation with cognate antigen," *J. Immunol.*, vol. 174, no. 11, pp. 6772–6780, 2005.

[185] C. Tanchot, F. Vasseur, C. Pontoux, C. Garcia, and A. Sarukhan, "Immune regulation by self-reactive T cells is antigen specific," *J. Immunol.*, vol. 172, no. 7, pp. 4285–4291, 2004.

[186] Q. Tang, J. Y. Adams, A. J. Tooley, M. Bi, B. T. Fife, P. Serra, *et al.*, "Visualizing regulatory T cell control of autoimmune responses in nonobese diabetic mice," *Nat. Immunol.*, vol. 7, no. 1, p. 83, 2006.

[187] J. Carneiro, K. León, Í. Caramalho, C. V van den Dool, R. Gardner, V. Oliveira, *et al.*, "When three is not a crowd: a Crossregulation model of the dynamics and repertoire selection of regulatory $CD4^+$ T cells," *Immunol. Rev.*, vol. 216, no. 1, pp. 48–68, 2007.

[188] C. Baecher-Allan, V. Viglietta, and D. A. Hafler, "Inhibition of human $CD4^+CD25^{+\text{high}}$ regulatory T cell function," *J. Immunol.*, vol. 169, no. 11, pp. 6210–6217, 2002.

[189] F. Fatehi, S. N. Kyrychko, A. Ross, Y. N. Kyrychko, and K. B. Blyuss, "Stochastic effects in autoimmune dynamics," *Front. Physiol.*, vol. 9, p. 45, 2018.

[190] F. Fatehi, Y. N. Kyrychko, and K. B. Blyuss, "Effects of viral and cytokine delays on dynamics of autoimmunity," *Mathematics*, vol. 6, p. 66, 2018.

[191] Y. A. Kuznetsov, *Elements of applied bifurcation theory.* Springer Verlag, 2nd ed., 1998.

[192] L. Anderson, S. Jang, and J.-L. Yu, "Qualitative behavior of systems of tumor-$CD4^+$-cytokine interactions with treatments," *Math. Meth. Appl. Sci.*, vol. 38, pp. 4330–4344, 2015.

[193] X. Li and H. Levine, "Bistability of the cytokine-immune cell network in a cancer microenvironment," *Converg. Sci. Phys. Oncol.*, vol. 3, p. 024002, 2017.

[194] A. Skapenko, J. Leipe, P. E. Lipsky, and H. Schulze-Koops, "The role of the T cell in autoimmune inflammation," *Arthritis Res. Ther.*, vol. 7(Suppl 2), pp. S4–S14, 2005.

[195] R. Antia, V. V. Ganusov, and R. Ahmed, "The role of models in understanding $CD8^+$ T-cell memory," *Nature Rev. Immunol.*, vol. 5, no. 2, pp. 101–111, 2005.

[196] L. J. S. Allen, *An introduction to stochastic processes with applications to biology*. CRC Press, Boca Raton, FL, 2nd ed., 2011.

[197] F. Brauer, P. van den Driessche, and J. Wu, *Mathematical Epidemiology*. Springer, 2008.

[198] E. Renshaw, *Modelling biological populations in space and time*, vol. 11. Cambridge University Press, 1993.

[199] N. G. van Kampen, *Stochastic processes in physics and chemistry*. Elsevier, 1992.

[200] P. S. Mandal, L. J. S. Allen, and M. Banerjee, "Stochastic modeling of phytoplankton allelopathy," *Appl. Math. Model.*, vol. 38, no. 5, pp. 1583–1596, 2014.

[201] D. T. Gillespie, "The chemical langevin equation," *J. Chem. Phys.*, vol. 113, no. 1, pp. 297–306, 2000.

[202] D. T. Gillespie, "The chemical langevin and fokker-planck equations for the reversible isomerization reaction," *J. Phys. Chem. A*, vol. 106, no. 20, pp. 5063–5071, 2002.

[203] B. Øksendal, *Stochastic Differential Equations: An Introduction with Applications*. Springer, 2010.

[204] C. A. Braumann, "Itô versus Stratonovich calculus in random population growth," *Math. Biosci.*, vol. 206, pp. 81–107, 2007.

[205] E. J. Allen, *Modeling with Itô stochastic differential equations*. Springer, 2007.

[206] E. J. Allen, L. J. S. Allen, A. Arciniega, and P. E. Greenwood, "Construction of equivalent stochastic differential equation models," *Stoch. Anal. Appl.*, vol. 26, no. 2, pp. 274–297, 2008.

[207] C. W. Gardiner, *Handbook of stochastic methods*. Springer, 1994.

[208] A. J. Black, A. J. McKane, A. Nunes, and A. Parisi, "Stochastic fluctuations in the susceptible-infective-recovered model with distributed infectious periods," *Phys. Rev. E*, vol. 80, no. 2, p. 021922, 2009.

[209] E. W. J. Wallace, D. T. Gillespie, K. R. Sanft, and L. R. Petzold, "Linear noise approximation is valid over limited times for any chemical system that is sufficiently large," *IET Syst. Biol.*, vol. 6, no. 4, pp. 102–115, 2012.

[210] F. Hayot and C. Jayaprakash, "The linear noise approximation for molecular fluctuations within cells," *Phys. Biol.*, vol. 1, pp. 205–210, 2004.

[211] J. Pahle, J. D. Challenger, P. Mendes, and A. J. McKane, "Biochemical fluctuations, optimisation and the linear noise approximation," *BMC Syst. Biol.*, vol. 6, no. 1, p. 1, 2012.

[212] J. M. Conway and D. Coombs, "A stochastic model of latently infected cell reactivation and viral blip generation in treated HIV patients," *PLoS Comput. Biol.*, vol. 7, no. 4, p. e1002033, 2011.

[213] M. Bruna, S. J. Chapman, and M. J. Smith, "Model reduction for slow-fast stochastic systems with metastable behaviour," *J. Chem. Phys.*, vol. 140, p. 174107, 2014.

[214] T. M. Earnest, E. Roberts, M. Assaf, D. K., and Z. Luthey-Schulten, "DNA looping increases the range of bistability in a stochastic model of the *lac* genetic switch," *Phys. Biol.*, vol. 10, p. 026002, 2013.

[215] P. G. Hufton, Y. T. Lin, T. Galla, and A. J. McKane, "Intrinsic noise in systems with switching environments," *Phys. Rev. E*, vol. 93, p. 052119, 2016.

[216] A. J. Black and A. J. McKane, "Stochastic formulation of ecological models and their applications," *Trends Ecol. Evol.*, vol. 27, no. 6, pp. 337–345, 2012.

[217] G. Neofytou, Y. N. Kyrychko, and K. B. Blyuss, "Time-delayed model of RNA interference," *Ecol. Complex.*, vol. 30, pp. 11–25, 2017.

[218] R. H. Bartels and G. W. Stewart, "Solution of the matrix equation AX+XB=C," *Comm. ACM*, vol. 15, pp. 820–826, 1972.

[219] S. J. Hammarling, "Numerical solution of the stable, non-negative definite lyapunov equation," *IMA J. Num. Anal.*, vol. 2, pp. 303–323, 1982.

[220] Y. Yuan and L. J. S. Allen, "Stochastic models for virus and immune system dynamics," *Math. Biosci.*, vol. 234, no. 2, pp. 84–94, 2011.

[221] A. J. Black and A. J. McKane, "Stochastic amplification in an epidemic model with seasonal forcing," *J. Theor. Biol.*, vol. 267, no. 1, pp. 85–94, 2010.

[222] A. J. McKane and T. J. Newman, "Predator-prey cycles from resonant amplification of demographic stochasticity," *Phys. Rev. Lett.*, vol. 94, no. 21, p. 218102, 2005.

[223] J. Boldison, T. K. Khera, D. A. Copland, M. L. Stimpson, G. L. Crawford, A. D. Dick, *et al.*, "A novel pathogenic RBP-3 peptide reveals epitope spreading in persistent experimental autoimmune uveoretinitis," *Immunol.*, vol. 146, pp. 301–311, 2015.

[224] P. Baccam, C. Beauchemin, C. A. Macken, F. G. Hayden, and A. S. Perelson, "Kinetics of influenza a virus infection in humans," *J. Virol.*, vol. 80, no. 15, pp. 7590–7599, 2006.

[225] J. Li, L. Zhang, and Z. Wang, "Two effective stability criteria for linear time-delay systems with complex coefficients," *J. Syst. Sci. Complex.*, vol. 24, no. 5, p. 835, 2011.

[226] B. Rahman, K. B. Blyuss, and Y. N. Kyrychko, "Dynamics of neural systems with discrete and distributed time delays," *SIAM J. Appl. Dyn. Syst.*, vol. 14, no. 4, pp. 2069–2095, 2015.

[227] D. Breda, S. Maset, and R. Vermiglio, "Numerical computation of characteristic multipliers for linear time periodic coefficients delay differential equations," *IFAC Proc. Vol.*, vol. 39, no. 10, pp. 163–168, 2006.

[228] R. Cavoretto, A. D. Rossi, E. Perracchione, and E. Venturino, "Reliable approximation of separatrix manifolds in competition models with safety niches," *Int. J. Comput. Math.*, vol. 92, no. 9, pp. 1826–1837, 2015.

[229] R. Cavoretto, A. De Rossi, E. Perracchione, and E. Venturino, "Robust approximation algorithms for the detection of attraction basins in dynamical systems," *J. Sci. Comput.*, vol. 68, no. 1, pp. 395–415, 2016.

[230] A. De Rossi, E. Perracchione, and E. Venturino, "Fast strategy for PU interpolation: An application for the reconstruction of separatrix manifolds," *Dolomites Res. Notes Approx.*, vol. 9, pp. 3–12, 2016.

[231] E. Francomano, F. M. Hilker, M. Paliaga, and E. Venturino, "On basins of attraction for a predator-prey model via meshless approximation," in *AIP Conference Proceedings*, vol. 1776, p. 070007, AIP Publishing, 2016.

[232] R. Cavoretto, A. De Rossi, E. Perracchione, and E. Venturino, "Graphical representation of separatrices of attraction basins in two and three-dimensional dynamical systems," *Int. J. Comput. Methods*, vol. 14, no. 01, p. 1750008, 2017.

[233] E. Francomano, F. M. Hilker, M. Paliaga, and E. Venturino, "Separatrix reconstruction to identify tipping points in an eco-epidemiological model," *Appl. Math. Comput.*, vol. 318, pp. 80–91, 2018.

[234] F. Fatehi, Y. N. Kyrychko, R. Molchanov, and K. B. Blyuss, "Bifurcations and multi-stability in a model of cytokine-mediated autoimmunity," *Int. J. Bif. Chaos*, vol. 29, no. 3, p. 1950034, 2019.

[235] K. S. Schluns, W. C. Kieper, S. C. Jameson, and L. Lefrancois, "Interleukin-7 mediates the homeostasis of naïve and memory CD8 T cells *in vivo*," *Nature Immunol.*, vol. 1, pp. 426–432, 2000.

[236] F. Fatehi Chenar, Y. N. Kyrychko, and K. B. Blyuss, "Mathematical model of immune response to hepatitis B," *J. Theor. Biol.*, vol. 447, pp. 98–110, 2018.

[237] F. Fatehi, Y. N. Kyrychko, and K. B. Blyuss, "Time-delayed model of autoimmune dynamics." submitted.

[238] H. Risken, *The Fokker-Planck equation, methods of solution and applications*. Springer-Verlag, 1989.

Appendix A

Coefficients of the Hopf frequency function

$$b_2 = \Big(-{\delta_1}^4{\delta_2}^4{\rho_1}^2Y^2 + 2\,{d_r}^2{\delta_1}^4{\delta_2}^4\Big){T^*_{reg}}^8 + \Big(-2\,{\delta_1}^3{\delta_2}^3\rho_1\Big(d_a\delta_2\rho_1 + d_i\delta_1\rho_1 - 2\,d_r\delta_2\rho_3\Big)I^{*2} + 8\,{d_r}^2{\delta_1}^3{\delta_2}^3\Big(d_a\delta_2 + d_i\delta_1\Big)\Big){T^*_{reg}}^7 + \Big(-2\,{\delta_1}^2{\delta_2}^3{\rho_1}^2\rho_3\Big(4\,\delta_1\rho_1 + \delta_2\rho_1 + 5\,\delta_2\rho_3\Big)I^{*4} - {\delta_1}^2{\delta_2}^2\Big({d_a}^2{\delta_2}^2{\rho_1}^2 + 2\,d_ad_i\delta_1\delta_2{\rho_1}^2 - 8\,d_ad_r\delta_2{}^2\rho_1\rho_3 + {d_i}^2{\delta_1}^2{\rho_1}^2 - 12\,d_id_r\delta_1\delta_2\rho_1\rho_3 + 2\,{d_r}^2{\delta_1}^2{\rho_1}^2 + 2\,{d_r}^2\delta_1\delta_2{\rho_1}^2 + 6\,{d_r}^2\delta_1\delta_2\rho_1\rho_3 + {d_r}^2{\delta_2}^2{\rho_1}^2 + 8\,{d_r}^2{\delta_2}^2{\rho_3}^2\Big)I^{*2} + 2\,{d_r}^2{\delta_1}^2{\delta_2}^2\Big(6\,{d_a}^2{\delta_2}^2 + 16\,d_ad_i\delta_1\delta_2 + 6\,{d_i}^2{\delta_1}^2 + {d_r}^2{\delta_1}^2 + {d_r}^2{\delta_2}^2\Big)\Big){T^*_{reg}}^6 + \Big(-2\,\rho_3{\delta_2}^2\rho_1\delta_1\Big(6\,d_a\delta_1\delta_2{\rho_1}^2 + 6\,d_a\delta_2{}^2\rho_1\rho_3 + 9\,d_i{\delta_1}^2{\rho_1}^2 + 5\,d_i\delta_1\delta_2{\rho_1}^2 + 22\,d_i\delta_1\delta_2\rho_1\rho_3 + 6\,d_r{\delta_1}^2{\rho_1}^2 + 2\,d_r\delta_1\delta_2{\rho_1}^2 - 4\,d_r{\delta_2}^2{\rho_3}^2\Big)I^{*4} + 2\,\delta_1\delta_2\Big({d_a}^2d_i\delta_1{\delta_2}^2{\rho_1}^2 + 2\,{d_a}^2d_r{\delta_2}^3\rho_1\rho_3 + d_a{d_i}^2{\delta_1}^2\delta_2{\rho_1}^2 + 10\,d_ad_id_r\delta_1{\delta_2}^2\rho_1\rho_3 - 3\,d_a{d_r}^2{\delta_1}^2\delta_2{\rho_1}^2 - 2\,d_a{d_r}^2\delta_1{\delta_2}^2{\rho_1}^2 - 8\,d_a{d_r}^2\delta_1{\delta_2}^2\rho_1\rho_3 - 8\,d_a{d_r}^2\delta_1{\delta_2}^3{\rho_3}^2 + 6\,{d_i}^2d_r{\delta_1}^2\delta_2\rho_1\rho_3 - d_i{d_r}^2{\delta_1}^3{\rho_1}^2 - 3\,d_i{d_r}^2{\delta_1}^2\delta_2{\rho_1}^2 - 8\,d_i{d_r}^2{\delta_1}^2\delta_2\rho_1\rho_3 - d_i{d_r}^2\delta_1{\delta_2}^2{\rho_1}^2 - 2\,d_i{d_r}^2\delta_1{\delta_2}^2\rho_1\rho_3 - 16\,d_i{d_r}^2\delta_1{\delta_2}^2{\rho_3}^2 + {d_r}^3{\delta_1}^2\delta_2\rho_1\rho_3 + 2\,{d_r}^3\delta_1{\delta_2}^2\rho_1\rho_3 + 2\,{d_r}^3{\delta_2}^3\rho_1\rho_3\Big)I^{*2} + 4\,{d_r}^2\delta_1\delta_2\Big(2\,{d_a}^3{\delta_2}^3 + 12\,{d_a}^2d_i\delta_1{\delta_2}^2 + 12\,d_a{d_i}^2{\delta_1}^2\delta_2 + 2\,d_a{d_r}^2{\delta_1}^2\delta_2 + d_a{d_r}^2{\delta_2}^3 + 2\,{d_i}^3{\delta_1}^3 + d_i{d_r}^2{\delta_1}^3 + 2\,d_i{d_r}^2\delta_1{\delta_2}^2\Big)\Big){T^*_{reg}}^5 + \Big(-2\,{\delta_2}^2{\rho_1}^2{\rho_3}^2\Big({\delta_1}^2{\rho_1}^2 + \delta_1\delta_2{\rho_1}^2 + 3\,\delta_1\delta_2\rho_1\rho_3 + 2\,{\delta_2}^2{\rho_3}^2\Big)I^{*6} - 2\,\rho_3\delta_2\rho_1\Big(2\,{d_a}^2{\delta_1}\delta_2{}^2{\rho_1}^2 + {d_a}^2{\delta_2}^3\rho_1\rho_3 + 9\,d_ad_i{\delta_1}^2\delta_2{\rho_1}^2 + 24\,d_ad_i\delta_1{\delta_2}^2\rho_1\rho_3 + 12\,d_ad_r{\delta_1}^2\delta_2{\rho_1}^2 - 4\,d_ad_r{\delta_2}^3{\rho_3}^2 + 4\,{d_i}^2{\delta_1}^3{\rho_1}^2 + 8\,{d_i}^2{\delta_1}^2\delta_2{\rho_1}^2 + 33\,{d_i}^2{\delta_1}^2\delta_2\rho_1\rho_3 + 9\,d_id_r{\delta_1}^3{\rho_1}^2 + 9\,d_id_r{\delta_1}^2\delta_2{\rho_1}^2 + 2\,d_id_r\delta_1{\delta_2}^2{\rho_1}^2 - 20\,d_id_r\delta_1{\delta_2}^2{\rho_3}^2 - 4\,{d_r}^2{\delta_1}^2\delta_2\rho_1\rho_3 - 6\,{d_r}^2\delta_1{\delta_2}^2\rho_1\rho_3 - 4\,{d_r}^2{\delta_1}^2{\delta_2}^2{\rho_3}^2 + {d_r}^2{\delta_2}^3\rho_1\rho_3 - 4\,{d_r}^2{\delta_2}^3{\rho_3}^2\Big)I^{*4} + \Big(2\,{d_a}^3d_i\delta_1{\delta_2}^3{\rho_1}^2 + 6\,{d_a}^2{d_i}^2{\delta_1}^2{\delta_2}^2{\rho_1}^2 + 4\,{d_a}^2d_id_r\delta_1{\delta_2}^3\rho_1\rho_3 - 7\,{d_a}^2{d_r}^2{\delta_1}^2{\delta_2}^2{\rho_1}^2 - 2\,{d_a}^2{d_r}^2\delta_1{\delta_2}^3{\rho_1}^2 - 14\,{d_a}^2{d_r}^2\delta_1{\delta_2}^3\rho_1\rho_3 - 8\,{d_a}^2{d_r}^2{\delta_2}^4{\rho_3}^2 + 2\,d_a{d_i}^3{\delta_1}^3\delta_2{\rho_1}^2 + 12\,d_a{d_i}^2d_r{\delta_1}^2{\delta_2}^2\rho_1\rho_3 - 6\,d_ad_i{d_r}^2{\delta_1}^3\delta_2{\rho_1}^2 - 12\,d_ad_i{d_r}^2{\delta_1}^2{\delta_2}^2{\rho_1}^2 - 42\,d_ad_i{d_r}^2{\delta_1}^2{\delta_2}^2\rho_1\rho_3 + 2\,d_ad_i{d_r}^2\delta_1{\delta_2}^3{\rho_1}^2 - 8\,d_ad_i{d_r}^2\delta_1{\delta_2}^3\rho_1\rho_3 - 64\,d_ad_i{d_r}^2\delta_1{\delta_2}^3{\rho_3}^2 + 2\,d_a{d_r}^3{\delta_1}^2{\delta_2}^2\rho_1\rho_3 + 8\,d_a{d_r}^3\delta_1{\delta_2}^3\rho_1\rho_3 + 4\,{d_i}^3d_r{\delta_1}^3\delta_2\rho_1\rho_3 - {d_i}^2{d_r}^2{\delta_1}^4{\rho_1}^2 - 6\,{d_i}^2{d_r}^2{\delta_1}^3\delta_2{\rho_1}^2 - 14\,{d_i}^2{d_r}^2{\delta_1}^3\delta_2\rho_1\rho_3 - 2\,{d_i}^2{d_r}^2{\delta_1}^2{\delta_2}^2{\rho_1}^2 - 12\,{d_i}^2{d_r}^2{\delta_1}^2{\delta_2}^2\rho_1\rho_3 - 48\,{d_i}^2{d_r}^2{\delta_1}^2{\delta_2}^2{\rho_3}^2 +$$

$$10\,d_i{d_r}^3{\delta_1}^2{\delta_2}^2\rho_1\rho_3+12\,d_i{d_r}^3\delta_1{\delta_2}^3\rho_1\rho_3-5\,{d_r}^4{\delta_1}^2{\delta_2}^2{\rho_3}^2-4\,{d_r}^4{\delta_2}^4{\rho_3}^2\Big)I^{*2}+2\,{d_r}^2\Big({d_a}^4{\delta_2}^4+16\,{d_a}^3d_i\delta_1{\delta_2}^3+36\,{d_a}^2{d_i}^2{\delta_1}^2{\delta_2}^2+6\,{d_a}^2{d_r}^2{\delta_1}^2{\delta_2}^2+{d_a}^2{d_r}^2{\delta_2}^4+16\,d_a{d_i}^3{\delta_1}^3\delta_2+8\,d_ad_i{d_r}^2{\delta_1}^3\delta_2+8\,d_ad_i{d_r}^2\delta_1{\delta_2}^3+{d_i}^4{\delta_1}^4+{d_i}^2{d_r}^2{\delta_1}^4+6\,{d_i}^2{d_r}^2{\delta_1}^2{\delta_2}^2\Big)\Big){T^*_{reg}}^4+\Big(-2\,{\delta_2}{\rho_1}^2{\rho_3}^2\Big(d_a\delta_1\delta_2{\rho_1}^2+2\,{d_a}{\delta_2}^2\rho_1\rho_3+2\,d_i{\delta_1}^2{\rho_1}^2+5\,d_i\delta_1\delta_2{\rho_1}^2+14\,d_i\delta_1\delta_2\rho_1\rho_3+2\,d_i{\delta_2}^2\rho_1\rho_3+12\,d_i{\delta_2}^2{\rho_3}^2-d_r\delta_1\delta_2\rho_1\rho_3-2\,d_r{\delta_2}^2\rho_1\rho_3\Big)I^{*6}+2\,\rho_3\rho_1\Big(2\,{d_a}^2d_i\delta_1{\delta_2}^2{\rho_1}^2-2\,{d_a}^2d_i{\delta_2}^3\rho_1\rho_3-7\,{d_a}^2d_r\delta_1{\delta_2}^2{\rho_1}^2+4\,d_a{d_i}^2{\delta_1}^2\delta_2{\rho_1}^2+2\,d_a{d_i}^2\delta_1{\delta_2}^2{\rho_1}^2-30\,d_a{d_i}^2\delta_1{\delta_2}^2\rho_1\rho_3-15\,d_ad_i{d_r}\delta_1^2\delta_2{\rho_1}^2-4\,d_ad_id_r\delta_1{\delta_2}^2{\rho_1}^2+20\,d_ad_id_r{\delta_2}^3{\rho_3}^2+8\,d_a{d_r}^2\delta_1{\delta_2}^2\rho_1\rho_3+4\,d_a{d_r}^2{\delta_2}^3{\rho_3}^2-4\,{d_i}^3{\delta_1}^2\delta_2{\rho_1}^2-20\,{d_i}^3{\delta_1}^2\delta_2\rho_1\rho_3-2\,{d_i}^2d_r{\delta_1}^3{\rho_1}^2-12\,{d_i}^2d_r{\delta_1}^2\delta_2{\rho_1}^2-7\,{d_i}^2d_r\delta_1{\delta_2}^2{\rho_1}^2+36\,{d_i}^2d_r\delta_1{\delta_2}^2{\rho_3}^2+6\,d_i{d_r}^2{\delta_1}^2\delta_2\rho_1\rho_3+20\,d_i{d_r}^2\delta_1{\delta_2}^2\rho_1\rho_3+12\,d_i{d_r}^2\delta_1{\delta_2}^2{\rho_3}^2-2\,d_i{d_r}^2{\delta_2}^3\rho_1\rho_3+20\,d_i{d_r}^2{\delta_2}^3{\rho_3}^2+3\,{d_r}^3\delta_1{\delta_2}^2{\rho_3}^2-4\,{d_r}^3{\delta_2}^3{\rho_3}^2\Big)I^{*4}+\Big(2\,{d_a}^3{d_i}^2\delta_1{\delta_2}^2{\rho_1}^2-4\,{d_a}^3d_id_r{\delta_2}^3\rho_1\rho_3-4\,{d_a}^3{d_r}^2\delta_1{\delta_2}^2{\rho_1}^2-4\,{d_a}^3{d_r}^2{\delta_2}^3\rho_1\rho_3+2\,{d_a}^2{d_i}^3{\delta_1}^2\delta_2{\rho_1}^2-12\,{d_a}^2{d_i}^2d_r\delta_1{\delta_2}^2\rho_1\rho_3-8\,{d_a}^2d_i{d_r}^2{\delta_1}^2\delta_2{\rho_1}^2-6\,{d_a}^2d_i{d_r}^2\delta_1{\delta_2}^2{\rho_1}^2-36\,{d_a}^2d_i{d_r}^2\delta_1{\delta_2}^2\rho_1\rho_3-4\,{d_a}^2d_i{d_r}^2{\delta_2}^3\rho_1\rho_3-32\,{d_a}^2d_i{d_r}^2{\delta_2}^3{\rho_3}^2-2\,{d_a}^2{d_r}^3\delta_1{\delta_2}^2\rho_1\rho_3+4\,{d_a}^2{d_r}^3\delta_2{}^3\rho_1\rho_3-4\,d_a{d_i}^3d_r{\delta_1}^2\delta_2\rho_1\rho_3-4\,d_a{d_i}^2{d_r}^2{\delta_1}^3{\rho_1}^2-12\,d_a{d_i}^2{d_r}^2{\delta_1}^2\delta_2{\rho_1}^2-36\,d_a{d_i}^2{d_r}^2{\delta_1}^2\delta_2\rho_1\rho_3+2\,d_a{d_i}^2{d_r}^2\delta_1{\delta_2}^2{\rho_1}^2-24\,d_a{d_i}^2{d_r}^2\delta_1{\delta_2}^2\rho_1\rho_3-96\,d_a{d_i}^2{d_r}^2\delta_1{\delta_2}^2{\rho_3}^2-8\,d_ad_i{d_r}^3{\delta_1}^2\delta_2\rho_1\rho_3+20\,d_ad_i{d_r}^3\delta_1{\delta_2}^2\rho_1\rho_3-4\,d_ad_i{d_r}^3{\delta_2}^3\rho_1\rho_3-10\,d_a{d_r}^4\delta_1{\delta_2}^2{\rho_3}^2-2\,{d_i}^3{d_r}^2{\delta_1}^3{\rho_1}^2-4\,{d_i}^3{d_r}^2{\delta_1}^3\rho_1\rho_3-2\,{d_i}^3{d_r}^2{\delta_1}^2\delta_2{\rho_1}^2-12\,{d_i}^3{d_r}^2{\delta_1}^2\delta_2\rho_1\rho_3-32\,{d_i}^3{d_r}^2{\delta_1}^2\delta_2{\rho_3}^2-2\,{d_i}^2{d_r}^3{\delta_1}^3\rho_1\rho_3+8\,{d_i}^2{d_r}^3{\delta_1}^2\delta_2\rho_1\rho_3+12\,{d_i}^2{d_r}^3\delta_1{\delta_2}^2\rho_1\rho_3-10\,d_i{d_r}^4{\delta_1}^2\delta_2{\rho_3}^2-16\,d_i{d_r}^4{\delta_2}^3{\rho_3}^2\Big)I^{*2}+8\,{d_r}^2\Big({d_a}^4d_i{\delta_2}^3+6\,{d_a}^3{d_i}^2\delta_1{\delta_2}^2+{d_a}^3{d_r}^2\delta_1{\delta_2}^2+6\,{d_i}^3{\delta_1}^2\delta_2{d_a}^2+3\,{d_a}^2d_i{d_r}^2{\delta_1}^2\delta_2+{d_a}^2d_i{d_r}^2{\delta_2}^3+d_a{d_i}^4{\delta_1}^3+d_a{d_i}^2{\delta_1}^3{d_r}^2+3\,d_a{d_i}^2\delta_1{d_r}^2{\delta_2}^2+{d_i}^3{\delta_1}^2\delta_2{d_r}^2\Big)\Big){T^*_{reg}}^3+\Big(2\,{\delta_2}^2{\rho_1}^4{\rho_3}^4I^{*8}-{\rho_1}^2{\rho_3}^2\Big({d_a}^2{\delta_2}^2{\rho_1}^2+6\,d_ad_i\delta_1\delta_2{\rho_1}^2+18\,d_ad_i{\delta_2}^2\rho_1\rho_3+2\,d_a{d_r}{\delta_2}^2\rho_1\rho_3+4\,{d_i}^2{\delta_1}^2{\rho_1}^2+16\,{d_i}^2\delta_1\delta_2{\rho_1}^2+40\,{d_i}^2\delta_1\delta_2\rho_1\rho_3+{d_i}^2{\delta_2}^2{\rho_1}^2+20\,{d_i}^2{\delta_2}^2\rho_1\rho_3+52\,{d_i}^2{\delta_2}^2{\rho_3}^2+4\,d_id_r\delta_1\delta_2\rho_1\rho_3-18\,d_id_r{\delta_2}^2\rho_1\rho_3+5\,{d_r}^2{\delta_2}^2{\rho_3}^2\Big)I^{*6}+2\,\rho_1\rho_3\Big(2\,{d_a}^3d_i{\delta_2}^2{\rho_1}^2-{d_a}^3d_r{\delta_2}^2{\rho_1}^2+12\,{d_a}^2{d_i}^2\delta_1\delta_2{\rho_1}^2+{d_a}^2{d_i}^2{\delta_2}^2{\rho_1}^2+3\,{d_a}^2{d_i}^2{\delta_2}^2\rho_1\rho_3-5\,{d_a}^2d_id_r\delta_1\delta_2{\rho_1}^2-2\,{d_a}^2d_id_r{\delta_2}^2{\rho_1}^2+4\,{d_a}^2{d_r}^2{\delta_2}^2\rho_1\rho_3+4\,d_a{d_i}^3{\delta_1}^2{\rho_1}^2+6\,d_a{d_i}^3\delta_1\delta_2{\rho_1}^2-12\,d_a{d_i}^3\delta_1\delta_2\rho_1\rho_3-8\,d_a{d_i}^2d_r\delta_1\delta_2{\rho_1}^2+d_a{d_i}^2d_r{\delta_2}^2{\rho_1}^2+36\,d_a{d_i}^2d_r{\delta_2}^2{\rho_3}^2+14\,d_ad_i{d_r}^2\delta_1\delta_2\rho_1\rho_3+12\,d_ad_i{d_r}^2{\delta_2}^2{\rho_3}^2+3\,d_a{d_r}^3{\delta_2}^2{\rho_3}^2-4\,{d_i}^4{\delta_1}^2\rho_1\rho_3-4\,{d_i}^3d_r{\delta_1}^2{\rho_1}^2-7\,{d_i}^3d_r\delta_1\delta_2{\rho_1}^2+28\,{d_i}^3d_r\delta_1\delta_2{\rho_3}^2+3\,{d_i}^2{d_r}^2{\delta_1}^2\rho_1\rho_3+22\,{d_i}^2{d_r}^2\delta_1\delta_2\rho_1\rho_3+12\,{d_i}^2{d_r}^2\delta_1\delta_2{\rho_3}^2+3\,{d_i}^2{d_r}^2{\delta_2}^2\rho_1\rho_3+36\,{d_i}^2{d_r}^2{\delta_2}^2{\rho_3}^2+9\,d_i{d_r}^3\delta_1\delta_2{\rho_3}^2-12\,d_i{d_r}^3{\delta_2}^2{\rho_3}^2\Big)I^{*4}+\Big(-{d_a}^4{d_i}^2{\delta_2}^2{\rho_1}^2-{d_a}^4{d_r}^2{\delta_2}^2{\rho_1}^2-2\,{d_a}^3{d_i}^3\delta_1\delta_2{\rho_1}^2-12\,{d_a}^3{d_i}^2d_r{\delta_2}^2\rho_1\rho_3-6\,{d_a}^3d_i{d_r}^2\delta_1\delta_2{\rho_1}^2-10\,{d_a}^3d_i{d_r}^2{\delta_2}^2\rho_1\rho_3-2\,{d_a}^3{d_r}^3{\delta_2}^2\rho_1\rho_3-{d_a}^2{d_i}^4{\delta_1}^2{\rho_1}^2-20\,{d_a}^2{d_i}^3d_r\delta_1\delta_2\rho_1\rho_3-7\,{d_a}^2{d_i}^2{d_r}^2{\delta_1}^2{\rho_1}^2-6\,{d_a}^2{d_i}^2{d_r}^2\delta_1\delta_2{\rho_1}^2-30\,{d_a}^2{d_i}^2{d_r}^2\delta_1\delta_2\rho_1\rho_3-2\,{d_a}^2{d_i}^2{d_r}^2{\delta_2}^2{\rho_1}^2-12\,{d_a}^2{d_i}^2{d_r}^2{\delta_2}^2\rho_1\rho_3-48\,{d_a}^2{d_i}^2{d_r}^2{\delta_2}^2{\rho_3}^2-16\,{d_a}^2d_i{d_r}^3\delta_1\delta_2\rho_1\rho_3+10\,{d_a}^2d_i{d_r}^3{\delta_2}^2\rho_1\rho_3-5\,{d_a}^2{d_r}^4{\delta_2}^2{\rho_3}^2-4\,d_a{d_i}^4d_r{\delta_1}^2\rho_1\rho_3-4\,d_a{d_i}^3{d_r}^2{\delta_1}^2{\rho_1}^2-10\,d_a{d_i}^3{d_r}^2{\delta_1}^2\rho_1\rho_3-2\,d_a{d_i}^3{d_r}^2\delta_1\delta_2{\rho_1}^2-24\,d_a{d_i}^3{d_r}^2\delta_1\delta_2\rho_1\rho_3-64\,d_a{d_i}^3{d_r}^2\delta_1\delta_2{\rho_3}^2-10\,d_a{d_i}^2{d_r}^3{\delta_1}^2\rho_1\rho_3+$$

$$16\,d_a{d_i}^2{d_r}^3\delta_1\delta_2\rho_1\rho_3 - 12\,d_a{d_i}^2{d_r}^3{\delta_2}^2\rho_1\rho_3 - 20\,d_a d_i{d_r}^4\delta_1\delta_2{\rho_3}^2 - {d_i}^4{d_r}^2{\delta_1}^2{\rho_1}^2 -$$
$$4\,{d_i}^4{d_r}^2{\delta_1}^2\rho_1\rho_3 - 8\,{d_i}^4{d_r}^2{\delta_1}^2{\rho_3}^2 + 2\,{d_i}^3{d_r}^3{\delta_1}^2\rho_1\rho_3 + 4\,{d_i}^3{d_r}^3\delta_1\delta_2\rho_1\rho_3 - 5\,{d_i}^2{d_r}^4{\delta_1}^2{\rho_3}^2 -$$
$$24\,{d_i}^2{d_r}^4{\delta_2}^2{\rho_3}^2\Big)I^{*2} + 2\,{d_r}^2\Big(6\,{d_a}^4{d_i}^2{\delta_2}^2 + {d_a}^4{d_r}^2{\delta_2}^2 + 16\,{d_a}^3{d_i}^3\delta_1\delta_2 + 8\,{d_a}^3 d_i{d_r}^2\delta_1\delta_2 +$$
$$6\,{d_a}^2{d_i}^4{\delta_1}^2 + 6\,{d_a}^2{d_i}^2{d_r}^2{\delta_1}^2 + 6\,{d_a}^2{d_i}^2{d_r}^2{\delta_2}^2 + 8\,d_a{d_i}^3{d_r}^2\delta_1\delta_2 + {d_i}^4{d_r}^2{\delta_1}^2\Big)\Big){T^*_{reg}}^2 +$$
$$\Big(8\,d_i\delta_2{\rho_1}^4{\rho_3}^4I^{*8} - 4\,d_i{\rho_1}^2{\rho_3}^2\Big({d_a}^2\delta_2{\rho_1}^2 + 2\,d_a d_i\delta_1{\rho_1}^2 + 6\,d_a d_i\delta_2\rho_1\rho_3 + 3\,d_a d_r\delta_2\rho_1\rho_3 +$$
$$2\,{d_i}^2\delta_1{\rho_1}^2 + 4\,{d_i}^2\delta_1\rho_1\rho_3 + {d_i}^2\delta_2{\rho_1}^2 + 8\,{d_i}^2\delta_2\rho_1\rho_3 + 12\,{d_i}^2\delta_2{\rho_3}^2 + 2\,d_i d_r\delta_1\rho_1\rho_3 - 6\,d_i d_r\delta_2\rho_1\rho_3 +$$
$$3\,{d_r}^2\delta_2{\rho_3}^2\Big)I^{*6} + 2\,d_i\rho_1\rho_3\Big(4\,{d_a}^3 d_i\delta_2{\rho_1}^2 + {d_a}^3 d_r\delta_2{\rho_1}^2 + 5\,{d_a}^2{d_i}^2\delta_1{\rho_1}^2 + 3\,{d_a}^2{d_i}^2\delta_2{\rho_1}^2 +$$
$$8\,{d_a}^2{d_i}^2\delta_2\rho_1\rho_3 + 5\,{d_a}^2 d_i d_r\delta_1{\rho_1}^2 - 4\,{d_a}^2 d_i d_r\delta_2{\rho_1}^2 + 8\,{d_a}^2{d_r}^2\delta_2\rho_1\rho_3 + 4\,d_a{d_i}^3\delta_1{\rho_1}^2 -$$
$$2\,d_a{d_i}^2 d_r\delta_1{\rho_1}^2 + 3\,d_a{d_i}^2 d_r\delta_2{\rho_1}^2 + 28\,d_a{d_i}^2 d_r\delta_2{\rho_3}^2 + 8\,d_a d_i{d_r}^2\delta_1\rho_1\rho_3 + 12\,d_a d_i{d_r}^2\delta_2{\rho_3}^2 +$$
$$9\,d_a{d_r}^3\delta_2{\rho_3}^2 - 2\,{d_i}^3 d_r\delta_1{\rho_1}^2 + 8\,{d_i}^3 d_r\delta_1{\rho_3}^2 + 8\,{d_i}^2{d_r}^2\delta_1\rho_1\rho_3 + 4\,{d_i}^2{d_r}^2\delta_1{\rho_3}^2 +$$
$$8\,{d_i}^2{d_r}^2\delta_2\rho_1\rho_3 + 28\,{d_i}^2{d_r}^2\delta_2{\rho_3}^2 + 6\,d_i{d_r}^3\delta_1{\rho_3}^2 - 12\,d_i{d_r}^3\delta_2{\rho_3}^2\Big)I^{*4} - 2\,d_i\Big({d_a}^4{d_i}^2\delta_2{\rho_1}^2 +$$
$${d_a}^4{d_r}^2\delta_2{\rho_1}^2 + {d_a}^3{d_i}^3\delta_1{\rho_1}^2 + 6\,{d_a}^3{d_i}^2 d_r\delta_2\rho_1\rho_3 + 3\,{d_a}^3 d_i{d_r}^2\delta_1{\rho_1}^2 + 4\,{d_a}^3 d_i{d_r}^2\delta_2\rho_1\rho_3 +$$
$$4\,{d_a}^3{d_r}^3\delta_2\rho_1\rho_3 + 4\,{d_a}^2{d_i}^3 d_r\delta_1\rho_1\rho_3 + {d_a}^2{d_i}^2{d_r}^2\delta_1{\rho_1}^2 + 4\,{d_a}^2{d_i}^2{d_r}^2\delta_1\rho_1\rho_3 + 2\,{d_a}^2{d_i}^2{d_r}^2\delta_2{\rho_1}^2 +$$
$$6\,{d_a}^2{d_i}^2{d_r}^2\delta_2\rho_1\rho_3 + 16\,{d_a}^2{d_i}^2{d_r}^2\delta_2{\rho_3}^2 + 7\,{d_a}^2 d_i{d_r}^3\delta_1\rho_1\rho_3 - 4\,{d_a}^2 d_i{d_r}^3\delta_2\rho_1\rho_3 + 5\,{d_a}^2{d_r}^4\delta_2{\rho_3}^2 +$$
$$d_a{d_i}^3{d_r}^2\delta_1{\rho_1}^2 + 4\,d_a{d_i}^3{d_r}^2\delta_1\rho_1\rho_3 + 8\,d_a{d_i}^3{d_r}^2\delta_1{\rho_3}^2 - 2\,d_a{d_i}^2{d_r}^3\delta_1\rho_1\rho_3 + 6\,d_a{d_i}^2{d_r}^3\delta_2\rho_1\rho_3 +$$
$$5\,d_a d_i{d_r}^4\delta_1{\rho_3}^2 + 8\,{d_i}^2{d_r}^4\delta_2{\rho_3}^2\Big)I^{*2} + 4\,d_a d_i{d_r}^2\Big(2\,{d_a}^3{d_i}^2\delta_2 + {d_a}^3{d_r}^2\delta_2 + 2\,{d_a}^2{d_i}^3\delta_1 +$$
$$2\,{d_a}^2 d_i{d_r}^2\delta_1 + 2\,d_a{d_i}^2{d_r}^2\delta_2 + {d_i}^3{d_r}^2\delta_1\Big)\Big){T^*_{reg}} + 8\,{d_i}^2{\rho_1}^4{\rho_3}^4I^{*8} - {d_i}^2{\rho_1}^2{\rho_3}^2\Big(5\,{d_a}^2{\rho_1}^2 +$$
$$8\,d_a d_i\rho_1\rho_3 + 12\,d_a d_r\rho_1\rho_3 + 4\,{d_i}^2{\rho_1}^2 + 16\,{d_i}^2\rho_1\rho_3 + 16\,{d_i}^2{\rho_3}^2 - 8\,d_i d_r\rho_1\rho_3 + 8\,{d_r}^2{\rho_3}^2\Big)I^{*6} +$$
$$2\,{d_i}^2\rho_1\rho_3\Big({d_a}^3 d_i{\rho_1}^2 + 3\,{d_a}^3 d_r{\rho_1}^2 + 2\,{d_a}^2{d_i}^2{\rho_1}^2 + 4\,{d_a}^2{d_i}^2\rho_1\rho_3 - {d_a}^2 d_i d_r{\rho_1}^2 + 5\,{d_a}^2{d_r}^2\rho_1\rho_3 +$$
$$2\,d_a{d_i}^2 d_r{\rho_1}^2 + 8\,d_a{d_i}^2 d_r{\rho_3}^2 + 4\,d_a d_i{d_r}^2{\rho_3}^2 + 6\,d_a{d_r}^3{\rho_3}^2 + 4\,{d_i}^2{d_r}^2\rho_1\rho_3 + 8\,{d_i}^2{d_r}^2{\rho_3}^2 -$$
$$4\,d_i{d_r}^3{\rho_3}^2\Big)I^{*4} - {d_i}^2\Big({d_a}^4{d_i}^2{\rho_1}^2 + 2\,{d_a}^4{d_r}^2{\rho_1}^2 + 4\,{d_a}^3{d_i}^2 d_r\rho_1\rho_3 + 2\,{d_a}^3 d_i{d_r}^2\rho_1\rho_3 +$$
$$6\,{d_a}^3{d_r}^3\rho_1\rho_3 + 2\,{d_a}^2{d_i}^2{d_r}^2{\rho_1}^2 + 4\,{d_a}^2{d_i}^2{d_r}^2\rho_1\rho_3 + 8\,{d_a}^2{d_i}^2{d_r}^2{\rho_3}^2 - 2\,{d_a}^2 d_i{d_r}^3\rho_1\rho_3 +$$
$$5\,{d_a}^2{d_r}^4{\rho_3}^2 + 4\,d_a{d_i}^2{d_r}^3\rho_1\rho_3 + 4\,{d_i}^2{d_r}^4{\rho_3}^2\Big)I^{*2} + 2\,{d_a}^2{d_i}^2{d_r}^2\Big({d_a}^2{d_i}^2 + {d_a}^2{d_r}^2 + {d_i}^2{d_r}^2\Big).$$

$$b_4 = {T^*_{reg}}^8{\delta_1}^4{\delta_2}^4 + 4\,{\delta_1}^3{\delta_2}^3\left(d_a\delta_2 + d_i\delta_1\right){T^*_{reg}}^7 + \Big(- {\delta_1}^2{\delta_2}^2\Big(2\,{\delta_1}^2{\rho_1}^2 + 2\,\delta_1\delta_2{\rho_1}^2 +$$
$$6\,\delta_1\delta_2\rho_1\rho_3 + {\delta_2}^2{\rho_1}^2 + 4\,{\delta_2}^2{\rho_3}^2\Big)I^{*2} + 2\,{\delta_1}^2{\delta_2}^2\Big(3\,{d_a}^2{\delta_2}^2 + 8\,d_a d_i\delta_1\delta_2 + 3\,{d_i}^2{\delta_1}^2 + 2\,{d_r}^2{\delta_1}^2 +$$
$$2\,{d_r}^2{\delta_2}^2\Big)\Big){T^*_{reg}}^6 + \Big(- 2\,\delta_1\delta_2\Big(3\,d_a{\delta_1}^2\delta_2{\rho_1}^2 + 2\,d_a\delta_1{\delta_2}^2{\rho_1}^2 + 8\,d_a\delta_1{\delta_2}^2\rho_1\rho_3 + 4\,d_a{\delta_2}^3{\rho_3}^2 +$$
$$d_i{\delta_1}^3{\rho_1}^2 + 3\,d_i{\delta_1}^2\delta_2{\rho_1}^2 + 8\,d_i{\delta_1}^2\delta_2\rho_1\rho_3 + d_i\delta_1{\delta_2}^2{\rho_1}^2 + 2\,d_i\delta_1{\delta_2}^2\rho_1\rho_3 + 8\,d_i\delta_1{\delta_2}^2{\rho_3}^2 -$$
$$d_r{\delta_1}^2\delta_2\rho_1\rho_3 - 2\,d_r\delta_1{\delta_2}^2\rho_1\rho_3 - 2\,d_r{\delta_2}^3\rho_1\rho_3\Big)I^{*2} + 4\,\delta_1\delta_2\Big({d_a}^3{\delta_2}^3 + 6\,{d_a}^2 d_i\delta_1{\delta_2}^2 + 6\,d_a{d_i}^2{\delta_1}^2\delta_2 +$$
$$4\,d_a{d_r}^2{\delta_1}^2\delta_2 + 2\,d_a{d_r}^2{\delta_2}^3 + {d_i}^3{\delta_1}^3 + 2\,d_i{d_r}^2{\delta_1}^3 + 4\,d_i{d_r}^2\delta_1{\delta_2}^2\Big)\Big){T^*_{reg}}^5 + \Big(2\,\rho_3\delta_2\rho_1\Big(4\,{\delta_1}^3{\rho_1}^2 +$$
$$4\,{\delta_1}^2\delta_2\rho_1\rho_3 - 2\,\delta_1{\delta_2}^2{\rho_1}^2 + 6\,\delta_1{\delta_2}^2\rho_1\rho_3 + 4\,\delta_1{\delta_2}^2{\rho_3}^2 - {\delta_2}^3\rho_1\rho_3 + 4\,{\delta_2}^3{\rho_3}^2\Big)Y^4 + \Big(-$$
$$7\,{d_a}^2{\delta_1}^2{\delta_2}^2{\rho_1}^2 - 2\,{d_a}^2\delta_1{\delta_2}^3{\rho_1}^2 - 14\,{d_a}^2\delta_1{\delta_2}^3\rho_1\rho_3 - 4\,{d_a}^2{\delta_2}^4{\rho_3}^2 - 6\,d_a d_i{\delta_1}^3\delta_2{\rho_1}^2 -$$
$$12\,d_a d_i{\delta_1}^2{\delta_2}^2{\rho_1}^2 - 42\,d_a d_i{\delta_1}^2{\delta_2}^2\rho_1\rho_3 + 2\,d_a d_i\delta_1{\delta_2}^3{\rho_1}^2 - 8\,d_a d_i\delta_1{\delta_2}^3\rho_1\rho_3 - 32\,d_a d_i\delta_1{\delta_2}^3{\rho_3}^2 +$$
$$2\,d_a d_r{\delta_1}^2{\delta_2}^2\rho_1\rho_3 + 8\,d_a d_r\delta_1{\delta_2}^3\rho_1\rho_3 - {d_i}^2{\delta_1}^4{\rho_1}^2 - 6\,{d_i}^2{\delta_1}^3\delta_2{\rho_1}^2 - 14\,{d_i}^2{\delta_1}^3\delta_2\rho_1\rho_3 -$$
$$2\,{d_i}^2{\delta_1}^2{\delta_2}^2{\rho_1}^2 - 12\,{d_i}^2{\delta_1}^2{\delta_2}^2\rho_1\rho_3 - 24\,{d_i}^2{\delta_1}^2{\delta_2}^2{\rho_3}^2 + 10\,d_i d_r{\delta_1}^2{\delta_2}^2\rho_1\rho_3 + 12\,d_i d_r\delta_1{\delta_2}^3\rho_1\rho_3 -$$

$$d_r{}^2\delta_1{}^4\rho_1{}^2 - 2\,d_r{}^2\delta_1{}^3\delta_2\rho_1{}^2 - 6\,d_r{}^2\delta_1{}^3\delta_2\rho_1\rho_3 - 3\,d_r{}^2\delta_1{}^2\delta_2{}^2\rho_1{}^2 - 2\,d_r{}^2\delta_1{}^2\delta_2{}^2\rho_1\rho_3 -$$
$$10\,d_r{}^2\delta_1{}^2\delta_2{}^2\rho_3{}^2 - 2\,d_r{}^2\delta_1\delta_2{}^3\rho_1{}^2 - 6\,d_r{}^2\delta_1\delta_2{}^3\rho_1\rho_3 - 8\,d_r{}^2\delta_2{}^4\rho_3{}^2\Big)I^{*2} + d_a{}^4\delta_2{}^4 + 16\,d_a{}^3d_i\delta_1\delta_2{}^3 +$$
$$36\,d_a{}^2d_i{}^2\delta_1{}^2\delta_2{}^2 + 24\,d_a{}^2d_r{}^2\delta_1{}^2\delta_2{}^2 + 4\,d_a{}^2d_r{}^2\delta_2{}^4 + 16\,d_ad_i{}^3\delta_1{}^3\delta_2 + 32\,d_ad_id_r{}^2\delta_1{}^3\delta_2 +$$
$$32\,d_ad_id_r{}^2\delta_1\delta_2{}^3 + d_i{}^4\delta_1{}^4 + 4\,d_i{}^2d_r{}^2\delta_1{}^4 + 24\,d_i{}^2d_r{}^2\delta_1{}^2\delta_2{}^2 + d_r{}^4\delta_1{}^4 + 4\,d_r{}^4\delta_1{}^2\delta_2{}^2 +$$
$$d_r{}^4\delta_2{}^4\Big)T^*_{reg}{}^4 + \Big(2\,\rho_3\rho_1\Big(10\,d_a\delta_1{}^2\delta_2\rho_1{}^2 - 2\,d_a\delta_1\delta_2{}^2\rho_1{}^2 + 8\,d_a\delta_1\delta_2{}^2\rho_1\rho_3 + 4\,d_a\delta_2{}^3\rho_3{}^2 +$$
$$3\,d_i\delta_1{}^3\rho_1{}^2 + 3\,d_i\delta_1{}^2\delta_2\rho_1{}^2 + 6\,d_i\delta_1{}^2\delta_2\rho_1\rho_3 - 2\,d_i\delta_1\delta_2{}^2\rho_1{}^2 + 20\,d_i\delta_1\delta_2{}^2\rho_1\rho_3 + 12\,d_i\delta_1\delta_2{}^2\rho_3{}^2 -$$
$$2\,d_i\delta_2{}^3\rho_1\rho_3 + 20\,d_i\delta_2{}^3\rho_3{}^2 + d_r\delta_1{}^3\rho_1{}^2 - 2\,d_r\delta_1{}^2\delta_2\rho_1{}^2 - 5\,d_r\delta_1\delta_2{}^2\rho_1{}^2 + 3\,d_r\delta_1\delta_2{}^2\rho_3{}^2 -$$
$$4\,d_r\delta_2{}^3\rho_3{}^2\Big)I^{*4} + \Big(-4\,d_a{}^3\delta_1\delta_2{}^2\rho_1{}^2 - 4\,d_a{}^3\delta_2{}^3\rho_1\rho_3 - 8\,d_a{}^2d_i\delta_1{}^2\delta_2\rho_1{}^2 - 6\,d_a{}^2d_i\delta_1\delta_2{}^2\rho_1{}^2 -$$
$$36\,d_a{}^2d_i\delta_1\delta_2{}^2\rho_1\rho_3 - 4\,d_a{}^2d_i\delta_2{}^3\rho_1\rho_3 - 16\,d_a{}^2d_i\delta_2{}^3\rho_3{}^2 - 2\,d_a{}^2d_r\delta_1\delta_2{}^2\rho_1\rho_3 + 4\,d_a{}^2d_r\delta_2{}^3\rho_1\rho_3 -$$
$$4\,d_ad_i{}^2\delta_1{}^3\rho_1{}^2 - 12\,d_ad_i{}^2\delta_1{}^2\delta_2\rho_1{}^2 - 36\,d_ad_i{}^2\delta_1{}^2\delta_2\rho_1\rho_3 + 2\,d_ad_i{}^2\delta_1\delta_2{}^2\rho_1{}^2 - 24\,d_ad_i{}^2\delta_1\delta_2{}^2\rho_1\rho_3 -$$
$$48\,d_ad_i{}^2\delta_1\delta_2{}^2\rho_3{}^2 - 8\,d_ad_id_r\delta_1{}^2\delta_2\rho_1\rho_3 + 20\,d_ad_id_r\delta_1\delta_2{}^2\rho_1\rho_3 - 4\,d_ad_id_r\delta_2{}^3\rho_1\rho_3 -$$
$$4\,d_ad_r{}^2\delta_1{}^3\rho_1{}^2 - 4\,d_ad_r{}^2\delta_1{}^2\delta_2\rho_1{}^2 - 16\,d_ad_r{}^2\delta_1{}^2\delta_2\rho_1\rho_3 - 4\,d_ad_r{}^2\delta_1\delta_2{}^2\rho_1{}^2 - 4\,d_ad_r{}^2\delta_1\delta_2{}^2\rho_1\rho_3 -$$
$$20\,d_ad_r{}^2\delta_1\delta_2{}^2\rho_3{}^2 - 4\,d_ad_r{}^2\delta_2{}^3\rho_1\rho_3 - 2\,d_i{}^3\delta_1{}^3\rho_1{}^2 - 4\,d_i{}^3\delta_1{}^3\rho_1\rho_3 - 2\,d_i{}^3\delta_1{}^2\delta_2\rho_1{}^2 -$$
$$12\,d_i{}^3\delta_1{}^2\delta_2\rho_1\rho_3 - 16\,d_i{}^3\delta_1{}^2\delta_2\rho_3{}^2 - 2\,d_i{}^2d_r\delta_1{}^3\rho_1\rho_3 + 8\,d_i{}^2d_r\delta_1{}^2\delta_2\rho_1\rho_3 + 12\,d_i{}^2d_r\delta_1\delta_2{}^2\rho_1\rho_3 -$$
$$2\,d_id_r{}^2\delta_1{}^3\rho_1{}^2 - 4\,d_id_r{}^2\delta_1{}^3\rho_1\rho_3 - 4\,d_id_r{}^2\delta_1{}^2\delta_2\rho_1{}^2 - 8\,d_id_r{}^2\delta_1{}^2\delta_2\rho_1\rho_3 - 20\,d_id_r{}^2\delta_1{}^2\delta_2\rho_3{}^2 -$$
$$6\,d_id_r{}^2\delta_1\delta_2{}^2\rho_1{}^2 - 16\,d_id_r{}^2\delta_1\delta_2{}^2\rho_1\rho_3 - 4\,d_id_r{}^2\delta_2{}^3\rho_1\rho_3 - 32\,d_id_r{}^2\delta_2{}^3\rho_3{}^2 - 2\,d_r{}^3\delta_1{}^3\rho_1\rho_3 +$$
$$4\,d_r{}^3\delta_1{}^2\delta_2\rho_1\rho_3 + 2\,d_r{}^3\delta_1\delta_2{}^2\rho_1\rho_3 + 4\,d_r{}^3\delta_2{}^3\rho_1\rho_3\Big)I^{*2} + 4\,d_a{}^4d_i\delta_2{}^3 + 24\,d_a{}^3d_i{}^2\delta_1\delta_2{}^2 +$$
$$16\,d_a{}^3d_r{}^2\delta_1\delta_2{}^2 + 24\,d_i{}^3\delta_1{}^2\delta_2d_a{}^2 + 48\,d_a{}^2d_id_r{}^2\delta_1{}^2\delta_2 + 16\,d_a{}^2d_id_r{}^2\delta_2{}^3 + 4\,d_ad_i{}^4\delta_1{}^3 +$$
$$16\,d_ad_i{}^2\delta_1{}^3d_r{}^2 + 48\,d_ad_i{}^2\delta_1d_r{}^2\delta_2{}^2 + 4\,d_ad_r{}^4\delta_1{}^3 + 8\,d_ad_r{}^4\delta_1\delta_2{}^2 + 16\,d_i{}^3\delta_1{}^2\delta_2d_r{}^2 + 8\,d_id_r{}^4\delta_1{}^2\delta_2 +$$
$$4\,d_id_r{}^4\delta_2{}^3\Big)T^*_{reg}{}^3 + \Big(-\rho_1{}^2\rho_3{}^2\Big(\delta_1{}^2\rho_1{}^2 + 2\,\delta_1\delta_2\rho_1{}^2 + 6\,\delta_1\delta_2\rho_1\rho_3 + \delta_2{}^2\rho_1{}^2 + 2\,\delta_2{}^2\rho_1\rho_3 +$$
$$5\,\delta_2{}^2\rho_3{}^2\Big)I^{*6} + 2\,\rho_3\rho_1\Big(8\,d_a{}^2\delta_1\delta_2\rho_1{}^2 - d_a{}^2\delta_2{}^2\rho_1{}^2 + 4\,d_a{}^2\delta_2{}^2\rho_1\rho_3 + 7\,d_ad_i\delta_1{}^2\rho_1{}^2 + 2\,d_ad_i\delta_1\delta_2\rho_1{}^2 +$$
$$14\,d_ad_i\delta_1\delta_2\rho_1\rho_3 + 2\,d_ad_i\delta_2{}^2\rho_1{}^2 + 12\,d_ad_i\delta_2{}^2\rho_3{}^2 + 3\,d_ad_r\delta_1{}^2\rho_1{}^2 - 4\,d_ad_r\delta_1\delta_2\rho_1{}^2 - d_ad_r\delta_2{}^2\rho_1{}^2 +$$
$$3\,d_ad_r\delta_2{}^2\rho_3{}^2 + 4\,d_i{}^2\delta_1{}^2\rho_1{}^2 + 3\,d_i{}^2\delta_1{}^2\rho_1\rho_3 + 4\,d_i{}^2\delta_1\delta_2\rho_1{}^2 + 22\,d_i{}^2\delta_1\delta_2\rho_1\rho_3 + 12\,d_i{}^2\delta_1\delta_2\rho_3{}^2 +$$
$$d_i{}^2\delta_2{}^2\rho_1{}^2 + 3\,d_i{}^2\delta_2{}^2\rho_1\rho_3 + 36\,d_i{}^2\delta_2{}^2\rho_3{}^2 - d_id_r\delta_1{}^2\rho_1{}^2 - 7\,d_id_r\delta_1\delta_2\rho_1{}^2 + 9\,d_id_r\delta_1\delta_2\rho_3{}^2 -$$
$$2\,d_id_r\delta_2{}^2\rho_1{}^2 - 12\,d_id_r\delta_2{}^2\rho_3{}^2 + d_r{}^2\delta_1{}^2\rho_1\rho_3 + 2\,d_r{}^2\delta_1\delta_2\rho_1\rho_3 + 2\,d_r{}^2\delta_1\delta_2\rho_3{}^2 + 4\,d_r{}^2\delta_2{}^2\rho_1\rho_3 +$$
$$3\,d_r{}^2\delta_2{}^2\rho_3{}^2\Big)I^{*4} + \Big(-d_a{}^4\delta_2{}^2\rho_1{}^2 - 6\,d_a{}^3d_i\delta_1\delta_2\rho_1{}^2 - 10\,d_a{}^3d_i\delta_2{}^2\rho_1\rho_3 - 2\,d_a{}^3d_r\delta_2{}^2\rho_1\rho_3 -$$
$$7\,d_a{}^2d_i{}^2\delta_1{}^2\rho_1{}^2 - 6\,d_a{}^2d_i{}^2\delta_1\delta_2\rho_1{}^2 - 30\,d_a{}^2d_i{}^2\delta_1\delta_2\rho_1\rho_3 - 2\,d_a{}^2d_i{}^2\delta_2{}^2\rho_1{}^2 - 12\,d_a{}^2d_i{}^2\delta_2{}^2\rho_1\rho_3 -$$
$$24\,d_a{}^2d_i{}^2\delta_2{}^2\rho_3{}^2 - 16\,d_a{}^2d_id_r\delta_1\delta_2\rho_1\rho_3 + 10\,d_a{}^2d_id_r\delta_2{}^2\rho_1\rho_3 - 6\,d_a{}^2d_r{}^2\delta_1{}^2\rho_1{}^2 - 2\,d_a{}^2d_r{}^2\delta_1\delta_2\rho_1{}^2 -$$
$$14\,d_a{}^2d_r{}^2\delta_1\delta_2\rho_1\rho_3 - 2\,d_a{}^2d_r{}^2\delta_2{}^2\rho_1{}^2 - 2\,d_a{}^2d_r{}^2\delta_2{}^2\rho_1\rho_3 - 10\,d_a{}^2d_r{}^2\delta_2{}^2\rho_3{}^2 - 4\,d_ad_i{}^3\delta_1{}^2\rho_1{}^2 -$$
$$10\,d_ad_i{}^3\delta_1{}^2\rho_1\rho_3 - 2\,d_ad_i{}^3\delta_1\delta_2\rho_1{}^2 - 24\,d_ad_i{}^3\delta_1\delta_2\rho_1\rho_3 - 32\,d_ad_i{}^3\delta_1\delta_2\rho_3{}^2 - 10\,d_ad_i{}^2d_r\delta_1{}^2\rho_1\rho_3 +$$
$$16\,d_ad_i{}^2d_r\delta_1\delta_2\rho_1\rho_3 - 12\,d_ad_i{}^2d_r\delta_2{}^2\rho_1\rho_3 - 4\,d_ad_id_r{}^2\delta_1{}^2\rho_1{}^2 - 10\,d_ad_id_r{}^2\delta_1{}^2\rho_1\rho_3 -$$
$$6\,d_ad_id_r{}^2\delta_1\delta_2\rho_1{}^2 - 16\,d_ad_id_r{}^2\delta_1\delta_2\rho_1\rho_3 - 40\,d_ad_id_r{}^2\delta_1\delta_2\rho_3{}^2 - 10\,d_ad_id_r{}^2\delta_2{}^2\rho_1\rho_3 -$$
$$6\,d_ad_r{}^3\delta_1{}^2\rho_1\rho_3 + 8\,d_ad_r{}^3\delta_1\delta_2\rho_1\rho_3 - 2\,d_ad_r{}^3\delta_2{}^2\rho_1\rho_3 - d_i{}^4\delta_1{}^2\rho_1{}^2 - 4\,d_i{}^4\delta_1{}^2\rho_1\rho_3 - 4\,d_i{}^4\delta_1{}^2\rho_3{}^2 +$$
$$2\,d_i{}^3d_r\delta_1{}^2\rho_1\rho_3 + 4\,d_i{}^3d_r\delta_1\delta_2\rho_1\rho_3 - 3\,d_i{}^2d_r{}^2\delta_1{}^2\rho_1{}^2 - 6\,d_i{}^2d_r{}^2\delta_1{}^2\rho_1\rho_3 - 10\,d_i{}^2d_r{}^2\delta_1{}^2\rho_3{}^2 -$$

$$6\,{d_i}^2{d_r}^2{\delta_1}{\delta_2}{\rho_1}^2-14\,{d_i}^2{d_r}^2{\delta_1}{\delta_2}{\rho_1}{\rho_3}-{d_i}^2{d_r}^2{\delta_2}^2{\rho_1}^2-12\,{d_i}^2{d_r}^2{\delta_2}^2{\rho_1}{\rho_3}-48\,{d_i}^2{d_r}^2{\delta_2}^2{\rho_3}^2+2\,{d_i}{d_r}^3{\delta_1}^2{\rho_1}{\rho_3}+10\,{d_i}{d_r}^3{\delta_2}^2{\rho_1}{\rho_3}-{d_r}^4{\delta_1}^2{\rho_3}^2-5\,{d_r}^4{\delta_2}^2{\rho_3}^2\Big)I^{*2}+6\,{d_a}^4{d_i}^2{\delta_2}^2+4\,{d_a}^4{d_r}^2{\delta_2}^2+16\,{d_a}^3{d_i}^3{\delta_1}{\delta_2}+32\,{d_a}^3{d_i}{d_r}^2{\delta_1}{\delta_2}+6\,{d_a}^2{d_i}^4{\delta_1}^2+24\,{d_a}^2{d_i}^2{d_r}^2{\delta_1}^2+24\,{d_a}^2{d_i}^2{d_r}^2{\delta_2}^2+6\,{d_a}^2{d_r}^4{\delta_1}^2+4\,{d_a}^2{d_r}^4{\delta_2}^2+32\,{d_a}{d_i}^3{d_r}^2{\delta_1}{\delta_2}+16\,{d_a}{d_i}{d_r}^4{\delta_1}{\delta_2}+4\,{d_i}^4{d_r}^2{\delta_1}^2+4\,{d_i}^2{d_r}^4{\delta_1}^2+6\,{d_i}^2{d_r}^4{\delta_2}^2\Big){T^*_{reg}}^2+\Big(-2\,{\rho_1}^2{\rho_3}^2\Big({d_a}{\delta_1}{\rho_1}^2+2\,{d_a}{\delta_2}{\rho_1}{\rho_3}+{d_i}{\delta_1}{\rho_1}^2+2\,{d_i}{\delta_1}{\rho_1}{\rho_3}+2\,{d_i}{\delta_2}{\rho_1}^2+6\,{d_i}{\delta_2}{\rho_1}{\rho_3}+6\,{d_i}{\delta_2}{\rho_3}^2+{d_r}{\delta_1}{\rho_1}{\rho_3}-2\,{d_r}{\delta_2}{\rho_1}{\rho_3}\Big)I^{*6}+2\,{\rho_3}{\rho_1}\Big(2\,{d_a}^3{\delta_2}{\rho_1}^2+5\,{d_a}^2{d_i}{\delta_1}{\rho_1}^2+{d_a}^2{d_i}{\delta_2}{\rho_1}^2+8\,{d_a}^2{d_i}{\delta_2}{\rho_1}{\rho_3}+3\,{d_a}^2{d_r}{\delta_1}{\rho_1}^2-2\,{d_a}^2{d_r}{\delta_2}{\rho_1}^2+6\,{d_a}{d_i}^2{\delta_1}{\rho_1}^2+8\,{d_a}{d_i}^2{\delta_1}{\rho_1}{\rho_3}+4\,{d_a}{d_i}^2{\delta_2}{\rho_1}^2+12\,{d_a}{d_i}^2{\delta_2}{\rho_3}^2-2\,{d_a}{d_i}{d_r}{\delta_1}{\rho_1}^2+{d_a}{d_i}{d_r}{\delta_2}{\rho_1}^2+9\,{d_a}{d_i}{d_r}{\delta_2}{\rho_3}^2+2\,{d_a}{d_r}^2{\delta_1}{\rho_1}{\rho_3}+2\,{d_a}{d_r}^2{\delta_2}{\rho_3}^2+3\,{d_i}^3{\delta_1}{\rho_1}^2+8\,{d_i}^3{\delta_1}{\rho_1}{\rho_3}+4\,{d_i}^3{\delta_1}{\rho_3}^2+3\,{d_i}^3{\delta_2}{\rho_1}^2+8\,{d_i}^3{\delta_2}{\rho_1}{\rho_3}+28\,{d_i}^3{\delta_2}{\rho_3}^2-{d_i}^2{d_r}{\delta_1}{\rho_1}^2+6\,{d_i}^2{d_r}{\delta_1}{\rho_3}^2-4\,{d_i}^2{d_r}{\delta_2}{\rho_1}^2-12\,{d_i}^2{d_r}{\delta_2}{\rho_3}^2+2\,{d_i}{d_r}^2{\delta_1}{\rho_1}{\rho_3}+{d_i}{d_r}^2{\delta_1}{\rho_3}^2+8\,{d_i}{d_r}^2{\delta_2}{\rho_1}{\rho_3}+9\,{d_i}{d_r}^2{\delta_2}{\rho_3}^2+{d_r}^3{\delta_1}{\rho_3}^2-2\,{d_r}^3{\delta_2}{\rho_3}^2\Big)I^{*4}+\Big(-2\,{d_a}^4{d_i}{\delta_2}{\rho_1}^2-6\,{d_a}^3{d_i}^2{\delta_1}{\rho_1}^2-8\,{d_a}^3{d_i}^2{\delta_2}{\rho_1}{\rho_3}-8\,{d_a}^3{d_i}{d_r}{\delta_2}{\rho_1}{\rho_3}-4\,{d_a}^3{d_r}^2{\delta_1}{\rho_1}^2-4\,{d_a}^3{d_r}^2{\delta_2}{\rho_1}{\rho_3}-2\,{d_a}^2{d_i}^3{\delta_1}{\rho_1}^2-8\,{d_a}^2{d_i}^3{\delta_1}{\rho_1}{\rho_3}-4\,{d_a}^2{d_i}^3{\delta_2}{\rho_1}^2-12\,{d_a}^2{d_i}^3{\delta_2}{\rho_1}{\rho_3}-16\,{d_a}^2{d_i}^3{\delta_2}{\rho_3}^2-14\,{d_a}^2{d_i}^2{d_r}{\delta_1}{\rho_1}{\rho_3}+8\,{d_a}^2{d_i}^2{d_r}{\delta_2}{\rho_1}{\rho_3}-2\,{d_a}^2{d_i}{d_r}^2{\delta_1}{\rho_1}^2-8\,{d_a}^2{d_i}{d_r}^2{\delta_1}{\rho_1}{\rho_3}-4\,{d_a}^2{d_i}{d_r}^2{\delta_2}{\rho_1}^2-8\,{d_a}^2{d_i}{d_r}^2{\delta_2}{\rho_1}{\rho_3}-20\,{d_a}^2{d_i}{d_r}^2{\delta_2}{\rho_3}^2-6\,{d_a}^2{d_r}^3{\delta_1}{\rho_1}{\rho_3}+4\,{d_a}^2{d_r}^3{\delta_2}{\rho_1}{\rho_3}-2\,{d_a}{d_i}^4{\delta_1}{\rho_1}^2-8\,{d_a}{d_i}^4{\delta_1}{\rho_1}{\rho_3}-8\,{d_a}{d_i}^4{\delta_1}{\rho_3}^2+4\,{d_a}{d_i}^3{d_r}{\delta_1}{\rho_1}{\rho_3}-12\,{d_a}{d_i}^3{d_r}{\delta_2}{\rho_1}{\rho_3}-6\,{d_a}{d_i}^2{d_r}^2{\delta_1}{\rho_1}^2-12\,{d_a}{d_i}^2{d_r}^2{\delta_1}{\rho_1}{\rho_3}-20\,{d_a}{d_i}^2{d_r}^2{\delta_1}{\rho_3}^2-8\,{d_a}{d_i}^2{d_r}^2{\delta_2}{\rho_1}{\rho_3}+4\,{d_a}{d_i}{d_r}^3{\delta_1}{\rho_1}{\rho_3}-8\,{d_a}{d_i}{d_r}^3{\delta_2}{\rho_1}{\rho_3}-2\,{d_a}{d_r}^4{\delta_1}{\rho_3}^2-2\,{d_i}^3{d_r}^2{\delta_1}{\rho_1}^2-4\,{d_i}^3{d_r}^2{\delta_1}{\rho_1}{\rho_3}-2\,{d_i}^3{d_r}^2{\delta_2}{\rho_1}^2-12\,{d_i}^3{d_r}^2{\delta_2}{\rho_1}{\rho_3}-32\,{d_i}^3{d_r}^2{\delta_2}{\rho_3}^2-2\,{d_i}^2{d_r}^3{\delta_1}{\rho_1}{\rho_3}+8\,{d_i}^2{d_r}^3{\delta_2}{\rho_1}{\rho_3}-10\,{d_i}{d_r}^4{\delta_2}{\rho_3}^2\Big)I^{*2}+4\,{d_a}^4{d_i}^3{\delta_2}+8\,{d_a}^4{d_i}{d_r}^2{\delta_2}+4\,{d_a}^3{d_i}^4{\delta_1}+16\,{d_a}^3{d_i}^2{d_r}^2{\delta_1}+4\,{d_a}^3{d_r}^4{\delta_1}+16\,{d_a}^2{d_i}^3{d_r}^2{\delta_2}+8\,{d_a}^2{d_i}{d_r}^4{\delta_2}+8\,{d_a}{d_i}^4{d_r}^2{\delta_1}+8\,{d_a}{d_i}^2{d_r}^4{\delta_1}+4\,{d_i}^3{d_r}^4{\delta_2}\Big){T^*_{reg}}+{I^*}^8{\rho_1}^4{\rho_3}^4-{\rho_1}^2{\rho_3}^2\Big({d_a}^2{\rho_1}^2+2\,{d_a}{d_i}{\rho_1}{\rho_3}+2\,{d_a}{d_r}{\rho_1}{\rho_3}+5\,{d_i}^2{\rho_1}^2+12\,{d_i}^2{\rho_1}{\rho_3}+8\,{d_i}^2{\rho_3}^2-2\,{d_i}{d_r}{\rho_1}{\rho_3}+{d_r}^2{\rho_3}^2\Big)I^{*6}+2\,{\rho_3}{\rho_1}\Big({d_a}^3{d_i}{\rho_1}^2+{d_a}^3{d_r}{\rho_1}^2+3\,{d_a}^2{d_i}^2{\rho_1}^2+5\,{d_a}^2{d_i}^2{\rho_1}{\rho_3}-{d_a}^2{d_i}{d_r}{\rho_1}^2+{d_a}^2{d_r}^2{\rho_1}{\rho_3}+{d_a}{d_i}^3{\rho_1}^2+4\,{d_a}{d_i}^3{\rho_3}^2+3\,{d_a}{d_i}^2{d_r}{\rho_1}^2+6\,{d_a}{d_i}^2{d_r}{\rho_3}^2+{d_a}{d_i}{d_r}^2{\rho_3}^2+{d_a}{d_r}^3{\rho_3}^2+2\,{d_i}^4{\rho_1}^2+4\,{d_i}^4{\rho_1}{\rho_3}+8\,{d_i}^4{\rho_3}^2-{d_i}^3{d_r}{\rho_1}^2-4\,{d_i}^3{d_r}{\rho_3}^2+5\,{d_i}^2{d_r}^2{\rho_1}{\rho_3}+6\,{d_i}^2{d_r}^2{\rho_3}^2-{d_i}{d_r}^3{\rho_3}^2\Big)I^{*4}+\Big(-2\,{d_a}^4{d_i}^2{\rho_1}^2-{d_a}^4{d_r}^2{\rho_1}^2-2\,{d_a}^3{d_i}^3{\rho_1}{\rho_3}-6\,{d_a}^3{d_i}^2{d_r}{\rho_1}{\rho_3}-2\,{d_a}^3{d_i}{d_r}^2{\rho_1}{\rho_3}-2\,{d_a}^3{d_r}^3{\rho_1}{\rho_3}-2\,{d_a}^2{d_i}^4{\rho_1}^2-4\,{d_a}^2{d_i}^4{\rho_1}{\rho_3}-4\,{d_a}^2{d_i}^4{\rho_3}^2+2\,{d_a}^2{d_i}^3{d_r}{\rho_1}{\rho_3}-4\,{d_a}^2{d_i}^2{d_r}^2{\rho_1}^2-6\,{d_a}^2{d_i}^2{d_r}^2{\rho_1}{\rho_3}-10\,{d_a}^2{d_i}^2{d_r}^2{\rho_3}^2+2\,{d_a}^2{d_i}{d_r}^3{\rho_1}{\rho_3}-{d_a}^2{d_r}^4{\rho_3}^2-4\,{d_a}{d_i}^4{d_r}{\rho_1}{\rho_3}-2\,{d_a}{d_i}^3{d_r}^2{\rho_1}{\rho_3}-6\,{d_a}{d_i}^2{d_r}^3{\rho_1}{\rho_3}-{d_i}^4{d_r}^2{\rho_1}^2-4\,{d_i}^4{d_r}^2{\rho_1}{\rho_3}-8\,{d_i}^4{d_r}^2{\rho_3}^2+2\,{d_i}^3{d_r}^3{\rho_1}{\rho_3}-5\,{d_i}^2{d_r}^4{\rho_3}^2\Big)I^{*2}+{d_a}^4{d_i}^4+4\,{d_a}^4{d_i}^2{d_r}^2+{d_a}^4{d_r}^4+4\,{d_a}^2{d_i}^4{d_r}^2+4\,{d_a}^2{d_i}^2{d_r}^4+{d_i}^4{d_r}^4.$$

$$b_6=2\,{\delta_1}^2{\delta_2}^2\Big({\delta_1}^2+{\delta_2}^2\Big){T^*_{reg}}^6+4\,{\delta_1}{\delta_2}\Big(2\,{d_a}{\delta_1}^2{\delta_2}+{d_a}{\delta_2}^3+{d_i}{\delta_1}^3+2\,{d_i}{\delta_1}{\delta_2}^2\Big){T^*_{reg}}^5+\Big(\Big(-{\delta_1}^4{\rho_1}^2-2\,{\delta_1}^3{\delta_2}{\rho_1}^2-6\,{\delta_1}^3{\delta_2}{\rho_1}{\rho_3}-3\,{\delta_1}^2{\delta_2}^2{\rho_1}^2-2\,{\delta_1}^2{\delta_2}^2{\rho_1}{\rho_3}-5\,{\delta_1}^2{\delta_2}^2{\rho_3}^2-2\,{\delta_1}{\delta_2}^3{\rho_1}^2-6\,{\delta_1}{\delta_2}^3{\rho_1}{\rho_3}-4\,{\delta_2}^4{\rho_3}^2\Big)I^{*2}+12\,{d_a}^2{\delta_1}^2{\delta_2}^2+2\,{d_a}^2{\delta_2}^4+16\,{d_a}{d_i}{\delta_1}^3{\delta_2}+16\,{d_a}{d_i}{\delta_1}{\delta_2}^3+2\,{d_i}^2{\delta_1}^4+12\,{d_i}^2{\delta_1}^2{\delta_2}^2+2\,{d_r}^2{\delta_1}^4+8\,{d_r}^2{\delta_1}^2{\delta_2}^2+2\,{d_r}^2{\delta_2}^4\Big){T^*_{reg}}^4+\Big(\Big(-4\,{d_a}{\delta_1}^3{\rho_1}^2-4\,{d_a}{\delta_1}^2{\delta_2}{\rho_1}^2-16\,{d_a}{\delta_1}^2{\delta_2}{\rho_1}{\rho_3}-4\,{d_a}{\delta_1}{\delta_2}^2{\rho_1}^2-4\,{d_a}{\delta_1}{\delta_2}^2{\rho_1}{\rho_3}-10\,{d_a}{\delta_1}{\delta_2}^2{\rho_3}^2-4\,{d_a}{\delta_2}^3{\rho_1}{\rho_3}-2\,{d_i}{\delta_1}^3{\rho_1}^2-$$

$$4\,d_i{\delta_1}^3\rho_1\rho_3 - 4\,d_i{\delta_1}^2\delta_2{\rho_1}^2 - 8\,d_i{\delta_1}^2\delta_2\rho_1\rho_3 - 10\,d_i{\delta_1}^2\delta_2{\rho_3}^2 - 6\,d_i\delta_1\delta_2^2{\rho_1}^2 - 16\,d_i\delta_1\delta_2^2\rho_1\rho_3 - 4\,d_i\delta_2^3\rho_1\rho_3 - 16\,d_i\delta_2^3{\rho_3}^2 - 2\,d_r{\delta_1}^3\rho_1\rho_3 + 4\,d_r{\delta_1}^2\delta_2\rho_1\rho_3 + 2\,d_r\delta_1\delta_2^2\rho_1\rho_3 + 4\,d_r\delta_2^3\rho_1\rho_3\Big)I^{*2} + 8\,{d_a}^3\delta_1\delta_2^2 + 24\,{d_a}^2d_i{\delta_1}^2\delta_2 + 8\,{d_a}^2d_i\delta_2^3 + 8\,d_a{d_i}^2{\delta_1}^3 + 24\,d_a{d_i}^2\delta_1\delta_2^2 + 8\,d_a{d_r}^2{\delta_1}^3 + 16\,d_a{d_r}^2\delta_1\delta_2^2 + 8\,{d_i}^3{\delta_1}^2\delta_2 + 16\,d_i{d_r}^2{\delta_1}^2\delta_2 + 8\,d_i{d_r}^2\delta_2^3\Big){T^*_{reg}}^3 + \Big(2\,\rho_1\rho_3\Big({\delta_1}^2{\rho_1}^2 + {\delta_1}^2\rho_1\rho_3 + 4\,\delta_1\delta_2{\rho_1}^2 + 2\,\delta_1\delta_2\rho_1\rho_3 + 2\,\delta_1\delta_2{\rho_3}^2 - {\delta_2}^2{\rho_1}^2 + 4\,{\delta_2}^2\rho_1\rho_3 + 3\,{\delta_2}^2{\rho_3}^2\Big)I^{*4} + \Big(-6\,{d_a}^2{\delta_1}^2{\rho_1}^2 - 2\,{d_a}^2\delta_1\delta_2{\rho_1}^2 - 14\,{d_a}^2\delta_1\delta_2\rho_1\rho_3 - 2\,{d_a}^2\delta_2^2{\rho_1}^2 - 2\,{d_a}^2\delta_2^2\rho_1\rho_3 - 5\,{d_a}^2\delta_2^2{\rho_3}^2 - 4\,d_a{d_i}{\delta_1}^2{\rho_1}^2 - 10\,d_a{d_i}{\delta_1}^2\rho_1\rho_3 - 6\,d_a{d_i}\delta_1\delta_2{\rho_1}^2 - 16\,d_a{d_i}\delta_1\delta_2\rho_1\rho_3 - 20\,d_a{d_i}\delta_1\delta_2{\rho_3}^2 - 10\,d_a{d_i}\delta_2^2\rho_1\rho_3 - 6\,d_a{d_r}{\delta_1}^2\rho_1\rho_3 + 8\,d_a{d_r}\delta_1\delta_2\rho_1\rho_3 - 2\,d_a{d_r}\delta_2^2\rho_1\rho_3 - 3\,{d_i}^2{\delta_1}^2{\rho_1}^2 - 6\,{d_i}^2{\delta_1}^2\rho_1\rho_3 - 5\,{d_i}^2{\delta_1}^2{\rho_3}^2 - 6\,{d_i}^2\delta_1\delta_2{\rho_1}^2 - 14\,{d_i}^2\delta_1\delta_2\rho_1\rho_3 - {d_i}^2\delta_2^2{\rho_1}^2 - 12\,{d_i}^2\delta_2^2\rho_1\rho_3 - 24\,{d_i}^2\delta_2^2{\rho_3}^2 + 2\,d_i{d_r}{\delta_1}^2\rho_1\rho_3 + 10\,d_i{d_r}\delta_2^2\rho_1\rho_3 - 2\,{d_r}^2{\delta_1}^2{\rho_1}^2 - 2\,{d_r}^2{\delta_1}^2\rho_1\rho_3 - 2\,{d_r}^2{\delta_1}^2{\rho_3}^2 - 2\,{d_r}^2\delta_1\delta_2{\rho_1}^2 - 6\,{d_r}^2\delta_1\delta_2\rho_1\rho_3 - {d_r}^2\delta_2^2{\rho_1}^2 - 2\,{d_r}^2\delta_2^2\rho_1\rho_3 - 10\,{d_r}^2\delta_2^2{\rho_3}^2\Big)I^{*2} + 2\,{d_a}^4\delta_2^2 + 16\,{d_a}^3d_i\delta_1\delta_2 + 12\,{d_a}^2{d_i}^2{\delta_1}^2 + 12\,{d_a}^2{d_i}^2\delta_2^2 + 12\,{d_a}^2{d_r}^2{\delta_1}^2 + 8\,{d_a}^2{d_r}^2\delta_2^2 + 16\,d_a{d_i}^3\delta_1\delta_2 + 32\,d_a{d_i}{d_r}^2\delta_1\delta_2 + 2\,{d_i}^4{\delta_1}^2 + 8\,{d_i}^2{d_r}^2{\delta_1}^2 + 12\,{d_i}^2{d_r}^2\delta_2^2 + 2\,{d_r}^4{\delta_1}^2 + 2\,{d_r}^4\delta_2^2\Big){T^*_{reg}}^2 + \Big(2\,\rho_1\rho_3\Big(2\,d_a\delta_1{\rho_1}^2 + 2\,d_a\delta_1\rho_1\rho_3 + 2\,d_a\delta_2{\rho_1}^2 + 2\,d_a\delta_2{\rho_3}^2 + 3\,d_i\delta_1{\rho_1}^2 + 2\,d_i\delta_1\rho_1\rho_3 + d_i\delta_1{\rho_3}^2 + d_i\delta_2{\rho_1}^2 + 8\,d_i\delta_2\rho_1\rho_3 + 9\,d_i\delta_2{\rho_3}^2 + d_r\delta_1{\rho_1}^2 + d_r\delta_1{\rho_3}^2 - 2\,d_r\delta_2{\rho_1}^2 - 2\,d_r\delta_2{\rho_3}^2\Big)I^{*4} + \Big(-4\,{d_a}^3\delta_1{\rho_1}^2 - 4\,{d_a}^3\delta_2\rho_1\rho_3 - 2\,{d_a}^2d_i\delta_1{\rho_1}^2 - 8\,{d_a}^2d_i\delta_1\rho_1\rho_3 - 4\,{d_a}^2d_i\delta_2{\rho_1}^2 - 8\,{d_a}^2d_i\delta_2\rho_1\rho_3 - 10\,{d_a}^2d_i\delta_2{\rho_3}^2 - 6\,{d_a}^2d_r\delta_1\rho_1\rho_3 + 4\,{d_a}^2d_r\delta_2\rho_1\rho_3 - 6\,d_a{d_i}^2\delta_1{\rho_1}^2 - 12\,d_a{d_i}^2\delta_1\rho_1\rho_3 - 10\,d_a{d_i}^2\delta_1{\rho_3}^2 - 8\,d_a{d_i}^2\delta_2\rho_1\rho_3 + 4\,d_a{d_i}{d_r}\delta_1\rho_1\rho_3 - 8\,d_a{d_i}{d_r}\delta_2\rho_1\rho_3 - 4\,d_a{d_r}^2\delta_1{\rho_1}^2 - 4\,d_a{d_r}^2\delta_1\rho_1\rho_3 - 4\,d_a{d_r}^2\delta_1{\rho_3}^2 - 4\,d_a{d_r}^2\delta_2\rho_1\rho_3 - 2\,{d_i}^3\delta_1{\rho_1}^2 - 4\,{d_i}^3\delta_1\rho_1\rho_3 - 2\,{d_i}^3\delta_2{\rho_1}^2 - 12\,{d_i}^3\delta_2\rho_1\rho_3 - 16\,{d_i}^3\delta_2{\rho_3}^2 - 2\,{d_i}^2d_r\delta_1\rho_1\rho_3 + 8\,{d_i}^2d_r\delta_2\rho_1\rho_3 - 2\,d_i{d_r}^2\delta_1{\rho_1}^2 - 4\,d_i{d_r}^2\delta_1\rho_1\rho_3 - 2\,d_i{d_r}^2\delta_2{\rho_1}^2 - 8\,d_i{d_r}^2\delta_2\rho_1\rho_3 - 20\,d_i{d_r}^2\delta_2{\rho_3}^2 - 2\,{d_r}^3\delta_1\rho_1\rho_3 + 4\,{d_r}^3\delta_2\rho_1\rho_3\Big)Y^2 + 4\,{d_a}^4d_i\delta_2 + 8\,{d_a}^3{d_i}^2\delta_1 + 8\,{d_a}^3{d_r}^2\delta_1 + 8\,{d_a}^2{d_i}^3\delta_2 + 16\,{d_a}^2d_i{d_r}^2\delta_2 + 4\,d_a{d_i}^4\delta_1 + 16\,d_a{d_i}^2{d_r}^2\delta_1 + 4\,d_a{d_r}^4\delta_1 + 8\,{d_i}^3{d_r}^2\delta_2 + 4\,d_i{d_r}^4\delta_2\Big){T^*_{reg}} - {\rho_1}^2{\rho_3}^2\Big(\rho_1+\rho_3\Big)^2I^{*6} + 2\,\rho_1\rho_3\Big({d_a}^2{\rho_1}^2 + {d_a}^2\rho_1\rho_3 + d_a{d_i}{\rho_1}^2 + d_a{d_i}{\rho_3}^2 + d_a{d_r}{\rho_1}^2 + d_a{d_r}{\rho_3}^2 + 3\,{d_i}^2{\rho_1}^2 + 5\,{d_i}^2\rho_1\rho_3 + 6\,{d_i}^2{\rho_3}^2 - d_i{d_r}{\rho_1}^2 - d_i{d_r}{\rho_3}^2 + {d_r}^2\rho_1\rho_3 + {d_r}^2{\rho_3}^2\Big)Y^4 + \Big(-{d_a}^4{\rho_1}^2 - 2\,{d_a}^3d_i\rho_1\rho_3 - 2\,{d_a}^3d_r\rho_1\rho_3 - 4\,{d_a}^2{d_i}^2{\rho_1}^2 - 6\,{d_a}^2{d_i}^2\rho_1\rho_3 - 5\,{d_a}^2{d_i}^2{\rho_3}^2 + 2\,{d_a}^2d_i{d_r}\rho_1\rho_3 - 2\,{d_a}^2{d_r}^2{\rho_1}^2 - 2\,{d_a}^2{d_r}^2\rho_1\rho_3 - 2\,{d_a}^2{d_r}^2{\rho_3}^2 - 2\,d_a{d_i}^3\rho_1\rho_3 - 6\,d_a{d_i}^2d_r\rho_1\rho_3 - 2\,d_a{d_i}{d_r}^2\rho_1\rho_3 - 2\,d_a{d_r}^3\rho_1\rho_3 - {d_i}^4{\rho_1}^2 - 4\,{d_i}^4\rho_1\rho_3 - 4\,{d_i}^4{\rho_3}^2 + 2\,{d_i}^3d_r\rho_1\rho_3 - 2\,{d_i}^2{d_r}^2{\rho_1}^2 - 6\,{d_i}^2{d_r}^2\rho_1\rho_3 - 10\,{d_i}^2{d_r}^2{\rho_3}^2 + 2\,d_i{d_r}^3\rho_1\rho_3 - {d_r}^4{\rho_3}^2\Big)I^{*2} + 2\,{d_a}^4{d_i}^2 + 2\,{d_a}^4{d_r}^2 + 2\,{d_a}^2{d_i}^4 + 8\,{d_a}^2{d_i}^2{d_r}^2 + 2\,{d_a}^2{d_r}^4 + 2\,{d_i}^4{d_r}^2 + 2\,{d_i}^2{d_r}^4.$$

$$b_8 = \Big({\delta_1}^4 + 4\,{\delta_1}^2\delta_2^2 + {\delta_2}^4\Big){T^*_{reg}}^4 + \Big(4\,d_a{\delta_1}^3 + 8\,d_a\delta_1\delta_2^2 + 8\,d_i{\delta_1}^2\delta_2 + 4\,d_i\delta_2^3\Big){T^*_{reg}}^3 + \Big(\Big(-2\,{\delta_1}^2{\rho_1}^2 - 2\,{\delta_1}^2\rho_1\rho_3 - {\delta_1}^2{\rho_3}^2 - 2\,\delta_1\delta_2{\rho_1}^2 - 6\,\delta_1\delta_2\rho_1\rho_3 - {\delta_2}^2{\rho_1}^2 - 2\,{\delta_2}^2\rho_1\rho_3 - 5\,{\delta_2}^2{\rho_3}^2\Big)I^{*2} + 6\,{d_a}^2{\delta_1}^2 + 4\,{d_a}^2{\delta_2}^2 + 16\,d_a{d_i}\delta_1\delta_2 + 4\,{d_i}^2{\delta_1}^2 + 6\,{d_i}^2{\delta_2}^2 + 4\,{d_r}^2{\delta_1}^2 + 4\,{d_r}^2{\delta_2}^2\Big){T^*_{reg}}^2 + \Big(\Big(-4\,d_a\delta_1{\rho_1}^2 - 4\,d_a\delta_1\rho_1\rho_3 - 2\,d_a\delta_1{\rho_3}^2 - 4\,d_a\delta_2\rho_1\rho_3 - 2\,d_i\delta_1{\rho_1}^2 - 4\,d_i\delta_1\rho_1\rho_3 - 2\,d_i\delta_2{\rho_1}^2 - 8\,d_i\delta_2\rho_1\rho_3 - 10\,d_i\delta_2{\rho_3}^2 - 2\,d_r\delta_1\rho_1\rho_3 + 4\,d_r\delta_2\rho_1\rho_3\Big)I^{*2} + 4\,{d_a}^3\delta_1 + 8\,{d_a}^2d_i\delta_2 + 8\,d_a{d_i}^2\delta_1 +$$

$$8\,d_a{d_r}^2\delta_1 + 4\,{d_i}^3\delta_2 + 8\,d_i{d_r}^2\delta_2\Big)T^*_{reg} + 2\,\rho_1\rho_3\Big({\rho_1}^2 + \rho_3\rho_1 + {\rho_3}^2\Big){I^*}^4 + \Big(- 2\,{d_a}^2{\rho_1}^2 - 2\,{d_a}^2\rho_1\rho_3 - {d_a}^2{\rho_3}^2 - 2\,d_ad_i\rho_1\rho_3 - 2\,d_ad_r\rho_1\rho_3 - 2\,{d_i}^2{\rho_1}^2 - 6\,{d_i}^2\rho_1\rho_3 - 5\,{d_i}^2{\rho_3}^2 + 2\,d_id_r\rho_1\rho_3 - {d_r}^2{\rho_1}^2 - 2\,{d_r}^2\rho_1\rho_3 - 2\,{d_r}^2{\rho_3}^2\Big){I^*}^2 + {d_a}^4 + 4\,{d_a}^2{d_i}^2 + 4\,{d_a}^2{d_r}^2 + {d_i}^4 + 4\,{d_i}^2{d_r}^2 + {d_r}^4.$$

$$b_{10} = \Big(2\,{\delta_1}^2 + 2\,{\delta_2}^2\Big){T^*_{reg}}^2 + \Big(4\,d_a\delta_1 + 4\,d_i\delta_2\Big)Treg^* - \Big(\rho_1 + \rho_3\Big)^2{I^*}^2 + 2\,{d_a}^2 + 2\,{d_i}^2 + 2\,{d_r}^2.$$

Appendix B

Construction of equivalent SDDE models

Using the method which is presented by Allen et al. [206] we show that in what conditions two different SDDE systems are equivalent.

Consider the two following Itô SDDE systems

$$\begin{aligned} d\mathbf{X}(t) =& \mathbf{f}\left(\mathbf{X}(t), \mathbf{X}(t-\tau_1), \ldots, \mathbf{X}(t-\tau_r), t\right) dt \\ &+ G\left(\mathbf{X}(t), \mathbf{X}(t-\tau_1), \ldots, \mathbf{X}(t-\tau_r), t\right) d\mathbf{W}(t), \end{aligned} \tag{B.1}$$

and

$$\begin{aligned} d\mathbf{X}^*(t) =& \mathbf{f}\left(\mathbf{X}^*(t), \mathbf{X}^*(t-\tau_1), \ldots, \mathbf{X}^*(t-\tau_r), t\right) dt \\ &+ B\left(\mathbf{X}^*(t), \mathbf{X}^*(t-\tau_1), \ldots, \mathbf{X}^*(t-\tau_r), t\right) d\mathbf{W}^*(t), \end{aligned} \tag{B.2}$$

where $\mathbf{X}(t) = [X_1(t), X_2(t), \ldots, X_n(t)]^T$, $\mathbf{X}^*(t) = [X_1^*(t), X_2^*(t), \ldots, X_n^*(t)]^T$, $\mathbf{W}(t) = [W_1(t), W_2(t), \ldots, W_m(t)]^T$, $\mathbf{W}^*(t) = [W_1^*(t), W_2^*(t), \ldots, W_n^*(t)]^T$, also G and B are related through the $n \times n$ matrix V, where $V = GG^T$ and $B = V^{1/2}$. Notice that V and B are symmetric positive semidefinite matrices and $V = BB^T$.

Finding the delay Fokker-Planck equation shows that solutions to (B.1) and (B.2) have the same probability distribution. Moreover, a sample path solution of one equation is also a sample path of the second one, i.e. given a Wiener trajectory $\mathbf{W}(t)$ with the sample path solution $\mathbf{X}(t)$ to (B.1), there exist a Wiener trajectory

$\mathbf{W}^*(t)$ with the sample path solution $\mathbf{X}^*(t) = \mathbf{X}(t)$ to (B.2) and vice versa.

Now assume that a Wiener trajectory $\mathbf{W}(t)$ for $0 \leq t \leq T$ with the sample path solution $\mathbf{X}(t)$ to (B.1) is given. Consider the following singular value decomposition

$$G(\mathbf{X}(t), \mathbf{X}(t-\tau_1), \ldots, \mathbf{X}(t-\tau_r), t) = G(t) = P(t)D(t)Q(t)$$

for $0 \leq t \leq T$, where $P(t)$ and $Q(t)$ are orthogonal matrices of sizes $n \times n$ and $m \times m$, respectively, and $D(t)$ is a $n \times m$ matrix with $d \leq n$ positive diagonal entries. since

$$V(t) = G(t)G(t)^T = P(t)D(t)D(t)^T P(t)^T = (B(t))^2,$$

then $B(t) = P(t)\Big(D(t)D(t)^T\Big)^{1/2}P(t)^T$. The Wiener trajectory $\mathbf{W}^*(t)$ is defined as

$$\mathbf{W}^*(t) = \int_0^t P(s)\bigg(\Big(D(s)D(s)^T\Big)^{1/2}\bigg)^+ D(s)Q(s)d\mathbf{W}(s) + \int_0^t P(s)d\mathbf{W}^{**}(s)$$

for $0 \leq t \leq T$, where $\mathbf{W}^{**}(s)$ is a vector of length n with the first d entries equal to zero and the next $n-d$ entries independent Wiener processes, and $(\cdot)^+$ is the pseudoinverse (If Σ is a $n \times m$ matrix with the only nonzero entries Σ_{ii} for $i = 1, 2, \ldots, d$, where $d \leq n \leq m$, then Σ^+ is a $m \times n$ matrix with the only nonzero entries $(\Sigma^+)_{ii} = (\Sigma_{ii})^{-1}$ for $i = 1, 2, \ldots, d$). It is clear that $\mathbb{E}(\mathbf{W}^*(t)(\mathbf{W}^*(t))^T) = tI_n$, where I_n is the $n \times n$ identity matrix. Now if we substitute $\mathbf{X}(t)$ in the diffusion term of (B.2), then

$$\begin{aligned} B(\mathbf{X}(t), \mathbf{X}(t-\tau_1), \ldots, \mathbf{X}(t-\tau_r), t)d\mathbf{W}^*(t) \\ &= B(t)\bigg(P(t)\Big(\Big(D(t)D(t)^T\Big)^{1/2}\Big)^+ D(t)Q(t)d\mathbf{W}(t) + P(t)d\mathbf{W}^{**}(t)\bigg) \\ &= G\left(\mathbf{X}(t), \mathbf{X}(t-\tau_1), \ldots, \mathbf{X}(t-\tau_r), t\right) d\mathbf{W}(t). \end{aligned}$$

Hence, $\mathbf{X}(t)$ is a sample path solution of (B.2).

Conversely, assume that a Wiener trajectory $\mathbf{W}^*(t)$ for $0 \leq t \leq T$ with the sample path solution $\mathbf{X}^*(t)$ to (B.2) is given. Consider the following singular value decomposition

$$G(\mathbf{X}^*(t), \mathbf{X}^*(t-\tau_1), \ldots, \mathbf{X}^*(t-\tau_r), t) = G(t) = P(t)D(t)Q(t)$$

for $0 \leq t \leq T$, where $P(t)$ and $Q(t)$ are orthogonal matrices of sizes $n \times n$ and $m \times m$, respectively, and $D(t)$ is a $n \times m$ matrix with $d \leq n$ positive diagonal entries. The Wiener trajectory $\mathbf{W}(t)$ is defined as

$$\mathbf{W}(t) = \int_0^t Q(s)^T D(s)^+ \Big(D(s)D(s)^T\Big)^{1/2} P(s)^T d\mathbf{W}^*(s) + \int_0^t Q(s)^T d\mathbf{W}^{***}(s)$$

for $0 \leq t \leq T$, where $\mathbf{W}^{***}(s)$ is a vector of length m with the first d entries equal to zero and the next $m - d$ entries independent Wiener processes. In a similar way we can show that $\mathbf{X}^*(t)$ is a sample solution of (B.1). Therefore, solutions to SDDE systems (B.1) and (B.2) have the same probability distribution, and a sample path solution of one system is a sample path solution of the other one, i.e. these two systems are equivalent.